核医学とともに30年

名古屋大学大学院医学系研究科
総合保健学専攻先端医療情報学領域
バイオメディカルイメージング情報科学
医用機能画像評価学講座
加藤克彦

最終講義
Mar. 21. 2025

Nagoya University Graduate School of Medicine

加 藤 克 彦

昭和35年2月28日生（64歳）名古屋市生まれ

本籍 〒461-0014 名古屋市東区橦木町1-17

昭和53年3月 愛知県立明和高等学校卒業

昭和59年3月 日本大学工学部土木工学科卒業

昭和59年4月 五洋建設株式会社入社

昭和61年1月 同退社

平成07年3月 川崎医科大学卒業

平成07年5月～8年3月 小牧市民病院

平成08年4月 名古屋大学大学院医学研究科博士課程内科系放射線医学専攻入学

平成12年3月 同修了

平成12年4月 名古屋大学医学部附属病院予防医療部医員

平成13年4月 名古屋大学医学部附属病院放射線科医員

平成14年4月 名古屋大学医学部附属病院放射線部助手

平成17年10月～12月 ドイツ、ミュンスター大学医学部核医学科へ日独放射線医学交流計画（German-Japanese Radiological Affiliation）により交換留学

平成19年4月 名古屋大学医学部放射線科医局長

平成19年4月 名古屋大学医学部講師

平成20年4月 名古屋大学医学部保健学科放射線技術科学専攻医用放射線技術学講座 教授

平成24年4月 名古屋大学大学院医学系研究科医療技術学専攻医用量子科学講座 教授

平成24年4月～26年3月 名古屋大学大学院医学系研究科医療技術学専攻医用量子科学講座 主任

平成28年 第56回日本核医学会学術総会（平成28年11月3日～5日）副会長

令和2年4月 名古屋大学大学院医学系研究科総合保健学専攻先端医療情報学領域バイオメディカルイメージング情報科学医用機能画像評価学講座 教授

令和4年4月 名古屋大学大学院医学系研究科総合保健学専攻先端医療情報学領域バイオメディカルイメージング情報科学 主任

平成07年4月 医師国家試験合格 医籍 第369970号

平成13年8月 日本核医学会認定医資格取得 第200207号

平成13年8月 放射線科専門医認定 第3744号

平成17年10月 PET核医学認定医 第P00272号

平成18年8月 日本核医学会専門医 第200207号

学位論文

An experimental teleradiology transmission system using a high-speed ATM backbone network（高速・広帯域バックボーンネットワークを利用した遠隔画像伝送システム）

所属学会

Radiological Society of North America (RSNA)
The Society of Nuclear Medicine (SNM)
European Association of Nuclear Medicine (EANM)
日本医学放射線学会
日本核医学会
日本放射線技術学会

役職
日本核医学会理事
日本核医学会評議員
日本医学放射線学会代議員
日本核医学会健保委員会委員長
日本核医学会編集委員会委員
日本医学放射線学会編集委員会委員
日本医学放射線学会保健委員会委員
日独放射線交流計画事務局長

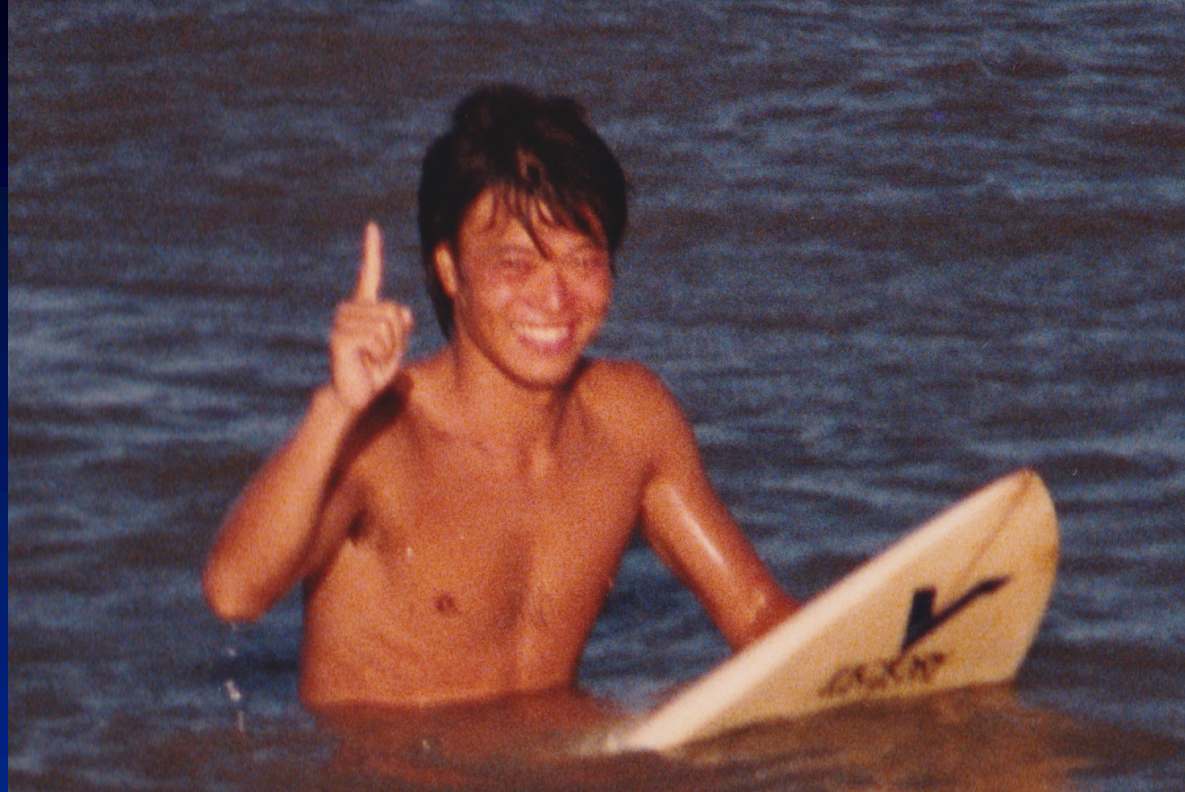平成30年～令和6年 診療放射線技師国家試験委員、診療放射線技師国家試験出題基準策定委員

専門領域

核医学全般、ポジトロン断層撮影（PET）、放射性同位元素内用療法

Giessen

坂 本 隧 道
昭和 60 年 2月
延長 23 M 幅員 9.5 M
横浜市
施工者 五洋建設株式会社

'84 12 6

骨シンチグラフィにおける膝蓋骨へのいわゆる正常集積の検討

加藤克彦，池田　充，田所匡典，吉田貴代，小林英敏，石垣武男

名古屋大学医学部放射線科
466　名古屋市昭和区鶴舞町 65

1. 緒言

^{99m}Tc-MDP[1] および ^{99m}Tc-HMDP[2] を用いた全身骨シンチグラフィは，癌の骨転移検索や骨，関節の退行性疾患の解析にも用いられている。骨シンチグラフィの集積は，加齢によって変化が見られるため，骨シンチグラフィ読影の際には性別，年齢を考慮することは臨床上必要なことと考えられている。しかし，加齢に伴う骨シンチグラフィ集積の変化についての定量的な検討は十分とはいえない。今回われわれは膝蓋骨に注目し，性別および年齢別による集積程度の違いおよび左右差につき検討を行ったので報告する。

2. 対象ならびに方法

平成7年1月から平成8年6月までに名古屋

た。

膝蓋骨の集積の評価には，正面全身像を用い大腿骨骨幹部の集積の度合と比較した。集積の程度により大腿骨骨幹部より明らかに集積が亢進している群を"陽性"とし，それ以外を"陰性"の2群に分けた (Fig. 1)。判定は放射線科医2名が共同で行った。

3. 結果

対象症例 828 例の性別は男性 508 例，女性320 例であった。年齢別では，60歳以上の男性が多い傾向がみられた (Table 1)。

男性，女性ともに膝蓋骨への集積は加齢により亢進した。男性において60歳以上の膝蓋骨への高集積率は 20 - 39 歳に比較して有意差をもっておいて
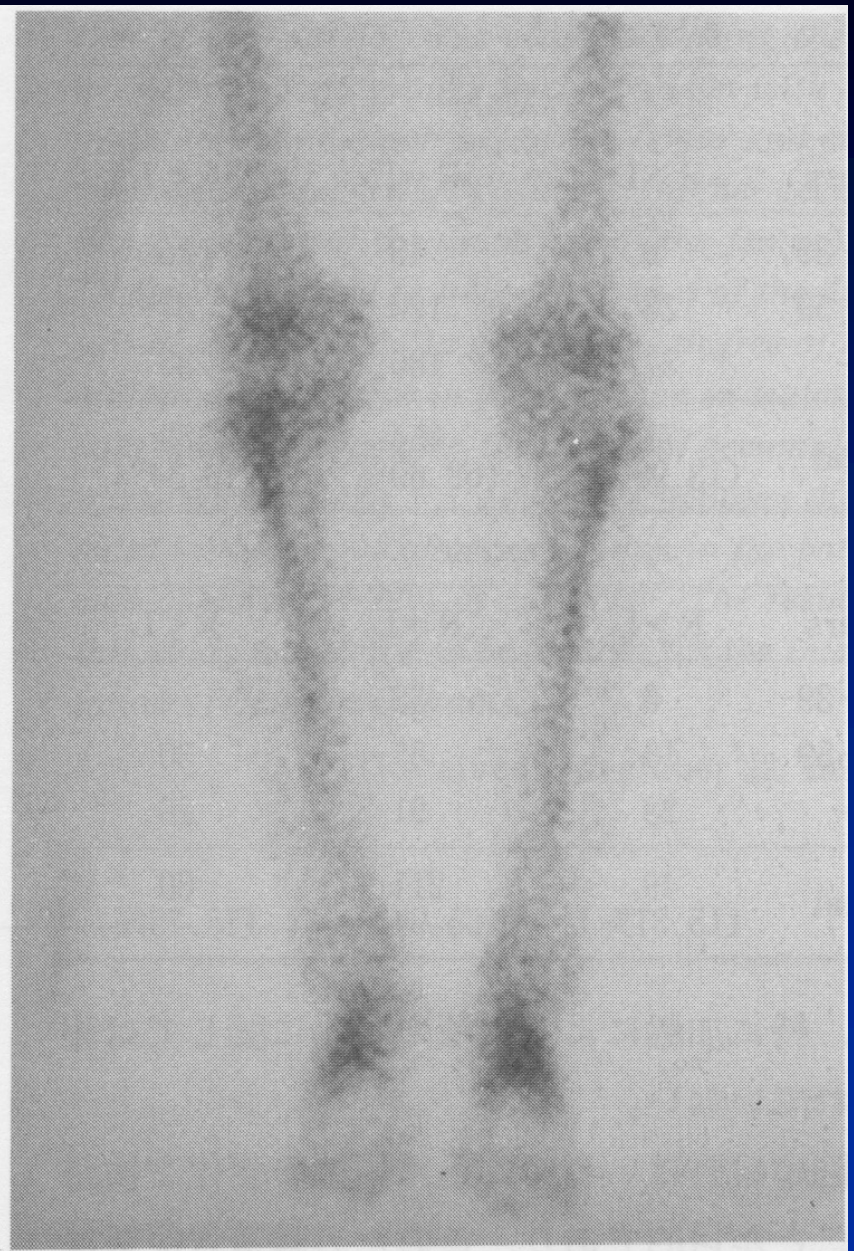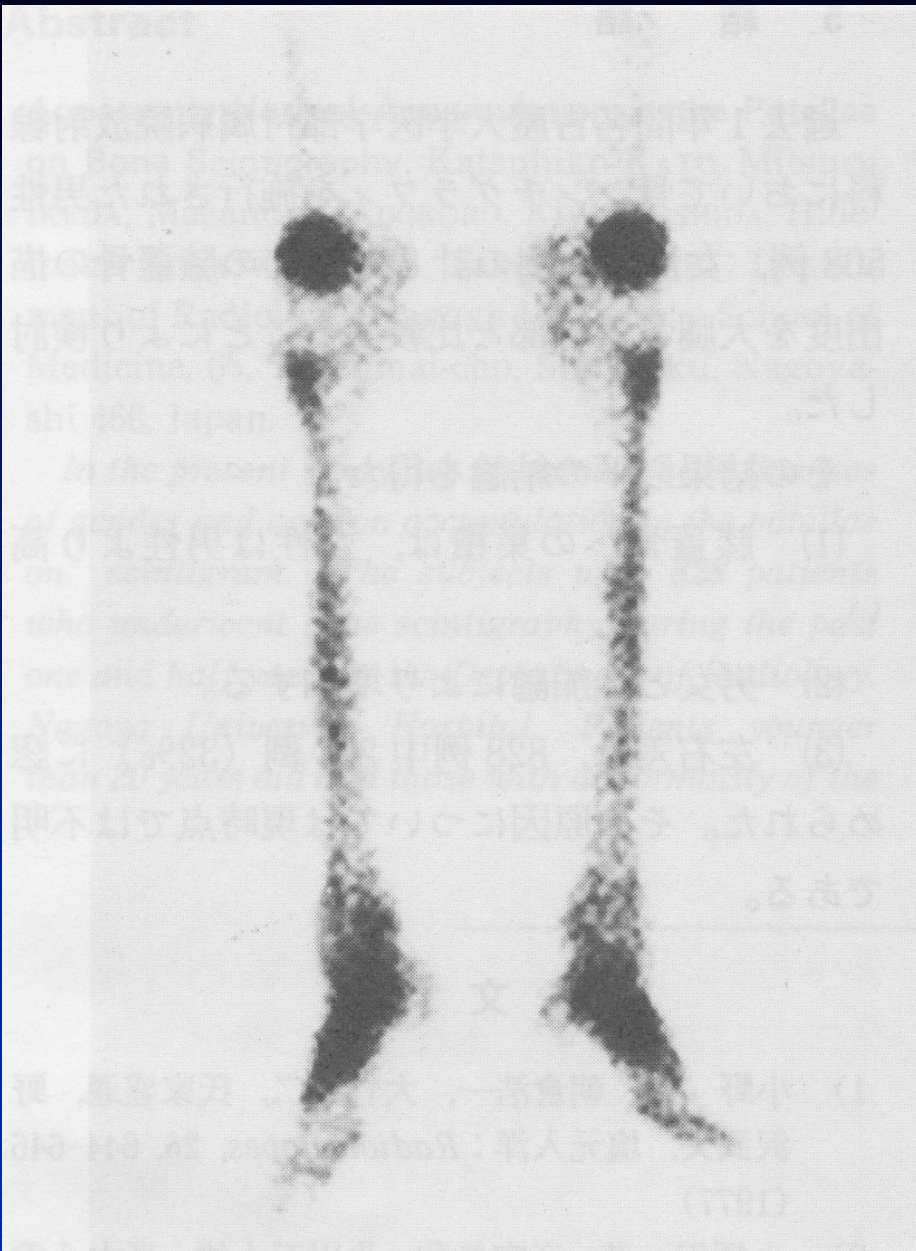
Fig. 1 "Positive" and "Negative" scintigraphy.

▶ An experimental teleradiology transmission system using a high-speed ATM backbone network

Katsuhiko Kato*, Kazuhiro Shimamoto†, Takeo Ishigaki*, Rie Niimi*, Tsuneo Ishiguchi*, Takeo Mimura‡, Kazunobu Yamauchi§, Mitsuru Ikeda§ and Akira Iwata**

*Department of Radiology, Nagoya University School of Medicine; †Department of Radiological Technology, Nagoya University School of Health Sciences; ‡Department of Radiology, Kamiiida Daiichi General Hospital; §Department of Medical Information and Records, Nagoya University Hospital; **Department of Electrical and Computer Engineering, Nagoya Institute of Technology, Japan

Summary

We evaluated the performance of an experimental teleradiology system based on a high-speed ATM backbone network. Image acquisition, transmission and the disk-to-display processing times were measured. Computerized tomography (CT) scans printed on 14 inch × 17 inch (36 cm × 43 cm) films were digitized and transferred over the network. The average time for the entire process was 1 min 30 s. Three radiologists interpreted 20 cases. For CT image interpretation, the reading time for one case ranged from 2 to 12 min (mean 6 min 46 s) on a monitor, and from 1 to 3 min (mean 1 min 31 s) with the original film. The ATM backbone network operating at 156 Mbit/s provided sufficient speed for remote consultation. However, further improvements in the operability of the system, especially the image viewing station, are necessary before it will be satisfactory for clinical use.

Introduction

Rapid advances in high-speed communications technology have made it possible to take advantage of multimedia (voice, data and image) communications in medicine. In order to develop new applications (different from those of the telephone era), the Nippon Telegraph and Telephone Corporation (NTT) has used high-speed ATM (asynchronous transfer mode) communications in a trial network (Fig 1). This provides a high-performance communications medium for medical image capture, data transmission and videoconferencing. We have evaluated the operability and clinical usefulness of an experimental teleradiology system based on the trial network.
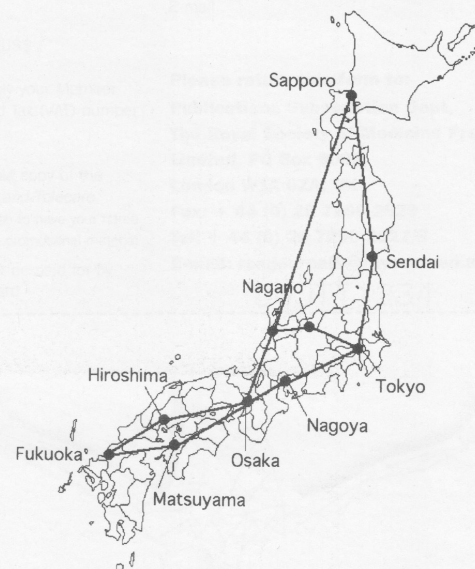
Fig 1 The site of the NTT high-speed, broadband backbone network in Japan.
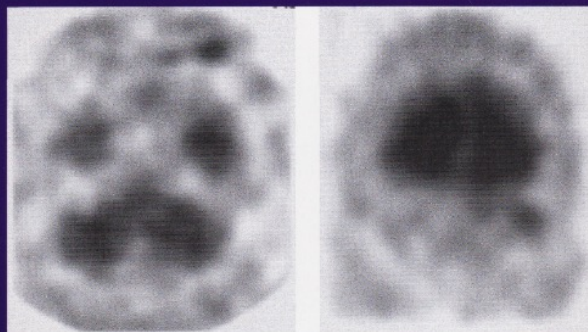
Annals of Nuclear Medicine

Fig. 1

Question:

^{123}I-IMP scintigram at delayed image (24 hr) from a 69-year-old male with impairment of visual acuity of the left eye (Fig. 1, left, axial image, right, coronal image). Examination of the fundus of the left eye revealed a tumor (4.4 × 7 mm). What is the diagnosis?   (See p. 612)

Answer and comments:

Uveal malignant melanoma

Katsuhiko Kato
Department of Radiology, Nagoya University Hospital

A 69-year-old male had noticed progressive impairment of visual acuity of the left eye. Examination of the fundus of the left eye revealed a tumor (4.4 × 7 mm). CT showed a mass in the left eye (Fig. 2). MRI showed a high intensity area on T1 weighted images and low intensity area on T2 weighted images in the left eye (Fig. 3). Scintigraphy with ^{123}I-IMP obtained at 24 hr after intravenous administration of ^{123}I-IMP delineated an area of increased uptake in the site corresponding to the left eye tumor (Fig. 1). From this finding the tumor was diagnosed as an uveal malignant melanoma. Later, laser photocoagulation therapy was performed to the tumor, but the follow-up ^{123}I-IMP scintigraphy showed a residual tumor (Fig. 4, left, axial image, right, coronal image).

^{123}I-IMP distributes in regions of melanin production, and therefore has been used in an attempt to detect malignant melanoma.[1–3] The accumulation of ^{123}I-IMP in malignant melanoma tissue is apparent not in the early image, but in the delayed image. It has been reported that melanoma lesions are best visualized at 16–24 hr.[1–3]
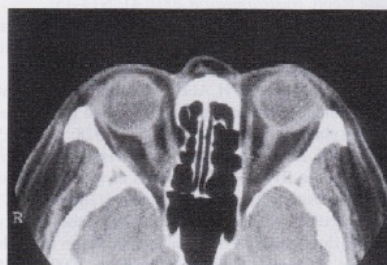

Fig. 2

References

1. Cohen MB, Saxton RE, Lake RR, Cagle L, Graham LS, Nizze A, et al. Detection of malignant melanoma with iodine-123 iodoamphetamine. *J Nucl Med* 1988; 29: 1200–1206.
2. Ono S, Fukunaga M. Otsuka N, Nagai K, Morita K, Furukawa T, et al. Visualization of ocular melanoma with *N*-isopropyl-*p*-[123I]-iodoamphetamine. *J Nucl Med* 1988; 29: 1448–1450.
3. Goto H, Usui M, Ishii I. Efficacy of *N*-isopropyl-*p*-[123I]-iodoamphetamine single photon emission computed tomography for the diagnosis of uveal malignant melanoma. *Am J Ophthalmol* 2001; 132: 937–939.
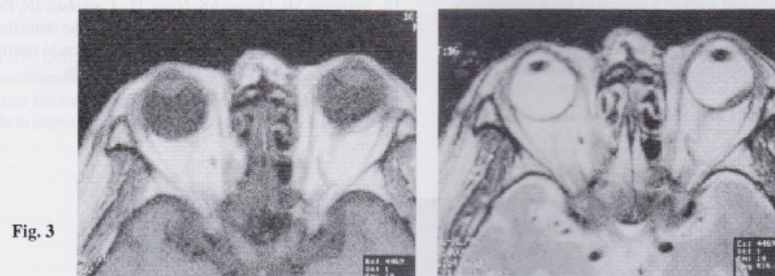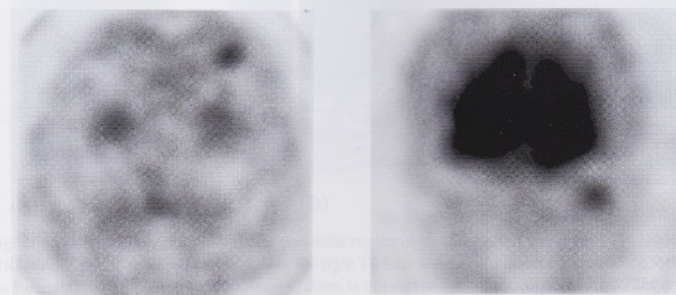
Fig. 3

Fig. 4

Low Efficacy of ^{18}F-FDG PET for Detection of Uveal Malignant Melanoma Compared with ^{123}I-IMP SPECT

Katsuhiko Kato, MD, PhD[1]; Toshinobu Kubota, MD[2]; Mitsuru Ikeda, MD, PhD[3]; Masanori Tadokoro, MD, PhD[4]; Shinji Abe, BSc, RT[5]; Satoshi Nakano, MSc, RT[5]; Masanari Nishino, BSc, RT[5]; Hidetoshi Kobayashi, MD, PhD[6]; and Takeo Ishigaki, MD, PhD[1]

[1]Department of Radiology, Nagoya University Graduate School of Medicine, Nagoya, Japan; [2]Department of Ophthalmology, National Hospital Organization, Nagoya Medical Center, Nagoya, Japan; [3]Department of Radiological Technology, Nagoya University School of Health Sciences, Nagoya, Japan; [4]Department of Radiology, Toyota Memorial Hospital, Toyota, Japan; [5]Department of Radiology, Nagoya University Hospital, Nagoya, Japan; and [6]Department of Radiology, Fujita Health University School of Health Science, Toyoake, Japan

Earlier investigations showed that N-isopropyl-p-^{123}I-iodoamphetamine SPECT (^{123}I-IMP SPECT) is useful for the diagnosis of uveal malignant melanoma, whereas the feasibility and usefulness of ^{18}F-FDG PET in uveal malignant melanoma have not yet been established. We compared the usefulness of ^{123}I-IMP SPECT and ^{18}F-FDG PET for the detection of uveal malignant melanoma on the same subjects. **Methods:** Nineteen patients (10 men, 9 women) with suspected uveal malignant melanoma were examined by ^{123}I-IMP SPECT. Thirteen of them were also examined by ^{18}F-FDG PET. ^{123}I-IMP SPECT was performed at 15 min or at 3 and 24 h after intravenous administration of ^{123}I-IMP. **Results:** In 12 of 19 study patients, ^{123}I-IMP SPECT obtained at 24 h after intravenous administration of ^{123}I-IMP delineated an area of increased uptake in the site corresponding to the ocular tumor. All of the ocular tumors in the 12 ^{123}I-IMP SPECT–positive patients were confirmed histopathologically and clinically to be uveal malignant melanoma. The other 7 ^{123}I-IMP-SPECT–negative patients have been monitored under the diagnosis of choroidal nevus, choroidal hemangioma, hyperplasia of the pigment epithelium of the retina, or idiopathic inflammatory lesions without any complications. In a total of 13 patients examined by ^{18}F-FDG PET, 9 of whom were ^{123}I-IMP SPECT positive and 4 were negative, only 1 patient showed abnormal uptake of ^{18}F-FDG PET in the site corresponding to the ocular tumor. Therefore, 8 of 9 patients with uveal malignant melanoma showed false-negative results in ^{18}F-FDG PET. The ^{18}F-FDG PET–positive patient with uveal malignant melanoma had the largest tumor mass with a short diameter of 12 mm, a long diameter of 17 mm, and a height of 7 mm. In the other 8 ^{18}F-FDG PET–negative patients, the tumors had a dimension of $11 \times 13 \times 7$ mm or less. **Conclusion:** ^{123}I-IMP SPECT is a sensitive and accurate method for the detection of uveal malignant melanoma, whereas the efficacy of ^{18}F-FDG PET for this purpose is low because of a high incidence of false-negative results. ^{123}I-IMP SPECT is far more superior in comparison with ^{18}F-FDG PET in detecting uveal malignant melanoma.

Key Words: uveal malignant melanoma; ^{123}I-IMP SPECT; ^{18}F-FDG PET

Uveal melanoma, which is the most common primary intraocular malignant neoplasm in adults (1), has been reported to occur in 6–7 cases per million in caucasians (1–3) or 4.3 cases per million in the United States, most of which occurred in the white population (4). In contrast, the annual incidence of uveal melanoma in Japan was 0.25 per million (5).

It was shown that the typical uveal melanoma signal in MRI was found in 69.4% (6). It was also shown that contrast CT could diagnose uveal melanoma in 75% of patients with 2.5- and 3-mm prominence, whereas in the noncontrast CT it was only evident in 34% (7).

A number of earlier reports showed that N-isopropyl-p-^{123}I-iodoamphetamine (^{123}I-IMP) scintigraphy was useful for the detection of primary and metastatic lesions of cutaneous malignant melanoma (8–14). Moreover, ^{123}I-IMP scintigraphy has been shown to be useful also for the detection of uveal malignant melanoma (15–18). These studies, except for 1 study reported in 1988 (15), were the results of imaging using ^{123}I-IMP SPECT (16–18). ^{123}I-IMP is incorporated into melanocytes actively producing melanin.

On the other hand, according to more recent studies, ^{18}F-FDG PET does not seem to be sensitive enough for the diagnosis of uveal malignant melanoma (19–21), despite the fact that it is a sensitive and accurate method for detecting primary and metastatic lesions of cutaneous malignant melanoma (22–28). The reason for this discrepancy in the efficacies of ^{18}F-FDG PET for the detection of cutaneous and uveal malignant melanomas has not yet been elucidated.
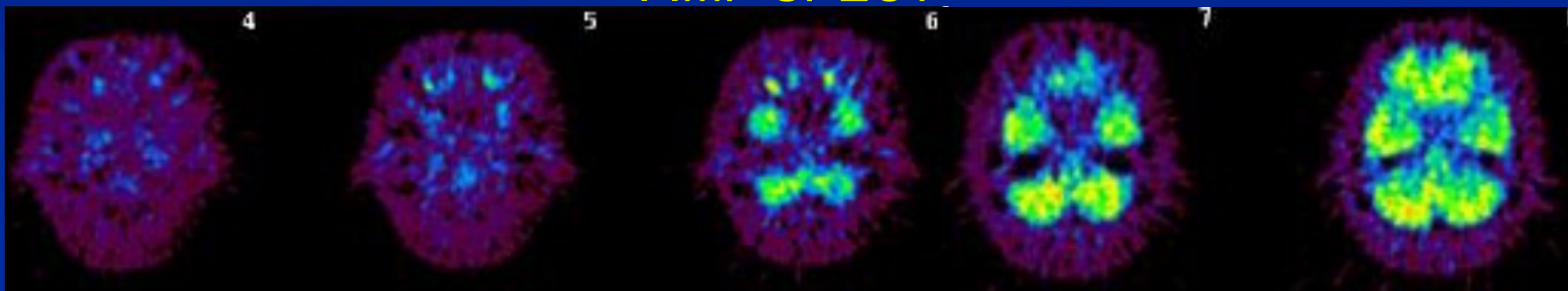
69歳男性 右脈絡膜悪性黒色腫
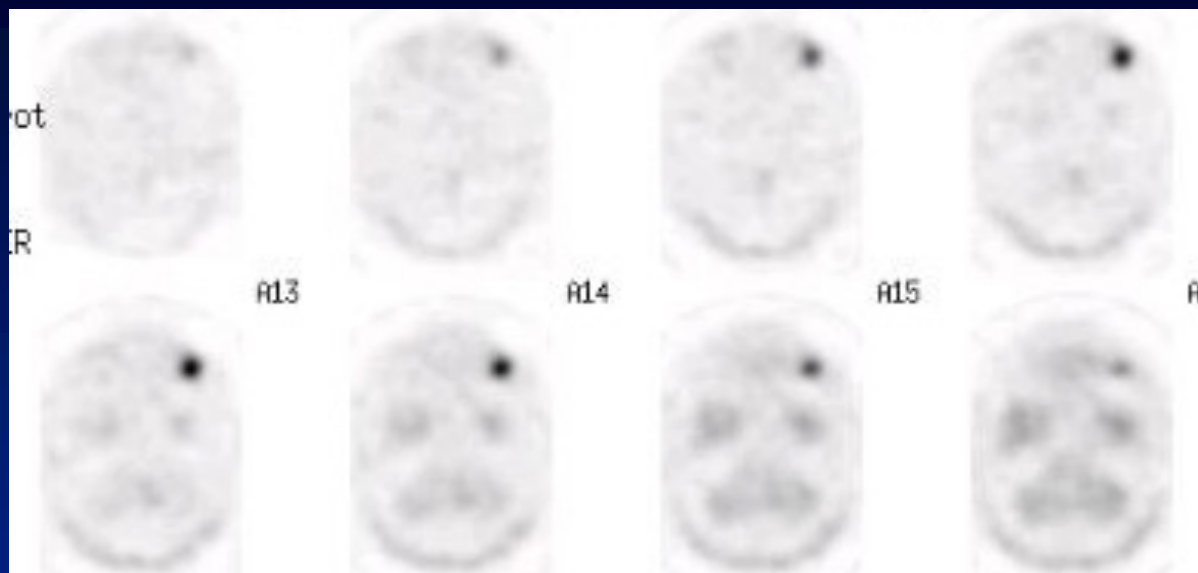

CT

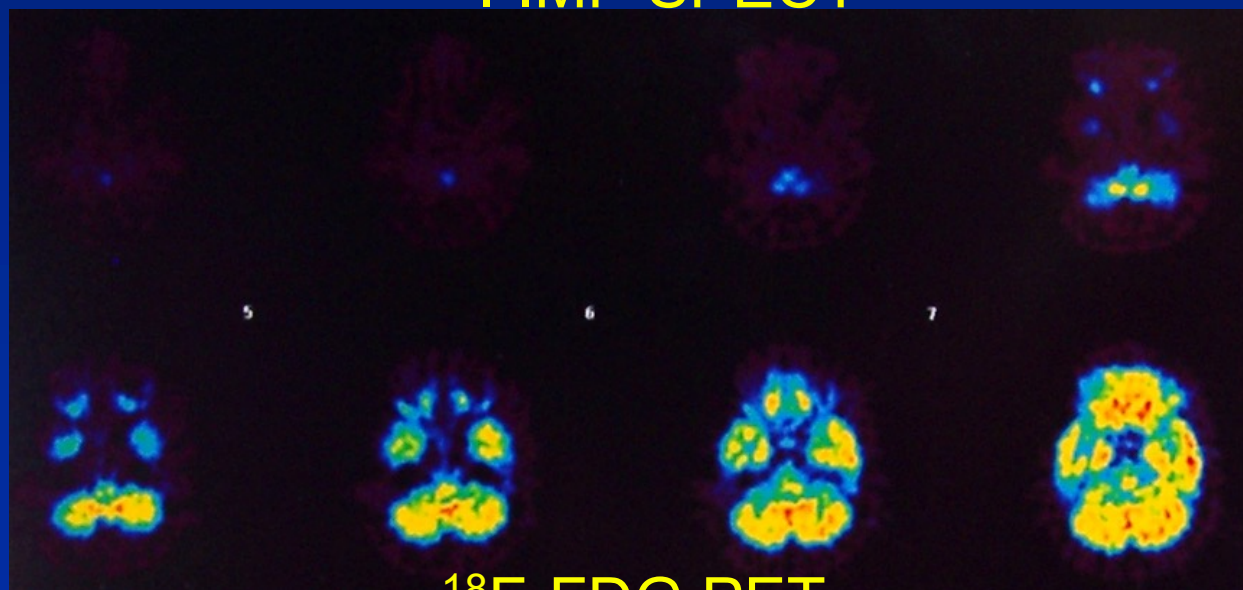MRI T1強調像

T2強調像

¹²³I-IMP SPECT

¹⁸F-FDG PET

70歳男性 右脈絡膜悪性黒色腫

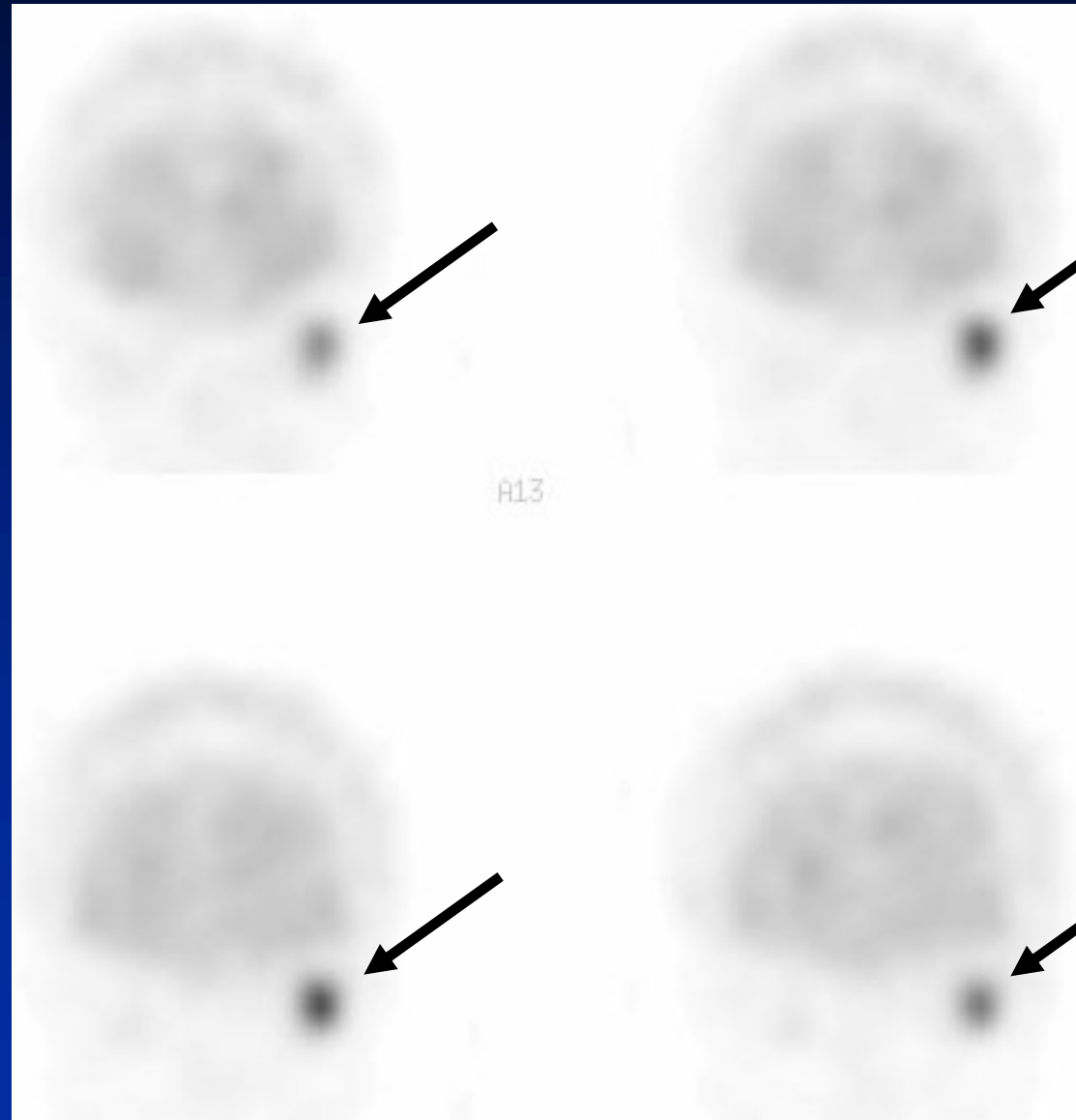^{123}I-IMP SPECT

^{18}F-FDG PET

脈絡膜悪性黒色腫

- 眼腫瘍19症例中悪性黒色腫12症例
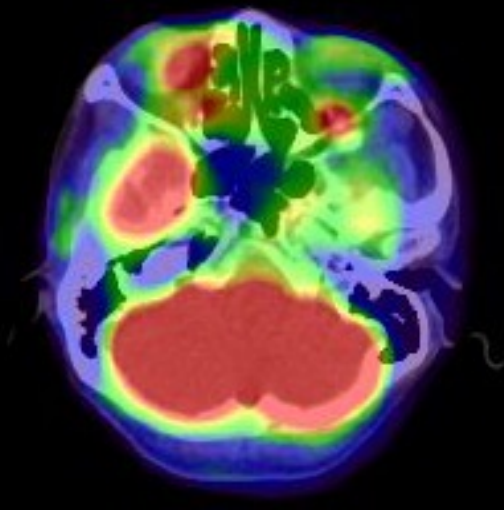12症例 ^{123}I-IMP SPECT陽性、
1例のみ ^{18}F-FDG PET陽性

Kato K, et al. J Nucl Med 2006; 47:404-409

Images of left choroidal melanoma (62-y-old woman)
^{123}I-IMP (N-isopropyl-p-(^{123}I) iodoamphetamine) SPECT

A13

Kato K, et al. J Nucl Med. 2006;47:404-409

^{18}F-FDG PET/CT

^{123}I-IMP SPECT

79 y male with choroidal melanoma (10.0 × 10.0 × 6.5mm)

| ^{123}I-IMP SPECT | CT | ^{18}F- FDG PET | ^{18}F- FDOPA PET |

Kato K, et al. RSNA 2015
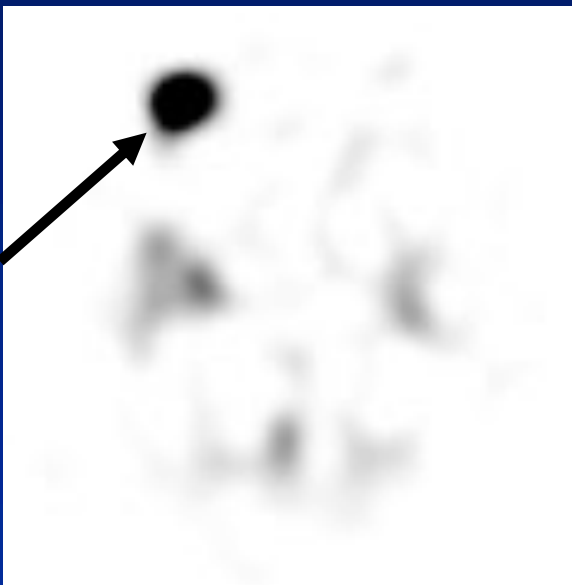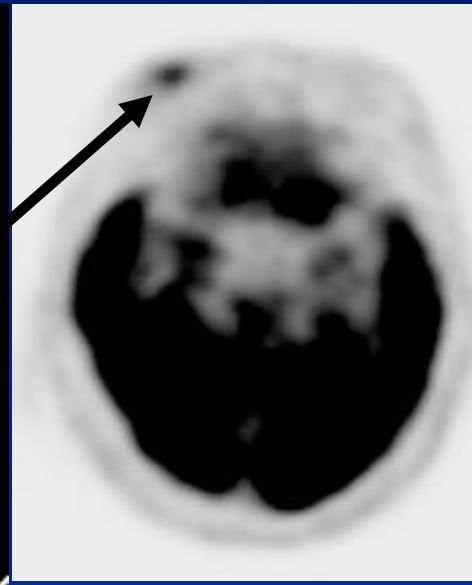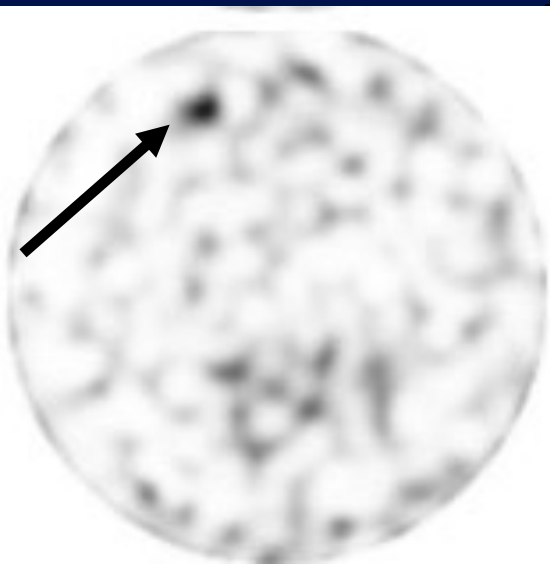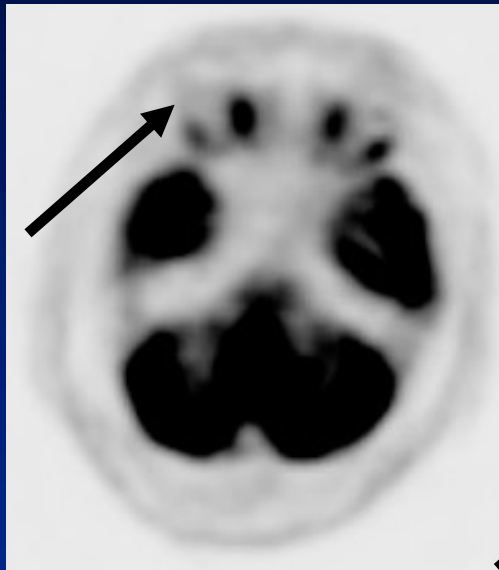
123I-IMP SPECT   CT   18F-FDG PET
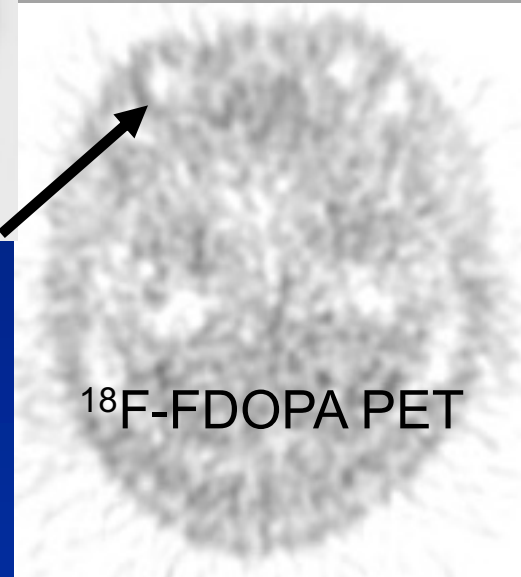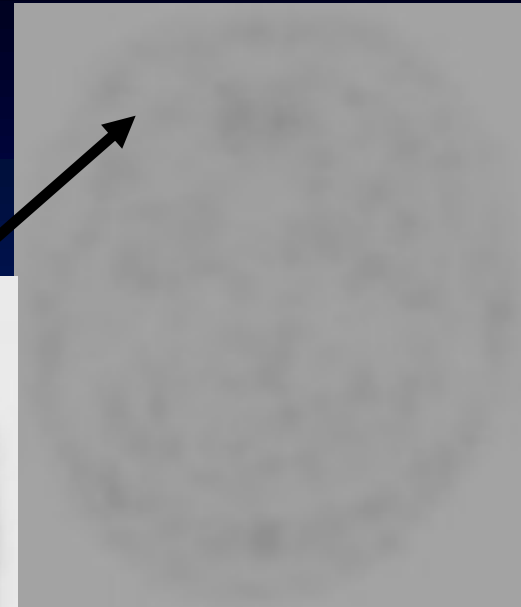
18F-FDOPA PET

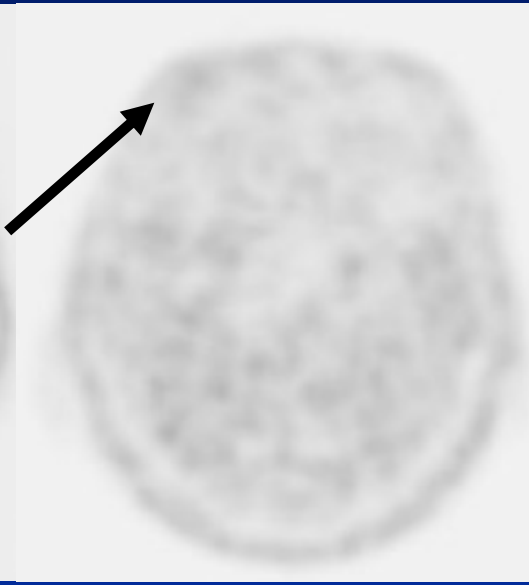Fig. 5. Images of choroidal melanoma
(6.9 × 6.9 × 4.4mm) in Case 5.
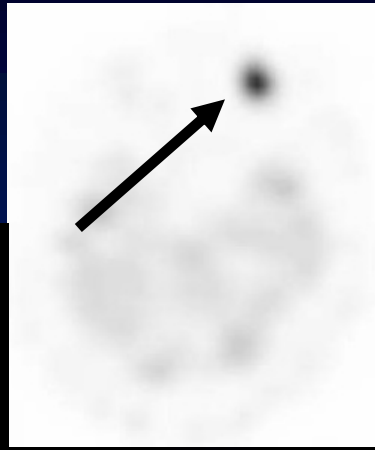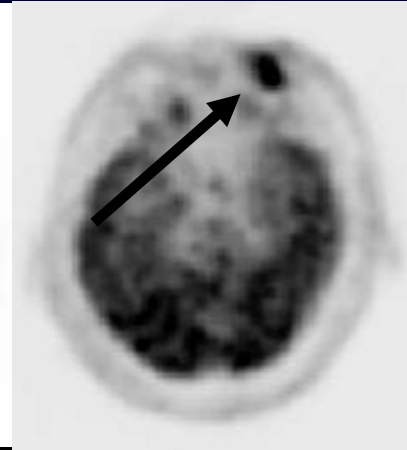
CT ^{123}I-IMP SPECT ^{18}F- FDG PET ^{18}F- FDOPA PET
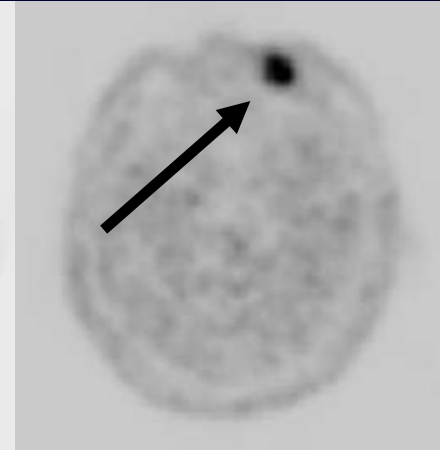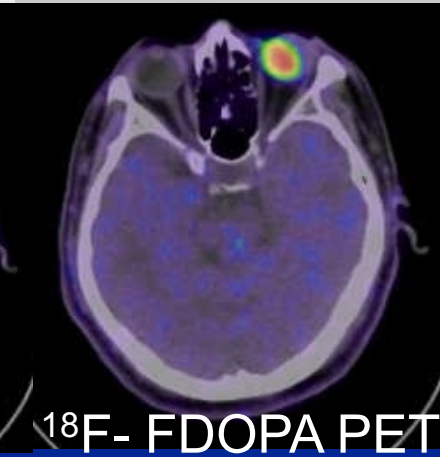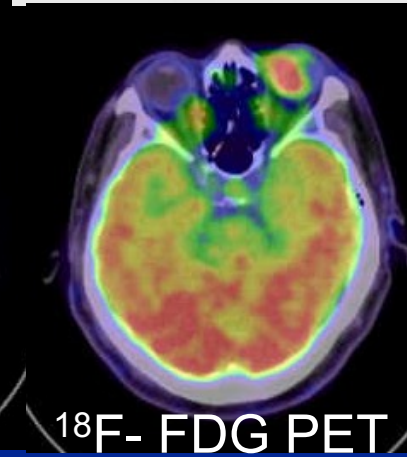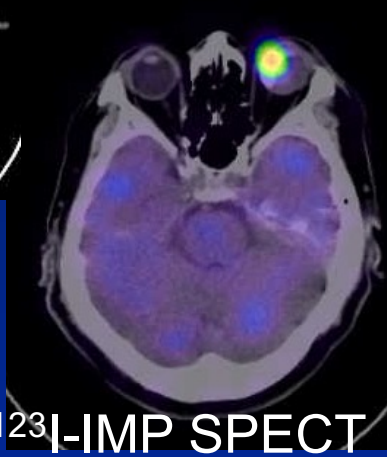
Fig. 6. Images of choroidal malignant melanoma (20 × 19 × 13mm) in Case 38.

Prof. A. schober   Prof. Otmar Schober
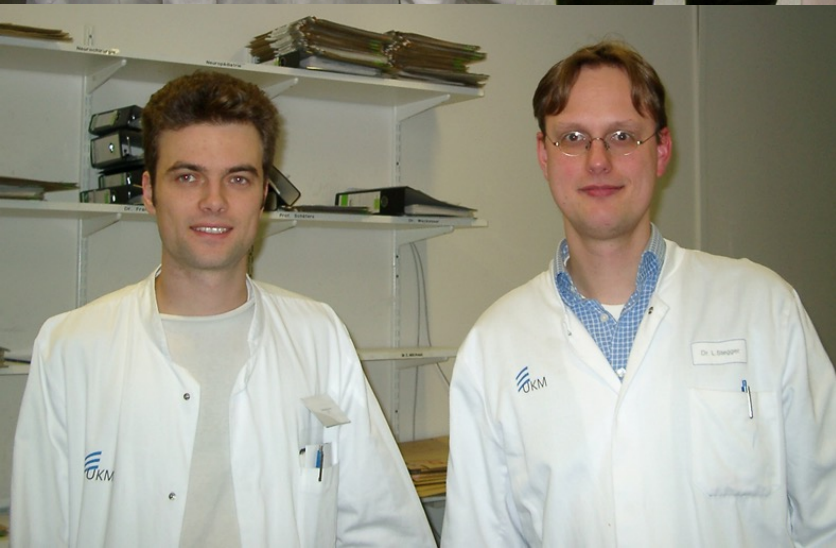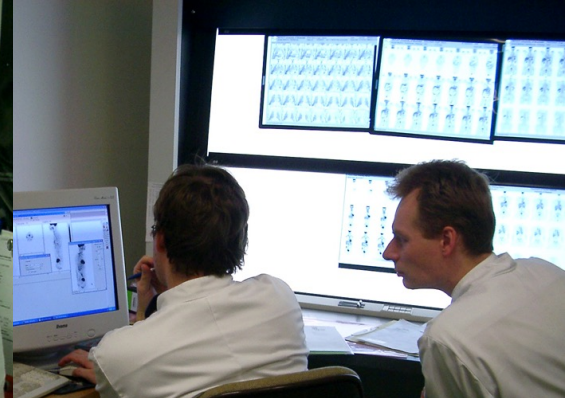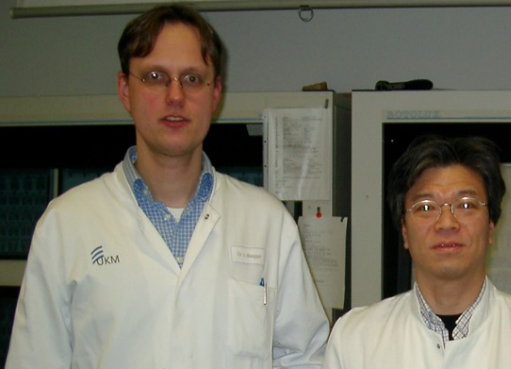
Fig. 2 ^{11}C-choline PET/CT images of the aortic arch of a 69-year-old male patient: (**a**) CT image, (**b**) fused PET/CT image, (**c**) PET image. ^{11}C-choline uptake geographically coincides with calcification (*arrows* calcification site)

Fig. 3 ^{11}C-choline PET/CT images of aortic the arch of a 60-year-old male patient: (**a**) CT image, (**b**) fused PET/CT image, (**c**) PET image. ^{11}C-choline uptake does not coincide with calcification. (*arrows* calcification site)

ORIGINAL ARTICLE

Evaluation and comparison of ^{11}C-choline uptake and calcification in aortic and common carotid arterial walls with combined PET/CT

Katsuhiko Kato · Otmar Schober · Mitsuru Ikeda ·
Michael Schäfers · Takeo Ishigaki · Peter Kies ·
Shinji Naganawa · Lars Stegger

Abstract

Purpose Inflamed atherosclerotic plaques may rupture and cause acute myocardial infarction, stroke and other thrombotic events. Early detection of these unstable plaques could, in many cases, prevent such potentially fatal events. ^{11}C-choline or ^{18}F-labelled choline derivatives for visualizing the synthesis of phospholipids, are promising markers of plaque inflammation with potential advantages over ^{18}F-FDG. Their potential for plaque characterization in humans is, however, unclear. In this study the prevalence and distribution of ^{11}C-choline uptake in the aortic and common carotid arterial walls of elderly male patients was evaluated with combined PET/CT. Additionally, the localization of radiotracer uptake and calcification was correlated in various vessel segments.

Methods Image data from 93 consecutive male patients between 60 and 80 years old who had undergone whole-body ^{11}C-choline PET/CT assessment for prostate cancer were evaluated retrospectively. ^{11}C-choline uptake and calcification were analysed qualitatively and semiquantitatively and compared.

Results ^{11}C-choline uptake was found in 95% of patients, calcification in 94% throughout all vessel segments. In 6% of the patients radiotracer uptake was colocalized with calcifications, whereas less than 1% of calcification sites showed increased radiotracer uptake.

Conclusion Both ^{11}C-choline uptake and calcification in the aortic and common carotid arterial walls are common in elderly men. Radiotracer uptake and calcification are, however, only rarely colocalized. ^{11}C-choline has the potential to provide information about atherosclerotic plaques independent of calcification measurement.

Katsuhiko Kato and Lars Stegger contributed equally to this work.

K. Kato · O. Schober · P. Kies · L. Stegger (✉)
Department of Nuclear Medicine, University of Münster,
Münster, Germany
e-mail: stegger@uni-muenster.de

K. Kato · T. Ishigaki · S. Naganawa
Department of Radiology,
Nagoya University Graduate School of Medicine,
Nagoya, Japan

K. Kato · M. Ikeda
Department of Radiological Technology,
Nagoya University School of Health Sciences,
Nagoya, Japan

M. Schäfers
European Institute of Molecular Imaging, University of Münster,
Münster, Germany

Introduction

Atherosclerotic plaques in coronary, carotid and other arteries can rupture and lead to myocardial infarction, stroke or other thrombotic events. Aggressive risk factor modification and pharmacological treatment with 3-hydroxy-3-methylglutaryl coenzyme A (HMG-CoA) reductase inhibitors ("statins") can stabilize plaques [1].

Several pathophysiological mechanisms such as inflammation, apoptosis and matrix degradation are implicated in plaque formation and rupture and may be imaged by molecular imaging technologies such as positron emission tomography (PET) whereas vessel calcification, a structural

Evaluation of ^{11}C-choline or ^{18}F-FDG Uptake and Arterial Wall Calcifications at PET/CT

Katsuhiko Kato, MD[1]; Lars Stegger, MD[2]; Michael Schäfers, MD[2]; Mitsuru Ikeda, MD[3]; Takeo Ishigaki, MD[1]; Otmar Schober, MD[2]

1) Department of Radiology, Nagoya University Graduate School of Medicine, Nagoya, Japan

2) Department of Nuclear Medicine, Münster University Hospital, Münster, Germany

3) Department of Radiological Technology, Nagoya University School of Health Sciences, Nagoya, Japan

Conclusion

In both ^{11}C-choline uptake and ^{18}F-FDG uptake at PET/CT, the area of uptake disagrees mostly with the area of calcifications of the arterial wall. Rate of ^{18}F-FDG uptake is relatively high as compared with that of ^{11}C-choline uptake. The relationship between the area of ^{11}C-choline or ^{18}F-FDG uptake and the area of atherosclerosis and the following pathological changes has to be determined.

Kato K, et al. Eur J Nucl Med Mol Imaging. 2009;36:1622-1628

加藤研究室

- 博士後期課程学位取得者 阿部真治、堤 貴紀、藤田尚利
- 大学院博士課程（後期課程）

3年 大橋俊夫、田村美香

2年 池田陽菜

博士前期課程学位取得者 末澤正太郎、丹羽亜利紗、藤田佑介、土屋沙貴、小芝有美子、国本啓太、本田将之、松澤伸一郎、椋本竜斗、長谷川千夏、伊藤良典、大野里沙、多田智大、村山里奈、池田陽菜、越智優佳、西尾美穂、浅野有紀

- 大学院博士課程（前期課程）

2年 稲垣拓実

1年 磯邊亮太、長原朋香

学部学生（卒業研究）

4年 稲垣朝也、清瀬裕也、恒川諒太郎、岸川想（休学中）

- 名古屋大学医学部附属病院診療放射線技師　　阿部真治、山下雅人、藤田尚利、西本卓矢、堤 貴紀、櫻木庸博、末澤正太郎、丹羽亜利紗、土屋沙貴、小芝有美子、多田智大、大原千乃、池田陽菜、浅野有紀
- 薬剤合成担当 山口博司、山城 敬一
- 東部医療センター 柴田洋希 、藤田佑介 西部医療センター 伊藤良典

研究テーマ

研究一覧

- ^{18}F-FDG PET/CTにおける肝の^{18}F-FDGの集積の検討：CTとの比較
- 名古屋大学医学部付属病院RI検査室における^{123}I-MIBGを用いた心筋交感神経機能シンチグラフィの心筋／縦隔摂取比の正常値の検討
- ^{123}I-IMP SPECTにおける撮影時間と濃度分解能の検討
- ^{123}I-IMP SPECTにおける空間分解能の検討：腫瘍径について
- ^{123}I-IMP SPECTにおける空間分解能の検討：腫瘍厚について
- ^{18}F-FDG PETおよび^{18}F-FDG PET/CTにおける空間分解能の検討
- ^{123}I-IMPを使用した脳血流SPECT定量解析における新しい非採血法と一点動脈採血法との比較
- ^{18}F-FDG PET/CTの撮影体位によって生ずるアーチファクトが肝臓の集積に与える影響:両腕を上げて撮影した場合と下げて撮影した場合の比較
- 骨シンチグラフィ診断支援ソフトウェアの基本的特性および診断精度の評価
- PET装置の描出能の検討
- ^{123}I-IMP ARG法による脳血流測定法における定量性に影響を与える因子に関する検討
- 骨シンチグラフィ用コンピュータ支援診断ソフトウェアにおけるprefiltering処理の有用性に関する検討
- Pixon法を用いたノイズ低減処理におけるプラナー画像の画質改善機能の評価
- 心臓用多焦点型ファンビームコリメータを用いた心筋SPECTによる至適収集時間の検討

- 脈絡膜悪性黒色腫における^{123}I-IMP SPECT、^{18}F-FDG PET/CT、^{18}F-DOPA PET/CTの診断能の比較
- 皮膚悪性黒色腫における^{123}I-IMP SPECT、^{18}F-FDG PET/CT、^{18}F-DOPA PET/CTの診断能の比較
- センチネルリンパ節シンチの評価
- 頭頸部腫瘍の^{18}F-FDG PET/CTによる化学療法の治療効果判定
- ^{18}F-FDG PET/CTによる頭頸部癌手術マッピング
- 進行性大腸癌に対する治療効果判定におけるPETの有用性
- 多系統萎縮症における脳血流SPECT
- 筋萎縮性側索硬化症における脳血流SPECT
- ^{18}F-FDG PET/CTによる腫瘤形成性膵炎と膵癌の鑑別
- 動脈壁における^{11}C-cholineの集積の検討
- ^{11}C-cholinePET/CTによる尿管癌の検討
- 透析患者の心筋シンチの検討
- CPK患者の心筋シンチの検討
- ^{99m}Tc-sestamibiを用いた拡張型心筋症における心筋障害の評価
- ^{99m}Tc-sestamibiを用いたアドリアマイシンによる心筋障害の検出
- ^{123}I-MIBGを用いた肥大型心筋症における心筋障害の評価

- ^{123}I-MIBGシンチにおけるコリメータによるカウントの変動
- シンチレーションカウンタとガンマカメラによる甲状腺摂取率の比較
- 腫瘍径の違いによるガンマカメラの検出能の研究
- PET検査における診療放射線技師の被曝
- ^{18}F-FLT PET/CTによる悪性腫瘍の評価
- ^{18}F-Na PET/CTによる悪性腫瘍の骨転移の評価
- ^{11}C-ラクロプライドPETの検討
- ^{11}C-フルマゼニールPETの検討
- ^{18}F-DOPA PETにおける心筋の集積の評価
- 腎保存術後の虚血性障害、^{99m}Tc-MAG3による評価
- ^{99m}Tc-MAG3によるcERPFの測定
- 腎癌の^{18}F-FDG PET/CT、嚢胞腎
- てんかんのPET
- ^{11}C-酢酸PETによる悪性腫瘍の評価の検討
- ^{18}F- THK5351 PETタウイメージング（アルツハイマー型認知症等）
- ^{11}C-PBB3 PETタウイメージング
- ^{11}C-PiB PETアミロイドイメージング

- ^{18}F-FMISO PETによる低酸素細胞腫瘍の検出
- ^{18}F-FAZA PETによる低酸素細胞腫瘍の検出
- 甲状腺機能亢進症の^{131}I治療における分割投与についての検討
- ^{131}Iシンチグラフィによる甲状腺摂取率の定量性に関する研究
- バセドウ病の^{131}I内用療法における吸収線量の定量評価
- 分化型甲状腺癌のアブレーション成功率の算出に向けた技術的検討
- 分化型甲状腺癌の^{131}I内用療法後の^{131}I-SPECTの定量評価
- 分化型甲状腺癌の^{131}I内用療法後の^{131}I-SPECTと^{18}F-FDG PETとの比較
- I-131シンチグラフィを用いた甲状腺癌全摘後の転移巣の評価に関する研究
- 異なる解析ソフトにおけるSUV比較に関する研究
- ドパミントランスポータシンチグラフィの視覚評価の正当性に関する研究
- 脳のタウイメージング撮像における視野外からの散乱線の影響
- 多焦点ファンビームコリメータを用いた心筋2核種同時収集法に関する検討
- SPECT/CTを用いた甲状腺重量推定の検討
- Noninvasive estimation of regional cerebral blood flow using ^{123}I-IMP acquisition data: comparison with ^{15}O-water autoradiography method
- （^{123}I-IMPの収集データによる非侵襲性局所脳血流量の測定：^{15}O-water autoradiography法との比較）
- デュアルエナジーを用いた^{111}In・^{131}Iのプラナー収集による深度測定
- SPECT-CT装置を用いた^{131}Iの放射能濃度の推定に関する基礎的検討
- PERCISTを用いた^{18}F-FDG PET/CTによる悪性リンパ腫の治療効果判定の研究
- グラフプロット法を用いた^{123}I-IMP脳血流定量測定法の研究
- SPECT-CT装置を用いた^{123}I-MIBG製剤の定量的心筋集積評価

- Quantitative analysis of ^{123}I-MIBG cardiac scintigraphy using combined SPECT/CT system.
- 肺及び脳からのI-123 IMP収集データを用いる動脈採血中I-123 IMP放射能の簡便な非侵襲的推定法
- A simplified noninvasive method for estimation of I-123 IMP arterial blood activity using I-123 IMP acquisition data from the lungs and brain.
- 心臓用多焦点型ファンビームコリメータの基礎特性の評価
- Evaluation of the basic characteristics of the cardiac focusing-collimators
- ドパミントランスポータシンチグラフィにおける最適収集処理条件の検討
- ^{131}Iシンチグラフィによる甲状腺摂取率に関する研究
- アルゴリズムの異なる解析ソフトにおける心内腔容積の比較
- 空間分解能の異なるPET装置におけるSUVの比較に関する研究
- 異なる解析ソフトにおけるSUV比較に関する研究
- ドパミントランスポーターシンチグラフィの補正による影響に関する研究
- ドパミントランスポータシンチグラフィにおける解析ソフトの有用性に関する研究
- 甲状腺機能亢進症の^{131}I内用療法における吸収線量に関する検討
- SPECT-CT装置を用いた心縦隔比の計測精度向上に関する研究
- PET解析ソフトウェアにおける計測精度に関する検討
- 甲状腺機能亢進症に対するI-131内用療法後の甲状腺へのI-131集積定量と治療効果予測に関する検討
- 脳PET検査における視野外放射能の影響と散乱補正の効果に関する研究
- タウイメージング剤^{18}F-THK-5351の臨床応用に向けた基礎的研究
- 多焦点型ファンビームコリメータを用いた心筋二核種同時収集法における画像コントラストに関する検討

- ^{89}Srによる骨転移疼痛緩和内用療法の治療効果判定：骨SPECTと ^{18}F-fluoride PET/CTによる骨転移巣の定量値の比較
- ^{89}Srによる骨転移疼痛緩和内用療法の治療効果判定：骨SPECT, ^{18}F-fluoride PET/CT, ^{18}F-FDG PET/CTによる骨転移巣のSUV, MBV, TBUの比較
- ^{18}F-fluoride PET/CT画像および18F-FDG PET/CT画像における正常骨と骨転移のカットオフ値決定に向けた検討
- ドパミントランスポータシンチグラフィにおける部分容積効果を考慮した半定量指標算出の検討
- 心サルコイドーシス^{18}F-FDG PET検査における病変部位検出のための至適閾値に関する基礎的検討
- ^{11}C-PiBを用いたPET画像におけるアルツハイマー型認知症の評価方法
- ^{123}I製剤脳血流SPECTの標準化と正常データベースに関する多施設研究
- 甲状腺機能亢進症に対する放射性ヨウ素内用療法における投与放射能決定法の再構築と甲状腺吸収線量を用いる治療効果予測法の確立
- Evaluation of Chronic Thromboembolic Pulmonary Hypertension by Dual-Energy CT in Pulmonary Circulation Phase
- 肺循環相を用いたDual-Energy CTによる慢性血栓塞栓性肺高血圧症の重症度評価
- バセドウ病のアイソトープ治療の効果を高めるためのヨウ素制限の意義
- バセドウ病の放射性ヨウ素治療におけるヨウ素制限と栄養士介在の意義
- Assessment of severity in chronic thromboembolic pulmonary hypertension by quantitative parameters of dual energy computed tomography

業績一覧

- Rintaro Ito, Keita Kato, Kosuke Nanataki, Yumi Abe, Hiroshi Ogawa, Ryogo Minamimoto, Katsuhiko Kato, Toshiaki Taoka, Shinji Naganawa. Assessing large language models for Lugano classification of malignant lymphoma in Japanese FDG-PET reports. EJNMMI Rep. 2025 Mar 10;9(1):8. doi: 10.1186/s41824-025-00246-8.

- Ryogo Minamimoto, Yumi Abe, Shinichiro Kamiya, Toshiki Nakane, Rintaro Ito, Katsuhiko Kato, Shinji Naganawa. Imaging insights of FDG-PET from neonates to infants. Jpn J Radiol. 2025 Mar 5.　doi: 10.1007/s11604-025-01763-z.

- Mai Hatanaka, Kazuhiro Hara, Chisato Ohba, Masashi Suzuki, Aya Ogura, Kazuya Kawabata, Yoshinori Ito, Tomohiro Tada, Naotoshi Fujita, Daisuke Mori, Satoshi Maesawa, Katsuhiko Kato, Masahisa Katsuno. Combined quantitative analysis of the nigro-striata system in multiple system atrophy and Parkinson's disease. J Neurol Sci. 2025 Jan 15:468:123331. doi: 10.1016/j.jns.2024.123331.

- Ryogo Minamimoto, Katsuhiko Kato, Shinji Naganawa. Clinical scenarios of unusual FDG uptake in muscle. Jpn J Radiol. 2025 Feb;43(2):177-185. DOI: 10.1007/s11604-024-01672-7

- Kohei Nakanishi, Naotoshi Fujita, Haruna Iwanaga, Yuki Asano, Shinji Abe, Ryuichi Nishii, Katsuhiko Kato. A Monte Carlo study comparing dead-time losses of a gamma camera between tungsten functional paper and lead sheet for dosimetry in targeted radionuclide therapy with Lu-177. Ann Nucl Med. 2025 Feb;39(2):199-207. doi: 10.1007/s12149-024-01987-5.

- Haruna Iwanaga, Naotoshi Fujita, Shinji Abe, Shinji Naganawa, Katsuhiko Kato. Correlation between the thyroid computed tomography value and thyroid function in hyperthyroidism: a retrospective study. Ann Nucl Med. 2024 Aug;38(8):659-665.　doi: 10.1007/s12149-024-01938-0.

- Eita Uenishi, Yusuke Seino, Akira Nakashima, Katsuhiko Kato, Mitsuhiro Kato, Hiroshi Nagasaki, Kota Ishikawa, Takako Izumoto, Masaaki Yamamoto, Yutaka Takahashi, Yoshihisa Sugimura, Yutaka Oiso, Shin Tsunekawa. A novel mechanism of idiopathic orthostatic hypotension and hypocatecholaminemia due to autoimmunity against aromatic l-Amino acid decarboxylase. Biochem Biophys Res Commun. 2024 Jun 25:714:149940.doi: 10.1016/j.bbrc.2024.149940.

- Kohei Nakanishi, Naotoshi Fujita, Shinji Abe, Ryuichi Nishii, Katsuhiko Kato. A simple method to shorten the apparent dead time in the dosimetry of Lu-177 for targeted radionuclide therapy using a gamma camera. Phys Med. 2024 Feb 2:119:103298. doi: 10.1016/j.ejmp.2024.103298.

- Takashi Mamiya, Yoshio Araki, Toshiaki Taoka, Naotoshi Fujita, Kinya Yokoyama, Kenji Uda, Shinsuke Muraoka, Fumiaki Kanamori, Kai Takayanagi, Kazuki Ishii, Masahiro Nishihori, Takashi Izumi, Katsuhiko Kato, Ryuta Saito. Characteristics of donor vessels and cerebral blood flow in the chronic phase after combined revascularization surgery for moyamoya disease. Clin Neurol Neurosurg. 2023 Dec 30: doi: 10.1016/j.clineuro.2023.108110.

- Yusuke Yoshida, Takamasa Yokoi, Kazuhiro Hara, Hirohisa Watanabe, Hiroshi Yamaguchi, Epifanio Bagarinao, Michihito Masuda, Toshiyasu Kato, Aya Ogura, Reiko Ohdake, Kazuya Kawabata, Masahisa Katsuno, Katsuhiko Kato, Shinji Naganawa, Nobuyuki Okamura, Kazuhiko Yanai, Gen Sobue. Pattern of THK 5351 retention in normal aging involves core regions of resting state networks associated with higher cognitive function. Nagoya J Med Sci. 2023 Nov;85(4):758-771. doi: 10.18999/nagjms.85.4.758.

- Mika Tamura, Kunihiro Nakada, Haruna Ikeda, Naotoshi Fujita, Katsuhiko Kato. Effect of previous administration of potassium iodine and different durations of low iodine diets for radioiodine therapy on the treatment of Graves' disease in iodine-rich areas. Eur J Nucl Med Mol Imaging. 2023 Nov 27. PMID: 38008728. DOI: 10.1007/s00259-023-06523-7

- Tomohiro Tada, Kazuhiro Hara, Naotoshi Fujita, Yoshinori Ito, Hiroshi Yamaguchi, Reiko Ohdake, Kazuya Kawabata, Aya Ogura, Toshiyasu Kato, Takamasa Yokoi, Michihito Masuda, Shinji Abe, Shinichi Miyao, Shinji Naganawa, Masahisa Katsuno, Hirohisa Watanabe, Gen Sobue, Katsuhiko Kato. Comparative examination of the pons and corpus callosum as reference regions for quantitative evaluation in positron emission tomography imaging for Alzheimer's disease using 11C-Pittsburgh Compound-B. Ann Nucl Med. 2023;37(7):410-418. DOI: 10.1007/s12149-023-01843-y.

- Ryota Morimoto, Kazumasa Unno, Naotoshi Fujita, Yasuhiro Sakuragi, Takuya Nishimoto, Masato Yamashita, Tasuku Kuwayama, Hiroaki Hiraiwa, Toru Kondo, Yachiyo Kuwatsuka, Takahiro Okumura, Satoru Ohshima, Hiroshi Takahashi, Masahiko Ando, Hideki Ishii, Katsuhiko Kato, Toyoaki Murohara. Prospective Analysis of Immunosuppressive Therapy in Cardiac Sarcoidosis With Fluorodeoxyglucose Myocardial Accumulation: PRESTIGE Study. JACC Cardiovasc Imaging. 2023 Jun 30;S1936-878X(23)00273-5. DOI: 10.1016/j.jcmg.2023.05.017

- Toshio Ohashi, Shinji Naganawa, Yusuke Nasu, Kayao Kuno, Katsuhiko Kato. Magnetic resonance imaging of endolymphatic hydrops: a comparison of methods with and without gadolinium-based contrast agent administration. Nagoya J Med Sci. 2023 May;85(2):299-309. DOI: 10.18999/nagjms.85.2.299

- Makoto Hattori, Keita Hiraga, Yuki Satake, Takashi Tsuboi, Daigo Tamakoshi, Maki Sato, Katsunori Yokoi, Keisuke Suzuki, Yutaka Arahata, Akihiro Hori, Motoshi Kawashima, Hideaki Shimizu, Hiroshi Matsuda, Katsuhiko Kato, Yukihiko Washimi, Masahisa Katsuno. Clinico-imaging features of subjects at risk of Lewy body disease in NaT-PROBE baseline analysis. NPJ Parkinsons Dis. 2023 Apr 26;9(1):67. doi: 10.1038/s41531-023-00507-y.

- Satoya Yoshida, Kazumasa Unno, Mamoru Nanasato, Takanaga Niimi, Kohei Inukai, Hidenori Morisaki, Tomoki Hattori, Miku Hirose, Takumi Hayashi, Noriya Uchida, Masahiro Simoda, Hideo Oishi, Monami Ando, Kenshi Hirayama, Masaki Takenaka, Mayuho Maeda, Ruka Yoshida, Yasuhiro Ogura, Hirohiko Suzuki, Kenji Furusawa, Ryota Morimoto, Katsuhiko Kato, Satoshi Isobe, Yukihiko Yoshida, Toyoaki Murohara. The potential of dynamic 99mTc-sestamibi cadmium zinc telluride-single-photon emission computed tomography camera assessing myocardial flow reserve in patients with heart failure with preserved ejection fraction. Eur Heart J Open. 2023;3(2):oead028. doi: 10.1093/ehjopen/oead028.

- Katsuhiko Kato, Soichi Nakamura, Hiroyasu Sugano, Seigo Kinuya. A Report on Health Resource Use of Internal Radiation Therapy with 131I-MIBG (2nd Survey). Kaku Igaku. 2023;60(1):13-18. DOI: 10.18893/kakuigaku.tr.2301.

- Yuri Shimizu, Hiroko Satake, Satoko Ishigaki, Kazuhiro Shimamoto, Fuga Uota, Masanori Tadokoro, Tomohiro Sato, Katsuhiko Kato, Tsuneo Ishiguchi, Shinji Naganawa. Physiological background parenchymal uptake of 18F-FDG in normal breast tissues using dedicated breast PET: correlation with mammographic breast composition, menopausal status, and menstrual cycle. Ann Nucl Med.2022;36(8):728-735. doi: 10.1007/s12149-022-01754-4.

- Yoshinori Ito, Naotoshi Fujita, Kazuhiro Hara, Tomohiro Tada, Shinji Abe, Masahisa Katsuno, Shinji Naganawa, Katsuhiko Kato. Novel approach to semi-quantification of tracer accumulation in dopamine transporter scan. J Appl Clin Med Phys. 2022; e13626. doi: 10.1002/acm2.13626.

- Yoshio Araki, Takashi Mamiya, Naotoshi Fujita, Kinya Yokoyama, Kenji Uda, Fumiaki Kanamori, Kai Takayanagi, Kazuki Ishii, Masahiro Nishihori, Kazuhito Takeuchi, Kuniaki Tanahashi, Yuichi Nagata, Yusuke Nishimura, Takafumi Tanei, Shinsuke Muraoka, Takashi Izumi, Katsuhiko Kato, Ryuta Saito. Symptomatic hyperperfusion after combined revascularization surgery in patients with pediatric moyamoya disease: patient series. J Neurosurg Case Lessons 3(19): CASE2274. 2022 DOI: 10.3171/CASE2274

- Yoshinori Tsutsumi, Shiro Adachi, Yoshihisa Nakano, Shingo Iwano, Shinji Abe, Katsuhiko Kato, Shinji Naganawa. End-Systolic Eccentricity Index Obtained by Enhanced Computed Tomography Is a Predictor of Pulmonary Vascular Resistance in Patients with Chronic Thromboembolic Pulmonary Hypertension. Life (Basel). 2022;12(4):593. doi: 10.3390/life12040593.

- Yoshio Araki, Takashi Mamiya, Naotoshi Fujita, Kenji Uda, Kinya Yokoyama, Fumiaki Kanamori, Kai Takayanagi, Kazuki Ishii, Masahiro Nishihori, Kazuhito Takeuch, Kuniaki Tanahashi, Yuichi Nagata, Yusuke Nishimura, Takafumi Tanei, Masaki Sumitomo, Sho Okamoto, Takashi Izumi, Katsuhiko Kato, Ryuta Saito. Changes in cerebral blood flow in the postoperative chronic phase after combined cerebral revascularization for moyamoya disease with ischaemic onset. Neurosurg Rev. 2022 Mar 23. doi: 10.1007/s10143-022-01774-8.PMID: 35319072

- Katsuhiko Kato, Soichi Nakamura, Yoshinori Matoba, Seigo Kinuya. A Report on Health Resource Use in Internal Radiation Therapy Using 177 Lu-DOTA-TATE. Kaku Igaku. 2021;58(1):39-46. doi: 10.18893/kakuigaku.tr.2104.

- Katsuhiko Kato, Soichi Nakamura, Yoshinori Matoba, Seigo Kinuya. A Report on Health Resource Use in Internal Radiation Therapy with 131 I-MIBG. Kaku Igaku. 2021;58(1):33-38. doi: 10.18893/kakuigaku.tr.2103.

- Yoko Satoh, Masami Kawamoto , Kazunori Kubota, Koji Murakami, Makoto Hosono, Michio Senda, Masayuki Sasaki, Toshimitsu Momose, Kengo Ito, Terue Okamura, Keiichi Oda, Yuji Kuge, Minoru Sakurai, Ukihide Tateishi, Yasuhisa Fujibayashi, Yasuhiro Magata, Takeshi Yoshida, Atsuo Waki, Katsuhiko Kato, Teisuke Hashimoto, Mayuki Uchiyama, Seigo Kinuya, Tatsuya Higashi, Yasuhiro Magata, Akihiro Machitori, Hirotaka Maruno, Ryogo Minamimoto, Keiichiro Yoshinaga. Clinical practice guidelines for high-resolution breast PET, 2019 edition. Ann Nucl Med. 2021 Mar;35(3):406-414.2021. doi: 10.1007/s12149-021-01582-y.

- Naotoshi Fujita, Katsuhiko Kato, Shinji Abe, Shinji Naganawa. Variation in thyroid volumes due to differences in the measured length or area of the cross-sectional plane: A validation study of the ellipsoid approximation method using CT images. Journal of Applied Clinical Medical Physics. 2021;22(4):15-25. doi: 10.1002/acm2.13125.

- Yoshinori Tsutsumi, Shingo Iwano, Naoki Okumura, Shiro Adachi, Shinji Abe, Takahisa Kondo, Katsuhiko Kato, Shinji Naganawa. Assessment of Severity in Chronic Thromboembolic Pulmonary Hypertension by Quantitative Parameters of Dual-Energy Computed Tomography. J Comput Assist Tomogr. 2020;44(4):578-585. doi: 10.1097/RCT.0000000000001052.

- Jun Natsume, Naoko Ishihara, Yoshiteru Azuma, Tomohiko Nakata, Tomoya Takeuchi, Masaharu Tanaka, Yoko Sakaguchi, Yu Okai, Yuji Ito, Hiroyuki Yamamoto, Atsuko Ohno, Hiroyuki Kidokoro, Ayako Hattori, Shin Nabatame, Katsuhiko Kato. Lenticular nuclei to thalamic ratio on PET is useful for diagnosis of GLUT1 deficiency syndrome. Brain Dev.2020;S0387-7604(20)30184-4. doi: 10.1016/j.braindev.2020.07.001.

- Shingo Iwano, Shinji Ito, Shinichiro Kamiya, Rintaro Ito, Katsuhiko Kato, Shinji Naganawa. Unexpected radioactive iodine accumulation on whole-body scan after I-131 ablation therapy for differentiated thyroid cancer. Nagoya J Med Sci. 2020 May;82(2):205-215. doi: 10.18999/nagjms.82.2.205.

- Naotoshi Fujita, Yumiko Koshiba, Shinji Abe, Katsuhiko Kato. Investigation of post-therapeutic image-based thyroid dosimetry using quantitative SPECT/CT, iodine biokinetics, and the MIRD's voxel S values in Graves' disease. EJNMMI Phys. 2020 Jan 28;7(1):6. doi: 10.1186/s40658-020-0274-7.
- Seiichi Yamamoto, Katsuhiko Kato, Shinji Abe. Optical imaging of produced light in water during irradiation of gamma photons lower energy than the Cerenkov-light threshold. Appl Radiat Isot. 2020 Mar;157:109037. doi: 10.1016/j.apradiso.2020.109037.

- Shingo Iwano, Shinji Ito, Shinichiro Kamiya, Rintaro Ito, Katsuhiko Kato, Shinji Naganawa. Utility of Metabolic Parameters on FDG PET/CT in the Classification of Early-Stage Lung Adenocarcinoma: Prediction of Pathological Invasive Size. Clin Nucl Med. 2019 Jul;44(7):560-565. doi: 10.1097/RLU.0000000000002591.
- Hiroaki Mori, Satoshi Isobe, Susumu Suzuki, Kazumasa Unno, Ryota Morimoto, Naoaki Kano, Takahiro Okumura, Yoshinari Yasuda, Katsuhiko Kato, Toyoaki Murohara. Prognostic value of left ventricular dyssynchrony evaluated by gated myocardial perfusion imaging in patients with chronic kidney disease and normal perfusion defect scores. J Nucl Cardiol. 2019;26(1):288-297. doi: 10.1007/s12350-017-0889-9.
- Takamasa Yokoi, Hirohisa Watanabe, Hiroshi Yamaguchi, Epifanio Bagarinao, Michihito Masuda, Kazunori Imai, Aya Ogura, Reiko Ohdake , Kazuya Kawabata, Kazuhiro Hara, Yuichi Riku, Shinsuke Ishigaki, Masahisa Katsuno, Shinichi Miyao, Katsuhiko Kato, Shinji Naganawa, Ryuichi Harada, Nobuyuki Okamura, Kazuhiko Yanai, Mari Yoshida, Gen Sobue. Involvement of the Precuneus/Posterior Cingulate Cortex Is Significant for the Development of Alzheimer's Disease: A PET (THK5351, PiB) and Resting fMRI Study. Front Aging Neurosci. 2018 Oct 5;10:304. doi: 10.3389/fnagi.2018.00304.
- Masayuki Inubushi, Mitsuaki Tatsumi, Yuka Yamamoto, Katsuhiko Kato, Tetsuya Tsujikawa, Ryuichi Nishii. European research trends in nuclear medicine. Ann Nucl Med. 2018 Nov;32(9):579-582. doi: 10.1007/s12149-018-1303-7.
- Seiichi Yamamoto, Katsuhiko Kato, Naotoshi Fujita, Masato Yamashita, Takuya Nishimoto, Hiroshi Kameyama, Shinji Abe. Detection of alpha radionuclides in air from patients during Ra-223 alpha radionuclide therapy. Scientific Reports. 2018(8):10976 | DOI:10.1038/s41598-018-29449-9
- Yoko Sakaguchi, Hiroyuki Kidokoro, Chikako Ogawa, Yu Okai, Yuji Ito, Hiroyuki Yamamoto, Atsuko Ohno, Tomohiko Nakata, Takeshi Tsuji, Toshiki Nakane, Hisashi Kawai, Katsuhiko Kato, Shinji Naganawa, Jun Natsume. Longitudinal findings of MRI and PET in West syndrome with subtle focal cortical dysplasia. AJNR Am J Neuroradiol. 2018 Oct;39(10):1932-1937. doi: 10.3174/ajnr. A5772.
- Shinji Ito, Shingo Iwano, Katsuhiko Kato, Shinji Naganawa. Predictive factors for the outcomes of initial I-131 low-dose ablation therapy to Japanese patients with differentiated thyroid cancer. Ann Nucl Med. 2018. 32(6):418-424. doi: 10.1007/s12149-018-1261-0.
- Hiroaki Ishiguchi, Shinji Ito, Katsuhiko Kato, Yusuke Sakurai, Hisashi Kawai, Naotoshi Fujita, Shinji Abe, Atsushi Narita, Nobuhiro Nishio, Hideki Muramatsu, Yoshiyuki Takahashi, Shinji Naganawa. Diagnostic performance of 18F-FDG PET/CT and whole-body diffusion-weighted imaging with background body suppression (DWIBS) in detection of lymph node and bone metastases from pediatric neuroblastoma. Ann Nucl Med. 2018 Jun;32(5):348-362. doi: 10.1007/s12149-018-1254-z. Epub 2018 Apr 17.
- Yoshitaka Inui, Takashi Ichihara, Masaki Uno, Masanobu Ishiguro, Kengo Ito, Katsuhiko Kato, Hajime Sakuma, Hidehiko Okazawa, Hiroshi Toyama. CT-based attenuation correction and resolution compensation for I-123 IMP brain SPECT normal database: a multicenter phantom study. Ann Nucl Med. 2018;32(5):311-318. doi: 10.1007/s12149-018-1248-x.
- Rintaro Ito, Shingo Iwano, Hironori Shimamoto, Hiroyasu Umakoshi, Koji Kawaguchi, Shinji Ito, Katsuhiko Kato, Shinji Naganawa. A comparative analysis of dual-phase dual-energy CT and FDG-PET/CT for the prediction of histopathological invasiveness of non-small cell lung cancer. Eur J Radiol. 2017;95:186-191.

- Takayuki Fukui, Katsuhiko Kato, Toshiki Okasaka, Koji Kawaguchi, Koichi Fukumoto, Shota Nakamura, Shuhei Hakiri, Naoki Ozeki, Kohei Yokoi. Predictors for hilar/intrapulmonary lymph node metastasis in discrete type of clinical N1 non-small cell lung cancer. Gen Thorac Cardiovasc Surg. 2017;65(11):640-645.

- Seigo Kinuya, Katsuhiko Kato, Takeshi Kamioka, Toshiyuki Shimmura, Yoshinori Matoba, Kengo Ito. A Report on Health Resource Use in Internal Radiation Therapy with Radium Chloride (223Ra) (2nd Survey). Kaku Igaku. 2017;54(1):603-621.

- Hidenori Suzuki, Katsuhiko Kato, Masami Nishio, Tsuneo Tamaki, Yasushi Fujimoto, Mariko Hiramatsu, Nobuhiro Hanai, Takeshi Kodaira, Yoshiyuki Itoh, Shinji Naganawa, Michihiko Sone, Yasuhisa Hasegawa. FDG-PET/CT predicts survival and lung metastasis of hypopharyngeal cancer in a multi-institutional retrospective study. Ann Nucl Med. 2017 Aug;31(7):514-520.

- Koichi Fukumoto, Takayuki Fukui, Toshiki Okasaka, Koji Kawaguchi, Shota Nakamura, Shuhei Hakiri, Naoki Ozeki, Tomoshi Sugiyama, Katsuhiko Kato, Kohei Yokoi. The Role of 18F-fluorodeoxyglucose Positron Emission Tomography-Computed Tomography for Predicting Pathologic Response After Induction Therapy for Thymic Epithelial Tumors. World J Surg. 2017 Jul;41(7):1828-1833.

- Hiroaki Mori, Satoshi Isobe, Susumu Suzuki, Kazumasa Unno, Ryota Morimoto, Naoaki Kano, Takahiro Okumura, Yoshinari Yasuda, Katsuhiko Kato, Toyoaki Murohara. Prognostic value of left ventricular dyssynchrony evaluated by gated myocardial perfusion imaging in patients with chronic kidney disease and normal perfusion defect scores. J Nucl Cardiol. 2017 Apr 21. doi: 10.1007/s12350-017-0889-9.

- Naoaki Kano, Takahiro Okumura, Satoshi Isobe, Akinori Sawamura, Naoki Watanabe, Kenji Fukaya, Hiroaki Mori, Ryota Morimoto, Katsuhiko Kato, Yasuko K. Bando, Toyoaki Murohara. Left ventricular phase entropy: Novel prognostic predictor in patients with dilated cardiomyopathy and narrow QRS. J Nucl Cardiol. 2017. Feb 7. doi: 10.1007/s12350-017-0807-1.

- Yusuke Fujita, Shinji Abe, Tetsuro Odagawa, Arisa Niwa, Saki Tsuchiya, Yumiko Koshiba, Naotoshi Fujita, Hidetaka Kono, Seiichi Yamamoto, Katsuhiko Kato. Validity of a Newly Developed Noninvasive Method for Estimating Cerebral Blood Flow Using 123I-IMP Acquisition Data from the Lungs and Brain. Medical Research Archives. 4(6),2016. DOI: http://dx.doi.org/10.18103/mra.v4i6.634

- Seiichi Yamamoto, Tadashi Watabe, Hayato Ikeda, Yasukazu Kanai, Kazuhiro Ichikawa, Motonao Nakao, Katsuhiko Kato, Jun Hatazawa. Development of a PET/OMRI combined system for simultaneous imaging of positron and free radical probes for small animals. Med Phys. 43(10):5676-5684. 2016.

- Katsuhiko Kato. Reply to the letter of Zattoni et al. Radiolabelled choline and FDG PET/CT: two alternatives for the assessment of lymph node metastases in patients with upper urinary tract urothelial carcinoma Reply. Eur J Nucl Med Mol Imaging. 2016;43(3):578-9.

- Seiichi Yamamoto, Hiroshi Watabe, Tadashi Watabe, Hayato Ikeda, Yasukazu Kanai, Yoshimune Ogata, Katsuhiko Kato, Jun Hatazawa, Development of ultrahigh resolution Si-PM-based PET system using 0.32 mm pixel scintillators, Nuclear Inst. and Methods in Physics Research-A. 2016;836, 7–12.

- Seiichi Yamamoto, Mayumi Suzuki, Katsuhiko Kato, Tadashi Watabe, Hayato Ikeda, Yasukazu Kanai, Yoshimune Ogata, Jun Hatazawa, Development of gamma-photon/Cerenkov-light hybrid system for simultaneous imaging of I-131 radionuclide, Nuclear Instruments and Methods in Physics Research Section A830, 444–448, 2016

- Rintaro Ito, Shingo Iwano , Mariko Kishimoto, Shinji Ito, Katsuhiko Kato, Shinji Naganawa. Correlation between FDG-PET/CT findings and solid type non-small cell cancer prognostic factors: are there differences between adenocarcinoma and squamous cell carcinoma? Ann Nucl Med. 2015 Dec;29(10):897-905.

- Seiichi Yamamoto, Satoshi Okumura, Tadashi Watabe, Hayato Ikeda, Yasukazu Kanai, Toshiyuki Toshito, Masataka Komori, Yoshimune Ogata, Katsuhiko Kato, Jun Hatazawa. Development of a prototype Open-close positron emission tomography system. Rev Sci Instrum. 2015;86(8):084301. doi: 10.1063/1.4929329.

- Hirotaka Nakashima, Hiroyuki Umegaki, Taeko Makino, Katsuhiko Kato, Shinji Abe, Yusuke Suzuki, Masahumi Kuzuya. Neuroanatomical correlates of error types on the Clock Drawing Test in Alzheimer's disease patients. Geriatr Gerontol Int. 2016 Jul;16(7):777-84. doi: 10.1111/ggi.12550.

- 藤田尚利,阿部真治、櫻木庸博、西本卓矢、加藤克彦. ドパミントランスポータシンチグラフィにおけるSpecific Binding Ratioの空間分解能依存性に関する解析的検証.核医学技術 2018;38(2):191-198.

- 熊澤智宇,阿部真治,藤田尚利,加藤克彦. ¹²³I-IMP ARG法における画像再構成法および減弱補正法の違いによる脳血流定量値の比較. 核医学技術. 2018; 38(4): 479-486.

- 土屋沙貴、阿部真治,藤田尚利,西本卓矢、櫻木庸博、小芝有美子、米田和夫、加藤克彦. 分化型甲状腺癌のアブレーション効果判定に関する多施設共同研究：アンケート調査とファントム評価.核医学技術 2017;37(3):211-218.

- 藤田尚利,阿部真治,加藤克彦,青木卓,杉本美津夫.ドパミントランスポータシンチグラフィの検査標準化に向けた施設及び装置間差の要因に関する検討. 核医学技術 2016;36(2):177-187.

- 石原加純,阿部真治,藤田尚利,加藤克彦.ドパミントランスポータシンチグラフィにおける最適処理条件の検討. 核医学技術 2016;36(4):516-522.

国際学会発表

EANM'10(Annual congress of the European Association of Nuclear Medicine, 2010/10/9-13, Vienna, Austria.

•Katsuhiko Kato, Shinji Abe, Mitsuru Ikeda, Kazuhiro Shimamoto, Shinji Naganawa.

Comparison of I-123 IMP SPECT, F-18 FDG PET/CT and F-18 Dopa PET/CT in detection of primary and metastatic lesions of cutaneous malignant melanoma

•Shinji Abe, Katsuhiko Kato, Yoshitake Takahashi, Naotoshi Ohta, Shinji Naganawa

Estimation of the arterial blood sample activity using multiple regression analysis (Monte Carlo simulation) with time series of ^{123}I-IMP acquisition data

RSNA2010, Radiological Society of North America, Chicago, IL, United State.

•Katsuhiko Kato, Shinji Abe, Kenichi Tuchiya, Mitsuru Ikeda, Kazuhiro Shimamoto, Shinji Naganawa. Comparison of ^{123}I-IMP SPECT, ^{18}F-FDG PET/CT, and ^{18}F-DOPA PET/CT in detection of primary and metastatic lesions of cutaneous malignant melanoma

Society of Nuclear Medicine 58th Annual Meeting, 6.4-8.2011 San Antonio, Texas, United State.

•Shinji Abe, Katsuhiko Kato, Yoshitake Takahashi, Masato Yamashita, Naotoshi Fujita, Naotoshi Ohta, Shinji Naganawa. Estimation of cerebral blood flow using ^{123}I-IMP acquisition data without any blood sampling.

EANM'11, Annual congress of the European Association of Nuclear Medicine, 2011/10/15-19, Birmingham, UK.

•Shinji Abe, Katsuhiko Kato, Yoshitake Takahashi, Masato Yamashita, Naotoshi Fujita, Naotoshi Ohta, Masanori Tadokoro, Shinji Naganawa[5]

Estimation of regional cerebral blood flow using I-123 IMP without any blood sampling: A new method that can be the substitution of O-15 water PET autoradiography method

•Katsuhiko Kato, Shinji Abe, Naotoshi Ota, Kenichi Tsuchiya, Shotaro Suezawa, Naoto Sassa, Mitsuru Ikeda, Kazuhiro Shimamoto, Shinji Naganawa.

Detection of urinary tract cancer by 11C-choline PET/CT

•Shinji Ito, Shingo Iwano, Katsuhiko Kato, Shinji Naganawa.

Evaluation of I-131 radioiodine therapy for bone metastases of differentiated thyroid carcinoma by F-18 FDG-PET/CT

•Shotato Suezawa, Katsuhiko Kato, Shinji Abe, Masanori Tadokoro.

Estimation of radioactivity at various depths using dual photo peaks of ^{111}In planar imaging

•Naotoshi Ota, Katsuhiko Kato, Shingo Iwano, Shinji Ito, Kenichi Tsuchiya, Yoshiyuki Okochi, Yumiko Okada, Shinji Naganawa

Comparison of ^{18}F-fluoride PET/CT, ^{18}F-FDG PET/CT, and bone scintigraphy in detection of bone metastases of thyroid cancer

•Kenichi Tsuchiya, Katsuhiko Kato, Shingo Iwano, Naotoshi Ota, Shinji Ito, Shinji Naganawa.

Comparison of FLT-PET/CT and FDG-PET/CT in detection of metastases of differentiated thyroid cancer

RSNA2011 (2011/11/26-12/3) Radiological Society of North America, , Chicago, IL, United State.

•Katsuhiko Kato, Shinji Abe, Naoto Sassa, Mitsuru Ikeda, Kazuhiro Shimamoto, Shinji Naganawa.

Detection of urinary tract cancer by ^{11}C-choline PET/CT

16th Workshop of the Japanese-German Radiological Affiliation 5.24-29.2012 Muenster, Germany.
•Katsuhiko Kato
Comparison of ^{123}I-IMP SPECT, ^{18}F-FDG PET/CT, and ^{18}F-FDOPA PET/CT in detection of primary and metastatic lesions of cutaneous malignant melanoma
•M. Tadokoro, T. Kato, S. Shirakawa, K. Kato, K. Ito.
Assessment of the accuracy of 3D-PET/CT the quantitative brain study

EANM'12(Annual congress of the European Association of Nuclear Medicine, 2012/10/27-31, Milan, Italy.
•Shinji Ito, Katsuhiko Kato, Keiji Matsuo, Shingo Iwano, Shinji Naganawa.
Comparison of Met-PET and FDG-PET for renal cell carcinoma.
• Yumiko Okada, Takashi Nihashi, Masazumi Fujii, Yoshiyuki Okochi, Katsuhiko Kato, Yoshio Ando, Masato Yamashita, Satoshi Maesawa, Shigenori Takebayashi, Toshihiko Wakabayashi, Shinji Naganawa.
 Differentiation of newly diagnosed Glioblastoma multiforme and intracranial diffuse large B cell lymphoma using ^{11}C-Methionine and ^{18}F-FDG PET.
• Yoshiyuki Okochi , Takashi Nihashi, Masazumi Fujii, Katsuhiko Kato, Yumiko Okada , Yoshio Ando, Satoshi Maesawa, Shigenori Takebayashi, Toshihiko Wakabayashi, Shinji Naganawa.
Clinical use of 11C-methionine and 18F-FDG PET for germinoma in central nervous system.

RSNA2012, Radiological Society of North America, 2012/11/25-30, Chicago, IL, United State.
•Katsuhiko Kato, Tetsuro Odagawa, Shinji Abe, Mitsuru Ikeda, Kazuhiro Shimamoto, Shinji Naganawa.
 Detection of urinary tract cancer by ^{11}C-choline PET/CT or ^{18}F-FDG PET/CT.
•Katsuhiko Kato, Shinji Ito, Shinji Abe, Tetsuro Odagawa, Mitsuru Ikeda, Kazuhiro Shimamoto, Shinji Naganawa.
Uptake of ^{18}F-FDOPA in the corpus striatum of normal brain in ^{18}F-FDOPA PET
•Shinji Ito, Shingo Iwano, Katsuhiko Kato, Shinji Naganawa.
 F-18 FDG-PET/CT for Evaluation of I-131 Radioiodine Therapy for Bone Metastases of Differentiated Thyroid Carcinoma

EANM'13, Annual congress of the European Association of Nuclear Medicine, 2013/10/19-23, Lyon, France.
•Katsuhiko Kato, Shinji Abe, Tetsuro Odagawa, Yusuke Fujita, Arisa Niwa, Shingo Iwano, Shinji Ito, Mitsuru Ikeda, Shinji Naganawa.
Comparison of ^{18}F-FLT PET/CT and ^{18}F-FDG PET/CT in detection of metastases of differentiated thyroid cancer.
•Katsuhiko Kato, Shinji Abe, Tetsuro Odagawa, Yusuke Fujita, Arisa Niwa, Shinji Naganawa.
 Uptake of ^{18}F-FDOPA in the heart muscle of normal humans in ^{18}F-FDOPA PET.
•Shinji Abe, Katsuhiko Kato, Tetsuro Odagawa, Naotoshi Fujita, Yusuke Fujita, Arisa Niwa, Shinji Naganawa.
Evaluation of I-123 MIBG uptake into the adrenal medulla in I-123 MIBG scintigraphy.
•Yusuke Fujita, Shinji Abe, Hidetaka Kono, Naotoshi Fujita, Tomotaka Kumazawa, Arisa Niwa, Tetsuro Odagawa, Katsuhiko Kato.
A simplified noninvasive method for estimation of I-123 IMP arterial blood activity using I-123 IMP acquisition data from the lungs and brain.
•Arisa Niwa, Hidetaka Kono, Shinji Abe, Naotoshi Fujita, Tomotaka Kumazawa, Yusuke Fujita, Tetsuro Odagawa, Katsuhiko Kato.
Evaluation of the basic characteristics of the cardiac focusing-collimators.
•Shinji Ito, Katsuhiko Kato, Takahito Okuda, Shingo Iwano, Shinji Naganawa.
Evaluation of dual-time-point F-18 FDG-PET scans for diagnosis of cancer of the corpus uteri

Society of Nuclear Medicine and Molecular Imaging 61th Annual Meeting   67-11. 2014, St. Louis, MO, , United State.

•Katsuhiko Kato, Tetsuro Odagawa, Shinji Abe, Arisa Niwa, Yusuke Fujita, Saki Tsuchiya, Seiichi Yamamoto, Shinji Naganawa.
Evaluation and comparison of ^{18}F-fluoride and ^{18}F-FDG uptake and calcification in aortic and common carotid arterial walls with combined PET/CT
•Katsuhiko Kato, Shinji Abe, Tetsuro Odagawa, Arisa Niwa, Yusuke Fujita, Saki Tsuchiya, Seiichi Yamamoto, Shinji Naganawa·
Uptake of ^{18}F-FDOPA in the heart muscle of normal humans in ^{18}F-FDOPA PET

IAEA/RCA Regional Training Basic Course on Improving Cancer Management with Hybrid Nuclear Medicine Imaging, 2014.7.3 , Chiba

•Katsuhiko Kato
Diagnostic PET Imaging with Special Reference to Oncologic PET and ^{18}F-FDG PET

The 15th Asia Oceanian Congress of Radiology 2014.9.24-28 Kobe
•Shinji Ito, Katsuhiko Kato, Masazumi Fujii, Toshihiko Wakabayashi, Shinji Naganawa
Evaluation of C-11 methionine PET for cerebral non-neoplastic lesions in comparison with glioma

EANM'14, Annual congress of the European Association of Nuclear Medicine, 2014/10/18-22, Gothenburg, Sweden.

•Katsuhiko Kato, Tetsuro Odagawa, Shinji Abe, Naotoshi Fujita, Arisa Niwa, Yusuke Fujita, Saki Tsuchiya, Shinji Ito, Shingo Iwano, Mitsuru Ikeda, Shinji Naganawa
Comparison of 24 hours-uptake of ^{131}I in the thyroid gland between before and during radioiodine therapy in Graves' disease
•Katsuhiko Kato, Tetsuro Odagawa, Shinji Abe, Naotoshi Fujita, Arisa Niwa, Yusuke Fujita, Saki Tsuchiya, Shinji Ito, Shinji Naganawa
Evaluation and comparison of ^{18}F-fluoride and ^{18}F-FDG uptake and calcification in aortic and common carotid arterial walls with combined PET/CT
•Shinji Ito, Takashi Nihashi, Katsuhiko Kato, Masazumi Fujii, Toshihiko Wakabayashi, Shinji Naganawa
Comparison of uptake for cerebral non-neoplastic lesion glioma C-11 methionine PET
•Yusuke Fujita, Shinji Abe, Tetsuro Odagawa, Arisa Niwa, Saki Tsuchiya, Naotoshi Fujita, Hidetaka Kono, Kastuhiko Kato
 The validity of the newly developed noninvasive method for estimating cerebral blood flow using ^{123}I-IMP acquisition data from the lungs and brain
• Arisa Niwa, Shinji Abe, Naotoshi Fujita, Hidetaka Kono, Tetsuro Odagawa, Yusuke Fujita, Saki Tsuchiya, Katsuhiko Kato
Investigation of the spatial dependence in the SPECT spatial resolution with cardiac focusing-collimator
• Saki Tsuchiya, Shinji Abe, Naotoshi Fujita, Hidetaka Kono, Arisa Niwa, Yusuke Fujita, Tetsuro Odagawa, Katsuhiko Kato
Basic studies on measurement of ^{131}I activity using SPECT-CT

SPIE Medical Imaging 2015 21-26, February, 2015, Orlando, Florida, United State.

•Arisa Niwa, Shinji Abe, Naotoshi Fujita, Hidetaka Kono, Tetsuro Odagawa, Yusuke Fujita, Saki Tsuchiya, Katsuhiko Kato.
Investigation of optimal acquisition time of myocardial perfusion scintigraphy using cardiac focusing-collimator

Japan-China Nuclear Medicine Joint Symposium in Okinawa March 14 15, 2015, Okinawa, Japan

•Katsuhiko Kato, Tetsuro Odagawa, Shinji Abe, Naotoshi Fujita, Arisa Niwa, Yusuke Fujita, Saki Tsuchiya, Seiich Yamamoto, Shinji Naganawa
Evaluation and comparison of ^{18}F-fluoride and ^{18}F-FDG uptake and calcification in aortic and common carotid arterial walls with combined PET/CT.

Society of Nuclear Medicine and Molecular Imaging 62th Annual Meeting, 2015, 6.6-10. Baltimore, MD, United State.

•Katsuhiko Kato, Toshinobu Kubota, Shinji Abe, Saki Tsuchiya, Yumiko Koshiba, Hiroko Terasaki, Shinji Naganawa

Comparison of ^{123}I-IMP SPECT, ^{18}F-FDG PET, and ^{18}F-FDOPA PET in Detection of Choroidal Malignant Melanoma

• Yumiko Koshiba, Shinji Abe, Saki Tsuchiya, Naotoshi Fujita, Tetsuro Odagawa, Katsuhiko Kato

Studies on measurement of thyroid uptake rate on 131I scintigraphy images

•

EANM'15 Annual congress of the European Association of Nuclear Medicine, 2015/10/10-14, Hamburg, Germany.

• Katsuhiko Kato, Saki Tsuchiya, Yumiko Koshiba,Tetsuro Odagawa, Shinji Abe, Toshinobu Kubota, Hiroko Terasaki, Shinji Naganawa.

Comparison of ^{123}I-IMP SPECT, ^{18}F-FDG PET, and ^{18}F-FDOPA PET in Detection of Choroidal Malignant Melanoma.

•Saki Tsuchiya, Shinji Abe, Naotoshi Fujita, Yumiko Koshiba, Tetsuro Odagawa, Katsuhiko Kato.

Comparative study on recovery coefficients of SPECT-CT.

• Yumiko Koshiba, Shinji Abe, Saki Tsuchiya, Naotoshi Fujita, Tetsuro Odagawa, Katsuhiko Kato.

Studies on measurement of thyroid uptake rate on ^{131}I scintigraphy images.

•Shinji Ito, Shingo Iwano, Katsuhiko Kato, Shinji Naganawa.

Predictive factors for the outcome of I-131 1110MBq ablation therapy in the patients with differentiated thyroid cancer: urinary iodine, serum thyroglobulin, and uptake to thyroid bed.

• Hiroaki Ishiguchi, Shinji Ito, Katsuhiko Kato, Yusuke Sakurai, Hisashi Kawai, Asahito Hama, Hideki Muramatsu, Yoshiyuki Takahashi, Seiji Kojima, Shinji Naganawa.

Comparison between FDG-PET and DWIBS in diagnosing neuroblastoma of child

•

RSNA2015 Radiological Society of North America, 2015/11/29-12/4, Chicago, IL, United State.

•Katsuhiko Kato, Toshinobu Kubota, Shinji Abe, Saki Tsuchiya, Yumiko Koshiba, Hiroko Terasaki, Shinji Naganawa.

Comparison of ^{123}I-IMP SPECT, ^{18}F-FDG PET, and ^{18}F-FDOPA PET in Detection of Choroidal Malignant Melanoma.

2nd Asian Nuclear Medicine Academic Forum, May 6-7, 2016, Shanghai, China

•Katsuhiko Kato, Saki Tsuchiya, Yumiko Koshiba,Tetsuro Odagawa, Shinji Abe, Toshinobu Kubota, Hiroko Terasaki, Shinji Naganawa.

Comparison of ^{123}I-IMP SPECT, ^{18}F-FDG PET/CT, and ^{18}F-FDOPA PET/CT in Detection of Choroidal Malignant Melanoma.

•

18th Workshop of the Japanese-German Radiological Affiliation. June. 2-6, 2016, Munich, Germany

•Katsuhiko Kato

Comparison of ^{123}I-IMP SPECT, ^{18}F-FDG PET, and ^{18}F-FDOPA PET in Detection of Choroidal Malignant Melanoma.

Society of Nuclear Medicine and Molecular Imaging 63th Annual Meeting   6.11-15. 2016, San Diego, CA, United State.

•Katsuhiko Kato, Yumiko Koshiba, Shinji Abe, Saki Tsuchiya, Masayuki Honda, Keita Kunimoto, Teturo Odagawa, Seiichi Yamamoto, Shinji Naganawa.

Detection of urinary tract tumors by ^{18}F-FLT PET/CT.

• Yumiko Koshiba, Shinji Abe, Naotoshi Fujita, Takuya Nishimoto, Yasuhiro Sakuragi, Tetsuro Odagawa, Katsuhiko Kato

Studies on Fractionated Administration of Radioiodine-131 in Therapy for Hyperthyroidism

• Keita Kunimoto, Shinji Abe, Naotoshi Fujita, Yasuhiro Sakuragi, Tetsuro Odagawa, Yumiko Koshiba, Katsuhiko Kato

Studies on simultaneous myocardial imaging with dual radionuclides (^{123}I and ^{201}Tl) using cardiac focusing collimator.

• Masayuki Honda, Hiroshi Yamaguchi, Yasuhiro Sakuragi, Shinji Abe, Naotoshi Fujita, Yumiko Koshiba, Katsuhiko Kato

Studies on the Effect of Scattered Radiation Out of Field of View on Tau Imaging

EANM'16, Annual congress of the European Association of Nuclear Medicine, 2016/10/15-19, Barcelona, Spain.

•Katsuhiko Kato, Yumiko Koshiba, Shinji Abe, Saki Tsuchiya, Masayuki Honda, Keita Kunimoto, Teturo Odagawa, Seiichi Yamamoto, Shinji Naganawa.

Detection of primary and metastatic lesions of urinary tract tumors by ^{18}F-FLT PET/CT.

• Atsushi Murai, Katsuhiko Kato, Shingo Iwano, Shinji Ito, Shinji Naganawa.

Comparison of FLT-PET/CT and FDG-PET/CT in detection of metastases of differentiated thyroid cancer

•Yumiko Koshiba, Shinji Abe, Naotoshi Fujita, Takuya Nishimoto, Yasuhiro Sakuragi, Keita Kunimoto, Masayuki Honda , Tetsuro Odagawa, Katsuhiko Kato.

Dosimetry of absorbed doses of Radioiodine-131 in Therapy for Hyperthyroidism.

• Masayuki Honda, Yasuhiro Sakuragi, Shinji Abe, Naotoshi Fujita, Hiroshi Yamaguchi, Yumiko Koshiba, Katsuhiko Kato.

Studies on the Effect of Scattered Radiation Out of Field of View on Tau Imaging

•Keita Kunimoto , Shinji Abe, Naotoshi Fujita, Yasuhiro Sakuragi, Tetsuro Odagawa, Yumiko Koshiba, Masayuki Honda, Katsuhiko Kato.

Studies on simultaneous myocardial imaging with ^{123}I and ^{201}Tl dual radionuclides using cardiac focusing collimator.

•

RSNA2016, Radiological Society of North America, 2016/11/26-12/2, Chicago, IL, United State.

•Katsuhiko Kato, Yumiko Koshiba, Shinji Abe, Masayuki Honda, Keita Kunimoto, Teturo Odagawa, Atsushi Murai, Shinji Naganawa.

 Detection of Primary and Metastatic Lesions of Urinary Tract Tumors by ^{18}F-FLT PET/CT

Society of Nuclear Medicine and Molecular Imaging 64th Annual Meeting   6.10-14. 2017, Denver, Colorado, USA

• Katsuhiko Kato, Shinji Abe, Masayuki Honda, Keita Kunimoto, Shinichiro Matsuzawa, Ryuto Mukumoto, Teturo Odagawa, Seiichi Yamamoto, Shinji Naganawa.

Comparison of accumulation of ^{18}F-FLT PET/CT with histopathological findings of primary and metastatic lesions of urinary tract tumors

• Ryuto Mukumoto, Shinji Abe, Keita Kunimoto, Masayuki Honda, Tetsuro Odagawa, Katsuhiko Kato.

Studies on the precision improvement of the heart-to-mediastinum ratio measurement by using SPECT-CT

• Shinichiro Matsuzawa, Shinji Abe,Masayuki Honda, Keita Kunimoto, TetsuroOdagawa, KatsuhikoKato.

Studies on the measurement accuracy of analyzing software for PET/CT

EANM'17 Annual congress of the European Association of Nuclear Medicine, 2017/10/21-25, Vienna, Austria.

•Katsuhiko Kato, Toshinobu Kubota, Shinji Abe, Naotoshi Fujita, Teturo Odagawa, Masayuki Honda, Keita Kunimoto, Shinichiro Matsuzawa, Ryuto Mukumoto, Hiroko Terasaki, Shinji Naganawa.

Comparison of ^{123}I-IMP SPECT, ^{18}F-FDG PET, and ^{18}F-FDOPA PET in Detection of Choroidal Malignant Melanoma

• Masayuki Honda, Yasuhiro Sakuragi, Shinji Abe, Naotoshi Fujita, Tetsuro Odagawa, Keita Kunimoto, Katsuhiko Kato.

Studies on Scattered Radiation out of Field of View and Effect of Scatter Correction in 3D brain PET

• Keita Kunimoto, Shinji Abe、Naotoshi Fujita, Tetsuro Odagawa、Masayuki Honda、Shinichiro Matsuzawa, Ryuto Mukumoto、Katsuhiko Kato.

Studies on the crosstalk rate in simultaneous myocardial imaging with dual radionuclides using cardiac focusing collimator

• Shinichiro Matsuzawa, Shinji Abe , Yasuhiro Sakuragi, Naotoshi Fujita, Masayuki Honda, Tetsuro Odagawa, Katsuhiko Kato.

The measurement accuracy of analyzing software for PET/CT

RSNA2017 Radiological Society of North America, 2017/11/25-12/1, Chicago, IL, United State.

•Katsuhiko Kato, Toshinobu Kubota, Shinji Abe, Naotoshi Fujita, Teturo Odagawa, Shinji Ito, Shingo Iwano, Hiroko Terasaki, Shinji Naganawa.

Comparison of ^{123}I-IMP SPECT, ^{18}F-FDG PET/CT, and ^{18}F-FDOPA PET/CT in Detection of Choroidal Malignant Melanoma

12th Congress of The World Federation of Nuclear Medicine And Biology, 2018/4/20-24 Melbourne, Australia

•Ryuto Mukumoto, Tetsuro Odagawa, Naotoshi Fujita, Shinichiro Matsuzawa, Chinatsu Hasegawa, Shinji Abe, Katsuhiko Kato

Studies on the precision improvement of the heart-to-mediastinum ratio measurement by using SPECT-CT data extracted for the myocardium and mediastinum

19th Workshop of the German-Japanese Radiological Affiliation, 2018/5/24-28. Okayama.

• Katsuhiko Kato, Shinji Naganawa.

Detection of Primary and Metastatic Lesions of Urinary Tract Tumors by ^{18}F-FLT PET/CT

Society of Nuclear Medicine & Molecular Imaging 2018 Annual Meeting 2018/6/23-26 Philadelphia, Pennsylvania, United States.

•Katsuhiko Kato, Tetsuro Odagawa, Naotoshi Fujit, Yoshihiro Tsutsumi, Shinichiro Matsuzawa, Ryuto Mukumoto, chinatsu Hasegawa, Shinji Abe, Shinji Naganawa.

Evaluation of the tumoricidal and pain relief effects of ^{89}Sr on bone metastases of cancer by ^{18}F-fluoride PET/CT, ^{18}F-FDG PET/CT, bone scintigraphy/SPECT, and follow-up.

•Ryuto Mukumoto, Tetsuro Odagawa, Naotoshi Fujita, Shinichiro Matsuzawa, Chinatsu Hasegawa, Shinji Abe, Katsuhiko Kato

Influence of scatter correction on measurement of the heart-to-mediastinum ratio by SPECT-CT

•Shinichiro Matsuzawa, Shinji Abe, Ryuto Mukumoto, Chinatsu Hasegawa , Tetsuro Odagawa, Katsuhiko Kato

Studies on variation of the standardized uptake value and metabolic tumor volume in analysis software for PET/CT using digital phantoms

•Chinatsu Hasegawa, Naotoshi Fujita, Matsuzawa Shinichiro, Ryuto Mukumoto, Shinji Abe, Katsuhiko Kato

Radioactivity concentration dependence of BCF used in quantitative analysis of bone scintigraphy

Annual Congress of the European Association of Nuclear Medicine 2018/10/13-17, Dusseldorf, Germany.

•Shinichiro Matsuzawa, Shinji Abe, Ryuto Mukumoto, Chinatsu Hasegawa, Tetsuro Odagawa, Katsuhiko Kato

Variation of the indices in analysis software for PET/CT using digital phantoms

•Chinatsu Hasegawa, Naotoshi Fujita, Shinichiro Matsuzawa, Ryuto Mukumoto, Shinji Abe, Katsuhiko Kato

Measurement accuracy of BCF used in quantitative analysis of bone scintigraphy

•Shinji Ito, Shingo Iwano, Katsuhiko Kato, and Shinji Naganawa

Prediction of recurrence using volume-based metabolic index obtained by preoperative FDG-PET for non-small-cell lung cancer

European Conference of Radiology (ECR), 2019/2/27-3/3, Vienna, Austria.

•Yoshinori Tsutsumi, Shingo Iwano, Naoki Okumura, Shiro Adachi, Shinji Abe, Takahisa Kondo, Shinji Naganawa, Katsuhiko Kato

Assessment of severity in chronic thromboembolic pulmonary hypertension by quantitative parameters of dual-energy CT

Society of Nuclear Medicine & Molecular Imaging 2019 Annual Meeting, 2019/6/22-25 Anaheim, California, United States.

•Katsuhiko Kato, Tetsuro Odagawa, Naotoshi Fujita, Yoshinori Tsutsumi, Shinji Abe, Shinji Naganawa.

Evaluation of ^{223}Ra therapy on bone metastases of prostate cancer by ^{18}F-fluoride PET/CT, ^{18}F-FDG PET/CT and bone scintigraphy/SPECT

•Mika Tamura, Kunihiro Nakada, Tsunenori Mizukoshi, Katsuhiko Kato, Naoya Hattori, Noriyoshi Kato, Masayuki Sakurai.

Potassium iodide therapy may not impair efficacy of radioiodine therapy for Graves' hyperthyroidism if discontinued 2 weeks before administration of I-131

•Chinatsu Hasegawa, Naotoshi Fujita, Yoshinori Ito, Risa Ono, Tomohiro Tada, Rina Murayama, Yoshinori Tsutsumi, Tetsuro Odagawa, Mika Tamura, Shinji Abe, Katsuhiko Kato.

Evaluation of radionuclide therapy for the palliation of bone metastasis pain using ^{89}Sr: comparison of SUV values of bone metastases measured by ^{99m}Tc bone SPECT, ^{18}F-fluoride PET/CT, ^{18}F-FDG PET/CT.

•Tomohiro Tada, Naotoshi Fujita, Chinatsu Hasegawa, Yoshinori Ito, Risa Ono, Tomohiro Tada, Rina Murayama, Yoshinori Tsutsumi, Mika Tamura, Tetsuro Odagawa, Hiroshi Yamaguchi, Shinji Abe, Katsuhiko Kato.

Comparative examination of the cerebellum and pons as reference regions for quantitative evaluation in PET imaging for Alzheimer's disease using ^{11}C-Pittsburgh Compound-B

• Rina Murayama, Ryota Morimoto, Naotoshi Fujita, Chinatsu Hasegawa, Yoshinori Ito, Risa Ono, Tomohiro Tada, Yoshinori Tsutsumi, Mika Tamura, Tetsuro Odagawa, Shinji Abe, Katsuhiko Kato.

Optimal threshold for detection of the lesion site in ^{18}F-FDG PET studies on cardiac sarcoidosis.

32nd Annual Congress of the European Association of Nuclear Medicine, 2019/10/12-16 Barcelona, Spain.

- Risa Ono, Naotoshi Fujita, Chinatsu Hasegawa, Yoshinori Ito, Tomohiro Tada, Rina Murayama, Yoshinori Tsutsumi, Tetsuro Odagawa, Mika Tamura, Shinji Abe, Katsuhiko Kato.

Studies On Decision Of The Cut-off Standardized Uptake Values For Normal Bones In ^{18}F-fluoride PET/CT And ^{18}F-FDG PET/CT.

Society of Nuclear Medicine and Molecular Imaging 2020 Annual Meeting, 2020/6/11-14 New Orleans, Louisiana, United States.

- Yoshinori Ito, Naotoshi Fujita, Risa Ono, Tomohiro Tada, Rina Murayama, Haruna Ikeda, Yuka Ochi, Miho Nishio, Yoshinori Tsutsumi, Tetsuro Odagawa, Mika Tamura, Shinji Abe, Katsuhiko Kato.

Studies on Calculation of the Specific Binding Ratio with the Minimum Partial Volume Effect for the Caudate and Putamen by Generating the Analogy Image to the Image Obtained by SPECT Imaging.

- Tomohiro Tada, Naotoshi Fujita, Yoshinori Ito, Risa Ono, Rina Murayama, Haruna Ikeda, Yuka Ochi, Miho Nishio, Tetsuro Odagawa, Mika Tamura, Hiroshi Yamaguchi, Shinji Abe, Katsuhiko Kato.

Comparative study of various reference regions for standardized uptake value ratio using ^{11}C-Pittsburgh Compound-B PET and MR images.

- Haruna Ikeda, Naotoshi Fujita, Tomohiro Tada, Yoshinori Ito, Risa Ono, Rina Murayama, Miho Nishio, Yuka Ochi, Tetsuro Odagawa, Mika Tamura, Yoshinori Tsutsumi, Shinji Abe, Katsuhiko Kato.

Correlation between thyroid computed tomography density and thyroid function in hyperthyroidism.

- Yuka Ochi, Yoshinori Tsutsumi, Naotoshi Fujita, Takahisa Kondo, Shiro Adachi, Yoshinori Ito, Risa Ono, Tomohiro Tada, Rina Murayama, Haruna Ikeda, Miho Nishio, Mika Tamura, Tetsuro Odagawa, Shinji Abe, Katsuhiko Kato.

Comparison of pulmonary perfusion index using ^{99m}Tc-MAA SPECT and evaluation indices obtained from right-sided heart catheterization in chronic thromboembolic pulmonary hypertension.

33rd Annual Congress of the European Association of Nuclear Medicine, 2020/10/22-30, Vienna, Austria.

- Risa Ono, Naotoshi Fujita, Yoshinori Ito, Tomohiro Tada, Rina Murayama, Haruna Ikeda, Yuka Ochi, Miho Nishio, Yoshinori Tsutsumi, Tetsuro Odagawa, Mika Tamura, Shinji Abe, Katsuhiko Kato.

Studies on Decision of the Cut-off Standardized Uptake Values for Normal Bones and Bone Metastases in the Vertebrae in ^{18}F-fluoride PET/CT and 18F-FDG PET/CT.

- Rina Murayama, Ryota Morimoto, Naotoshi Fujita, Yoshinori Ito, Risa Ono, Tomohiro Tada, Haruna Ikeda, Yuka Ochi, Miho Nishio, Yoshinori Tsutsumi, Mika Tamura, Tetsuro Odagawa, Shinji Abe, Katsuhiko Kato.

Comparison of quantitative assessment for cardiac sarcoidosis inflammation site using 18F-FDG PET / CT images.

Society of Nuclear Medicine and Molecular Imaging 2021 Annual Meeting, 2021/6/11-15, Virtual Annual Meeting.

- Haruna Ikeda, Miho Nishio, Yuka Ochi, Mika Tamura, Katsuhiko Kato. Predictive Factors of the Therapeutic Effect of I-131 Therapy for Hyperthyroidism. (International Best Abstract Award Winners)

34th Annual Congress of the European Association of Nuclear Medicine, 2021/20−23, Virtual Annual Meeting.

- Haruna Ikeda, Naotoshi Fujita, Miho Nishio, Yuka Ochi, Yuki Asano, Shinji Abe, Katsuhiko Kato. Dosimetry prior to I-131 therapy in hyperthyroidism using thyroid computed tomography value.
- Yuka Ochi, Yoshinori Tsutsumi, Naotoshi Fujita, Haruna Ikeda, Miho Nishio, Yuki Asano, Shinji Abe, Katsuhiko Kato. Comparison of Low Pulmonary Perfusion Index Using ^{99m}Tc-MAA SPECT Images and Hemodynamic Indices in Chronic Thromboembolic Pulmonary Hypertension.
- Miho Nishio, Naotoshi Fujita, Haruna ikeda, Yuka Ochi, Shinuji Abe , Hiroshi Yamaguchi, Katsuhiko Kato. Basic study of imaging acquisition condition in somatostatin receptor scintigraphy with phantom.

Radiological Society of North America 107th Annual Meeting, 2021/11/28-12/2, Chicago, IL, United State.

- Haruna Ikeda, Naotoshi Fujita, Yuka Ochi, Miho Nishio, Yuki Asano, Katsuhiko Kato. Dosimetry of absorbed dose using single-photon emission computed tomography images in I-131 therapy for hyperthyroidism.

Society of Nuclear Medicine and Molecular Imaging 2022 Annual Meeting.

- Takumi Inagaki, Hiroshi Yamaguchi, Naotoshi Fujita, Yuki Asano, Shinji Abe, Katsuhiko Kato. Adsorption of ^{111}In solution on phantom walls: Effect of concentration nd pH.

13th Congress of the World Federation of Nuclear Medicine and Biology.

- Takumi Inagaki, Hiroshi Yamaguchi, Naotoshi Fujita, Yuki Asano, Shinji Abe, Katsuhiko Kato. A study on the adsorption of ^{111}In solution in a plastic syringe.

Society of Nuclear Medicine and Molecular Imaging 2023 Annual Meeting, Chicago, IL, United State.

- Haruna Ikeda, Naotoshi Fujita, Ryuichi Nishii, Shinji Abe, Katsuhiko Kato. Dose evaluation in iodine-131 therapy of hyperthyroidism with heterogeneous thyroid iodine distribution using SPECT images
- Takumi Inagaki, Naotoshi Fujita, Ryota Isobe, Tomoka Nagahara, Shinji Abe, Katsuhiko Kato. Comparison of adsorption of ^{111}In radiopharmaceuticals on acrylic and polypropylene
- Ryota Isobe, Yoshinori Ito, Naotoshi Fujita, Kohei Nakanishi, Haruna Ikeda, Takumi Inagaki, Shinji Abe, Katsuhiko Kato. New analysis method using successive approximations to obtain the H/M ratio in ^{123}I-MIBG scintigraphy

36th Annual Congress of the European Association of Nuclear Medicine, 2023/9/9-13, Vienna, Austria

- Takumi Inagaki, Hiroshi Yamaguchi, Naotoshi Fujita, Haruna Ikeda, Ryota Isobe, Tomoka Nagahara, Shinji Abe, Katsuhiko Kato. Comparison of ^{111}In and ^{201}Tl radiopharmaceutical adsorption on acrylic phantoms.
- Tomoka Nagahara, Naotoshi Fujita, Haruna Ikeda, Takumi Inagaki, Ryota Isobe, Shinji Abe, Katsuhiko Kato. Clinical application of SPECT phantoms created using paper phantoms.

Society of Nuclear Medicine and Molecular Imaging 2024 Annual Meeting, 2024/6/8-11, Toronto, Canada

- Comparison of image reconstruction methods by a SPECT phantom using an inkjet printer

  Tomoka Nagahara, Naotoshi Fujita, Tetsuro Katafuchi, Haruna Iwanaga, Ryota Isobe, Tomoya Inagaki, Ryotaro Tsunekawa, Kohei Nakanishi, Ryuichi Nishii, Katsuhiko Kato

- Age-related Variation in SUVR in ^{11}C-PiB PET Scans

  Tomoya Inagaki, Naotoshi Fujita, Tomohiro Tada, Haruna Iwanaga, Ryota Isobe, Tomoka Nagahara, Shinji Abe, Kohei Nakanishi, Ryuichi Nishii, Katsuhiko Kato

- Relationship between ^{99m}Tc-MAA Planar Image Accumulation Distribution in Pulmonary Hypertension and Indices Obtained by Right Heart Catheterization

  Ryotaro Tsunekawa, Naotoshi Fujita, Haruna Iwanaga, Ryota Isobe, Tomoka Nagahara, Tomoya Inagaki, Shinji Abe, Kohei Nakanishi, Ryuichi Nishii, Katsuhiko Kato

37th Annual Congress of the European Association of Nuclear Medicine, 2024/10/19-23, Hambrug, Germany

- Evaluation of voxel-based absorbed doses calculated using SPECT imaging in iodine-131 therapy for hyperthyroidism」

  Haruna Iwanaga, Naotoshi Fujita, Shinji Abe, Katsuhiko Kato

2010 RSNA Chicago
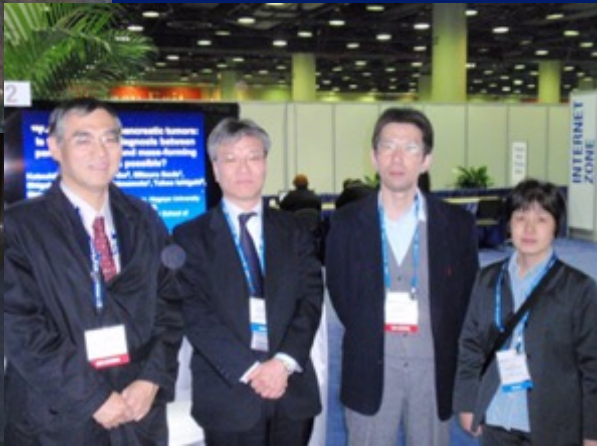
2010 SNM Salt Lake City

2012 日独放射線交流計画 Münster
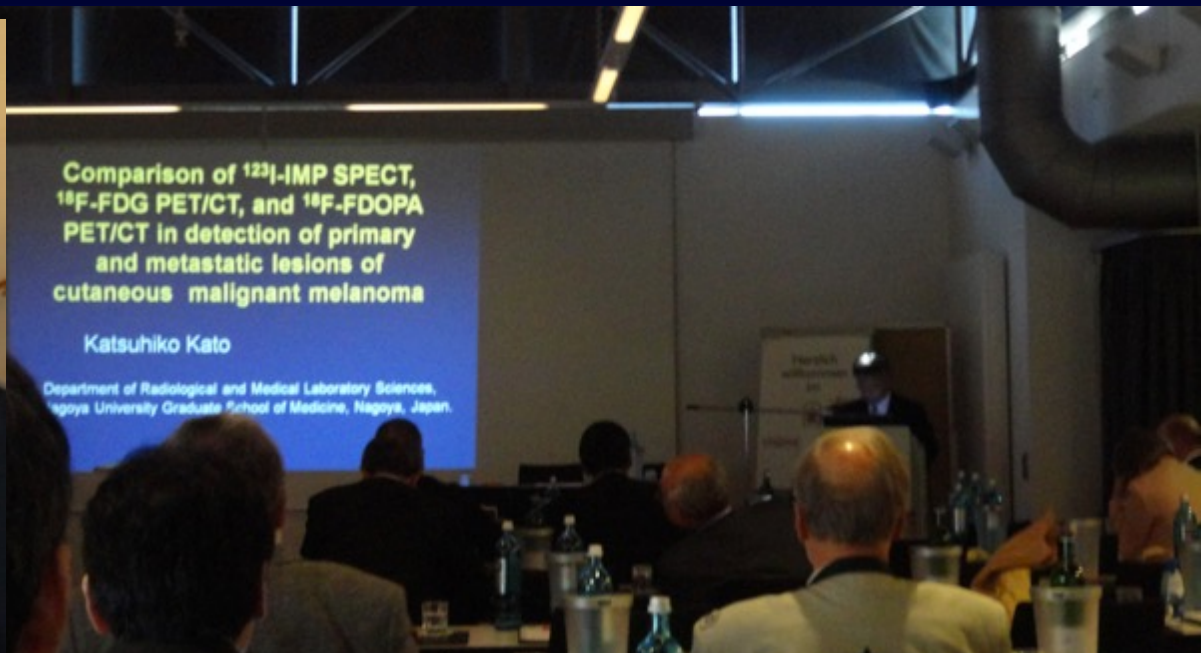
2012 EANM Milano
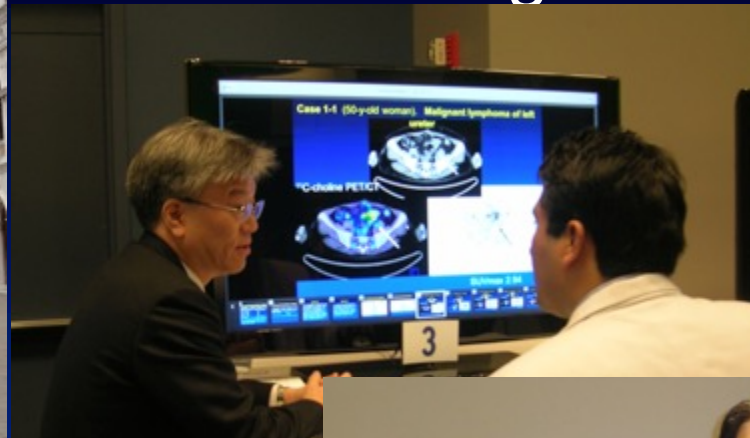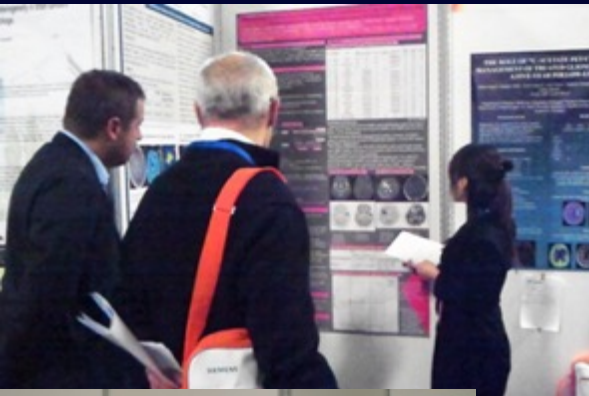
2012 RSNA Chicago

Comparison of ^{18}F-FDG PET and Bone Scintigraphy in Detection of Bone Metastases of Thyroid Cancer

Shinji Ito[1,2], Katsuhiko Kato[1], Mitsuru Ikeda[3], Shingo Iwano[1], Naoki Makino[2], Masanori Tadokoro[4], Shinji Abe[5], Satoshi Nakano[5], Masanari Nishino[5], Takeo Ishigaki[1], and Shinji Naganawa[1]

[1]Department of Radiology, Nagoya University Graduate School of Medicine, Nagoya, Japan; [2]Department of Radiology, Toyota Memorial Hospital, Toyota, Japan; [3]Department of Radiological Technology, Nagoya University School of Health Sciences, Nagoya, Japan; [4]Department of Radiology, Fujita Health University School of Health Science, Toyoake, Japan; and [5]Department of Radiology, Nagoya University Hospital, Nagoya, Japan

We compared the efficacies of ^{18}F-FDG PET and ^{99m}Tc-bone scintigraphy for the detection of bone metastases in patients with differentiated thyroid carcinoma (DTC). **Methods:** We examined 47 patients (32 women, 15 men; mean age ± SD, 57.0 ± 10.7 y) with DTC who had undergone total thyroidectomy and were hospitalized to be given ^{131}I therapy. All patients underwent both whole-body ^{18}F-FDG PET and ^{99m}Tc-bone scintigraphy. The skeletal system was classified into 11 anatomic segments and assessed for the presence of bone metastases. Bone metastases were verified either when positive findings were obtained on >2 imaging modalities—^{201}Tl scintigraphy, ^{131}I scintigraphy, and CT—or when MRI findings were positive if vertebral MRI was performed. **Results:** Bone metastases were confirmed in 59 of 517 (11%) segments in 18 (38%) of the 47 study patients. The sensitivities (visualization rate) for bone metastases on a segment basis using ^{18}F-FDG PET and ^{99m}Tc-bone scintigraphy were 50 of 59 (84.7%) and 46 of 59 (78.0%), respectively; the difference between these values was not statistically significant. There were only 2 (0.4%) false-positive cases in a total of 451 bone segments without bone metastases when examined by ^{18}F-FDG PET, whereas 39 (8.6%) were false-positive when examined by ^{99m}Tc-bone scintigraphy. Therefore, the specificities of ^{18}F-FDG PET and ^{99m}Tc-bone scintigraphy were 449 of 451 (99.6%) and 412 of 451 (91.4%), respectively; the difference between these values was statistically significant ($P < 0.001$). The overall accuracies of ^{18}F-FDG PET and ^{99m}Tc-bone scintigraphy were 499 of 510 (97.8%) and 458 of 510 (89.8%), respectively; the difference between these was also statistically significant ($P < 0.001$). **Conclusion:** The specificity and the overall accuracy of ^{18}F-FDG PET for the diagnosis of bone metastases in patients with DTC are higher than those of ^{99m}Tc-bone scintigraphy, whereas the difference in the sensitivities of both modalities is not statistically significant. In comparison with ^{99m}Tc-bone scintigraphy, ^{18}F-FDG PET is superior because of its lower incidence of false-positive results in the detection of bone metastases of DTC.

Skeletal imaging by ^{18}F-FDG PET has been shown to be useful in the detection of bone metastases of breast (*1–6*), lung (*1,4,7,8*), thyroid (*4*), esophageal (*4,9*), gastric (*4*), colorectal (*4*), endemic nasopharyngeal (*10*), renal cell (*11*), prostate (*1*), ovarian (*4*), and testicular (*4*) carcinomas. In most of these studies, ^{18}F-FDG PET was proven to be superior to conventional scintigraphic imaging using ^{99m}Tc-labeled phosphate compounds (^{99m}Tc-methylene diphosphonate [^{99m}Tc-MDP] or ^{99m}Tc-hydroxymethylene diphosphonate [^{99m}Tc-HMDP]). For the detection and evaluation of bone metastases of various kinds of carcinomas, ^{99m}Tc-bone scintigraphy has been used widely because of its overall high sensitivity and the easy evaluation of the entire skeleton (*12*). However, ^{99m}Tc-bone scintigraphy leads often to false-positive lesions and, consequently, its specificity is reduced, because degenerative or inflammatory foci will be often confused with metastatic diseases.

Differentiated thyroid carcinoma ([DTC] papillary and follicular) is characterized by good prognosis in comparison with carcinomas of other organs. The 10-y survival rate of DTC is >80% because of treatments such as total thyroidectomy and ablation of remnants with radioiodine (*13*). However, metastases of thyroid carcinoma develop in 7%–23% of patients; the distant metastases occur commonly in the lungs, bones, and brain, and bones are the second common site of metastases from thyroid carcinoma (*14*).

Several earlier reports showed that ^{18}F-FDG PET is highly sensitive in detecting DTC and is particularly useful for the evaluation of patients with negative radioactive iodine scintigraphy and elevated thyroglobulin levels (*15–20*). For the detection of bone metastases of thyroid

Comparison of ^{18}F-FDG PET and Bone Scintigraphy in Detection of Bone Metastases of Thyroid Cancer
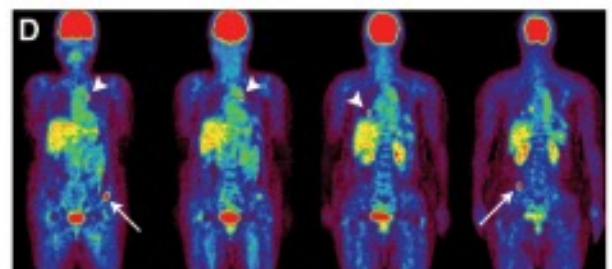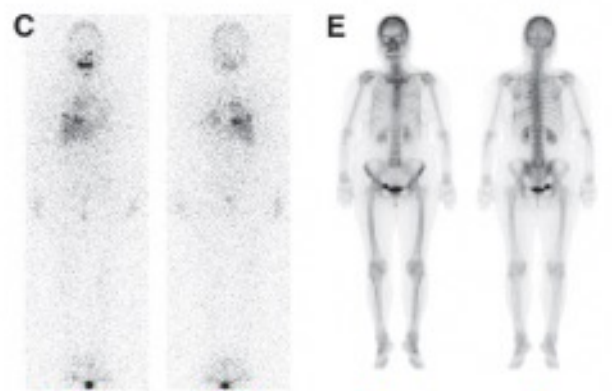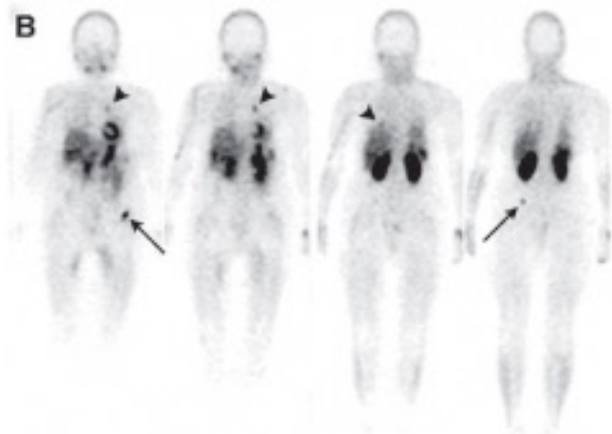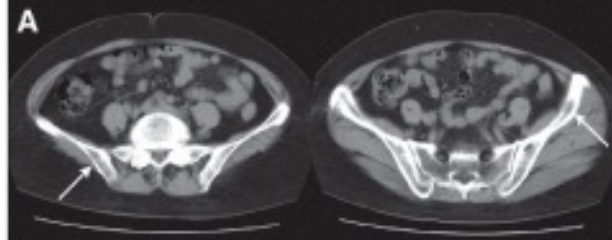
FIGURE 2. In this patient, there were multiple lung metastases besides bone metastases. (A) CT scan shows osteolytic lesions on both sides of iliac bones (arrows). (B) 201Tl SPECT image
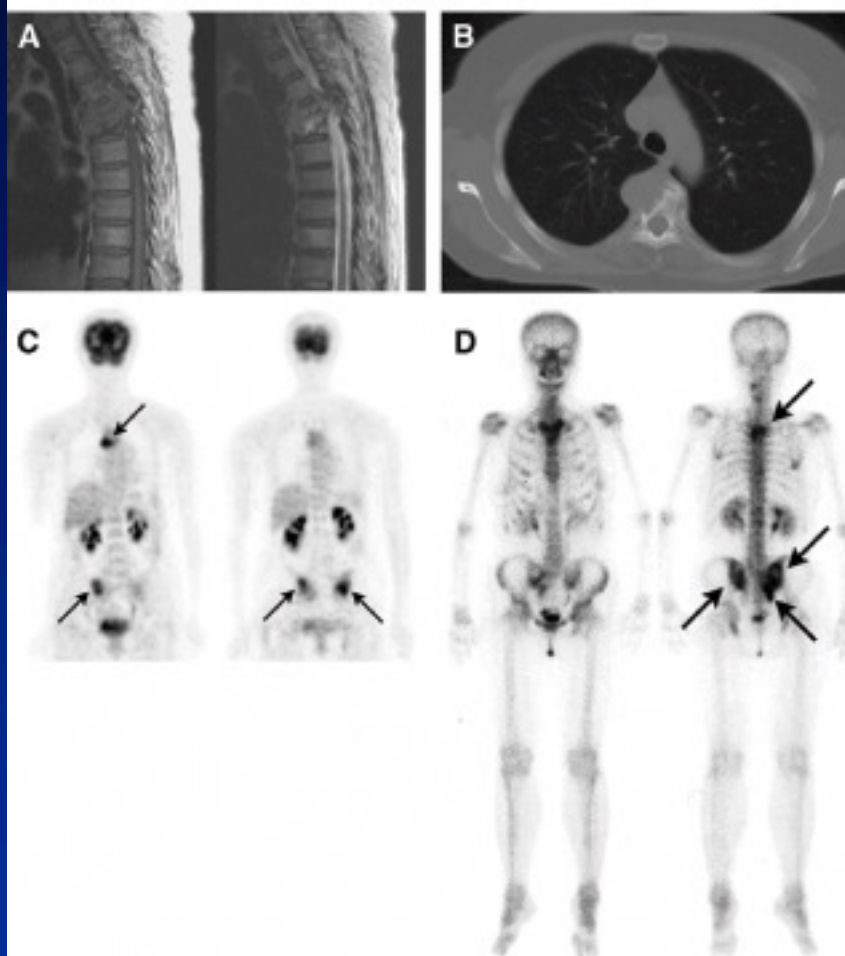
FIGURE 1. (A) T1-weighted MR image (left) shows massive lesion of low signal intensity, and T2-weighted MR image (right) shows lesion of high signal intensity. (B) CT scan shows osteolytic changes at thoracic spine (T4–T5). (C and D) ^{18}F-FDG PET coronal image (C) and ^{99m}Tc-bone whole-body scintigram (D) show high uptakes at thoracic spine (T4–T5), sacrum, and iliac bones (arrows).

TABLE 3

Sensitivity, Specificity, and Overall Accuracy of ^{18}F-FDG PET and ^{99m}Tc-Bone Scintigraphy in Detection of Bone Metastases in Patients with DTC

Parameter	^{18}F-FDG PET	^{99m}Tc-Bone scintigraphy	P
Sensitivity (%)	50/59 (84.7)	46/59 (78.0)	0.45*
Specificity (%)	449/451 (99.6)	412/451 (91.4)	<0.001
Accuracy (%)	449/510 (97.8)	458/510 (89.8)	<0.001

*Not significant.

Ito S, Kato K, et al. J Nucl Med. 2007;48:889-895

Nagoya University Graduate School of Medicine

FULL PAPER

Comparison of 18F-fluoride PET/CT, 18F-FDG PET/CT and bone scintigraphy (planar and SPECT) in detection of bone metastases of differentiated thyroid cancer: a pilot study

[1,2]NAOTOSHI OTA, MD, [3]KATSUHIKO KATO, MD, PhD, [1]SHINGO IWANO, MD, PhD, [1]SHINJI ITO, MD, PhD, [4]SHINJI ABE, RT, PhD, [4]NAOTOSHI FUJITA, RT, MS, [4]KEIICHI YAMASHIRO, MT, [3]SEIICHI YAMAMOTO, PhD and [1]SHINJI NAGANAWA, MD, PhD

[1]Department of Radiology, Nagoya University Graduate School of Medicine, Nagoya, Japan
[2]Department of Radiology, Toyohashi Municipal Hospital, Toyohashi, Japan
[3]Department of Radiological and Medical Laboratory Sciences, Nagoya University Graduate School of Medicine, Nagoya, Japan
[4]Department of Radiological Technology, Nagoya University Hospital, Nagoya, Japan

Address correspondence to: Professor Katsuhiko Kato
E-mail: katokt@med.nagoya-u.ac.jp

Objective: We compared the efficacies of 18F-fluoride positron emission tomography (18F-fluoride PET)/CT, 18F-fludeoxyglucose PET (18F-FDG PET)/CT, and 99mTc bone scintigraphy [planar and single photon emission CT (SPECT)] for the detection of bone metastases in patients with differentiated thyroid carcinoma (DTC).

Methods: We examined 11 patients (8 females and 3 males; mean age ± standard deviation, 61.9 ± 8.7 years) with DTC who had been suspected of having bone metastases after total thyroidectomy and were hospitalized to be given 131I therapy. Bone metastases were verified either when positive findings were obtained on both 131I scintigraphy and CT or when MRI findings were positive if MRI was performed.

Results: Metastases were confirmed in 24 (13.6%) of 176 bone segments in 9 (81.8%) of the 11 patients. The sensitivities of 18F-fluoride PET/CT and 99mTc bone scintigraphy (SPECT) were significantly higher than those of 18F-FDG PET/CT and 99mTc bone scintigraphy (planar) ($p < 0.05$). The accuracies of 18F-fluoride PET/CT and 99mTc bone scintigraphy (SPECT) were significantly higher than that of 99mTc bone scintigraphy (planar) ($p < 0.05$).

Conclusion: The sensitivity and accuracy of 18F-fluoride PET/CT for the detection of bone metastases of DTC are significantly higher than those of 99mTc bone scintigraphy (planar). However, the sensitivity and accuracy of 99mTc bone scintigraphy (planar) are improved near to those of 18F-fluoride PET/CT when SPECT is added to a planar scan. The sensitivity of 18F-FDG PET/CT is significantly lower than that of 18F-fluoride PET/CT or 99mTc bone scintigraphy (SPECT).

Advances in knowledge: This article has demonstrated first the high efficacy of 18F-fluoride PET/CT for the detection of bone metastases of DTC.

Differentiated thyroid carcinoma (DTC) shows a relatively good prognosis compared with carcinomas of other organs, and the 10-year survival rate of DTC is >80% because of treatments such as total thyroidectomy and ablation of remnants with radioiodine.[1] However, metastases of DTC develop in 7–23% of patients; the distant metastases occur commonly in the lungs, bones and brain, and the bones are the second most common site of metastases of DTC.[2] Bone scintigraphy using 99mTc-labelled phosphate compounds [99mTc-methylene diphosphonate (99mTc-MDP) or 99mTc-hydroxymethylene diphosphonate (99mTc-HMDP)] has been widely used for detecting and evaluating bone metastases of various kinds of carcinomas because of its overall high sensitivity and the easy evaluation of the entire skeleton.[3] However, there were often false-positive cases in 99mTc

bone scintigraphy, because degenerative or inflammatory foci were often confused with metastatic lesions. The addition of single photon emission CT (SPECT) to planar acquisition of 99mTc bone scintigraphy has been shown to exhibit a beneficial effect on the detection and evaluation of bone metastases.[4–6] Skeletal imaging by 18F-fludeoxyglucose positron emission tomography (18F-FDG PET)/CT has been shown to be useful in the detection of bone metastases of various carcinomas including DTC.[7]

Previously, we compared the efficacies of 18F-FDG PET and planar 99mTc bone scintigraphy for the detection of bone metastases in patients with DTC.[8] We found that the specificity and the overall accuracy of 18F-FDG PET for the detection of bone metastases in patients with DTC were

Comparison of ^{18}F-fluoride PET/CT, ^{18}F-FDG PET/CT and bone scintigraphy (planar and SPECT) in detection of bone metastases of differentiated thyroid cancer: a pilot study

Figure 1. Multiple bone metastases in Patient 5. (a) From left to right: ^{131}I scintigraphy, ^{18}F-fluoride positron emission tomography (^{18}F-fluoride PET)/CT, ^{18}F-fludeoxyglucose PET (^{18}F-FDG PET)/CT, and anterior and posterior planar bone scintigraphies. Bone metastases at left pelvis and thoracic spine could be detected by all four modalities. (b, c) From left to right (metastases are marked by arrows): ^{18}F-fluoride PET/CT, ^{18}F-FDG PET/CT and single photon emission CT (SPECT) bone scintigraphy. (b) Bone metastasis at right clavicle could be detected by ^{18}F-fluoride PET/CT and SPECT bone scintigraphy, but not by ^{18}F-FDG PET/CT. (c) Bone metastasis at left scapula could be detected by ^{18}F-fluoride PET/CT, but not by ^{18}F-FDG PET/CT and SPECT bone scintigraphy.
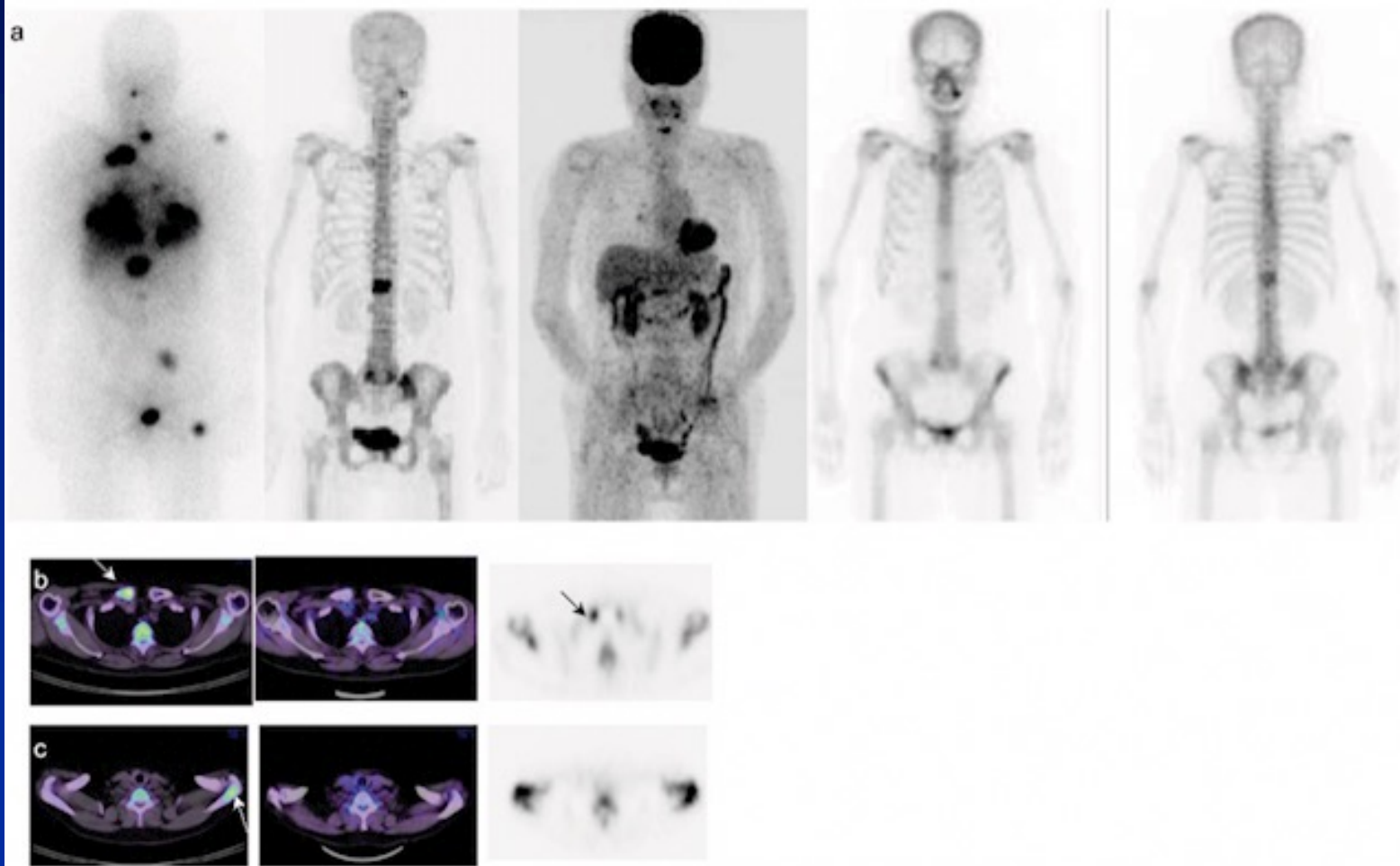
Table 3. Sensitivity, specificity and overall accuracy of ^{18}F-fluoride positron emission tomography (^{18}F-fluoride PET)/CT, ^{18}F-fludeoxyglucose PET (^{18}F-FDG PET)/CT and ^{99m}Tc bone scintigraphy [planar and single photon emission CT (SPECT)] in detection of bone metastases in patients with differentiated thyroid carcinoma (lesion based)

Parameter	^{18}F-fluoride PET/CT	^{18}F-FDG PET/CT	[99m]Tc bone scintigraphy (planar)	Scintigraphy (SPECT)
Sensitivity (%)	23/24 (95.8%)	17/24 (70.8%)[a]	14/22 (63.6%)[a]	21/24 (87.5%)
Specificity (%)	151/152 (99.3%)	152/152 (100.0%)	136/138 (98.6%)	150/152 (98.7%)
Accuracy (%)	174/176 (98.9%)	169/176 (96.0%)	150/160 (93.8%)[b]	171/176 (97.2%)

[a]The sensitivities of ^{18}F-fluoride PET/CT and ^{99m}Tc bone scintigraphy (SPECT) were significantly higher than those of ^{18}F-FDG PET/CT and ^{99m}Tc bone scintigraphy (planar) ($p < 0.05$).
[b]The accuracies of ^{18}F-fluoride PET/CT and ^{99m}Tc bone scintigraphy (SPECT) were significantly higher than that of ^{99m}Tc bone scintigraphy (planar) ($p < 0.05$).

Ota N, Kato K, et al. Br J Radiol. 2014;87(1034)20130444.

ORIGINAL ARTICLE

Diagnostic performance of ^{18}F-FDG PET/CT and whole-body diffusion-weighted imaging with background body suppression (DWIBS) in detection of lymph node and bone metastases from pediatric neuroblastoma

Hiroaki Ishiguchi[1,2] · Shinji Ito[1] · Katsuhiko Kato[3] · Yusuke Sakurai[1] · Hisashi Kawai[1] · Naotoshi Fujita[4] · Shinji Abe[4] · Atsushi Narita[5] · Nobuhiro Nishio[5] · Hideki Muramatsu[5] · Yoshiyuki Takahashi[5] · Shinji Naganawa[1]

Abstract

Objective Recent many studies have shown that whole body "diffusion-weighted imaging with background body signal suppression" (DWIBS) seems a beneficial tool having higher tumor detection sensitivity without ionizing radiation exposure for pediatric tumors. In this study, we evaluated the diagnostic performance of whole body DWIBS and ^{18}F-FDG PET/CT for detecting lymph node and bone metastases in pediatric patients with neuroblastoma.

Methods Subjects in this retrospective study comprised 13 consecutive pediatric patients with neuroblastoma (7 males, 6 females; mean age, 2.9 ± 2.0 years old) who underwent both ^{18}F-FDG PET/CT and whole-body DWIBS. All patients were diagnosed as neuroblastoma on the basis of pathological findings. Eight regions of lymph nodes and 17 segments of skeletons in all patients were evaluated. The images of ^{123}I-MIBG scintigraphy/SPECT-CT, bone scintigraphy/SPECT, and CT were used to confirm the presence of lymph node and bone metastases. Two radiologists trained in nuclear medicine evaluated independently the uptake of lesions in ^{18}F-FDG PET/CT and the signal-intensity of lesions in whole-body DWIBS visually. Interobserver difference was overcome through discussion to reach a consensus. The sensitivities, specificities, and overall accuracies of ^{18}F-FDG PET/CT and whole-body DWIBS were compared using McNemer's test. Positive predictive values (PPVs) and negative predictive values (NPVs) of both modalities were compared using Fisher's exact test.

Results The total numbers of lymph node regions and bone segments which were confirmed to have metastasis in the total 13 patients were 19 and 75, respectively. The sensitivity, specificity, overall accuracy, PPV, and NPV of ^{18}F-FDG PET/CT for detecting lymph node metastasis from pediatric neuroblastoma were 100, 98.7, 98.9, 95.0, and 100%, respectively, and those for detecting bone metastasis were 90.7, 73.1, 80.3, 70.1, and 91.9%, respectively. In contrast, the sensitivity, specificity, overall accuracy, PPV, and NPV of whole-body DWIBS for detecting bone metastasis from pediatric neuroblastoma were 94.7, 24.0, 53.0, 46.4 and 86.7%, respectively, whereas those for detecting lymph node metastasis were 94.7, 85.3, 87.2, 62.1, and 98.5%, respectively. The low specificity, overall accuracy, and PPV of whole-body DWIBS for detecting bone metastasis were due to a high incidence of false-positive findings (82/108, 75.9%). The specificity, overall accuracy, and PPV of whole-body DWIBS for detecting lymph node metastasis were also significantly lower than those of ^{18}F-FDG PET/CT for detecting lymph node metastasis, although the difference between these 2 modalities was less than that for detecting bone metastasis.

Conclusion The specificity, overall accuracy, and PPV of whole-body DWIBS are significantly lower than those of ^{18}F-FDG PET/CT because of a high incidence of false-positive findings particularly for detecting bone metastasis, whereas whole-body DWIBS shows a similar level of sensitivities for detecting lymph node and bone metastases to those of ^{18}F-FDG PET/CT. DWIBS should be carefully used for cancer staging in children because of its high incidence of false-positive findings in skeletons.

Keywords ^{18}F-FDG PET/CT · Whole-body DWIBS · Neuroblastoma · Metastasis

✉ Katsuhiko Kato
 katokt@med.nagoya-u.ac.jp

Extended author information available on the last page of the article
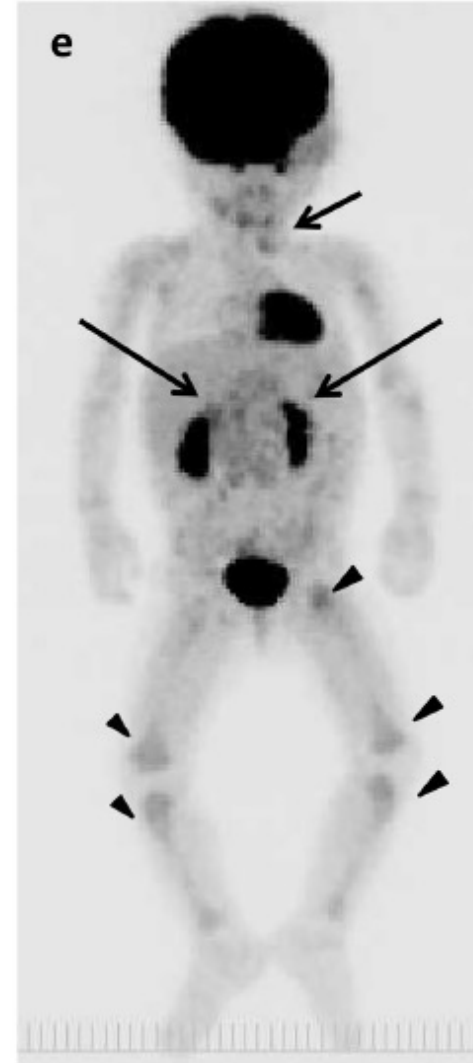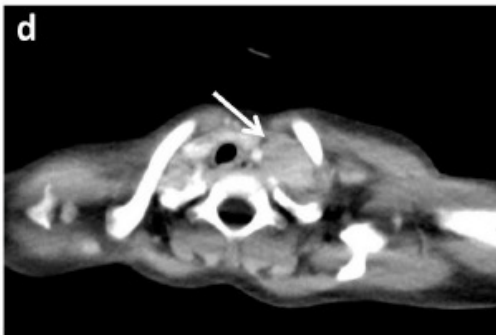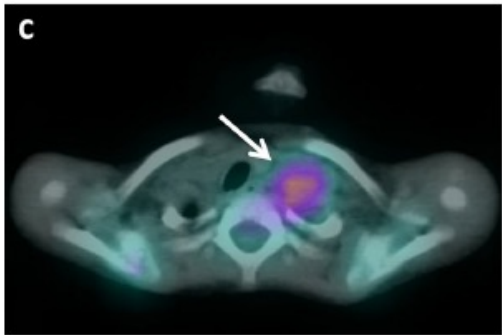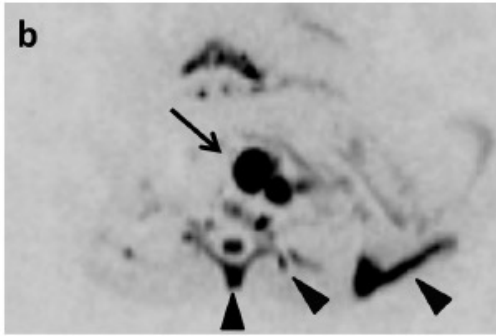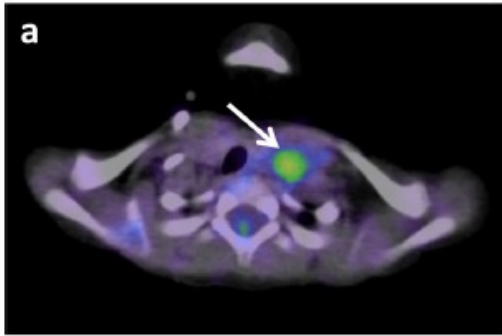
Evaluation of radionuclide therapy for the palliation of bone metastasis pain using ^{89}Sr: comparison of SUV values of bone metastases measured by ^{99m}Tc bone SPECT, ^{18}F-fluoride PET/CT, ^{18}F-FDG PET/CT

Chinatsu Hasegawa[1], Naotoshi Fujita[1,2], Yoshinori Ito[1],
Risa Ono[1], Tomohiro Tada[1], Rina Murayama[1],
Yoshinori Tsutsumi[1,2], Tetsuro Odagawa[1], Mika Tamura[1],
Shinji Abe[2], Katsuhiko Kato[1]

[1] Department of Radiological and Medical Laboratory Sciences,
Nagoya University Graduate School of Medicine
[2] Department of Radiological Technology, Nagoya University Hospital

Nagoya University Graduate School of Medicine

Patient 7

In this case SUV was increased only on bone SPECT

Bone SPECT — ^{18}F-fluoride PET/CT — ^{18}F-FDG PET/CT
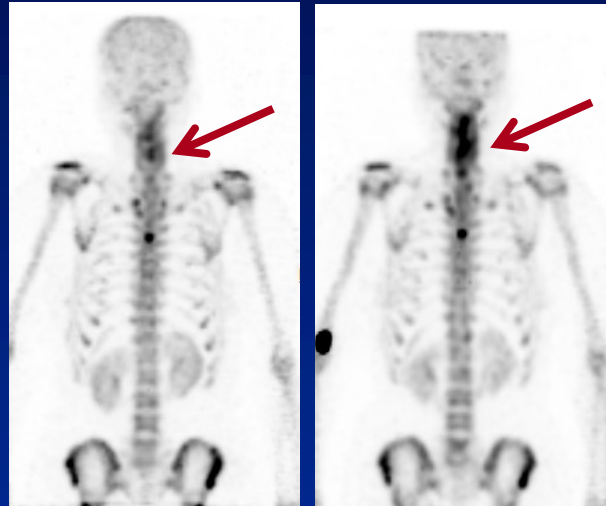
Before January 2016 — After February 2016 — After 1 month
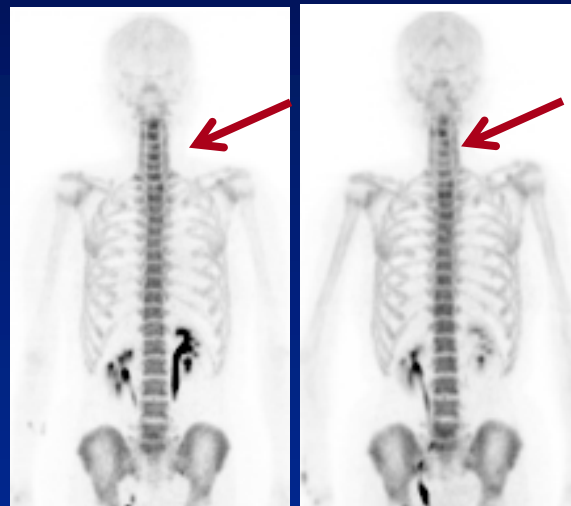
Before January 2016 — After March 2016 — After 2 months
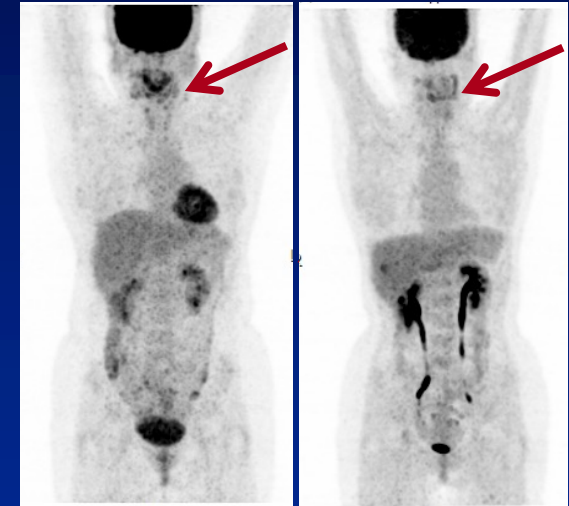
Before December 2015 — After March 2016 — After 3 months

Hasegawa C, et al. J Nucl Med. 2019; 60 (suppl 1): 2029.

Nagoya University Graduate School of Medicine

- ## Change in SUVs

bone SPECT

10.0 8.0 6.0 4.0 2.0 0.0

- SUVmax
- SUVpeak

2016
Jan. Feb. Mar. Apr. May Jun. Jul.

Fluoride PET/CT

20.0 15.0 10.0 5.0 0.0

- SUVmax
- SUVpeak

2016
Jan. Feb. Mar.

FDG PET/CT

5.0 4.0 3.0 2.0 1.0 0.0

- SUVmax
- SUVpeak

2015 2016
Dec. Jan. Feb. Mar.
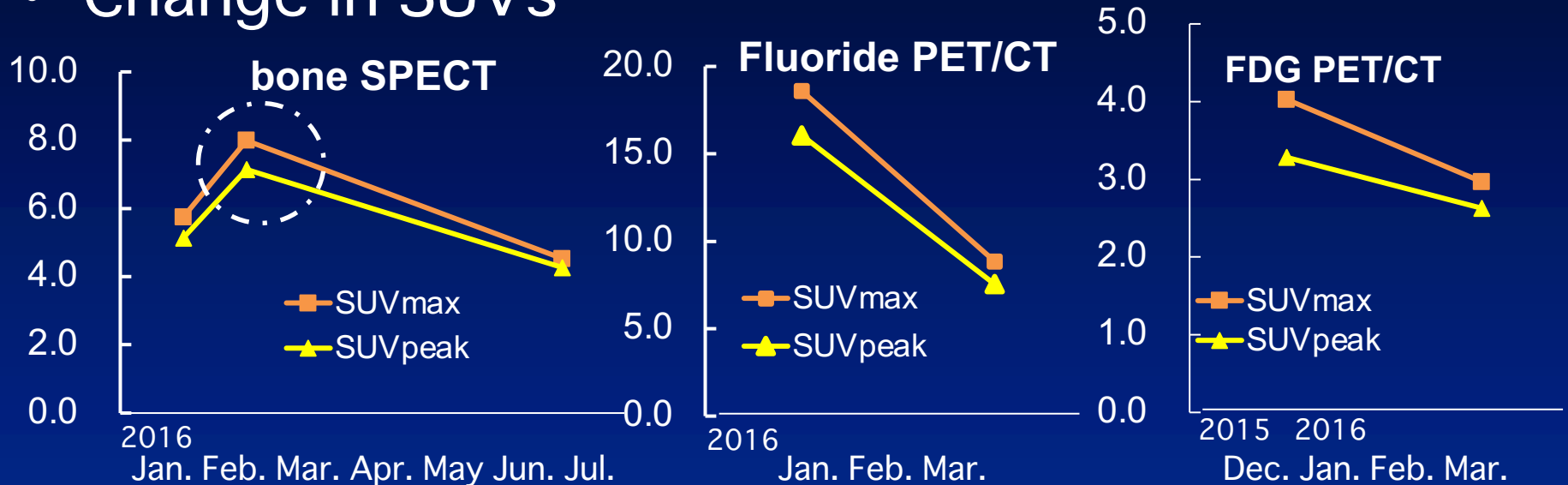
- The flare phenomenon often occurred in bone SPECT and ^{18}F-fluoride PET/CT .

- The flare phenomenon was characterized by an early and transient rise in uptake followed by a decline.

- The rise in SUV on bone SPECT may be attributed to the flare phenomenon.

Hasegawa C, et al. J Nucl Med. 2019; 60 (suppl 1): 2029.

Nagoya University Graduate School of Medicine

Patient 6
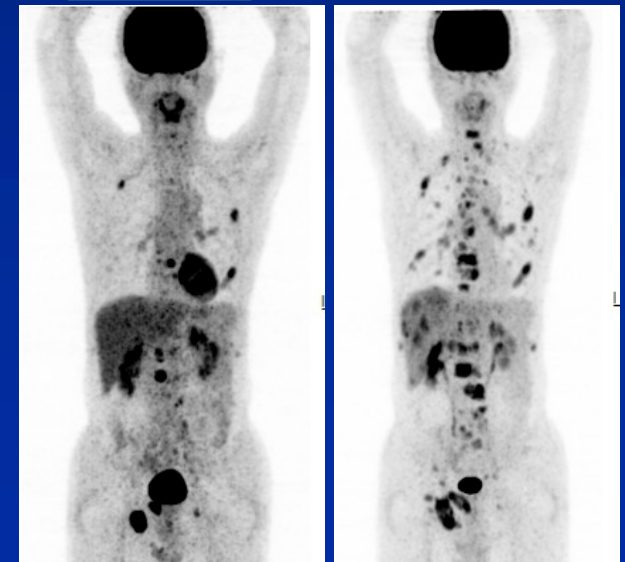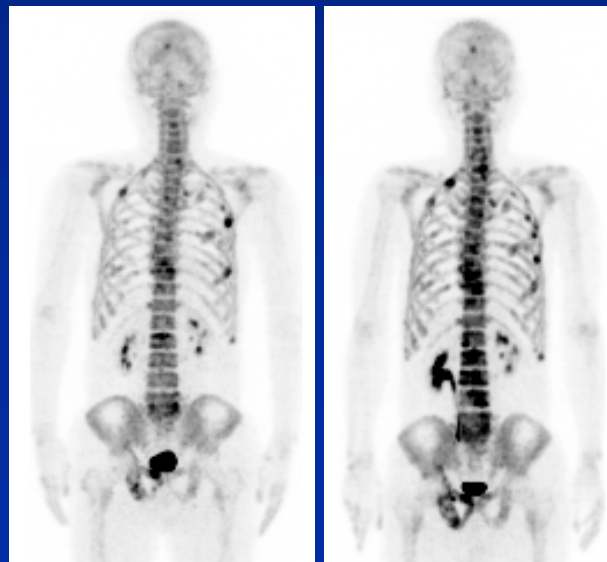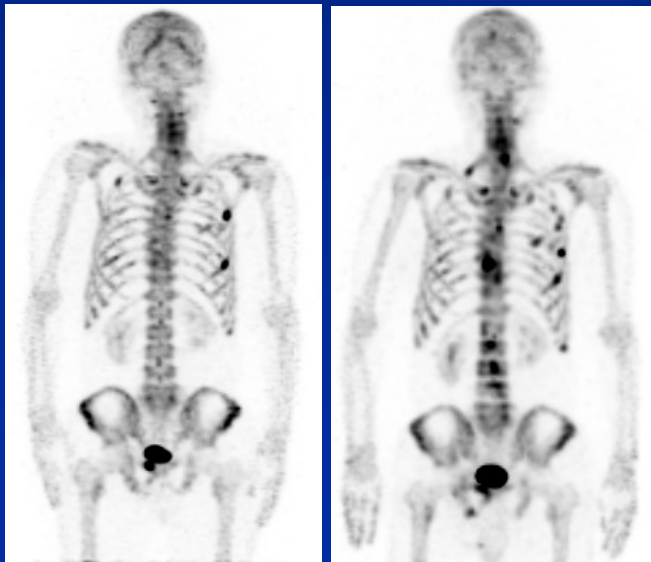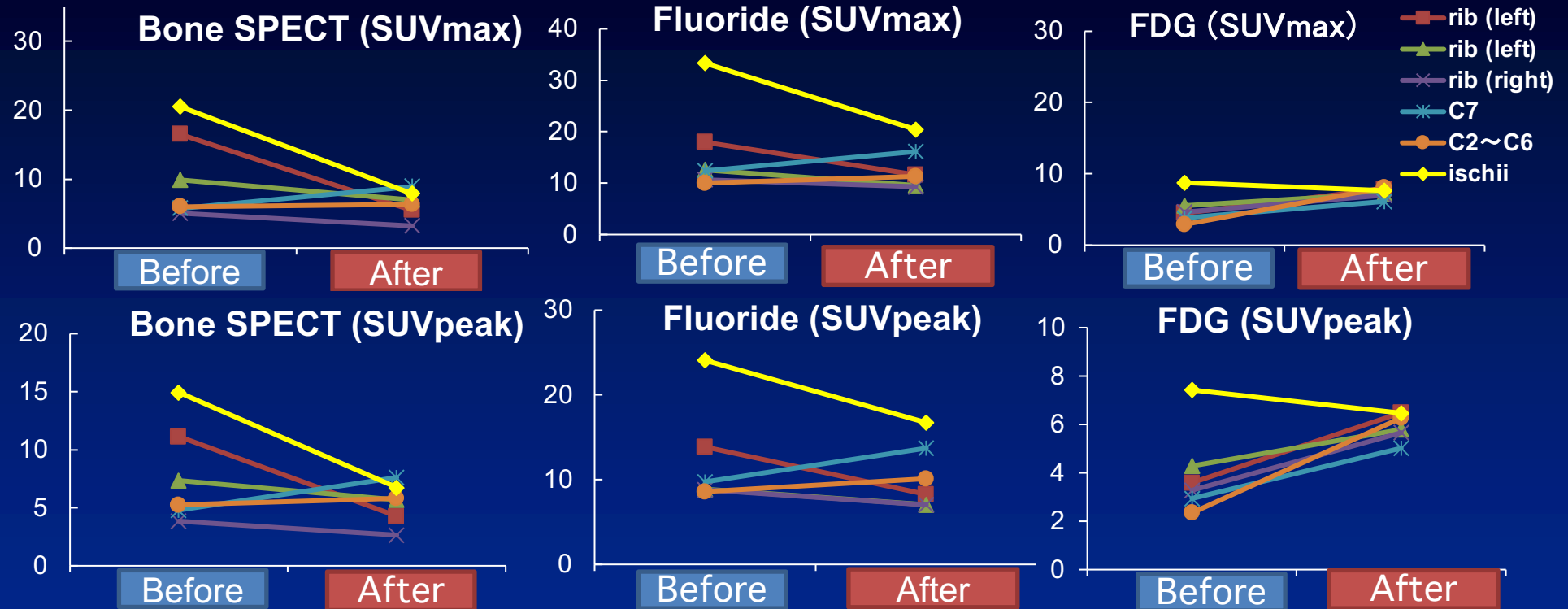
Conclusion

- The %SUV changes of ^{18}F-fluoride were most consistent with the results of clinical evaluation.

- In the evaluation of %SUV change using bone SPECT, many cases showed results that were not consistent with those of clinical evaluation because of the flare phenomenon.

- The %change in SUV of ^{18}F-FDG may not be related to patient symptoms.

Hasegawa C, et al. J Nucl Med. 2019; 60 (suppl 1): 2029.

Nagoya University Graduate School of Medicine

Studies on decision of the cut-off standardized uptake values for normal bones and bone metastases of the vertebrae in ^{18}F-fluoride PET/CT and ^{18}F-FDG PET/CT

Risa Ono [1], Naotoshi Fujita [1, 2], Yoshinori Ito [1], Tomohiro Tada [1], Rina Murayama [1], Haruna Ikeda [3], Yuka Ochi [3], Miho Nishio [3], Yoshinori Tsutsumi [2], Tetsuro Odagawa [1], Mika Tamura [1], Shinji Abe [2], Katsuhiko Kato [3]

[1] Department of Radiological and Medical Laboratory Sciences, Nagoya University Graduate School of Medicine, Nagoya, Japan

[2] Department of Radiological Technology, Nagoya University Hospital, Nagoya, Japan

[3] Department of Integrated Health Science, Nagoya University Graduate School of Medicine, Nagoya, Japan

Nagoya University Graduate School of Medicine

^{18}F-fluoride PET/CT及び^{18}F-FDG PET/CTを用いて,頸椎・胸椎・腰椎における正常骨及び骨転移を区別するためのSUVによるカットオフ値を設定し,その有用性を検討した.

Normal bone
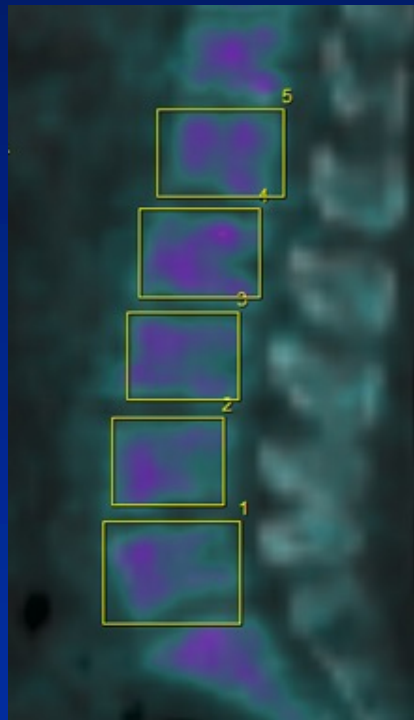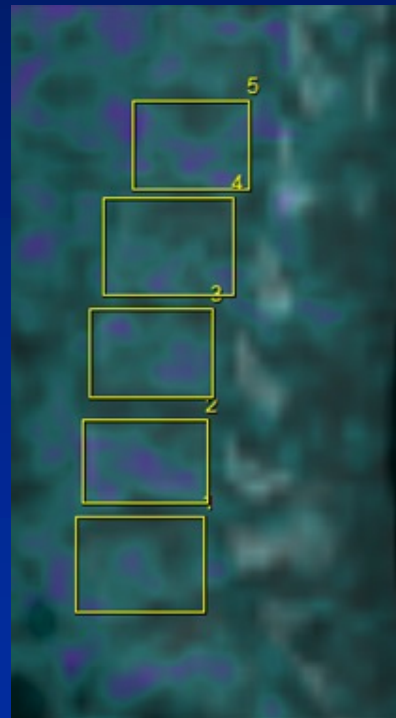
Bone metastases
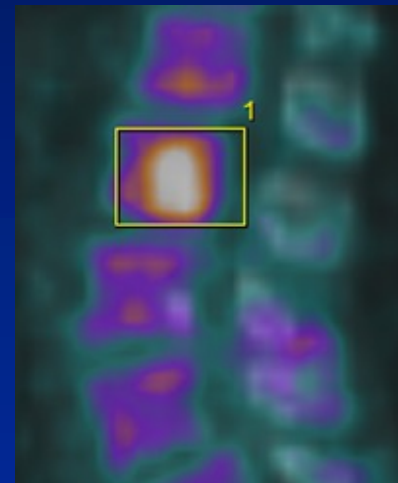
(A)
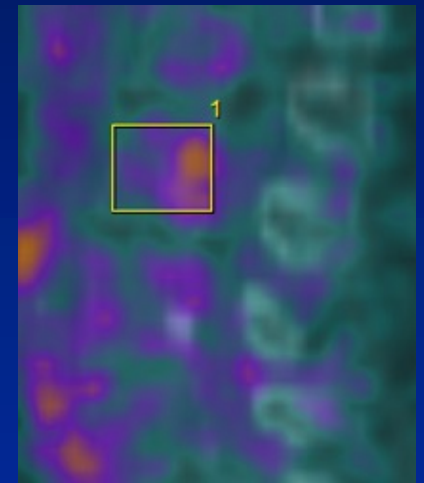
(B)

(A): ^{18}F-fluoride PET/CT
(B): ^{18}F-FDG PET/CT

(A)

(B)

Ono R, et al. Eur J Nucl Med Mol Imaging. 2020;47: S200.
Nagoya University Graduate School of Medicine

正常骨SUVの部位間の比較
(上: ^{18}F-fluoride PET/CT, 下: ^{18}F-FDG PET/CT)

∗: p<0.05, n.s.: not significant

Ono R, et al. Eur J Nucl Med Mol Imaging. 2020;47: S200.
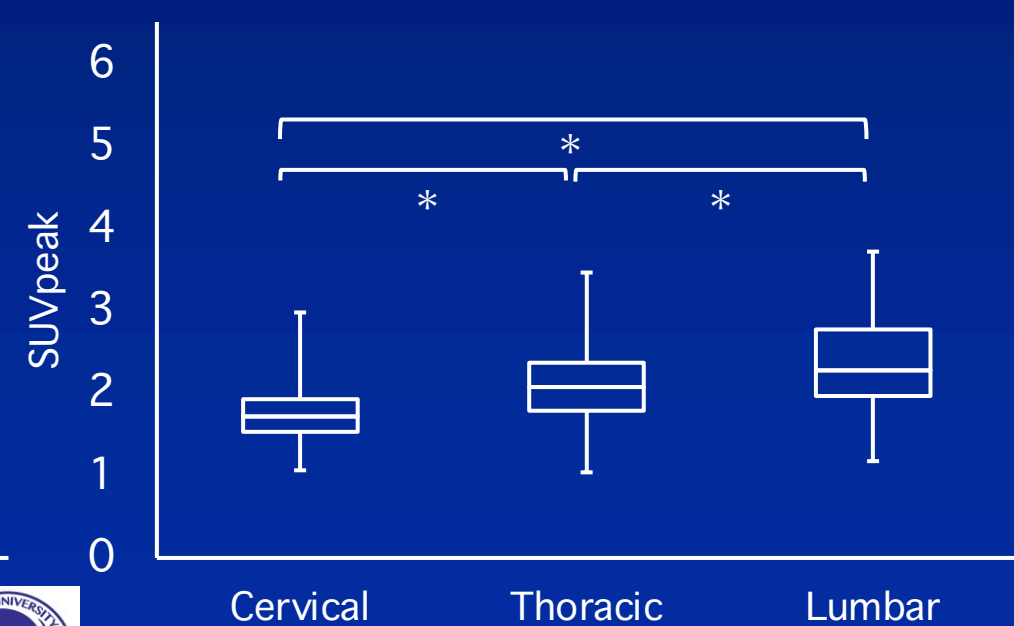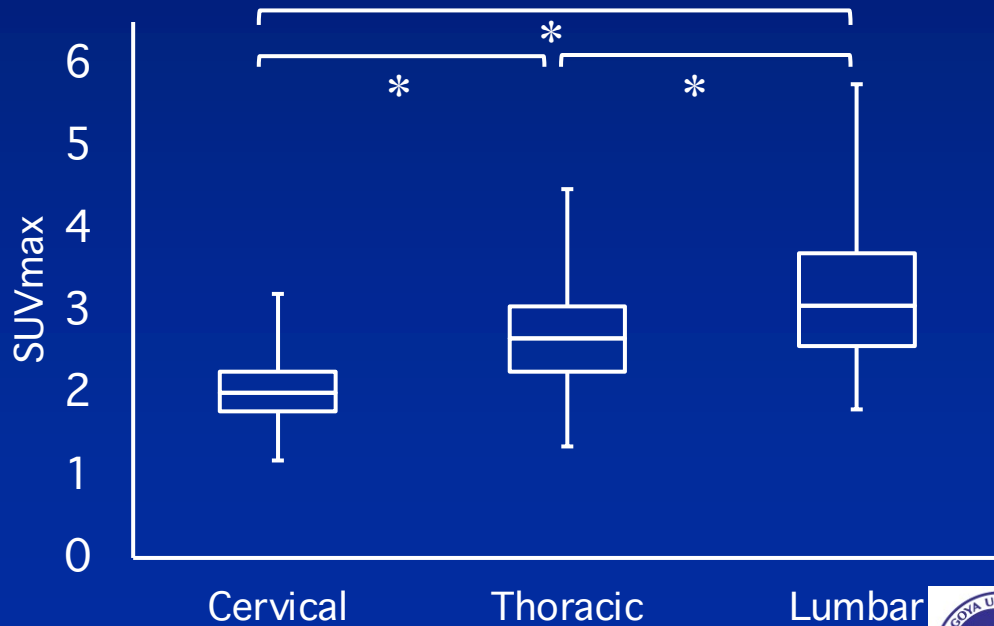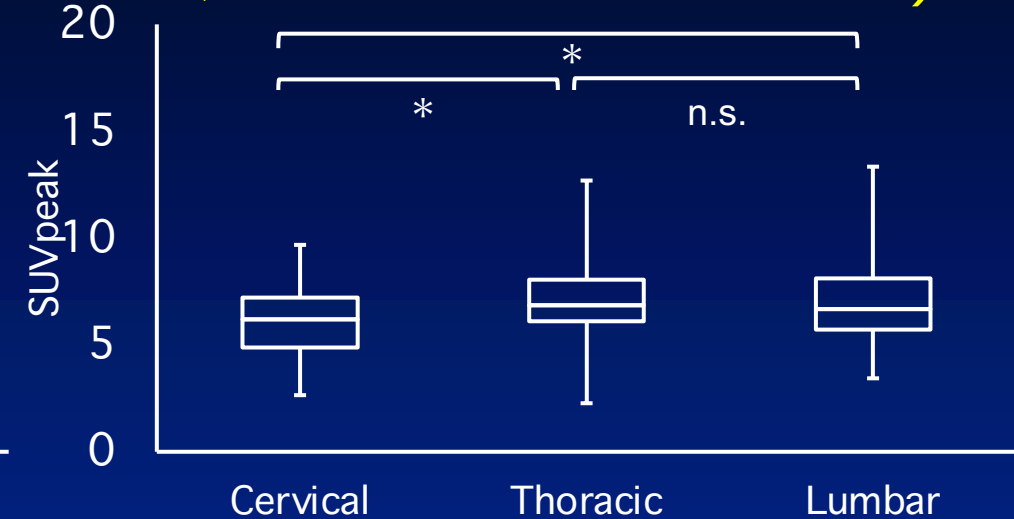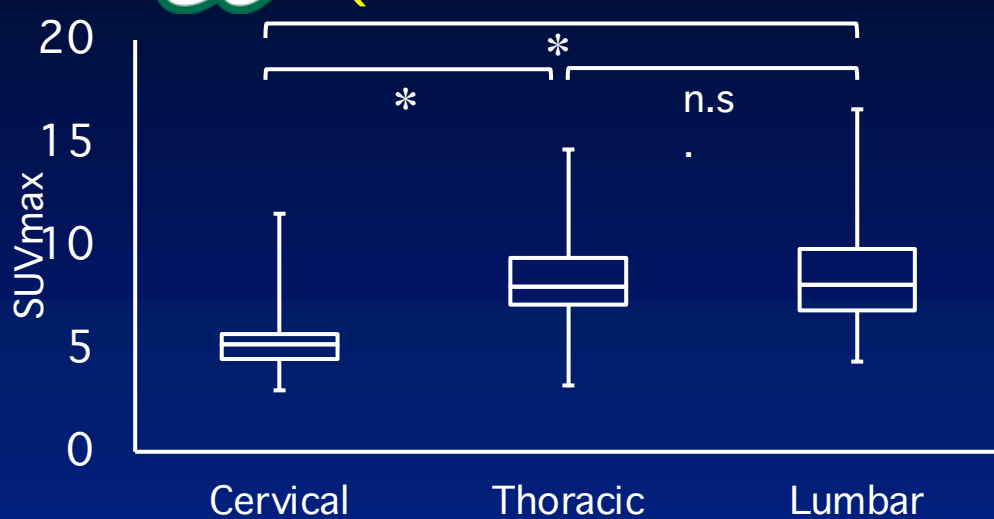
ROC解析の結果

		18F-fluoride PET/CT				18F-FDG PET/CT			
		Cut-off value	Sen.	Spe.	AUC	Cut-off value	Sen.	Spe.	AUC
SUVmax	Cervical	9.32	0.894	0.881	0.96	2.50	0.741	0.881	0.832
	Thoracic	10.05	0.873	0.819	0.926	3.05	0.654	0.750	0.753
	Lumbar	13.08	0.842	0.952	0.961	3.26	0.746	0.614	0.766
	C–L	10.71	0.841	0.882	0.941	2.94	0.712	0.711	0.772
SUVpeak	Cervical	8.42	0.835	0.938	0.961	2.04	0.753	0.850	0.824
	Thoracic	8.63	0.816	0.841	0.912	2.46	0.588	0.816	0.736
	Lumbar	10.85	0.816	0.950	0.954	2.42	0.754	0.593	0.751
	C–L	8.58	0.843	0.856	0.933	2.32	0.663	0.735	0.76

C–L: Cervical–Lumbar, Sen.: Sensitivity, Spe.: Specificity

部位毎のカットオフ値が適切な場合
- ^{18}F-fluoride PET/CTにおけるSUVmax
- ^{18}F-FDG PET/CTにおけるSUVmax
- ^{18}F-FDG PET/CTにおけるSUVpeak

部位共通のカットオフ値を用いることができる場合
- ^{18}F-fluoride PET/CTにおけるSUVpeak

Ono R, et al. Eur J Nucl Med Mol Imaging. 2020;47: S200.

Limited Efficacy of 18F-FDG PET/CT for Differentiation Between Metastasis-Free Pancreatic Cancer and Mass-Forming Pancreatitis

Katsuhiko Kato, MD, PhD,* Takashi Nihashi, MD, PhD,† Mitsuru Ikeda, MD, PhD,*
Shinji Abe, RT, PhD,† Shingo Iwano, MD, PhD,‡ Shigeki Itoh, MD, PhD,§
Kazuhiro Shimamoto, MD, PhD,* and Shinji Naganawa, MD, PhD‡

Objective: Differentiation between metastasis-free pancreatic cancer and mass-forming pancreatitis is important to avoid unnecessary operative procedures. This study was aimed at evaluating the efficacy of PET/CT with 18F-FDG (FDG PET/CT) for the differential diagnosis between them.

Patients and Methods: FDG-PET/CT was performed in 47 study patients with pancreatic masses and without any detectable metastases, 33 of which cases were finally diagnosed as pancreatic cancer and the other 14 as pancreatitis, and the corresponding imaging data were evaluated retrospectively. The maximal SUV (SUVmax) within the masses were determined at 1 hour and mostly at 2 hours after intravenous injection of FDG.

Results: SUVmax at 1 hour in pancreatic cancer was significantly higher than that in mass-forming pancreatitis, and the change in SUVmax from 1- to 2-hour time points was more consistent with pancreatic cancer than with mass-forming pancreatitis. However, there remained considerable overlapping between the SUVmax values of both diseases except either at the higher range for pancreatic cancer (>7.7 at 1 hour or >9.98 at 2 hours) or at the lower range for mass-forming pancreatitis (<3.37 at 1 hour or <3.53 at 2 hours). No obvious difference was found in the FDG uptake patterns of the mass areas between both diseases.

Conclusions: Differentiation between metastasis-free pancreatic cancer and mass-forming pancreatitis is difficult by FDG-PET/CT due to considerable overlapping between the SUVmax values of the two diseases, although the differential diagnosis may be possible either at the higher range of SUVmax (> 7.7 at 1 hour or >9.98 at 2 hours) for pancreatic cancer or at the lower range of SUVmax (<3.37 at 1 hour or <3.53 at 2 hours) for mass-forming pancreatitis.

Key Words: 18F-FDG PET/CT, pancreatic cancer, mass-forming pancreatitis

A number of earlier reports showed that PET or PET/CT with 18F-FDG (FDG-PET or FDG-PET/CT) was a sensitive and specific noninvasive technique for the diagnosis of pancreatic cancer and was therefore useful in differentiating pancreatic cancer from chronic pancreatitis.[1–8] Previous studies reported the sensitivity and specificity of FDG-PET for detecting pancreatic cancer as being 71%–100% and 64%–90%, respectively.[9] Recently, it was reported that FDG-PET/CT was more sensitive than multidetector row computed tomography (MDCT) and MRI in the diagnosis of both primary pancreatic adenocarcinoma and associated distant metastases, whereas the sensitivity of FDG-PET/CT

was poor in detecting local lymph node metastasis.[10] It was also shown that there were certain limitations to FDG-PET in the diagnosis of pancreatic cancer and that false-negative cases might occur when the tumor was less than 1 cm in diameter.[11] FDG-PET did not detect small-sized islet cell tumors ranging from 1.5 to 8 mm in diameter[12] or hepatic, peritoneal, and other distant metastases of pancreatic cancer that were less than 1 cm in diameter.[13] Besides, it was reported that a delayed FDG-PET scanning at 2 hours postinjection was useful in differentiating between malignant and benign pancreatic lesions in patients in whom routine PET findings obtained at 1 hour were inconclusive.[14]

On the other hand, because FDG is not a tumor-specific substance, accumulation of this tracer could occur in experimentally induced inflammatory lesions in rats.[15] In fact, it was reported that due to the increased glycolytic metabolism in activated leukocytes, patients with abdominal abscesses[16] and sarcoidosis[17] exhibited elevated FDG uptake. Inflammatory pancreatic diseases could give rise to focal FDG uptake in the same intensity range as pancreatic cancer.[18,19] These findings may result in low specificity of FDG-PET in differentiating malignant tumors from benign lesions. Thus, obscure points still remain about the usefulness of FDG-PET in differentiating pancreatic cancer from chronic pancreatitis.

It has been known that chronic pancreatitis clinically presents as a focal tumorous swelling at some stage of the disease process.[20] This feature has been variously called tumor-forming pancreatitis, focal pancreatic mass, pseudotumorous pancreatitis, inflammatory pancreatic mass,[21] or mass-forming pancreatitis.[22] Because this stage of chronic pancreatitis has often been suspected to be a carcinoma, a correct diagnosis in differentiating pancreatic cancer from mass-forming pancreatitis is important to avoid unnecessary operative procedures.[23]

The purpose of this study was to compare the FDG uptake findings of the mass areas in metastasis-free pancreatic cancer and mass-forming pancreatitis and to evaluate the efficacy of FDG-PET/CT for the differential diagnosis between both diseases. To the best of our knowledge, this study is the first large-scale assessment to compare FDG uptake findings in the mass areas in pancreatic cancer and mass-forming pancreatitis.

PATIENTS AND METHODS

Patients

Whole-body FDG-PET/CT was performed in 47 patients with suspected pancreatic tumors and without any detectable metastases, who were referred from the departments of internal medicine and surgery of Nagoya University Hospital between April 2007 and February 2009 (33 men, 14 women; age range, 44–81 years; mean age ± SD, 66 ± 8.6 years), and the corresponding imaging data were evaluated retrospectively. Thirty-three (20 men, 13 women; age range, 48–81 years; mean age ± SD, 66 ± 8.1 years) of the 47 study patients were finally diagnosed as having pancreatic cancer (32 adenocarcinoma and 1 ductal carcinoma) and the other 14 (13 men, 1 woman; age range, 44–79 years; mean age ± SD, 65 ± 9.5 years) had pancreatitis, including 5 cases of autoimmune pancreatitis.[24] In 33 cases of pancreatic cancer, 20 were operated on, 5 were

55 years old male. Pancreatic cancer

Early phase

Delayed phase

Head: SUV mean 4.16, max 9.55   SUV mean 5.81, max 10.27

Kato K, et al. Clin Nucl Med 2013;38(6):417-421.

Tail: SUV mean 3.97, max 6.0   SUV mean 3.98, max 5.76

Mass-forming pancreatitis
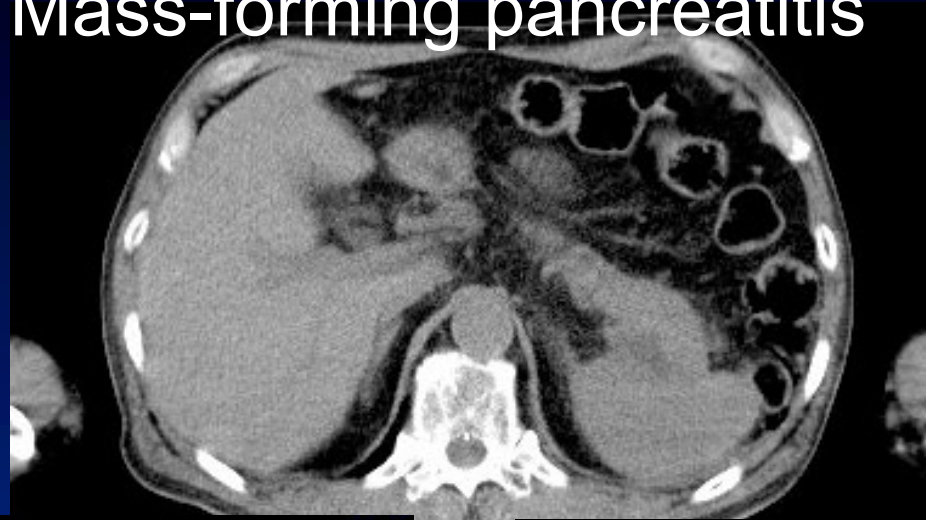
^{18}F-FDG PET/CT
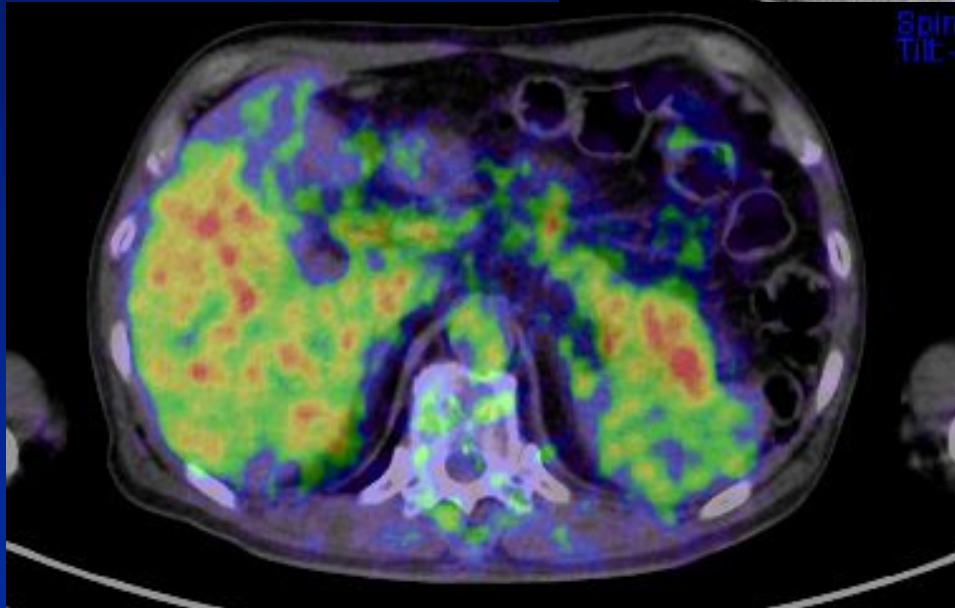
Early phase
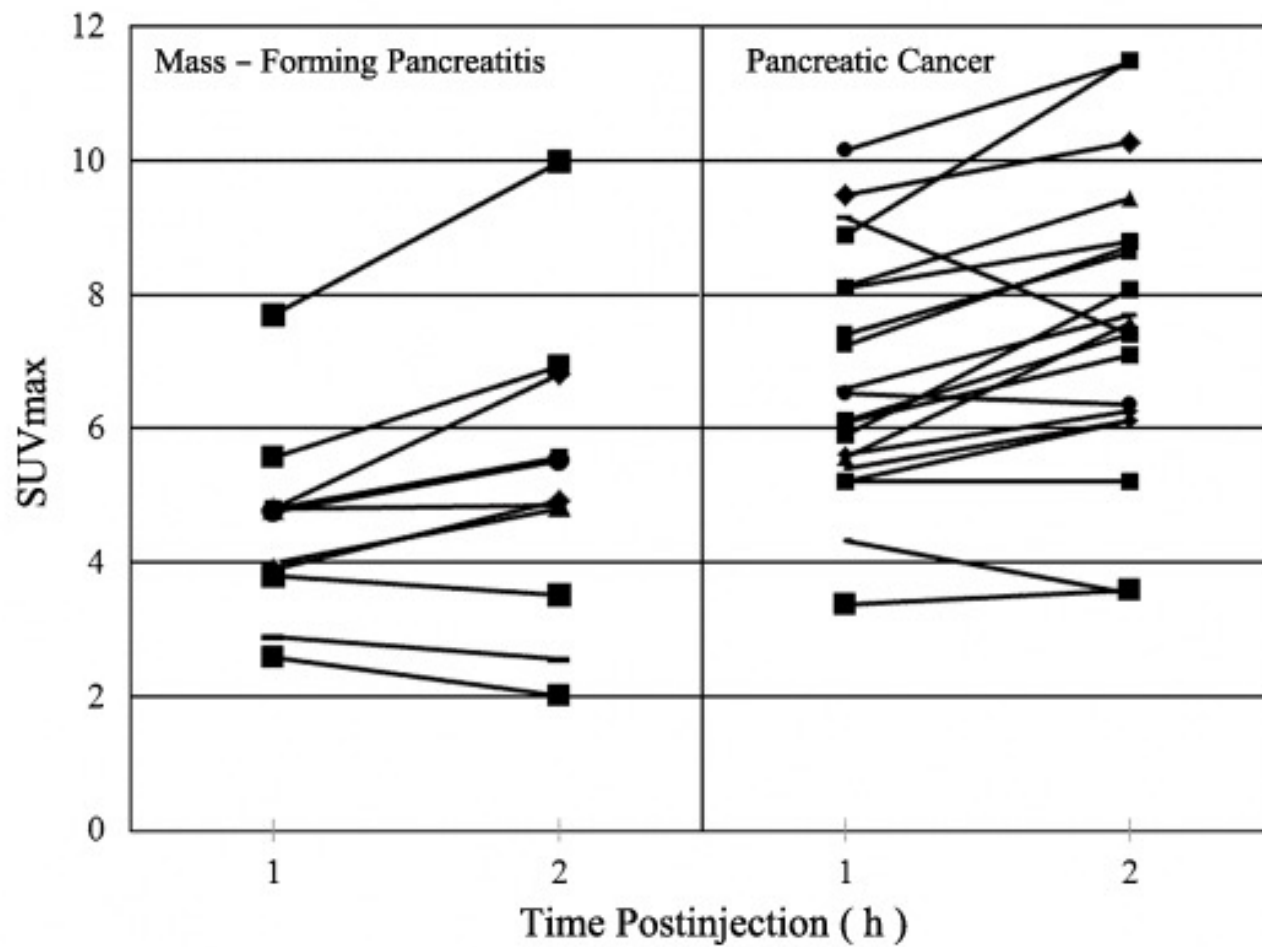SUV mean 3.04, max 4.81
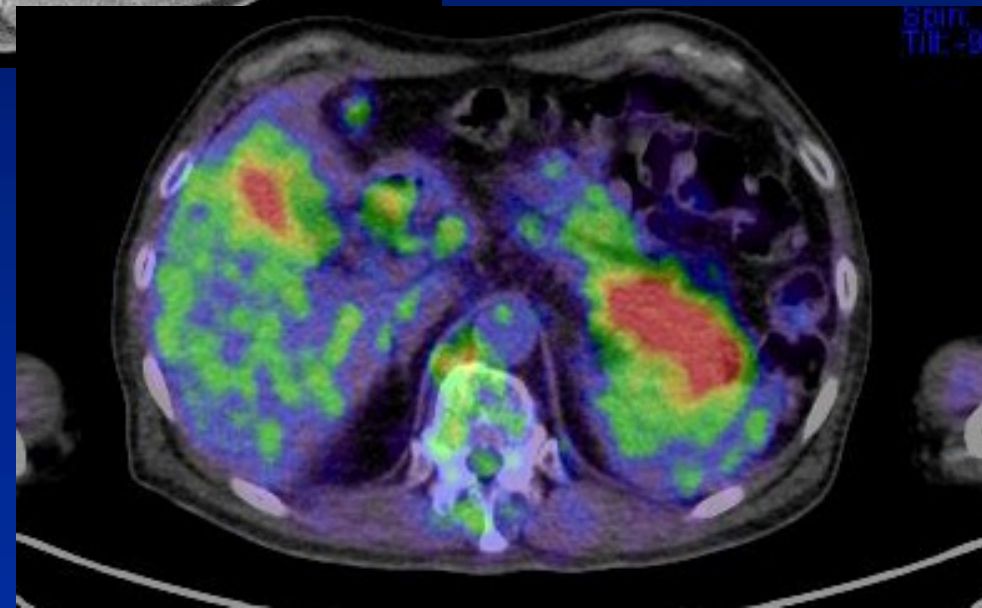
Delayed phase
SUV mean 3.72, max 5.56

Kato K, et al. Clin Nucl Med 2013;38(6):417-421.

FIGURE 1. SUVmax at 1 hour and 2 hours postinjection in metastasis-free pancreatic cancer and mass-forming pancreatitis.

Kato K, et al. Clin Nucl Med 2013;38(6):417-421.

- FDG投与後1hのSUVmaxは、膵癌が腫瘤形成性膵炎より高い。
- 1時間値と2時間値の差も膵癌の方が高い。
- しかし両者にはオーバーラップがあるので鑑別が難しい。
- SUVmax が >7.7 (1 h値) もしくは >9.98 (2 h値) の場合は膵癌、<3.37 (1 h値) もしくは <3.53 (2 h値) の場合は腫瘤形成性膵炎と診断が可能。

Kato K, et al. Clin Nucl Med 2013;38(6):417-421.

Images of a Case of Carney Triad by Combined F-18 FDG PET/CT

Katsuhiko Kato, MD, PhD,* Wataru Koike, MD,† Shingo Iwano, MD, PhD,† Norihiro Usami, MD, PhD,‡ Kohei Yokoi, MD, PhD,‡ Yuichi Ueda, MD, PhD,‡ and Shinji Naganawa, MD, PhD†

Abstract: Carney triad is a very rare condition with gastrointestinal stromal tumor, pulmonary chondroma, and extra-adrenal paragangliomas. We present the images of a patient with the complete triad, including total gastrectomy for gastrointestinal stromal tumor at the age of 13, and a left pneumonectomy for pulmonary chondroma at the age of 15. Results of F-18 FDG PET/CT that was performed at age of 22 for recurrent pulmonary chondroma also demonstrated new lesions in the neck, mediastinum, and abdomen representing extra-adrenal paragangliomas.

Key Words: Carney triad, gastrointestinal stromal tumor (GIST), pulmonary chondroma, extra-adrenal paragangliomas, F-18 FDG PET/CT, I-131MIBG

(*Clin Nucl Med* 2011;36: 698–700)

REFERENCES

1. Carney JA, Sheps SG, Go VL, et al. The triad of gastric leiomyosarcoma, functioning extra-adrenal paraganglioma and pulmonary chondroma. *N Engl J Med*. 1977;296:1517–1518.

2. Carney JA. Gastric stromal sarcoma, pulmonary chondroma, and extra-adrenal paraganglioma (Carney Triad): natural history, adrenocortical component, and possible familial occurrence. *Mayo Clin Proc*. 1999;74:543–552.

3. Lancha C, Diez L, Mitjuvila M, et al. Case of complete Carney's syndrome. *Clin Nucl Med*. 1994;19:1008–1010.

4. Jabbour SA, Miller JL. A case of the Carney triad. *Endocr Pract*. 1999;5:266–268.

5. Wales PW, Drab SA, Kim PC. An unusual case of complete Carney's triad in a 14-year-old boy. *J Pediatr Surg*. 2002;37:1228–1231.

6. Vogl TJ, Lehnert T, Wetter A, et al. Interventional radiology in Carney triad. *Eur Radiol*. 2005;15:833–837.

7. Diment J, Tamborini E, Casali P, et al. Carney triad: case report and molecular analysis of gastric tumor. *Hum Pathol*. 2005;36:112–116.

8. Bümming P, Nilsson B, Sörensen J, et al. Use of 2-tracer PET to diagnose gastrointestinal stromal tumour and pheochromocytoma in patients with Carney triad and neurofibromatosis type 1. *Scand J Gastroenterol*. 2006;41:626–630.

9. Colapinto MN, Weiser WJ. Answer to case of the month #131. Carney triad. *Can Assoc Radiol J*. 2008;59:86–88.

^{18}F-FDG PET   Carny Triad

gastrointestinal stromal tumor, pulmonary chondroma, and extra-adrenal paragangliomas.
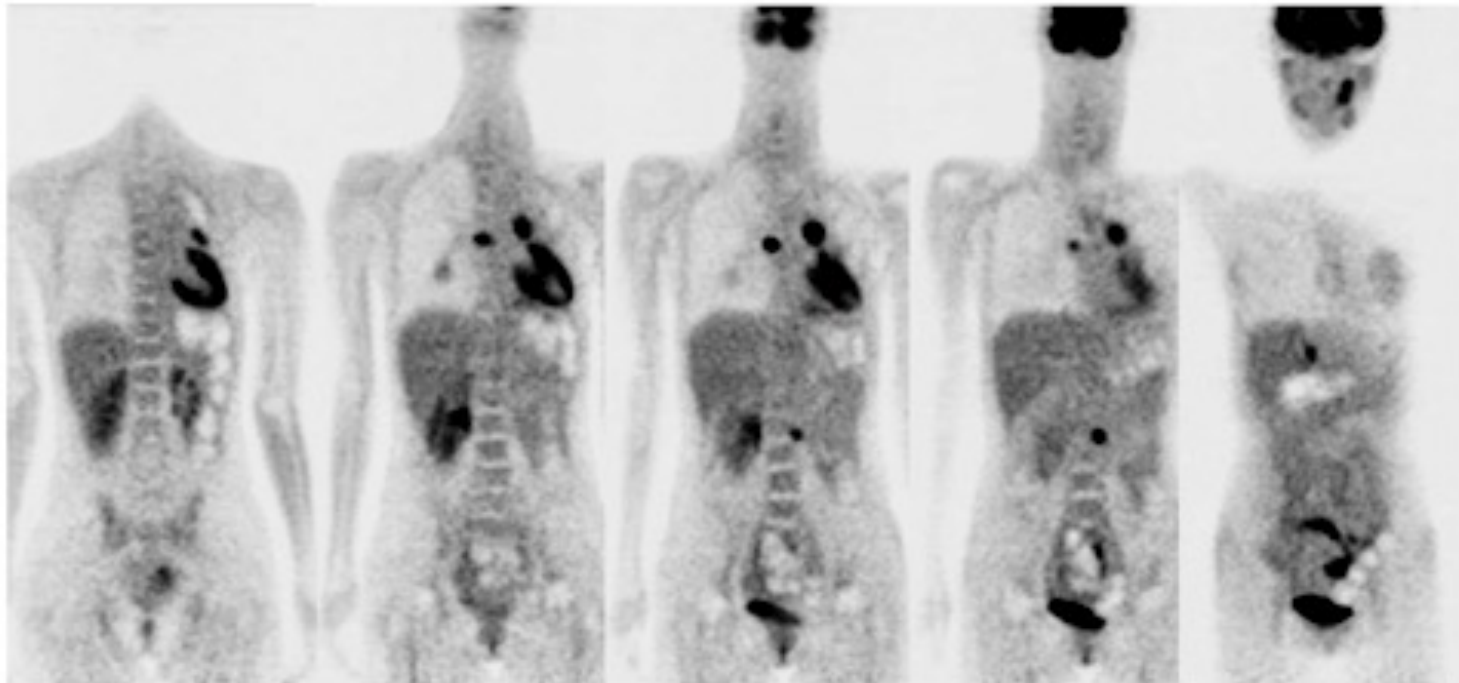
FIGURE 2. Results of F-18 FDG PET/CT (taken on February 10, 2009) revealed a large mass located in the lower lobe of the right lung and multiple masses of left neck, middle mediastinum, and left side of the abdominal aorta (PET and CT imaging was performed using a combined PET/CT system [Biograph Sensation 16; Siemens Medical Solutions]).
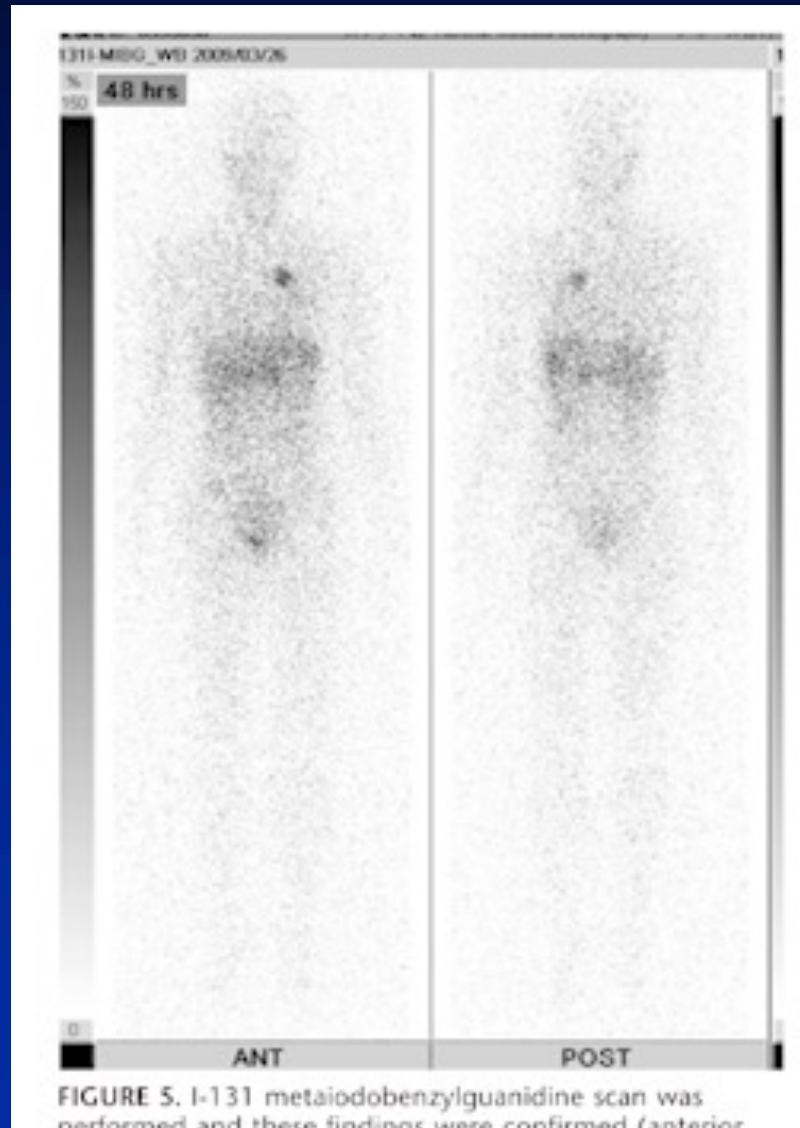
Kato K, et al. Clin Nucl Med 2011;36(8):698-700.

^{131}I-MIBG scintigraphy

FIGURE 5. I-131 metaiodobenzylguanidine scan was performed, and these findings were confirmed (anterior

Kato K, et al. Clin Nucl Med 2011;36(8):698-700.

ORIGINAL ARTICLE

Evaluation of ^{11}C-choline PET/CT for primary diagnosis and staging of urothelial carcinoma of the upper urinary tract: a pilot study

Naoto Sassa · Katsuhiko Kato · Shinji Abe · Shingo Iwano · Shinji Ito ·
Mitsuru Ikeda · Kazuhiro Shimamoto · Seiichi Yamamoto · Tokunori Yamamoto ·
Momokazu Gotoh · Shinji Naganawa

Abstract

Purpose We conducted a pilot study to prospectively evaluate the efficacy of PET/CT with ^{11}C-choline (choline PET/CT) for primary diagnosis and staging of urothelial carcinoma of the upper urinary tract (UUT-UC).

Methods Enrolled in this study were 16 patients (9 men, 7 women; age range 51 – 83 years, mean±SD 69±10.8 years) with suspected UUT-UC. The patients were examined by choline PET/CT, and 13 underwent laparoscopic nephroureterectomy and partial cystectomy. Lymphadenectomy and chemotherapy were also performed as necessary in some of the patients. Of the 16 patients, 12 were confirmed to have UUT-UC (7 renal pelvis carcinoma and 5 ureteral carcinoma), 1 had malignant lymphoma (ureter), 1 had IgG4-related disease (ureter), and 2 had other benign diseases (ureter).

Results Of the 16 study patients, 13 showed definite choline uptake in urothelial lesions, and of these, 11 had UUT-UC, 1 had malignant lymphoma, and 1 had IgG4-related disease.

Three patients without choline uptake comprised one with UUT-UC and two with benign diseases. Of the 12 patients with UUT-UC, 3 had distant metastases, 2 had metastases only in the regional lymph nodes, and 7 had no metastases. Distant metastases and metastases in the regional lymph nodes showed definite choline uptake. The outcome in patients with UUT-UC, which was evaluated 592 – 1,530 days after surgery, corresponded to the patient classification based on the presence or absence of metastases and locoregional or distant metastases. Choline uptake determined as SUVmax 10 min after administration was significantly higher than at 20 min in metastatic tumours of UUT-UC ($p < 0.05$), whereas there was no statistically significant difference between the SUVmax values at 10 and those at 20 min in primary tumours of UUT-UC.

Conclusion This study suggests that choline PET/CT is a promising tool for the primary diagnosis and staging of UUT-UC.

N. Sassa · T. Yamamoto · M. Gotoh
Department of Urology, Nagoya University Graduate School
of Medicine, Nagoya, Japan

K. Kato (✉) · M. Ikeda · K. Shimamoto · S. Yamamoto
Department of Radiological and Medical Laboratory Sciences,
Nagoya University Graduate School of Medicine, 1-20 Daikominami
1-chome, Higashi-ku, Nagoya 461-8673, Japan
e-mail: katokt@med.nagoya-u.ac.jp

S. Abe
Department of Radiological Technology, Nagoya University
Hospital, Nagoya, Japan

S. Iwano · S. Ito · S. Naganawa
Department of Radiology, Nagoya University Graduate School
of Medicine, Nagoya, Japan

Introduction

Urothelial carcinoma of the upper urinary tract (renal pelvis and ureter; UUT-UC) is an infrequent genitourinary malignancy accounting for 5 % of urothelial cancers and less than 10 % of renal tumours [1]. Analysis of epidemiological and survival patterns of UUT-UC over the past 30 years in a review of a large, population-based database in the USA has shown that the incidence of UUT-UC has slowly risen, and that increasing patient age, male gender, Afro-American race,
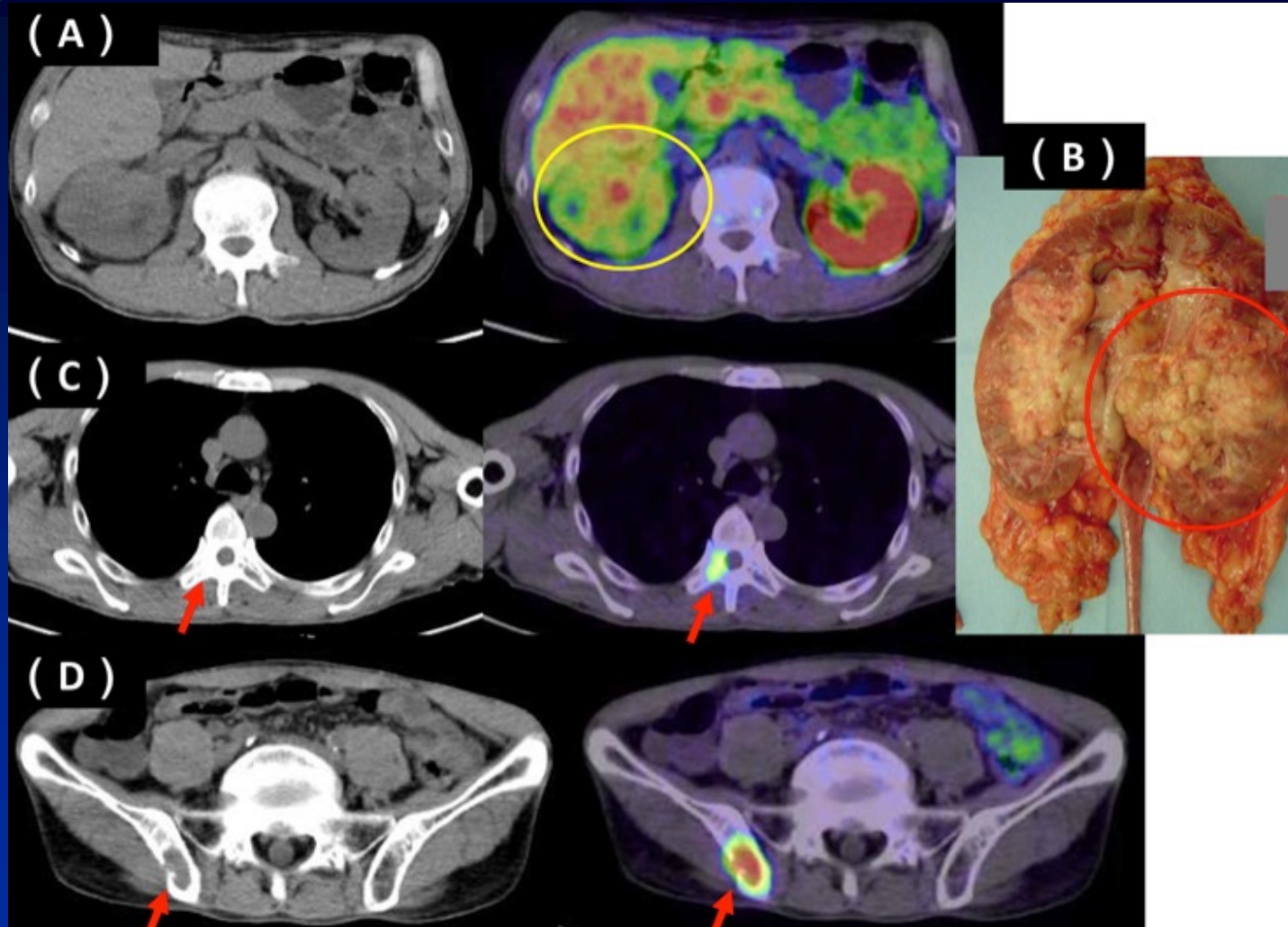
Sassa N, Kato K, et al. Eur J Nucl Med Mol Imaging. 2014;41(12):2232-41.

^{11}C-cholineは^{18}F-FDGが苦手とする尿管、膀胱周辺部の腫瘍の診断に有効

Nagoya University Graduate School of Medicine

右尿管癌

¹¹C-choline PET/CT
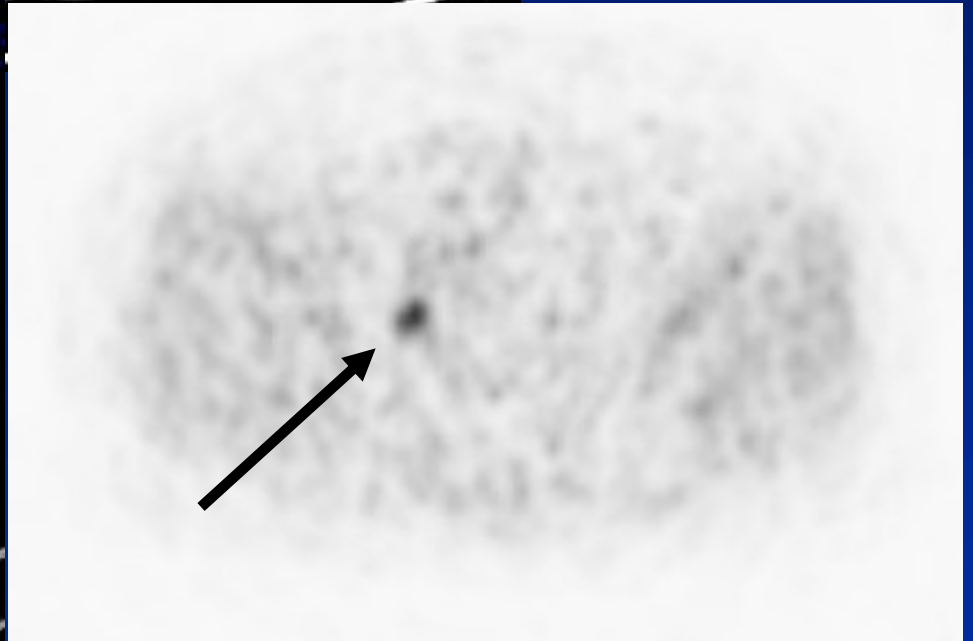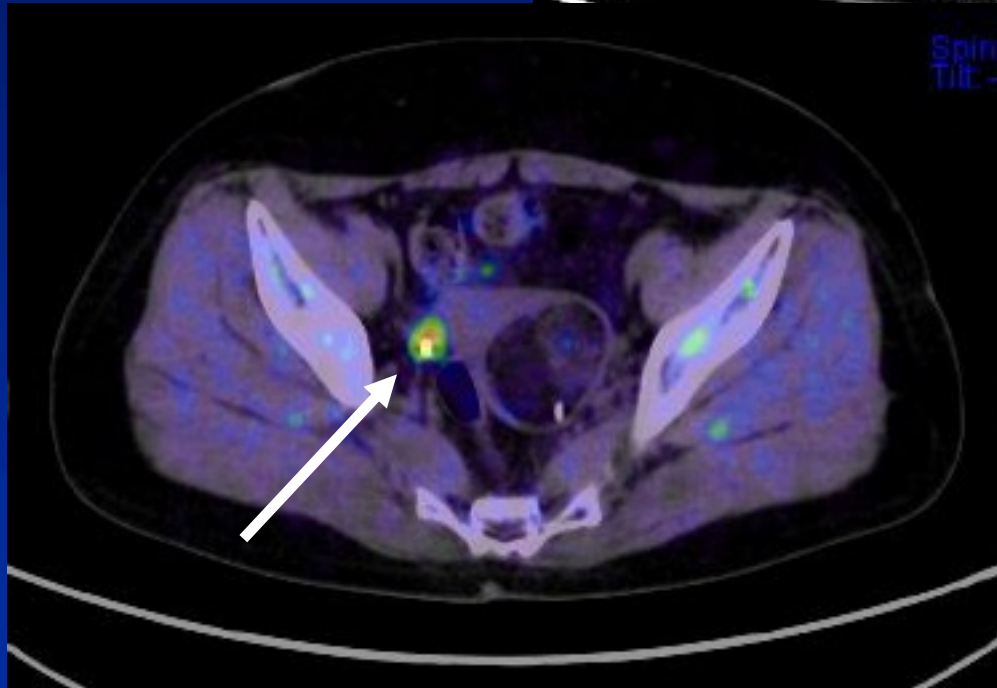
SUVmax 6.28

Sassa N, Kato K, et al. Eur J Nucl Med Mol Imaging. 2014;41(12):2232-41.

TABLE 3

Sensitivity, Specificity, Accuracy, Positive Predictive Value, and Negative Predictive Value of ^{11}C-choline PET/CT in Detection of UUT-UC

Parameter	Value	%
Sensitivity	12[*] / 13[*]	92%
Specificity	2 / 3[**]	67%
Accuracy	14 / 16	88%
Positive predictive value	12[*] / 13[**]	92%
Negative predictive value	2 / 3	67%

* Including malignant lymphoma ;
** Including IgG4-related disease.

Sassa N, Kato K, et al. Eur J Nucl Med Mol Imaging. 2014;41(12):2232-41.

Estimation of ^{123}I-IMP Arterial Blood Activity Using ^{123}I-IMP Acquisition Data From the Lungs and Brain Without Any Blood Sampling

Validation of Its Usefulness for Quantification of Regional Cerebral Blood Flow

Shinji Abe, RT,*† Katsuhiko Kato, MD, PhD,*‡ Yoshitake Takahashi, BPharm,§ Naotoshi Fujita, RT, MS,† Masato Yamashita, RT,† Masaki Shinoda, MT,† Mitsuru Ikeda, MD, PhD,‡ Naotoshi Ohta, MD,¶ Yasukazu Kajita, MD, PhD,‖ and Shinji Naganawa, MD, PhD¶

Objective: The conventional methods for the estimation of regional cerebral blood flow (rCBF) using ^{123}I-labeled N-isopropyl-p-iodoamphetamine (^{123}I IMP) autoradiography (ARG) require continuous or 1-point arterial blood sampling. Patients who need rCBF quantification benefit from the avoidance of arterial puncture. In this study, we attempted to develop a method without any blood sampling to estimate ^{123}I IMP activity in the arterial blood sample at 10 minutes after injection of ^{123}I IMP (Ca10) for the purpose of rCBF quantification. For the evaluation of validity of this method, the mean of rCBFs in various regions of the brain (mean CBF) calculated by ^{123}I IMP ARG method using the estimated Ca10 was compared with that calculated using the Ca10 directly measured with the actual arterial blood sample. Both groups of the mean CBF values were also compared with those measured by O-15 H$_2$O PET ARG method.

Methods: I-123 IMP ARG study was applied to 23 patients, and O-15 H$_2$O PET ARG was applied to 20 patients of them. Dynamic images of the lungs, time series of static images of the brain, and brain SPECT images were acquired after injection of ^{123}I IMP. Arterial blood sampling was done 10 minutes after injection of ^{123}I IMP. Multiple regression analysis was used to estimate Ca10 using 5 parameters from the lung washout counts, time series of brain static counts, and brain SPECT average counts as the explanatory variables and the Ca10 directly measured with the actual arterial blood sample as the objective variable, and the regression equation was calculated.

Results: The regression equation was calculated by multiple regression analysis as follows: Estimated Ca10 = (2.09 × 10^{-2} · LW3) − (2.29 × 10^{-4} · Cb5) − (9.87 × 10^{-3} · Cbpre-SPECT) + (1.06 · CbSPECTav) + (1.03 × 10^{-2} · Cbpost-SPECT) + 165 (counts/s/g), where LW3: lung washout count at 3 minutes after injection, Cb5: brain count at 5 minutes, Cb pre-SPECT: brain count before SPECT, Cb SPECT av: average brain count during SPECT, and Cb post-SPECT: brain count after SPECT. The estimated Ca10 values closely correlated with the directly measured Ca10 values ($r = 0.907$, $P < 0.01$). The mean CBF values (mL/min/100 g) calculated by ^{123}I IMP ARG method using the estimated Ca10 also closely correlated with those calculated using the directly measured Ca10 ($r = 0.818$, $P < 0.01$). The mean
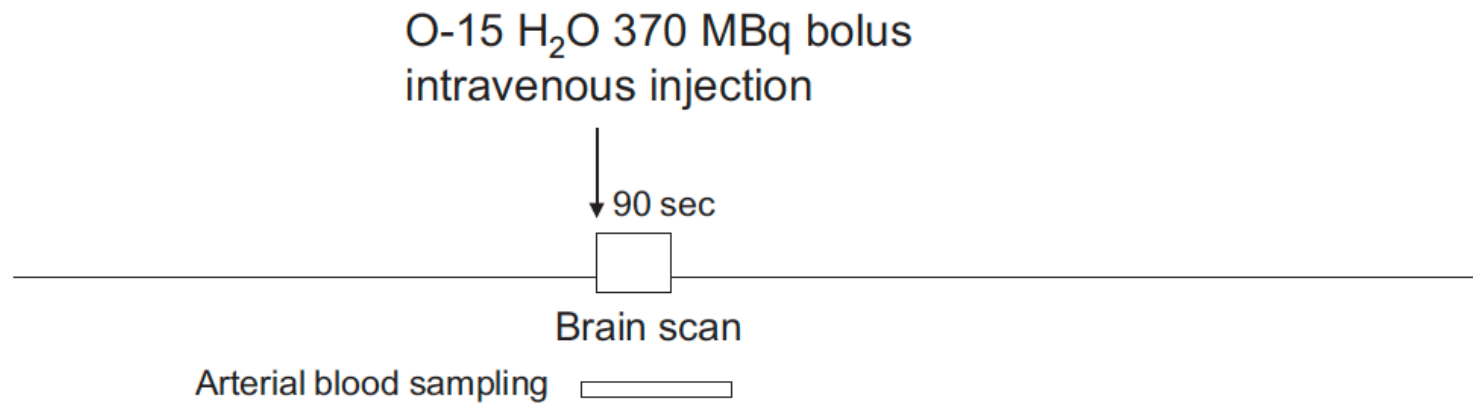
CBF values calculated by the ^{123}I IMP ARG method using either the directly measured or the estimated Ca10 significantly correlated ($r = 0.698$ and 0.590, respectively; $P < 0.01$) with those measured by O-15 H$_2$O PET ARG method.

Conclusions: The ^{123}I IMP arterial blood activity can be estimated reliably without any blood sampling using the ^{123}I IMP acquisition data from the lungs and brain. This method can serve for a convenient and noninvasive rCBF quantification technique instead of the conventional methods requiring arterial blood sampling.

Key Words: cerebral blood flow, ^{123}I IMP, O-15 H$_2$O, SPECT, PET

(Clin Nucl Med 2012;37: 258–263)

The measurement of regional cerebral blood flow (rCBF) is necessary for evaluation of the cerebral circulation in the diagnosis of pathologic changes of the brain. N-isopropyl-p[I-123] iodoamphetamine (^{123}I IMP) has been widely used as a tracer for the measurement of rCBF by SPECT. I-123 IMP has a higher first-pass extraction fraction into the cerebral tissue and negligible back diffusion from there within an early time after injection.[1,2] These characteristics of ^{123}I IMP bring about a good linear correlation between its accumulation into the cerebral tissue and rCBF. Moreover, ^{123}I IMP is one of the most suitable SPECT tracers used for the measurement of rCBF because it excels in the contrast between normal and defective cerebral areas.

In the past few decades, many studies were conducted for rCBF quantification using ^{123}I IMP. Quantification of rCBF using ^{123}I IMP and SPECT based on the microsphere model was performed by Kuhl et al.[1,3] In addition, there were several studies for rCBF quantification using ^{123}I IMP based on the 2-compartment model, the arterial blood as one compartment and the cerebral tissue as the other compartment.[4–8] These quantification methods for rCBF so far reported require continuous or 1-point arterial blood sampling by arterial puncture that is invasive for patients. A simple and reliable quantification method for rCBF using ^{123}I IMP SPECT has been developed by Iida et al (^{123}I IMP autoradiography [ARG] method).[7,8] In this method, continuous arterial blood sampling and measurement of the lipophilic fraction in the blood samples were avoided, but 1-point arterial blood sample is still necessary for determination of the arterial input function for each subject.

Recent studies indicated that rCBF could be calculated using ^{123}I IMP and SPECT with venous blood sampling[9] or without any blood sampling.[10–12] The methods without any blood sampling were based on the microsphere model, and calculated the input function by using dynamic lung images and estimated cardiac output.[10,11] In

Estimation of ^{123}I-IMP Arterial Blood Activity Using ^{123}I-IMP Acquisition Data From the Lungs and Brain Without Any Blood Sampling

Validation of Its Usefulness for Quantification of Regional Cerebral Blood Flow

Shinji Abe, RT,*† Katsuhiko Kato, MD, PhD,*‡ Yoshitake Takahashi, BPharm,§ Naotoshi Fujita, RT, MS,†
Masato Yamashita, RT,† Masaki Shinoda, MT,† Mitsuru Ikeda, MD, PhD,‡ Naotoshi Ohta, MD,¶
Yasukazu Kajita, MD, PhD,‖ and Shinji Naganawa, MD, PhD¶

Objective: The conventional methods for the estimation of regional cerebral blood flow (rCBF) using ^{123}I-labeled N-isopropyl-p-iodoamphetamine (^{123}I IMP) autoradiography (ARG) require continuous or 1-point arterial blood sampling. Patients who need rCBF quantification benefit from the avoidance of arterial puncture. In this study, we attempted to develop a method without any blood sampling to estimate ^{123}I IMP activity in the arterial blood sample at 10 minutes after injection of ^{123}I IMP (Ca10) for the purpose of rCBF quantification. For the evaluation of validity of this method, the mean of rCBFs in various regions of the brain (mean CBF) calculated by ^{123}I IMP ARG method using the estimated Ca10 was compared with that calculated using the Ca10 directly measured with the actual arterial blood sample. Both groups of the mean CBF values were also compared with those measured by O-15 H$_2$O PET ARG method.

CBF values calculated by the ^{123}I IMP ARG method using either the directly measured or the estimated Ca10 significantly correlated ($r = 0.698$ and 0.590, respectively; $P < 0.01$) with those measured by O-15 H$_2$O PET ARG method.

Conclusions: The ^{123}I IMP arterial blood activity can be estimated reliably without any blood sampling using the ^{123}I IMP acquisition data from the lungs and brain. This method can serve for a convenient and noninvasive rCBF quantification technique instead of the conventional methods requiring arterial blood sampling.

Key Words: cerebral blood flow, ^{123}I IMP, O-15 H$_2$O, SPECT, PET

(Clin Nucl Med 2012;37: 258–263)

FIGURE 1. Outlines of the procedure of O-15 H_2O PET ARG method and ^{123}I IMP data acquisition with a gamma camera.

Abe S, Kato K, et al. Clin Nucl Med. 2012;37:258-263
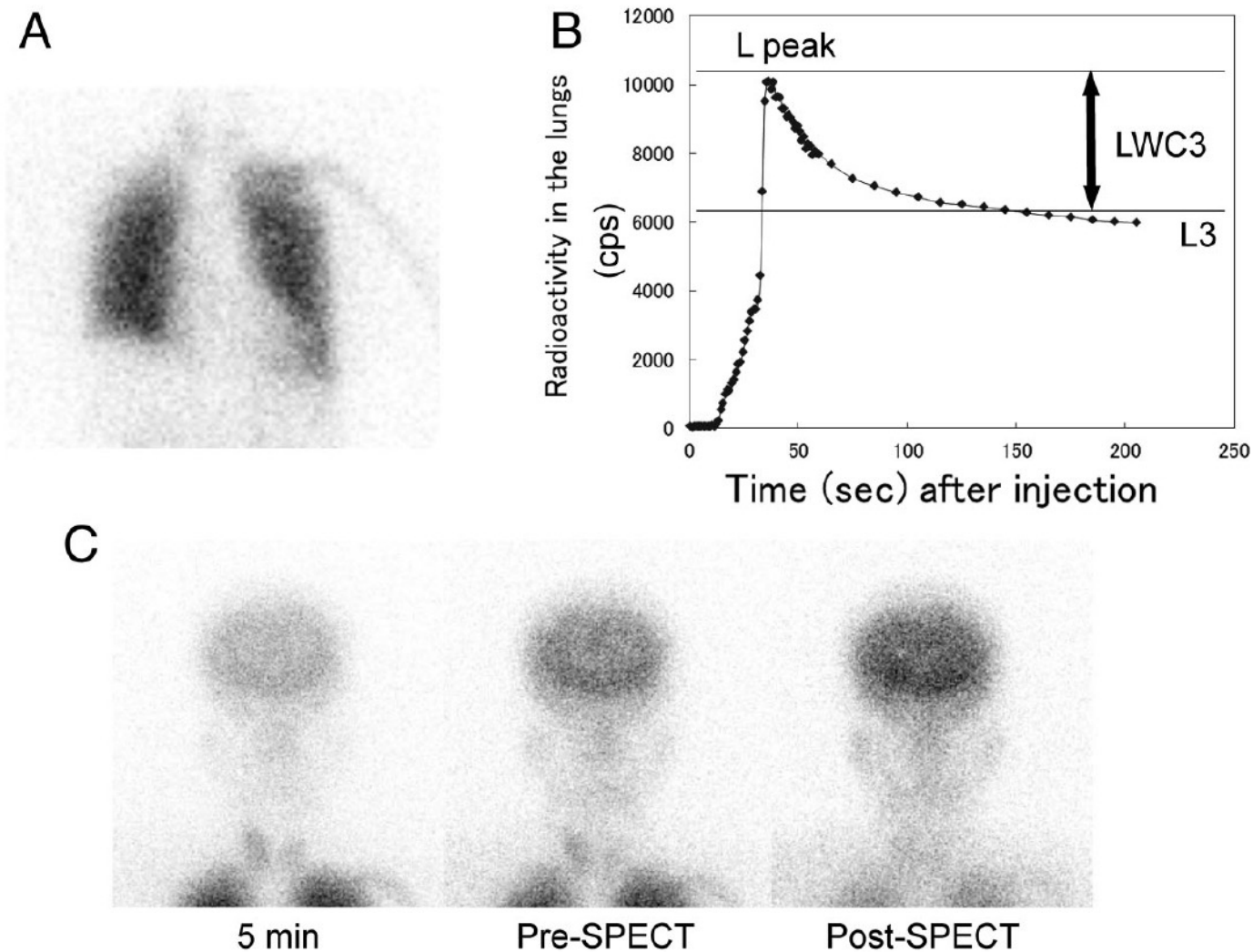
FIGURE 2. Data acquired after intravenous injection of ^{123}I IMP. A, Lung planar image taken at 3 minutes after injection. B, Time course of radioactivity of the lungs after injection. C, Brain static images at 5 minutes, 13 minutes (pre-SPECT), and 45 to 50 minutes (post-SPECT) after injection.

Abe S, Kato K, et al. Clin Nucl Med. 2012;37:258-263
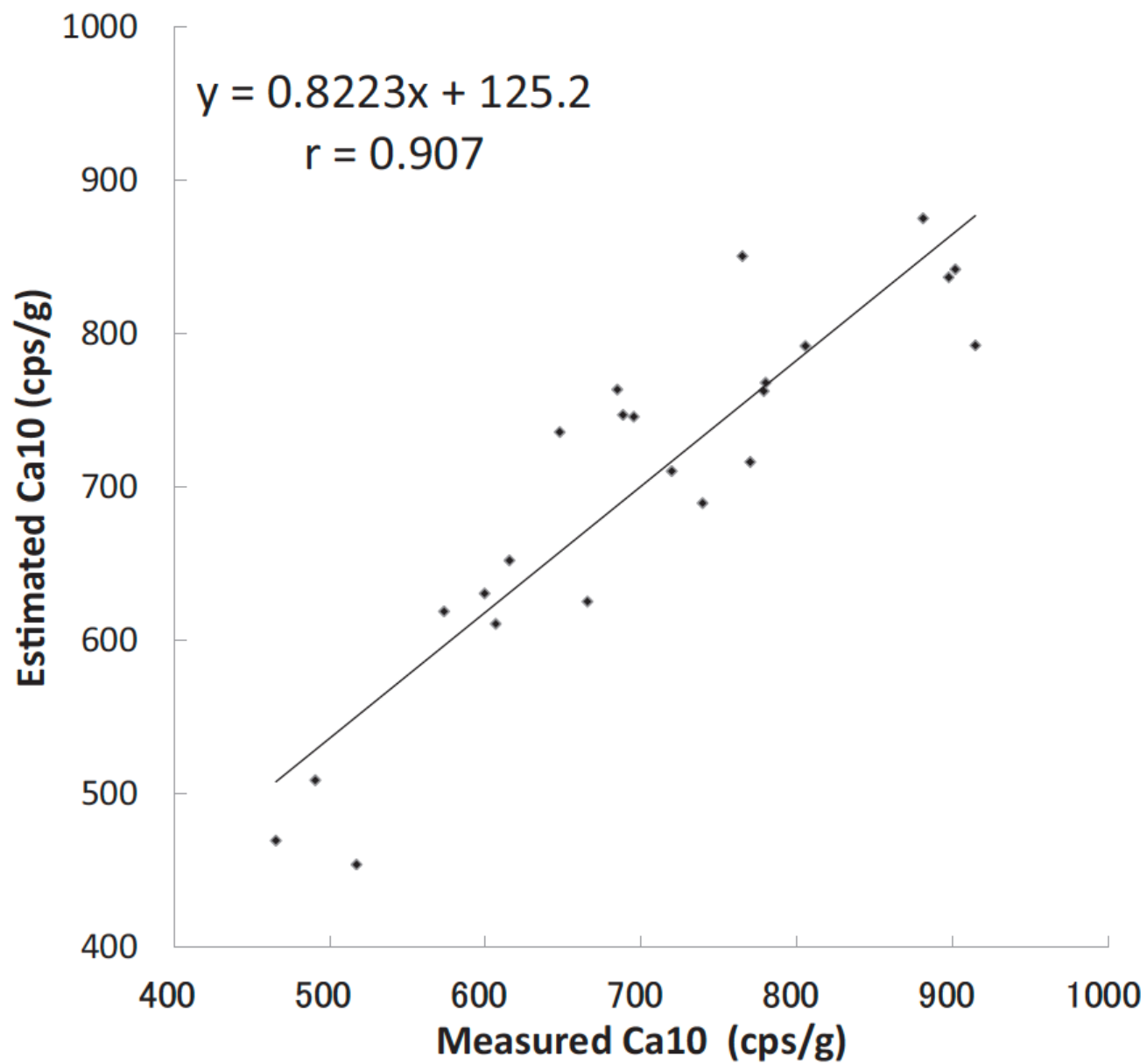
FIGURE 3. Comparison between the estimated Ca10 and the directly measured Ca.

Abe S, Kato K, et al. Clin Nucl Med. 2012;37:258-263
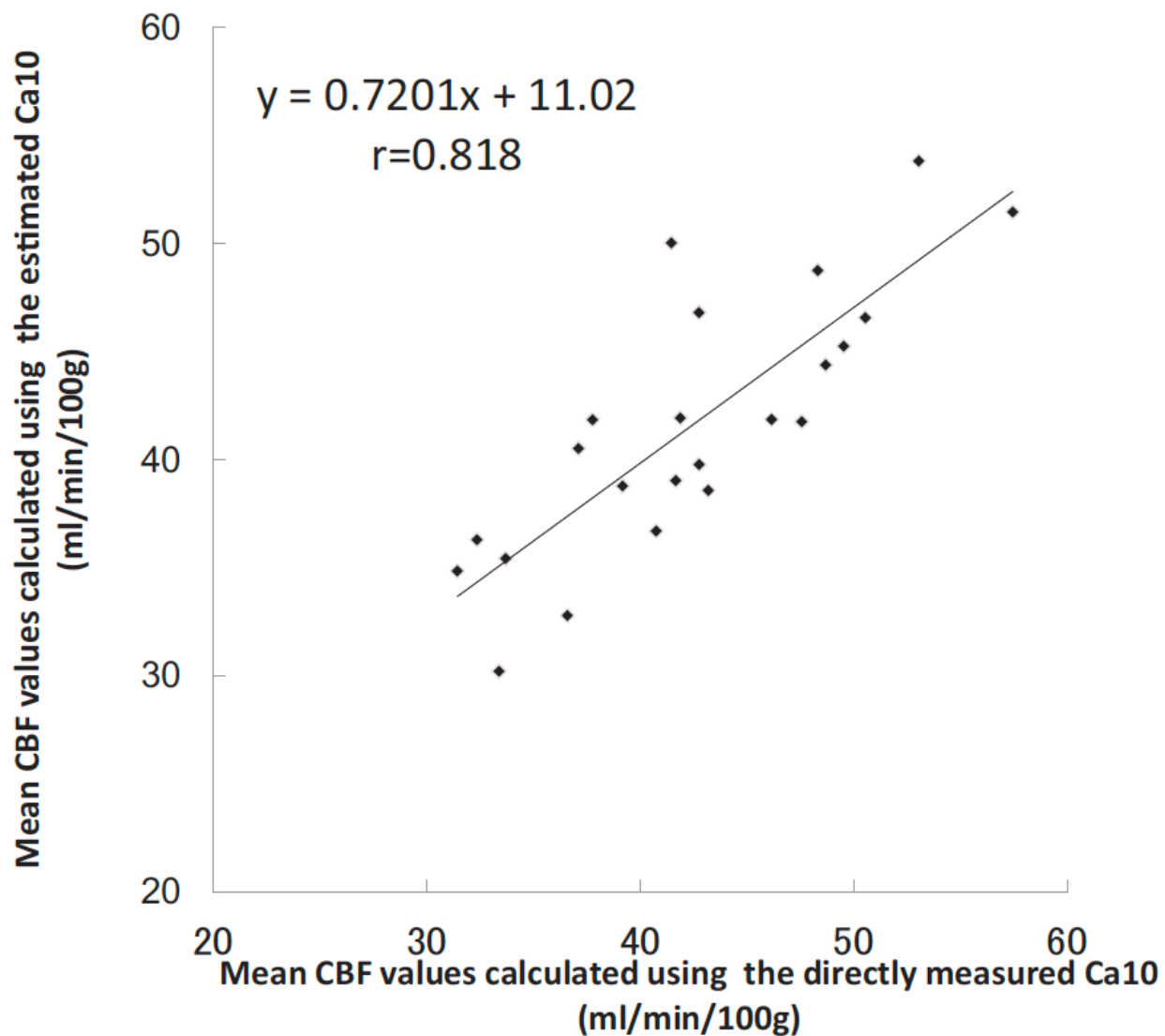
FIGURE 4. Comparison between the mean CBF values calculated using the estimated Ca10 and those calculated using the directly measured Ca10.

Abe S, Kato K, et al. Clin Nucl Med. 2012;37:258-263
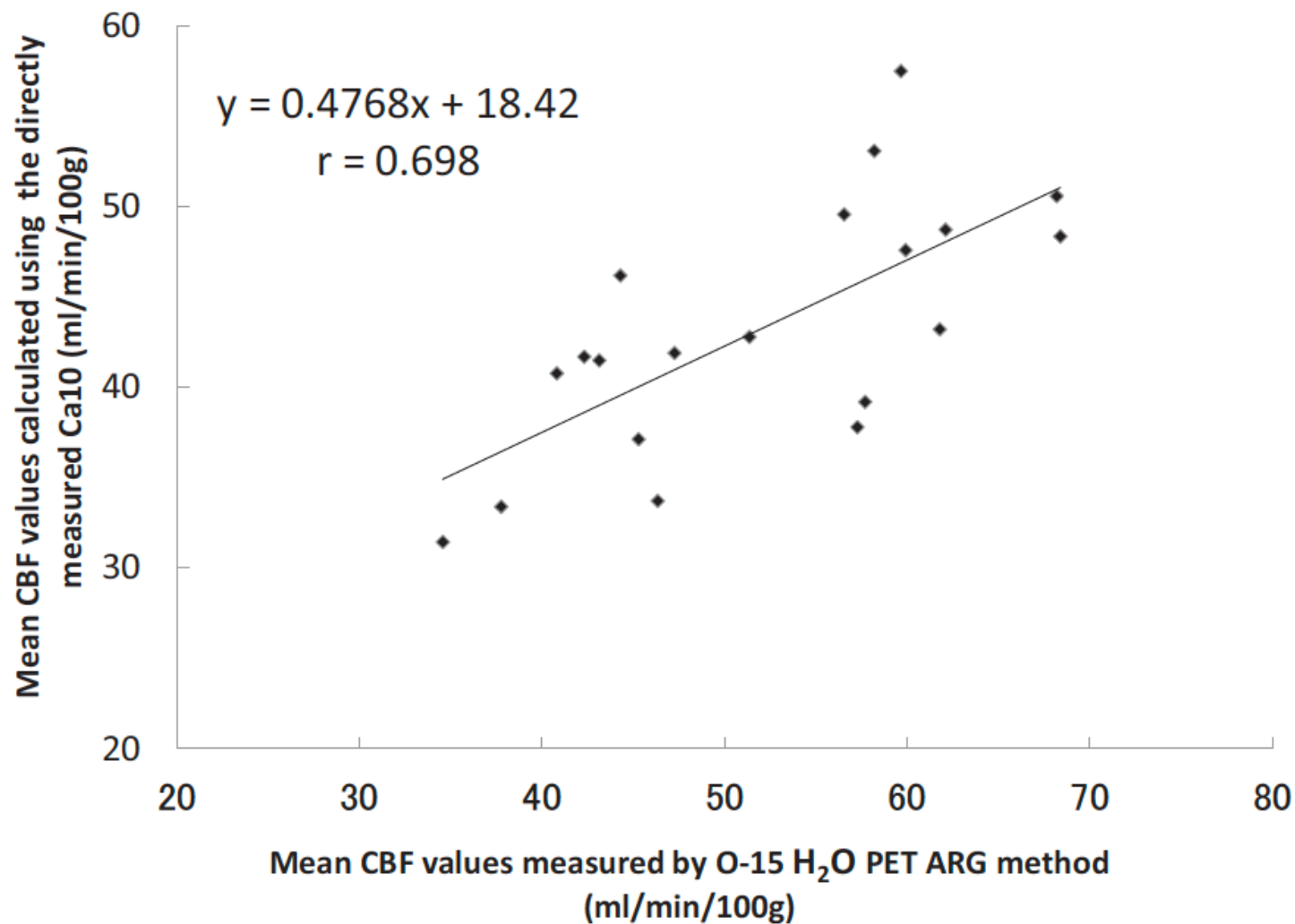
FIGURE 5. Comparison between the mean CBF values calculated by ^{123}I IMP ARG method using the measured Ca10 and those measured by O-15 H_2O PET ARG method.

Abe S, Kato K, et al. Clin Nucl Med. 2012;37:258-263
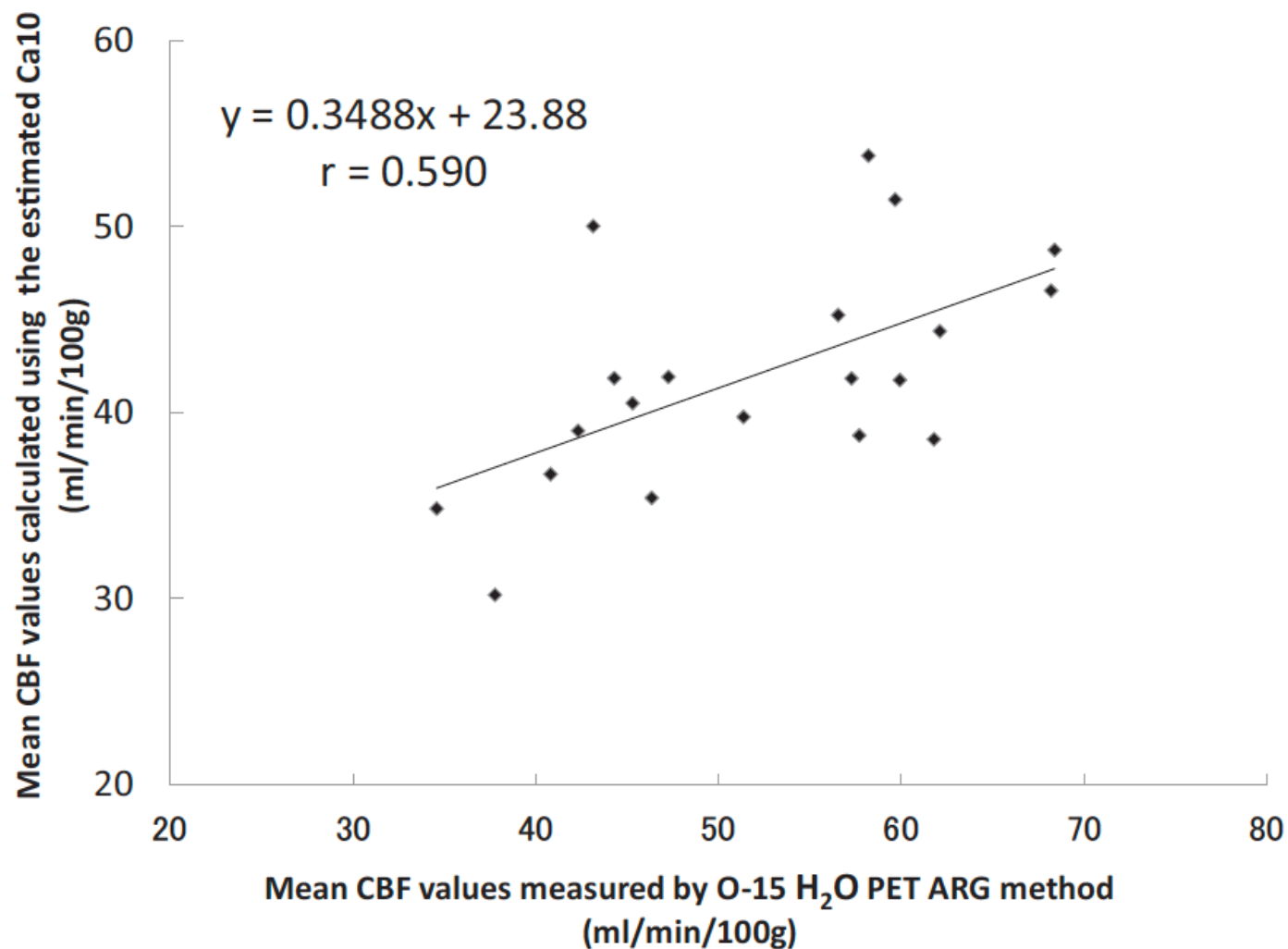
FIGURE 6. Comparison between the mean CBF values calculated by ^{123}I IMP ARG method using the estimated Ca10 and those measured by O-15 H_2O PET ARG method.

Abe S, Kato K, et al. Clin Nucl Med. 2012;37:258-263

Estimation of regional cerebral blood flow using N-isopropyl-p-^{123}I iodoamphetamine acquisition data from the lungs and brain

An improved non-invasive technique

S. Abe[1]; K. Kato[2]; Y. Takahashi[3]; N. Fujita[1]; M. Ikeda[2]; N. Ota[4]; Y. Kajita[5]; S. Yamamoto[2]; S. Naganawa[4]

[1]Department of Radiological Technology, Nagoya University Hospital, Nagoya, Japan; [2]Department of Radiological and Medical Laboratory Sciences, Nagoya University Graduate School of Medicine, Nagoya, Japan; [3]Rikkyo University Graduate School of Sociology, Tokyo, Japan; [4]Department of Radiology, Nagoya University Graduate School of Medicine, Nagoya, Japan; [5]Department of Neurosurgery, Nagoya University Graduate School of Medicine, Nagoya, Japan

Summary

Aim: Previously, we devised a method for estimating ^{123}I labeled N-isopropyl-p-iodoamphetamine (^{123}I IMP) arterial blood activity at 10 minutes after intravenous injection of ^{123}I IMP (Ca10) without any blood sampling using ^{123}I IMP autoradiography (ARG) acquisition data, and verified its usefulness for quantification of regional cerebral blood flow (rCBF). In this study, we attempted to develop an improved noninvasive method for estimating rCBF. **Patients, methods:** ^{123}I IMP studies with 23 patients and ^{15}O-H$_2$O positron emission tomography (PET) ARG studies with 20 patients were evaluated. Multiple regression analysis was used to estimate an integral of the arterial blood counts during the time after injection of ^{123}I ($\int$Ca) using parameters from the time series of the lung counts and brain counts as the explanatory variables and the fraction [brain single-photon emission computed tomography (SPECT) average count / the mean of rCBFs (mean CBF) measured by ^{15}O-H$_2$O PET ARG method] as the objective variable. **Results:** The regression equation was as follows: Estimated $\int$Ca = $(7.09\times10^{-3}\cdot\mathrm{Cb}12) - (1.57\times10^{-4}\cdot\mathrm{CbpreSPECT}) + (9.48\times10^{-5}\cdot\mathrm{CbpostSPECT}) + (1.35\times10^{-4}\cdot\mathrm{L}15) - (6.95\times10^{-4}\cdot\mathrm{L}33) + (7.61\times10^{-4}\cdot\mathrm{L}81) - (0.417)$, where Cb12: brain count at 12 minutes, Cbpre-SPECT: brain count before SPECT, Cbpost-SPECT: brain count after SPECT, L15, L33, and L81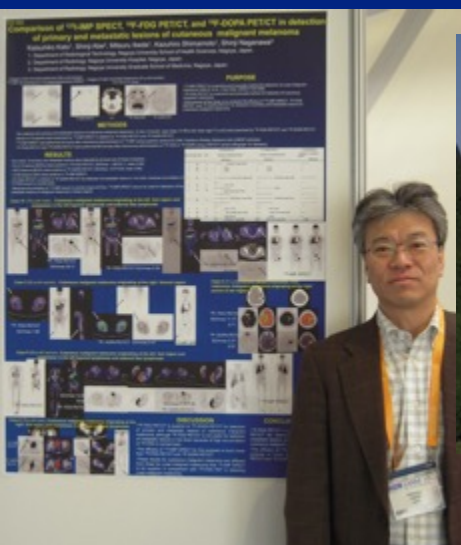: lung count at 15, 33, and 81 seconds, respectively. The mean CBF values (ml/min/100g) calculated using the estimated $\int$Ca values more closely correlated with those measured by ^{15}O-H$_2$O PET ARG method ($r = 0.833$, $p < 0.01$) than those obtained by our previous method ($r = 0.590$, $p < 0.01$). **Conclusion:** The rCBFs obtained by this method approximated more accurately to the values measured by ^{15}O-H$_2$O PET ARG method than those obtained by our previous method.

Correspondence to
Katsuhiko Kato, M.D., Ph.D.
Department of Radiological and Medical Laboratory Sciences, Nagoya University Graduate School of Medicine, 1–20, Daikominami 1-chome, Higashi-ku, Nagoya 461–8673, Japan
Tel. +81/52/719–1590; Fax +81/52/719–1589
E-mail: katokt@med.nagoya-u.ac.jp

Zusammenfassung

Ziel: In einer früheren Arbeit wurde eine Methode vorgestellt, ohne Blutentnahmen die Aktivität von ^{123}I-markiertem N-Isopropyl-p-Iodamphetamin (^{123}I-IMP) im arteriellen Blut 10 Minuten nach intravenöser Injektion abzuschätzen (Ca10), und deren Nutzen zur Quantifizierung des regionalen zerebralen Blutflusses (rCBF) mittels ^{123}I-IMP-Autoradiographie (ARG) verifiziert. In dieser Studie wurde versucht, eine verbesserte, nicht-invasive Methode zur Schätzung des rCBF zu entwickeln. **Patienten, Methoden:** Untersuchungen mit ^{123}I-IMP an 23 Patienten und ^{15}O-H$_2$O-Positronenemissionstomographie (PET) ARG an 20 Patienten wurden evaluiert. Zur Abschätzung des Zeitintegrals der Zählrate im arteriellen Blut ($\int$Ca) nach Injektion von ^{123}I wurde eine multiple Regressionsanalyse durchgeführt. Dabei wurden Parameter aus den Aufnahmeserien über der Lunge und dem Gehirn als erklärende Variablen verwendet. Zielvariable war der Quotient aus der durchschnittlichen Zählrate des Gehirns in der Einzelphotonen-Emissionscomputertomographie (SPECT) und dem Mittelwert der rCBFs (mittlerer CBF) gemessen mittels ^{15}O-H$_2$O-PET-ARG. **Ergebnisse:** Die Regressionsgleichung lautete: geschätztes $\int$Ca = $(7,09\times10^{-3}\cdot\mathrm{Cb}12) - (1,57\times10^{-4}\cdot\mathrm{Cbpre\text{-}SPECT}) + (9,48\times10^{-5}\cdot\mathrm{CbpostSPECT}) + (1,35\times10^{-4}\cdot\mathrm{L}15) - (6,95\times10^{-4}\cdot\mathrm{L}33) + (7,61\times10^{-4}\cdot\mathrm{L}81) - (0,417)$. Dabei ist Cb12 die Zählrate für das Gehirn 12 Minuten p. i., Cbpre-SPECT und Cbpost-SPECT sind die

Estimation of regional cerebral blood flow using ^{123}I-IMP without any blood sampling: A new method that can be the substitution of ^{15}O-water PET autoradiography method

Shinji Abe[1) 2)], Katsuhiko Kato[3)], Yoshitake Takahashi[4)], Masato Yamashita[1)], Naotoshi Fujita[1)], Naotoshi Ohta[5)], Masanori Tadokoro[6)], Yasukazu Kajita[7)], Shinji Naganawa[5)].

1) Department of Radiological Technology, Nagoya University Hospital
2) Department of Radiological Technology, Nagoya University Graduate School of Medicine
3) Department of Radiological Technology, Nagoya University School of Health Sciences
4) Department of Medical Engineering, Division of Allied Health Sciences, Osaka University Medical School
5) Department of Radiology, Nagoya University Graduate School of Medicine
6) Fujita Health University School of Health Science, Toyoake, JAPAN.
7) Department of Neurosurgery Nagoya University, Graduate School of Medicine, Nagoya, Japan.

EANM 2011

O-15 H$_2$O PET Scan

O-15 H$_2$O 370 MBq bolus
intravenous injection

90 sec

Brain scan

Arterial blood sampling

I-123 IMP data acquisition
with gamma camera

IMP 222 MBq
intravenous injection

5 min   12 min 13 min   45-50 min

3 min   1 min 10 sec 1 min   30 min   1 min

Lung dynamic
image

Brain dynamic and
static image (5 min
and Pre-SPECT)

Brain SPECT   Brain static image
(Post-SPECT)

Fig. 1
Outlines of the pro-
cedures of ^{15}O H$_2$O
PET ARG method and
^{123}I IMP data acquisi-
tion with gamma
camera
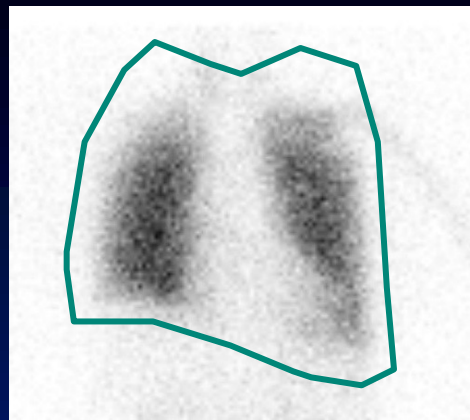
Lung planar image taken at approximately 3 min after injection

LW3:
Lung washout count at 3 min after injection

L15-150
Lung count after injection

L15   L33   L58   L81   L150
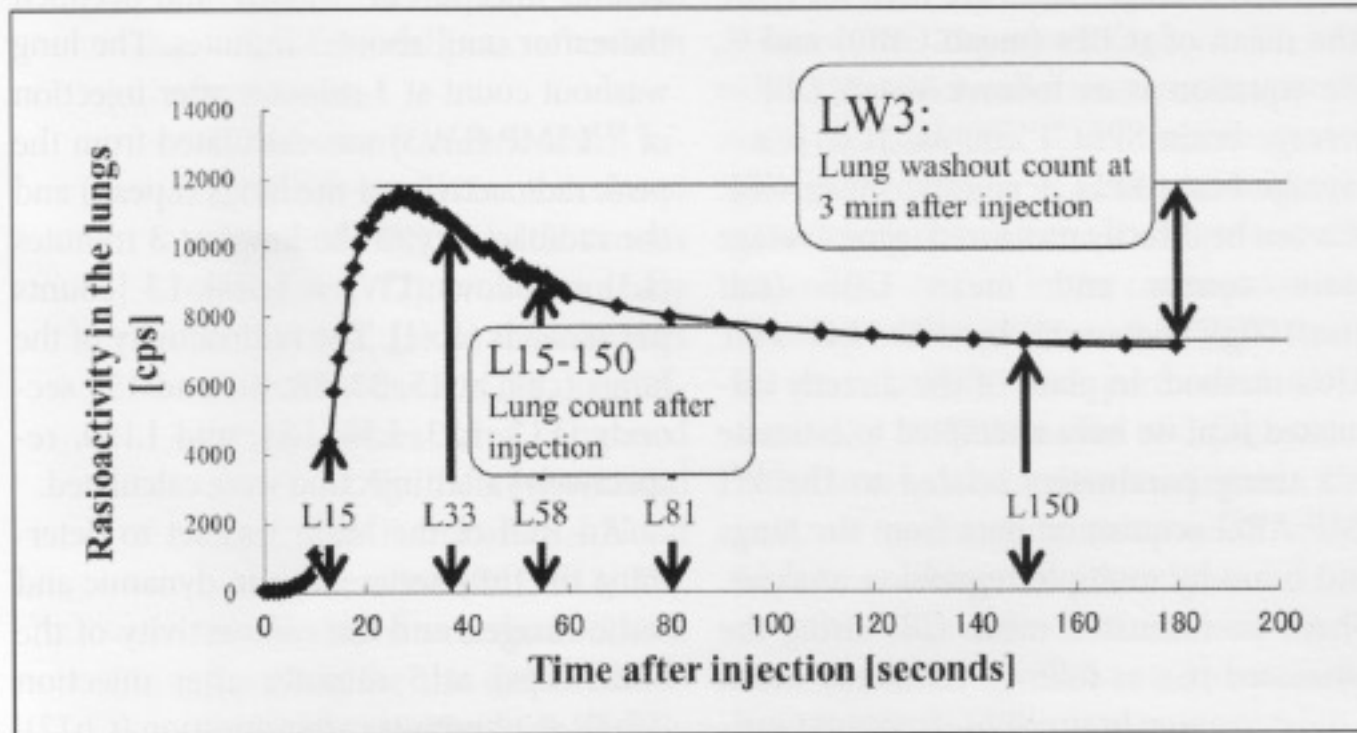
Fig. 2   Time course of the radioactivity of the lungs after intravenous injection of ^{123}I IMP

Abe S, Kato K, et al. Nuklearmedizin. 2014;53:221-226.

Brain static images

| 5 min | 12 min | 13 min | 48 min |
| Cb 5 | Cb 12 | Cb pre-SPECT | Cb post-SPECT |

Abe S, Kato K, et al. Nuklearmedizin. 2014;53:221-226.
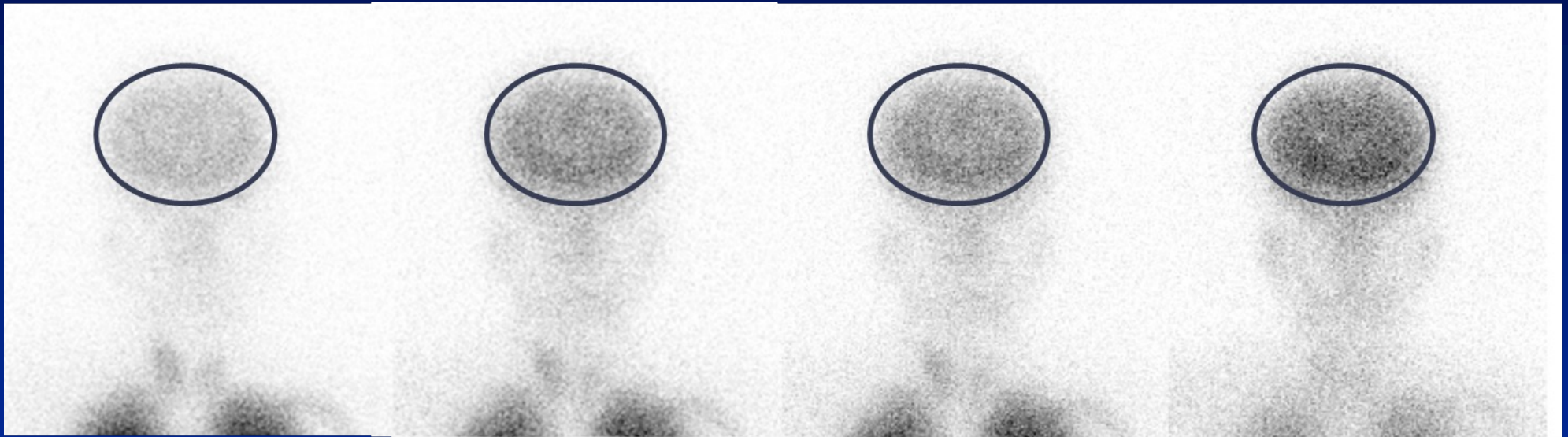
Multiple regression analysis

Explanatory variables

LW3: Lung washout count at 3 min after injection

L15: Lung count at 15 sec after injection

L33: Lung count at 33 sec after injection

L58: Lung count at 58 sec after injection

L81: Lung count at 63 sec after injection

L150: Lung count at 133 sec after injection

Cb5: Brain count at 5 min

Cb12: Brain count at 12 min

Cbpre-SPECT: Brain count before SPECT

Cbpost-SPECT: Brain count after SPECT

Objective variable

$F(x)$ = SPECT average counts / PET CBF

Abe S, Kato K, et al. Nuklearmedizin. 2014;53:221-226.

$$y = 0.7749x + 1.4661$$
$$r = 0.880$$
$$n = 20$$
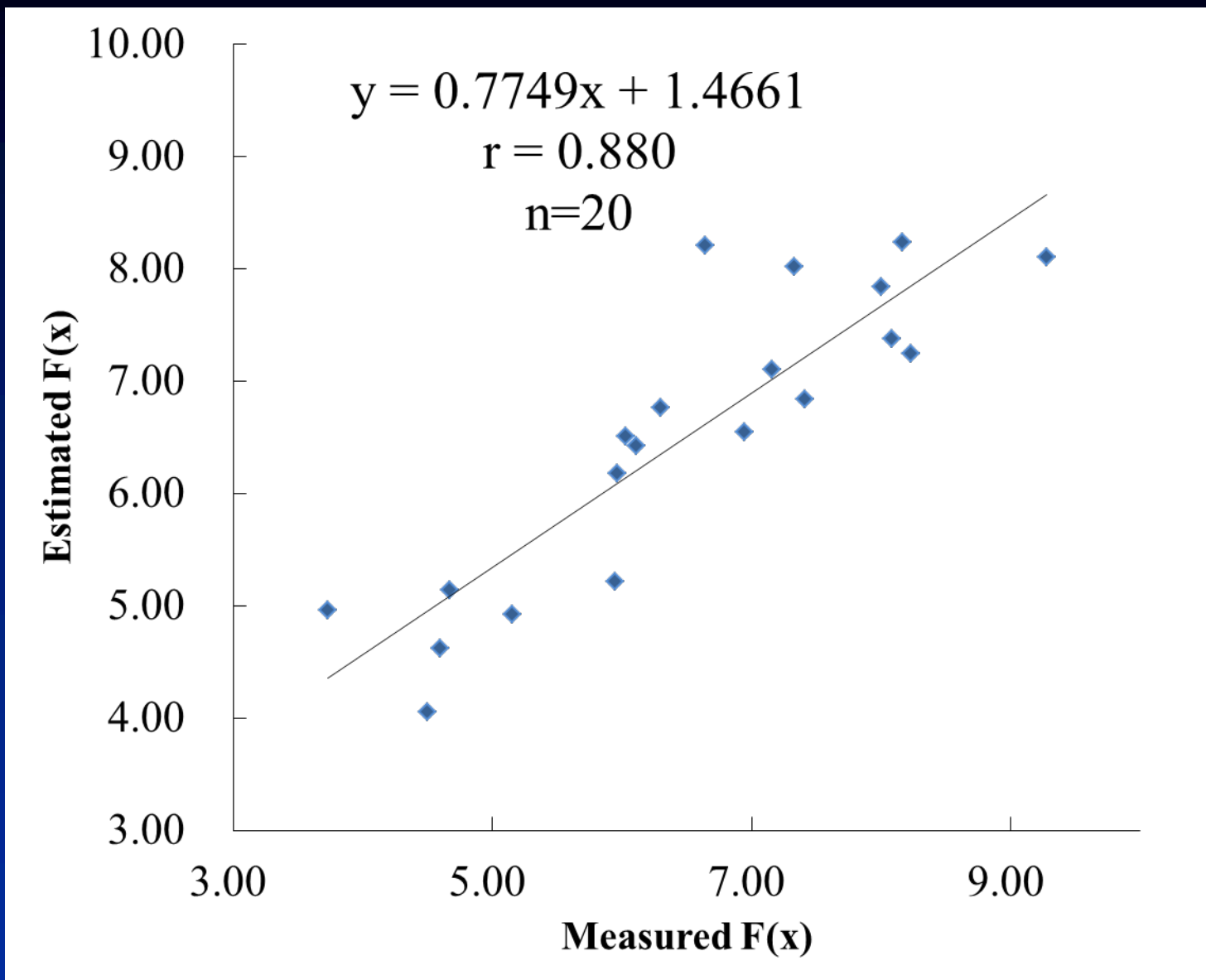
Estimated F(x) = $-1.57 \times 10^{-4} \cdot$ CbpreSPECT $+ 9.48 \times 10^{-5} \cdot$ CbpostSPECT $+ 1.35 \times 10^{-4} \cdot$ L15 $- 6.95 \times 10^{-4} \cdot$ L33 $+ 7.61 \times 10^{-4} \cdot$ L81 $+ 7.09 \times 10^{-3} \cdot$ Cb12 $- 0.417$

Abe S, Kato K, et al. Nuklearmedizin. 2014;53:221-226.

Abe S, Kato K, et al. Nuklearmedizin. 2014;53:221-226.
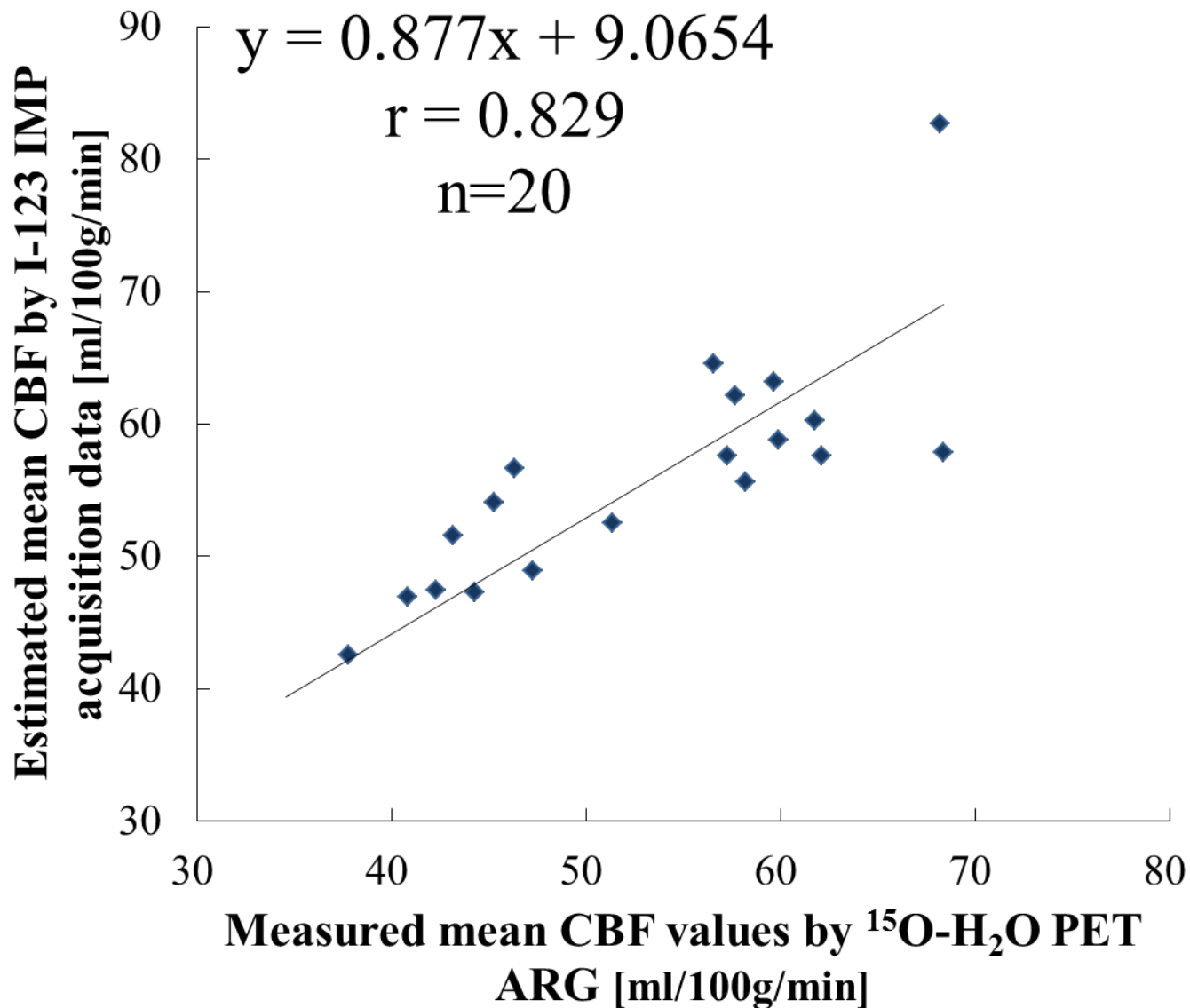
2010 EANM Wien
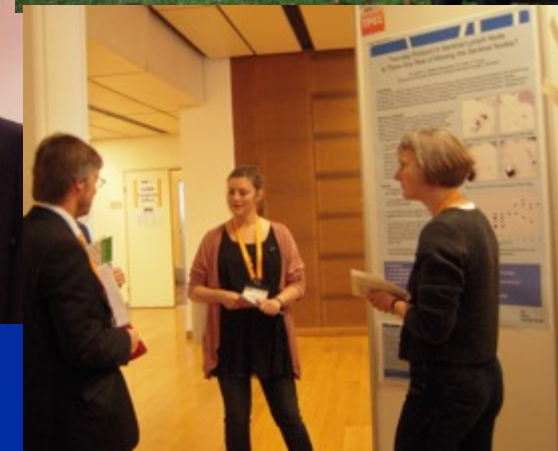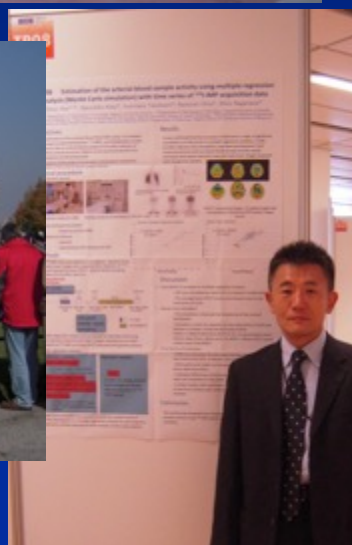
2011 EANM Birmingham

2011 RSNA Chicago
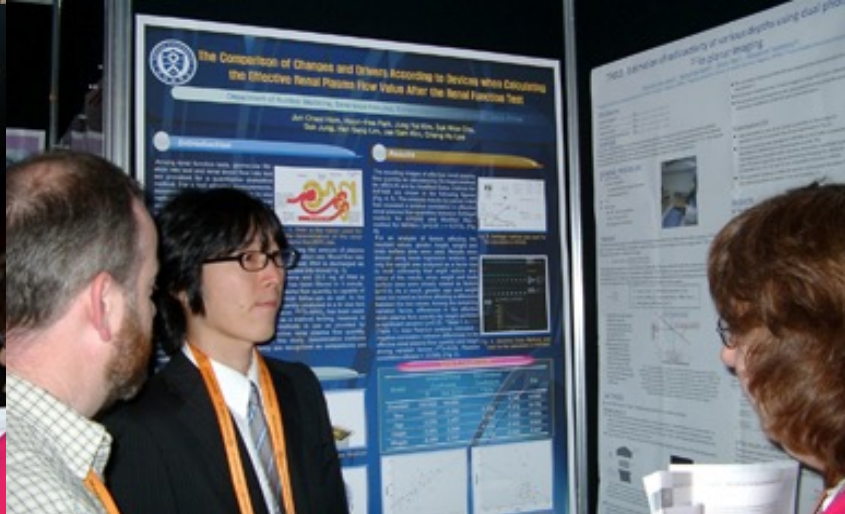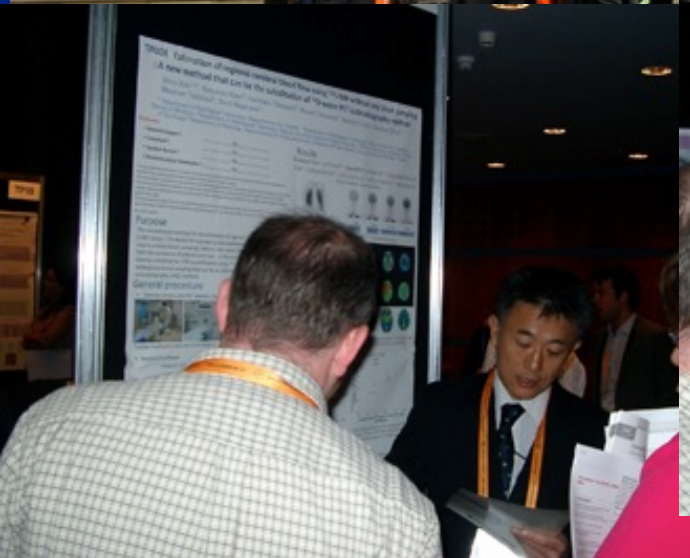
TP55 The validity of the newly developed noninvasive method for estimating cerebral blood flow using ^{123}I-IMP acquisition data from the lungs and brain

Yusuke Fujita[1], Shinji Abe[2], Tetsuro Odagawa[1], Arisa Niwa[1]
Saki Tsuchiya[1], Naotoshi Fujita[2], Hidetaka Kono[2], Kastuhiko Kato[1]

[1]Department of Radiological and Medical Laboratory Sciences, Nagoya University Graduate School of Medicine, Nagoya, Japan
[2]Departoment of Radiological Technology, Nagoya University Hospital, Nagoya, Japan

Background

· The ^{123}I-IMP autoradiography (ARG) method[*1] has been well used for quantification of the cerebral blood flow (CBF).This method requires the ^{123}I-IMP activity in the arterial blood sample obtained by arterial puncture at 10 min after IMP injection (Ca10). Arterial puncture is invasive and burden for patients.

[*1] Iida H, Itoh H, Nakazawa M, et al. Quantitative mapping of regional cerebral blood flow using iodine-123-IMP and SPECT. J Nucl Med 1994; 35:2019-2030.

· Previously, we devised a method for estimating Ca10 using multiple regression analysis without any blood sampling and proposed the noninvasive ARG method for quantification of CBF (the previous method)[*2] . There is a significant correlation between the CBF values obtained by the previous method and those obtained by the ^{15}O-PET method. The previous method does not require any blood sampling, but it needs 5 parameters from ^{123}I-IMP acquisition data.

[*2] Abe S, Kato K, Takahashi Y, et al. Estimation of I-123 IMP arterial blood activity using I-123 IMP acquisition data from the lungs and brain without any blood sampling. Clin Nncl Med 2012; 37:258-263.

· Then we developed a noninvasive method for the estimation of an integral of arterial blood counts of ^{123}I-IMP injection (∫Ca) using 6 parameters from the ^{123}I-IMP acquisition data. The CBF values calculated using the estimated ∫Ca closely correlated with those measured by the ^{15}O-PET method[*3]

[*3] Abe S, Kato K, Takahashi Y, et al. Estimation of regional cerebral blood flow using N-isopropyl-p-[123I] iodoamphetamine acquisition data from the lungs and brain. An improved non-invasive technique. Nuklearmedizin. 2014;53(6)

Purpose

· Recently we devised a more simplified method for estimating Ca10 (this method).
The purpose of this study is to evaluate the clinical usefulness of this method for quantification of CBF.

Patients

· Consecutive 134 patients underwent brain SPECT for ^{123}I-IMP ARG method for quantification of CBF in Nagoya University Hospital between April 2012 and February 2014.

The study was performed according to the approval of the Ethics Committee of Medicine at Nagoya University for Human studies. (No. 13-318)

Outline of this study

I. Calculate the regression equation for estimating Ca10 using multiple regression analysis in 35 patients.
II. Calculate the estimated Ca10 by applying the regression equation to the other 99 patients.
III. Calculate the mean CBF values using the estimated Ca10 (mean CBF: the average value of regional CBFs calculated by 3D-SRT).
IV. Compare between the mean CBF values calculated using the estimated Ca10 and those calculated using the measured Ca10 in each patient group.

Materials

· Gamma camera: Symbia-T (Siemens)
    · Collimator: Low medium energy general purpose (LMEGP)
    · Analysis software: syngo MI Applications VA60A
· Auto-well counter: AccuFLEX γ7000 (Aloka)
· 3D-auto ROI analysis software three-dimensional stereotaxic ROI template (3D-SRT) (Fuji Film RI Pharma)

Fujita Y, et al. EANM'14, Gothenburg, Sweden.

Nagoya University Graduate School of Medicine

Table 1 Profile of patients examined for calculating the regression equation to estimated Ca10

Patients	Age range (mean ± SD) years	Male /female	Number
Parkinson's disease	55-80 (69.13 ± 7.31)	10/13	23
Common or internal carotid artery occlusion or stenosis	21-77 (58.80 ± 21.74)	4/1	5
Moyamoya disease	17-45 (31 ± 19.80)	0/3	2
Cerebral infraction	42 (42 ± 0.00)	3/0	3
Common carotid artery dissection	65	1/0	1
Middle cerebral artery stenosis	77	1/0	1
Total	17-80 (62.76 ± 15.32)	19/16	35

Fig.1 Outline of the procedure of ^{123}I-IMP data acquisition in this method

123I-IMP(167MBq) IV injection — One- point arterial blood sampling at 10 min

Lung dynamic image for 5min — Brain SPECT for 30 min (6×5min) — CT

	Dynamic acquisition	Dynamic SPECT acquisition	Dynamic SPECT reconstruction	
Time	1sec × 300 frames	30min (6×5min)	Scatter correction	TEW
Start time	Immediately after IMP injection	10 min after IMP injection	Attenuation correction	CTAC
Matrix Size	128 × 128	128 × 128	Image reconstruction	FBP
Zoom	1.45	1.45	CCF	25.8

Fig.2 Outline of the procedure of ^{123}I-IMP data acquisition in the previous method

123I-IMP IV injection — One- point arterial blood sampling at 10 min

Lung dynamic image for 3 min — Brain static Image for 1 min — Brain static Image for 1 min — Brain SPECT For 30 min — Brain static Image for 1 min
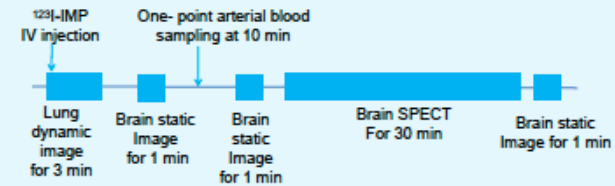
- The previous method requires lung dynamic image, three times of brain static images and brain SPECT.

Fig.3 Multiple regression analysis to calculate the regression equation in 35 patients

Objective variable	Explanatory variables
Measured Ca10	UCL
	Sum of UCL and CB1
	CB6
	Body weight (BW)

UCL — IMP injection — One-point arterial blood sampling at 10 min — CB1 10-15 min after IMP injection — CB6 35-40 min after IMP injection

Lung dynamic image for 5 min — Brain Dynamic SPECT for 30 min (6×5min) — CT
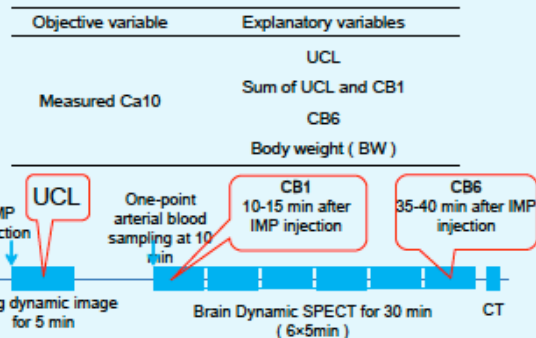
Fig.4 The area under the time-activity curve of the lungs (UCL)

Lung dynamic image (0-5 min after IMP injection)

counts / UCL / Time Time-activity curve 5 (min)
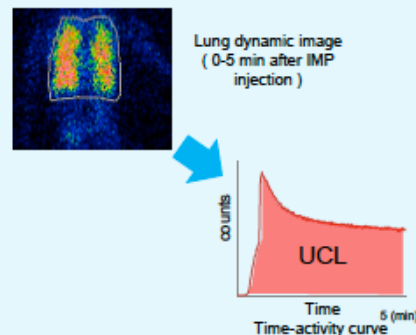
Fig.5 The counts of brain projection data (CB)
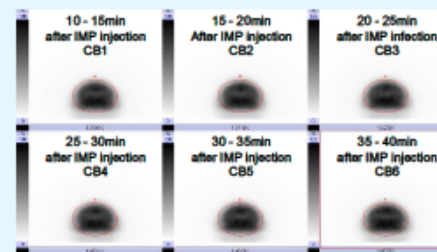
10 - 15min after IMP injection CB1
15 - 20min After IMP injection CB2
20 - 25min after IMP infection CB3
25 - 30min after IMP injection CB4
30 - 35min after IMP injection CB5
35 - 40min after IMP injection CB6

The regression equation for estimating Ca10

Estimated Ca10
$$= 1070.1 + 2.17 \times 10^{-3}a - 8.08 b - 2.23 \times 10^{-3}c + 2.47 \times 10^{-3}d$$

(a:UCL, b:BW, c:UCL+CB1, d:CB6)

This method can provide the estimated Ca10 values equivalent to those obtained by the previous method. The correlation coefficients between the estimated Ca10 and the measured Ca10 is obtained by this method (r = 0.894) and the previous method (0.907) are nearly equal.

Apply the regression equation to 99 patients of with different diseases

Estimated Ca10
$$= 1070.1 + 2.17 \times 10^{-3}a - 8.08b$$
$$- 2.23 \times 10^{-3}c + 2.47 \times 10^{-3}d$$
(a:UCL, b:BW, c:UCL+CB1, d:CB6)

Patients	Age range (mean ± SD) years	Male/Female	Number
Parkinson's disease	49-78 (68.55 ± 6.74)	9/20	29
Common or internal carotid artery occlusion or stenosis	49-81 (68.75 ± 9.11)	29/3	32
Moyamoya disease	25-66 (40.29 ± 12.44)	3/11	14
Cerebral infarction	36-71 (51.92 ± 12.24)	5/7	12
Others[*4]	38-79 (55.08 ± 13.58)	3/9	12
Total	25-81 (60.97 ± 14.40)	49/50	99

[*4]others : middle cerebral artery occlusion or stenosis, aortitis syndromes, motor neuron disease, essential tremor, spinocerebellar degeneration, dementia, amnesia, homonymous hemianopsia

Fujita Y, et al. EANM'14, Gothenburg, Sweden.

Nagoya University Graduate School of Medicine

Results

Fig.6 Comparison between the estimated Ca10 and the measured Ca10 in the total 99 patients
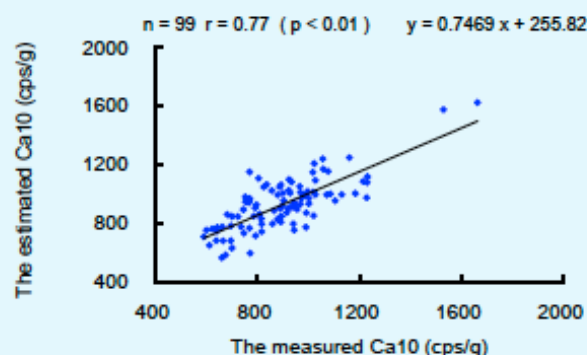
$n = 99$ $r = 0.77$ ($p < 0.01$) $y = 0.7469 x + 255.82$

(x-axis: The measured Ca10 (cps/g); y-axis: The estimated Ca10 (cps/g))

Comparison between the mean CBF values calculated using the estimated Ca10 and those calculated using the measured Ca10

Table 3 Correlation coefficients between the mean CBF values calculated using the estimated Ca10 and those calculated using the measured Ca10 in each patient group

Patients		Correlation coefficient ($p < 0.01$)
Parkinson' disease	(n=29)	0.795
Common or internal carotid artery occlusion or stenosis	(n=32)	0.784
Moyamoya disease	(n=14)	0.624
Cerebral infarction	(n=12)	0.771
Others	(n=12)	0.851
Total	(n=99)	0.785

Fig.7 Parkinson's disease
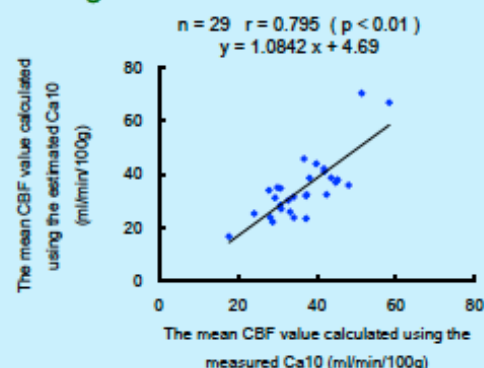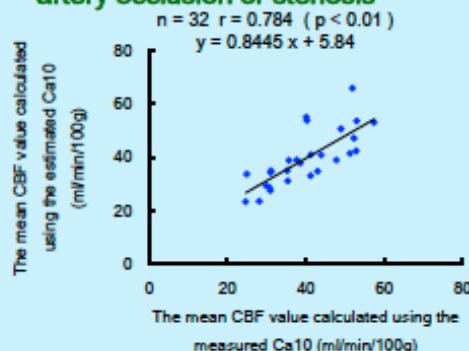
$n = 29$ $r = 0.795$ ($p < 0.01$)
$y = 1.0842 x + 4.69$

Fig.8 Common or internal carotid artery occlusion or stenosis

$n = 32$ $r = 0.784$ ($p < 0.01$)
$y = 0.8445 x + 5.84$

Fig.9 Moyamoya disease

$n = 14$ $r = 0.624$ ($p < 0.01$)
$y = 0.6016 x + 12.687$

Fig.10 Cerebral infarction

$n = 12$ $r = 0.771$ ($p < 0.01$)
$y = 0.8126 x + 6.79$

Fig.11 Others

$n = 12$ $r = 0.854$ ($p < 0.01$)
$y = 0.6842 x + 7.63$

Fig.12 Total patients

$n = 99$ $r = 0.785$ ($p < 0.01$)
$y = 0.8957 x + 2.80$

(Figs. 7–12 axes: The mean CBF value calculated using the measured Ca10 (ml/min/100g) vs. The mean CBF value calculated using the estimated Ca10 (ml/min/100g))
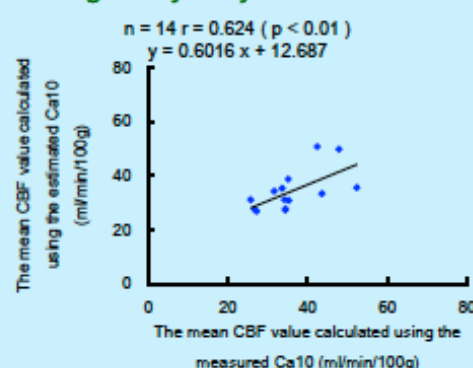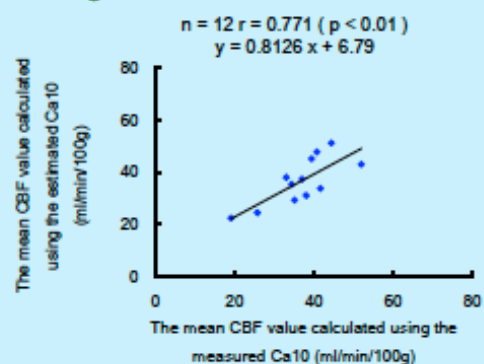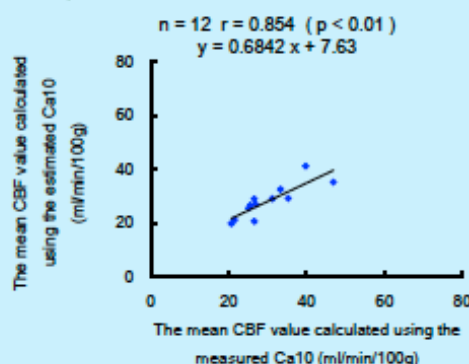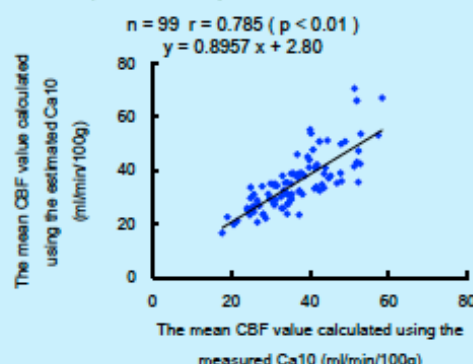
Conclusion

- This study verified that the newly developed noninvasive method, which is more simplified than the previous method, can estimate reliably the Ca10 values available for quantification of CBF in different patient groups.

- Fujita Y, Abe S, Odagawa T, Niwa A, Tsuchiya S, Koshiba Y, Fujita N, Kono H, Yamamoto S, Kato K. Validity of a Newly Developed Noninvasive Method for Estimating Cerebral Blood Flow Using 123I-IMP Acquisition Data from the Lungs and Brain. Medical Research Archives. 4(6),2016. DOI: http://dx.doi.org/10.18103/mra.v4i6.634

Fujita Y, et al. EANM'14, Gothenburg, Sweden.

Nagoya University Graduate School of Medicine

^{123}I-IMP ARG法による脳血流測定法における定量性に影響を与える因子に関する検討

藤田佑介　*阿部真治　**小田川哲郎　*藤田尚利　*河野秀隆
*熊澤智宇　小出若葉　小南かすみ　丹羽亜利紗　**加藤克彦

名古屋大学医学部保健学科放射線技術科学専攻
*名古屋大学医学部附属病院医療技術部放射線部門
**名古屋大学大学院医学系研究科医療技術学専攻医療量子科学講座

方法

IMP静注後、肺野動態像を
5分間収集する

⬇

動態像の肺野に関心領域を設
定し、肺野の時間放射能曲線 (
Time Activity Curve:TAC) を
求める

⬇

TACの個人差がCa10、
全脳平均脳血流量 (mCBF)に
与える影響について検討を行う
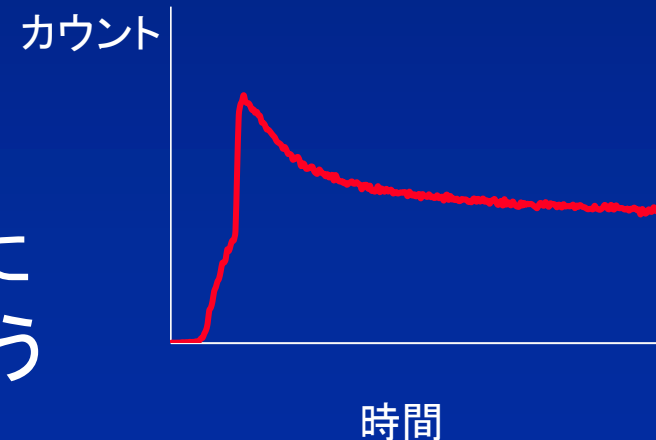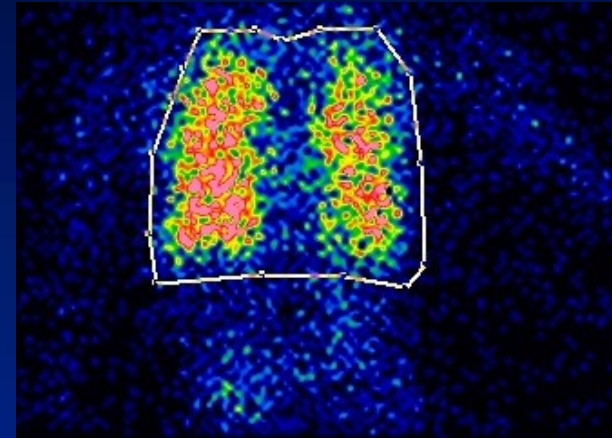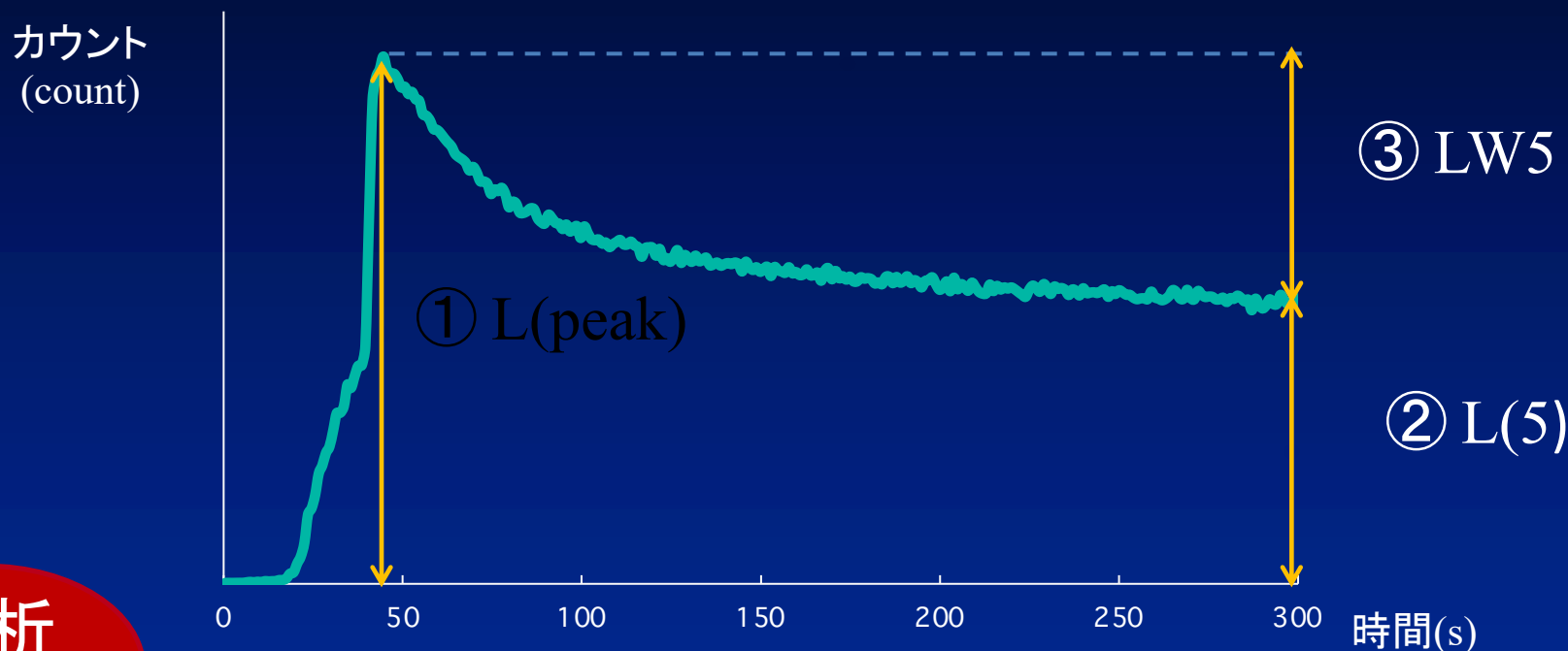
カウント

時間

結果

全症例の肺野のTAC
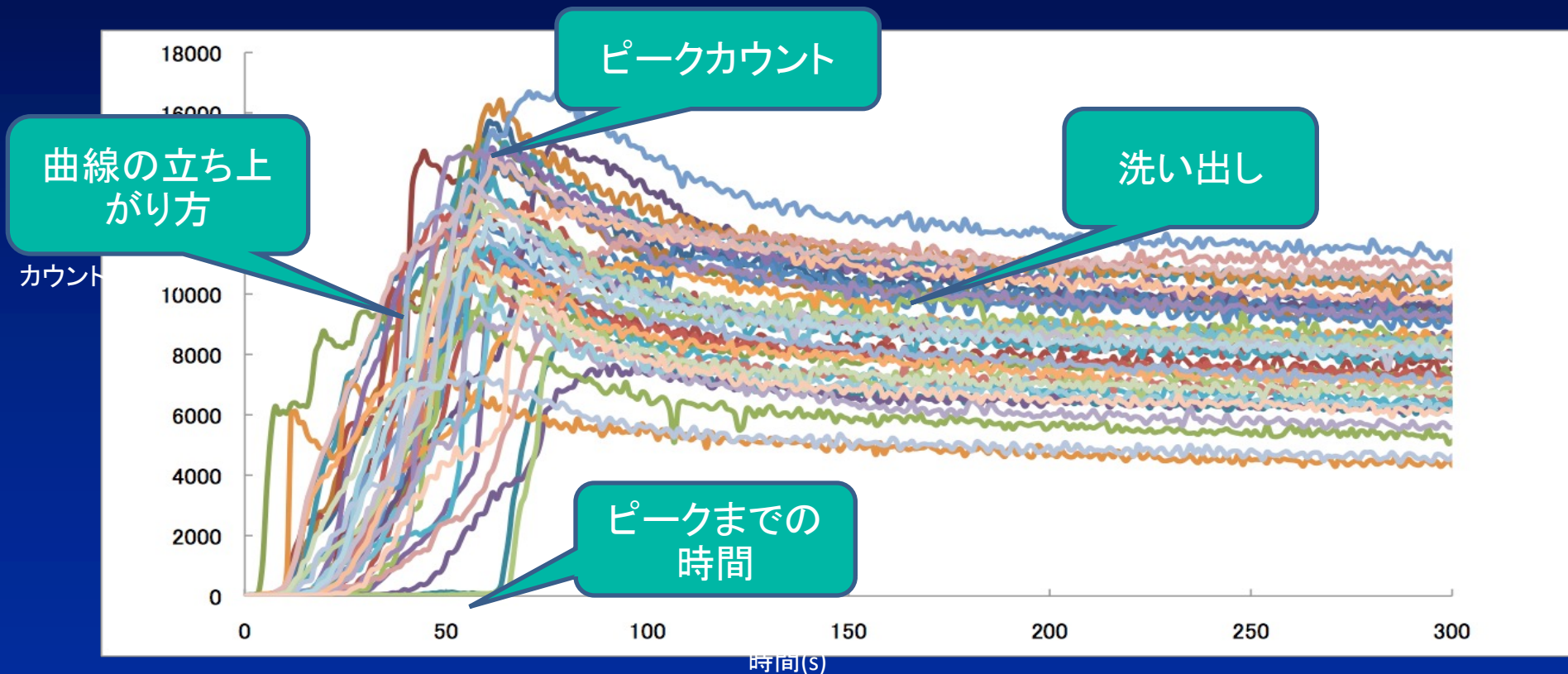
TACは個人差がある
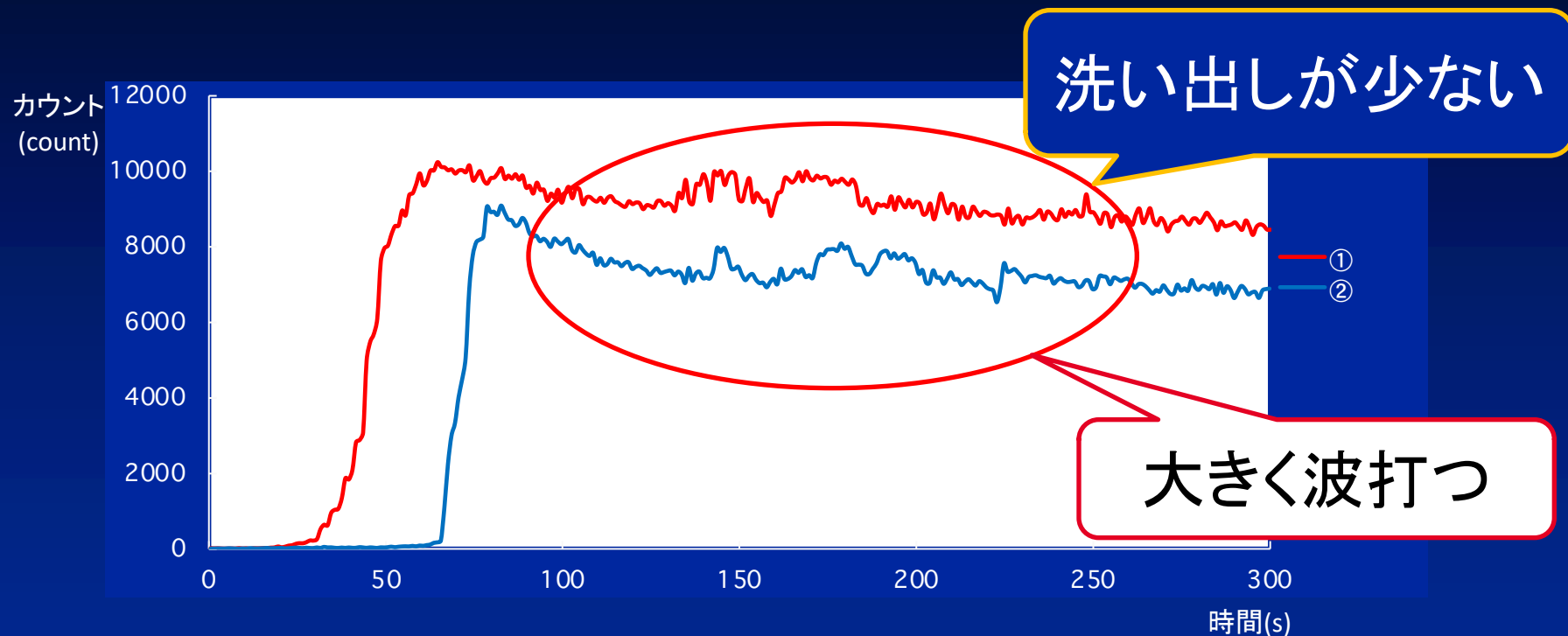
—原　著—

^{123}I-IMP ARG 法における画像再構成法および減弱補正法の違いによる脳血流定量値の比較

熊澤　智宇　　阿部　真治　　藤田　尚利
名古屋大学医学部附属病院

加藤　克彦
名古屋大学大学院医学系研究科医療技術学専攻医用量子科学講座

Comparison of the Cerebral Brood Flow Fixed Quantity Value by the Difference Between the Image Reconstruction and Attenuation Correction in the ^{123}I-IMP ARG Method

Tomotaka KUMAZAWA, Shinji ABE and Naotoshi FUJITA
Nagoya University Hospital

Katsuhiko KATO
Department of Radiological and Medical Laboratory Sciences, Nagoya University Graduate School of Medicine

(article received : Oct 17, 2017)

Summary

In the quantification of cerebral blood flow using the ^{123}I-IMP ARG method, the applicability of CT attenuation correction (CTAC) and image reconstruction by the ordered subsets-expectation maximization (OSEM) method is appropriate when compared with the conventional method. CBF was computed by changing the combination of the image reconstruction method and attenuation correction method to assess 38 patients' data, which enforced the ARG method. Combination of the disposal method was set to FBP + Chang, FBP + CTAC, and OSEM + CTAC. Regarding mCBF, a fixed quantity of grounds did not change with either CTAC or OSEM a lot, and it was shown that a value equivalent to the conventional method was acquired. The reason is considered to be the body that had taken CCF correctly. However, in rCBF, using CTAC, it was suggested that CBF, which also considered absorption of the skull, can be computed. Moreover, because image reconstruction by the OSEM method has the character to attach contrast, the fall part of a blood flow may be shown notably.

Key words : IMP, ARG, CTAC, OSEM

1. 諸　言

脳血流シンチグラフィは，脳の血流を評価する検査で，脳血管障害の病態評価，認知症や変性疾患の鑑別診断，癲癇焦点の検出などに役立ち，広く用いられている．脳血流シンチグラフィには定性と定量がある．再構成画像の視覚的な評価に加えて，定量値を考慮することでフォローアップや治療効果判定に有用である．古くから ^{125}I-N-isopropyl-p-iodoamphetamine （^{123}I-IMP）を使用した定量法にはマイクロスフェア法がある[1]．しかし，マイクロスフェア法は持続動脈採血が必要であり，侵襲性が高く，今日では Iida らが開発した Autoradiography （ARG）法が広く普及している[2-5]．^{123}I-IMP ARG 法は一回の動脈採血で脳血流を定量する簡便な手法であるが，正確な定量値

479

熊澤, 他. ^{123}I-IMP ARG法における画像再構成法および減弱補正法の違いによる脳血流定量値の比較. 核医学技術. 2018; 38(4): 479-486.

Nagoya University Graduate School of Medicine

¹²³I-IMP ARG法における画像再構成法および減弱補正法の違いによる脳血流定量値の比較

東芝 GCA-9300A (SPECT)

→ SIEMENS Symbia T (SPECT/CT)

機器更新によって，SPECT/CT装置を導入した（2012年3月）

¹²³I-IMP ARG法で用いる画像再構成法＋減弱補正法

FBP*+Chang法 →
- ・FBP*+Chang法
- ・FBP+CTAC**
- ・OSEM***+CTAC

使用可能な画像再構成法＋減弱補正法の組み合わせが増えた

* Filtered back projection
** CT based attenuation correction
*** Ordered subset expectation maximization

同一患者でfollow upを行う場合，どの組み合わせを用いるべきか？
画像再構成法＋減弱補正法組み合わせで脳血流定量値は変わるのか？
（当時はOSEM法で得られた定量値は懐疑的にみられていたため）
について検証した

Nagoya University Graduate School of Medicine

対象患者：2012年4月から2012年7月までに名古屋大学医学部附属病院にて
^{123}I-IMP ARG法を用いて脳血流定量SPECT/CT検査を行った患者38症例

比較する画像再構成法＋減弱補正法の組み合わせ：　　1) FBP+Chang法
　　　　　　　　　　　　　　　　　　　　　　　　　　2) FBP+CTAC
　　　　　　　　　　　　　　　　　　　　　　　　　　3) OSEM+CTAC

1症例につき3種類の定量画像を作成

作成した定量画像から12領域のregional cerebral blood flow (rCBF)と,その平均値であるmean cerebral blood flow (mCBF)を算出,3種類の定量画像間で定量値を比較
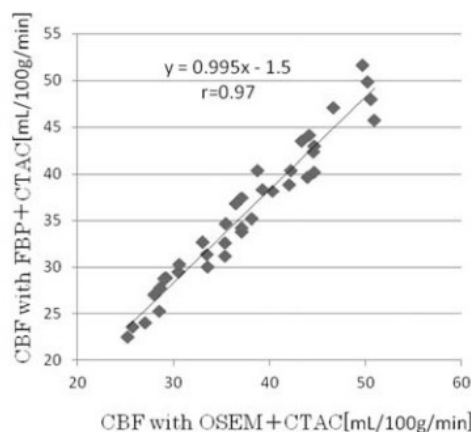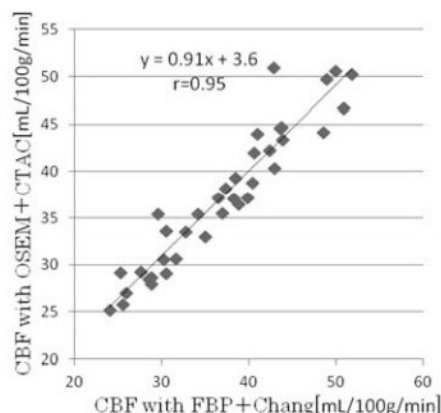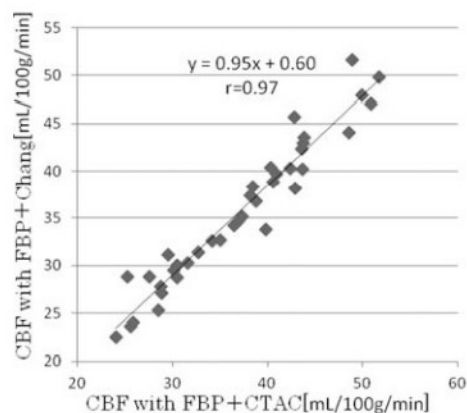
組み合わせ間の
mCBFの相関係数
は0.95以上

回帰式も
y = x に近い

FBP+Chang法	FBP+CTAC	OSEM+CTAC	→
36.95 ± 7.98	35.72 ± 7.56	37.39 ± 7.42	OSEM+CTACが統計的有意に高いが,その差は1 mL/100g/min　程度であり,臨床的意義は小さい

※単位はmL/100g/min

熊澤, 他. ^{123}I-IMP ARG法における画像再構成法および減弱補正法の違いによる脳血流定量値の比較. 核医学技術. 2018; 38(4): 479-486.
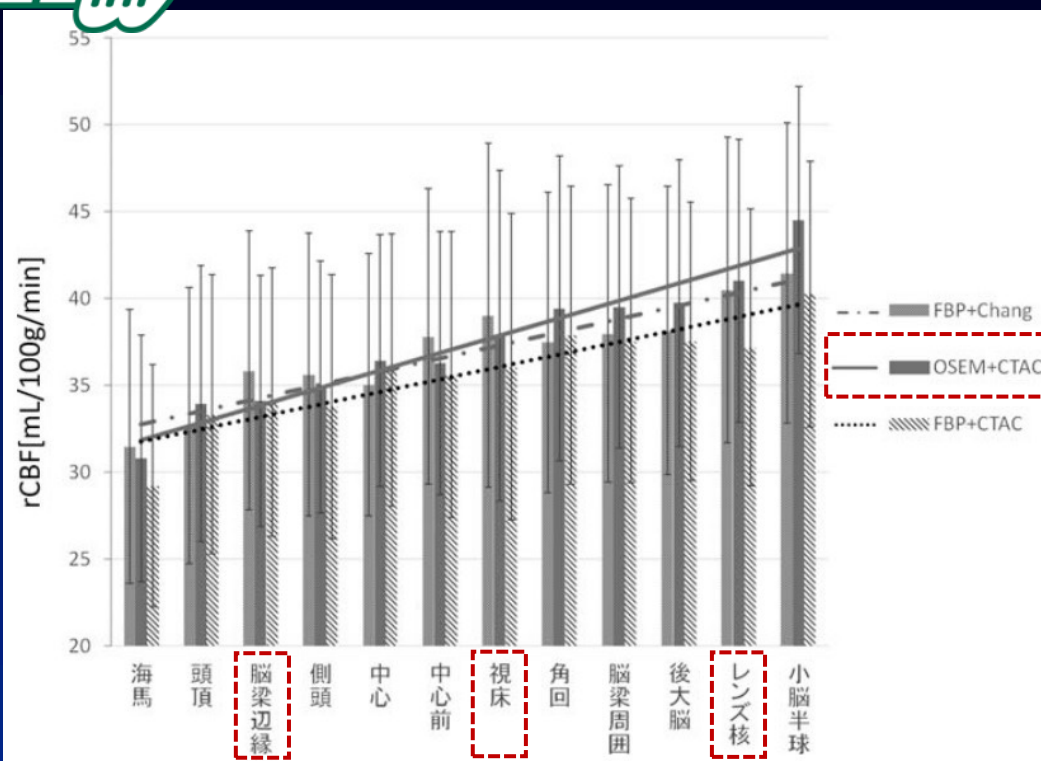
OSEM+CTACは全領域でrCBFが高め
になる傾向あり

脳梁辺縁, 視床, レンズ核のrCBFは,
FBP+Chang法とFBP+CTAC法を比較
すると, FBP+Chang法のほうが
3 mL/100g/min程度高めになる

Chang法における輪郭が, 実際の頭部
サイズより大きかったために, 回転中心
に近いほど過補正になったのでは?

mCBF：画像再構成法や減弱補正法の違いによって定量値が大きく変化しない
rCBF：OSEM+CTACは他の組み合わせと比較して定量値が異なる傾向があり, 定
性画像の見え方も変わる
➡ 装置間をまたいで同一患者でfollow upを行う場合, FBP+Chang法を
OSEM+CTACに切り替えるのは不適切といえる
FBP+CTACがFBP+Chang法に近いコントラストを持つ定量画像が得られる

熊澤, 他. ^{123}I-IMP ARG法における画像再構成法および減弱補正法の違いによる脳血流定量値の比較. 核医学技術. 2016; 38(4): 479-486

核医学技術 36：177-187 （2016）

—原　著—

ドパミントランスポータシンチグラフィの検査標準化に向けた施設および装置間差の要因に関する検討

藤田　尚利　　阿部　真治

名古屋大学医学部附属病院　医療技術部　放射線部門

加藤　克彦

名古屋大学大学院　医学系研究科　医療技術学専攻　医用量子科学講座

青木　卓

医療法人　豊田会　刈谷豊田総合病院　放射線技術科

杉本美津夫

名古屋第二赤十字病院　医療技術部　放射線科

Investigation of Factors Relevant to the Differences among Facilities and SPECT Scanners for Standardization of Dopamine Transporter Scintigraphy

Naotoshi Fujita and Shinji Abe

Department of Radiological Technology, Nagoya University Hospital

Katsuhiko Kato

Department of Radiological and Medical Laboratory Sciences,
Nagoya University Graduate School of Medicine

Taku Aoki

Department of Radiological Technology, Kariya Toyota General Hospital

Mitsuo Sugimoto

Department of Radiological Technology, Japanese Red Cross Nagoya Daini Hospital

(article received : Nov 17, 2015)

Summary

Although dopamine transporter scintigraphy with ^{123}I-ioflupane has been widely used in Japan since January 2014, there are actually differences among images acquired in various facilities. We evaluated and compared data about the dose linearity, single photon emission computed tomography (SPECT) spatial resolution, and specific binding ratio (SBR) on the images of dopamine transporter scintigraphy obtained from 11 hospitals. Based on the results, we investigated the factors relevant to the differences among facilities and SPECT scanners for realizing the standardization of dopamine transporter scintigraphy. Using 15 SPECT scanners (11 models), SPECT images were acquired according to either the acquisition and reconstruction

ドパミントランスポータシンチグラフィの検査標準化に向けた施設及び装置間差の要因に関する検討

Right SBR$_{Bolt}$: 7

Left SBR$_{Bolt}$: 3

設定SBR*
（CT画像）
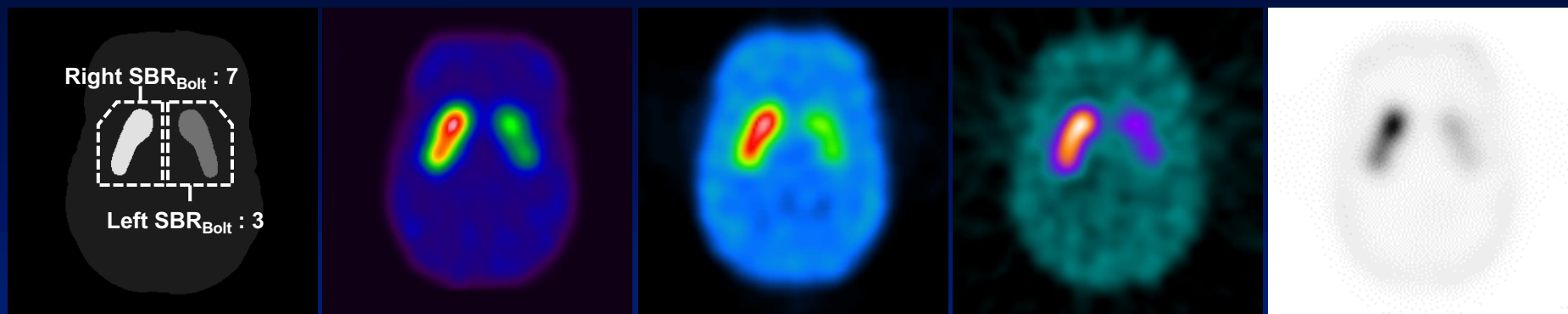
*SBR: specific binding ratio

施設A
GP系コリメータ

施設B
GP系コリメータ

施設C
GP系コリメータ

施設D
GP系コリメータ

読影基準, 保有装置の性能には多様性があるが,少なくとも診断の差が 生じないような基準作りが必要

➡

まずは施設・装置間でどれくらい違いがあるのかを調べないと標準化へ進めない
（メーカ推奨条件?自施設条件?）

東海地方会に所属する施設,装置/コリメータ毎に性能評価ファントムおよび線条体ファントムの画像収集,解析を行うことで,ドパミントランスポータシンチグラフィの標準化にあたり, 施設・装置間差を検証した

参加施設：11施設,使用装置：11機種 15台,コリメータとの組み合わせ：28種類

General purpose (GP)系,High resolution (HR)系,Fan beam系に分類

Nagoya University Graduate School of Medicine

a) 全収集データから算出した平均値は,理論値よりも低値となった
SBRが高値なほどばらつきが増加する傾向がある

b) 減弱補正を適用していない推奨条件にて得られた条件を抽出し,コリメータ群ごとに分類すると,SBRが低値であれば三群間に有意差は認められなかったが,高値では,GP系コリメータとHR系コリメータに統計的有意差が認められた
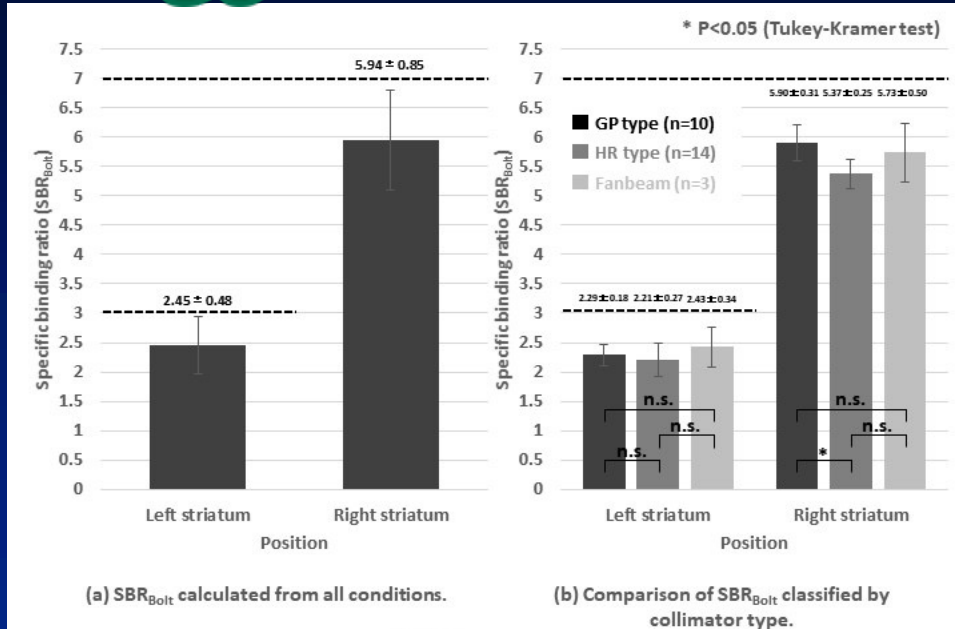
減弱補正の有無による比較
c) GP系コリメータ,d)HR系コリメータ

減弱補正を適用することにより,SBRは1.2から1.5倍程度の上昇があり,理論値に近づく傾向が認められた

藤田, 他. ドパミントランスポータシンチグラフィの検査標準化に向けた施設及び装置間差の要因に関する検討. 核医学技術. 2016; 36(2): 177-187.
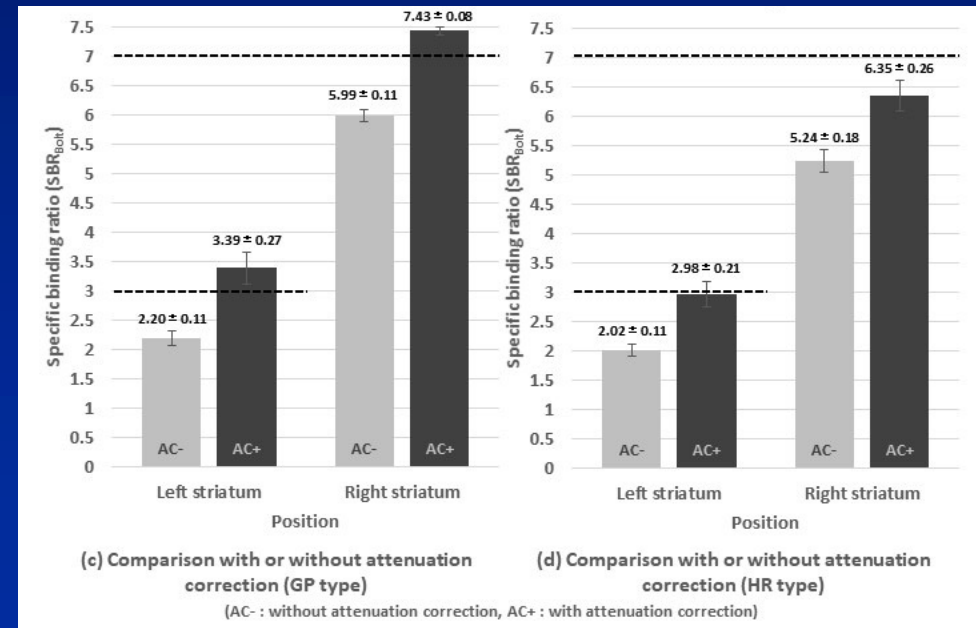
各施設で検討した自施設条件群（▲記号）や減弱補正を適用した
　推奨条件群（×記号）では,理論値の交点に近づいている
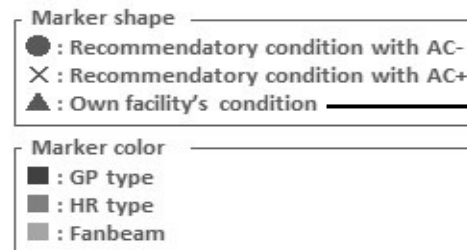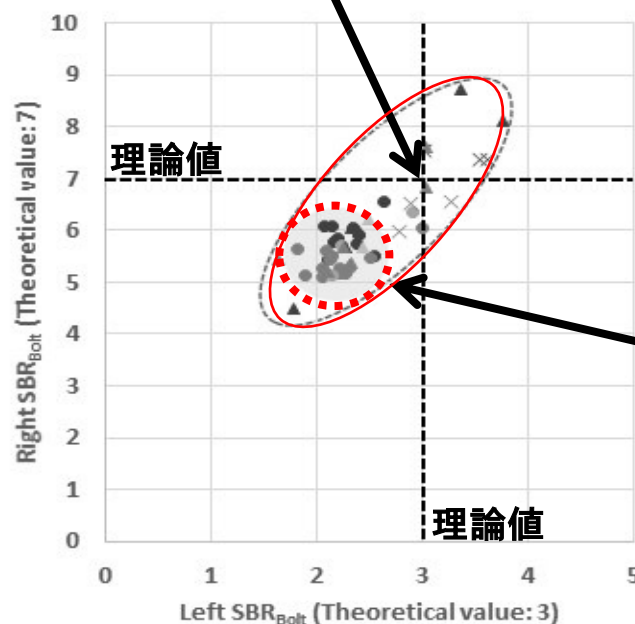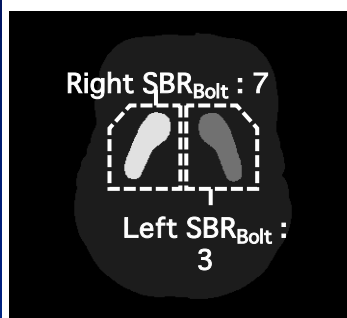
推奨条件（●記号）より算出したSBR
は,赤点線内に集簇している
※ただし,理論値から乖離は生じる

すべての条件が混在すると,SBRの
ばらつきは赤線で囲む範囲の
ように広がってしまう

撮像・処理条件を限定することにより,理論値との乖離は少なからず生じて
しまうものの,条件間のばらつきは低減できるため,検査標準化の観点から
すれば,撮像・処理条件を限定することは効果的である

藤田, 他.ドパミントランスポータシンチグラフィの検査標準化に向けた施設及び装置間差の要因に関する検討. 核医学技術. 2016; 36(2): 177-187.

—原 著—

ドパミントランスポータシンチグラフィにおける Specific Binding Ratio の空間分解能依存性に関する解析的検証

藤田 尚利 阿部 真治
櫻木 庸博 西本 卓矢

名古屋大学医学部附属病院 医療技術部 放射線部門

加藤 克彦

名古屋大学大学院 医学系研究科 医療技術学専攻 医用量子科学講座

Analytical Verification on Spatial Resolution Dependence of Specific Binding Ratio in Dopamine Transporter Scintigraphy

Naotoshi Fujita, Shinji Abe,
Yasuhiro Sakuragi and Takuya Nishimoto

Department of Radiological Technology, Nagoya University Hospital

Katsuhiko Kato

Department of Radiological and Medical Laboratory Sciences,
Nagoya University Graduate School of Medicine

Summary

We analytically verified the spatial resolution dependence of the specific binding ratio (SBR) excluding the variation factors (e.g. image noise) of the actual measured images by using a numerical phantom with various spatial resolution. Firstly, we created a numerical striatal phantom based on the Talairach atlas. Then, numerical phantom images with various spatial resolutions were obtained by applying three dimensional Gaussian filter to above numerical striatal phantom. Based on the method of Bolt et al. SBRs (SBR_{Bolt}) were calculated from numerical phantom images, we investigated the variability of SBR_{Bolt} and its factors accompanying the change of spatial resolution. As a result, in numerical phantom images simulating various spatial resolutions, SBR_{Bolt} tended to decrease with the spatial resolution deterioration. The SBR_{Bolt} decreased by about 3% from the theoretical value at the spatial resolution corresponding to the clinical condition (full width at half maximum : FWHM is about 13 mm). When the spatial resolution was further deteriorated (FWHM is about 20 to 30 mm), the SBR_{Bolt} decreased by 10 to 30% from the theoretical value. Although SBR_{Bolt} is a calculation method that considers partial volume effect due to spatial resolution deterioration, it was revealed that SBR_{Bolt} has spatial resolution dependence in this paper.

Key words : Dopamine transporter scintigraphy, Specific binding ratio (SBR), Spatial resolution, Numerical striatal phantom

1．緒 言

^{123}I-ioflupane を用いたドパミントランスポータシンチグラフィは，パーキンソン症候群やレビー小体型認知症の診断に対して有用な検査法として広く普及している。日米欧の各学会ガイドライン

ドパミントランスポータシンチグラフィにおける Specific Binding Ratioの空間分解能依存性に関する解析的検証

$$\mathrm{SBR_{Bolt}} = \left(\frac{1}{V_s} \right) \left\{ \frac{Ct_{\mathrm{VOI}}}{C_r} - V_{\mathrm{VOI}} \right\}$$

- V_s : The volume of striatum
- Ct_{VOI} : The total counts in the striatal VOI
- C_r : The counts concentration in the reference region
- V_{VOI} : The volume of the striatum VOI
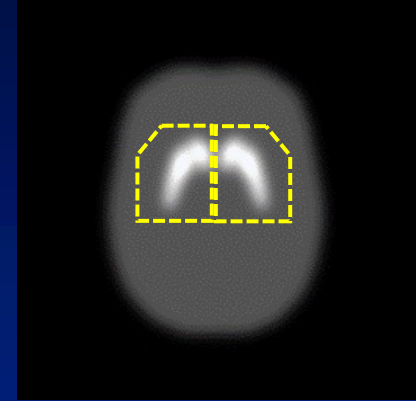
SPECT画像の低い空間分解能に起因する部分容積効果の影響を低減するために導入された手法

Tossici-Bolt L, et al. Eur J Nucl Med Mol Imaging, 33(12): 1491-1499

※国内ではDaTViewで得られるSBRが該当する
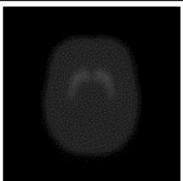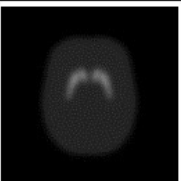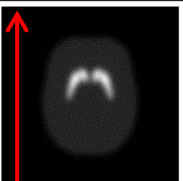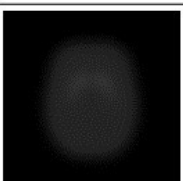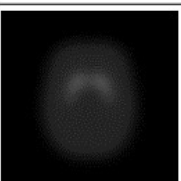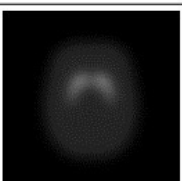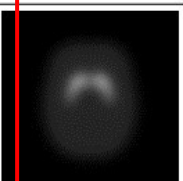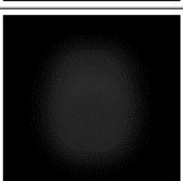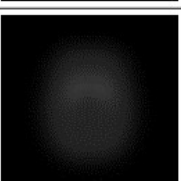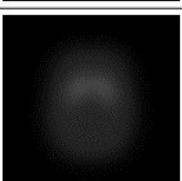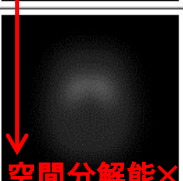
撮像・処理条件といった複合的な変化による検討は多く行われているが，SBR_{Bolt}の空間分解能固有の依存性に関する知見は得られていない

画像処理により空間分解能を変化させた数値ファントムを用いることで，実測画像の持つ変動要素を排除したSBR_{Bolt}の空間分解能依存性について，解析的な検証を行った

Nagoya University Graduate School of Medicine

	Expected SBR_{Bolt} : 1	Expected SBR_{Bolt} : 3	Expected SBR_{Bolt} : 5	Expected SBR_{Bolt} : 7
Original image (No Filter)				空間分解能〇
FWHM of kernel : 10 mm				
FWHM of kernel : 20 mm				
FWHM of kernel : 30 mm				空間分解能✕

Voxel size	2 mm × 2 mm × 2 mm
Number of matrix (Transaxial direction)	128 × 128
Number of slice (Longitudinal direction)	55
Background count	50 (const.)
Striatal counts	100, 150, 200, 250, 300, 350, 400
Expected SBR_{Bolt}	1, 2, 3, 4, 5, 6, 7
FWHM of kernel [mm]	No Filter, 4, 6, 8, 10, 12, 14, 16, 18, 20, 22, 24, 26, 28, 30
Number of phantom type	105 types

異なるSBR_{Bolt}における空間分解能依存性を検証するために,SBR_{Bolt}が1〜7の7通りのコントラストを有する画像を用意（original image）

⬇

数値ファントムに三次元Gaussian filterを適用することで,様々な空間分解能を有する線条体数値ファントムを作成した

⬇

得られた線条体数値ファントムから左右SBR_{Bolt}を算出し,その平均値を各画像に対するSBR_{Bolt}とした

藤田, 他.ドパミントランスポータシンチグラフィにおけるSpecific Binding Ratioの空間分解能依存性に関する解析的検証. 核医学技術. 2018; 38(2): 191-198.

空間分解能○　　　　　　　　空間分解能×

(a) Good ← **Spatial resolution** → Poor

SBR_{Bolt} : 7.0
SBR_{Bolt} : 6.0
SBR_{Bolt} : 5.0
SBR_{Bolt} : 4.0
SBR_{Bolt} : 3.0
SBR_{Bolt} : 2.0
SBR_{Bolt} : 1.0
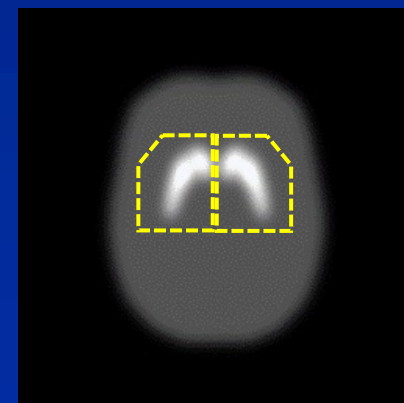
FWHM of Gaussian filter [mm]
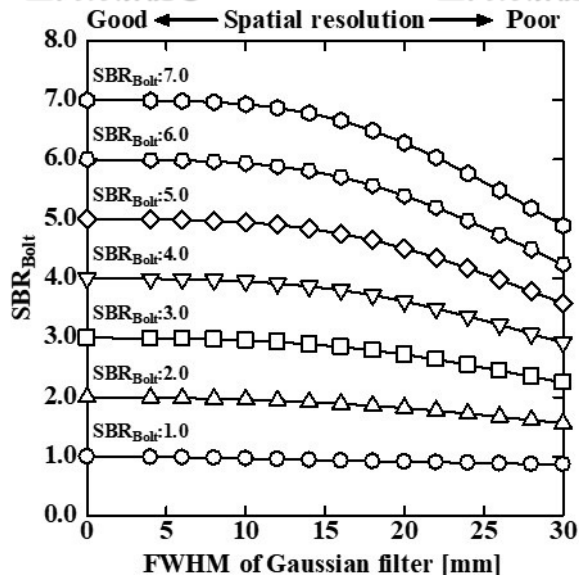
(a) Relationship of the spatial resolution (FWHM of Gaussian filter) and SBR_{Bolt}.

Good ← **Spatial resolution** → Poor

SBR_{Bolt} : 1.0
SBR_{Bolt} : 2.0
SBR_{Bolt} : 3.0
SBR_{Bolt} : 4.0
SBR_{Bolt} : 5.0
SBR_{Bolt} : 6.0
SBR_{Bolt} : 7.0

FWHM of Gaussian filter [mm]
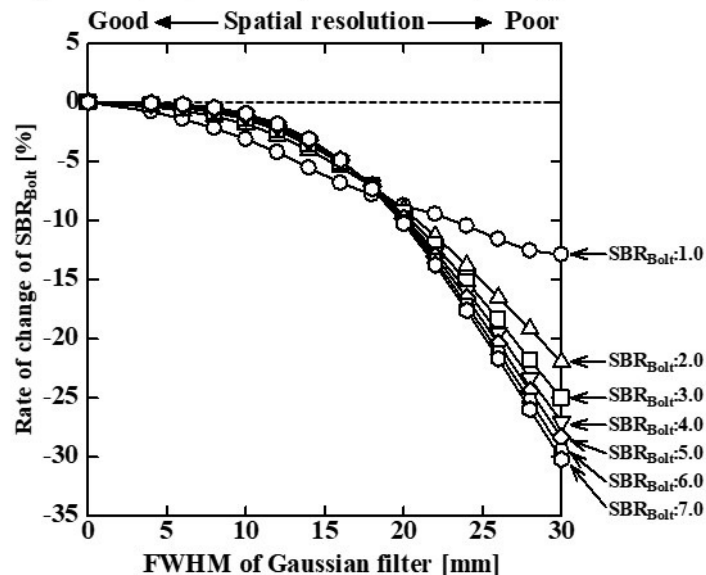
(b) Relationship of the spatial resolution (FWHM of Gaussian filter) and rates of change of SBR_{Bolt}. Each rates of change of SBR_{Bolt} were obtained by 100 × (measured SBR_{Bolt} - expected SBR_{Bolt})/ expected SBR_{Bolt}.

・空間分解能が劣化するとSBR_{Bolt}は減少
・設定したSBR_{Bolt}が大きい値ほど,空間分解能
　劣化に伴うSBR_{Bolt}減少の程度も大きくなる

⬇

理論値に対する実測値の比による比較

各空間分解能における
$$\frac{SBR_{Bolt}の実測値}{SBR_{Bolt}の理論値（基準値）} [\%]$$

・FWHM*：10mmでは約2%の低下
・FWHM：20mmでは約10%の低下を認めた

*FWHM: full width at half maximum

部分容積効果を考慮して算出されるSBR_{Bolt}であるが,空間分解能依存性が少なからず存在することを考慮したうえでの使用が望まれる

藤田, 他.ドパミントランスポータシンチグラフィにおけるSpecific Binding Ratioの空間分解能依存性に関する解析的検証. 核医学技術. 2018; 38(2): 191-198.

―原 著―

ドパミントランスポータシンチグラフィにおける最適処理条件の検討

石原　加純

聖隷予防検診センター　放射線課

阿部　真治　　　藤田　尚利

名古屋大学医学部附属病院　医療技術部　放射線部門

加藤　克彦

名古屋大学大学院　医学系研究科　医療技術学専攻　医用量子科学講座

Investigation about the Optimum Image Processing Condition of Dopamine Transporter Scintigraphy

Kasumi ISHIHARA

Department of Radiological Technology, Seirei Preventive Health-Care Center

Shinji ABE and Naotoshi FUJITA

Department of Radiological Technology, Nagoya University Hospital

Katsuhiko KATO

Department of Radiological and Medical Laboratory Sciences,
Nagoya University Graduate School of Medicine

Summary

Tracer accumulation in dopamine transporter scintigraphy is evaluated by visual assessment and quantitative measurements such as the specific binding ratio (SBR). SBR is changed by the acquisition and reconstruction parameters of SPECT imaging. To eliminate the difference in SBR among facilities or SPECT scanners, SPECT images were acquired according to the standardized acquisition and reconstruction parameters (clinical parameters). We determined the optimal acquisition and reconstruction parameters (optimal parameters) to obtain the correct SBR. Using the striatum phantom in which SBR of left and right striatum was 3 and 7, respectively, SPECT images were acquired by changing five parameters. We decided the optimal parameters to obtain the correct SBR. We compared the image quality and SBR of the patients' images obtained with the clinical and optimal parameters. The optimal parameters were as follows : OSEM 2D (subsets : 10, iterations : 8), FWHM of Gaussian filter : 7 mm, and CTAC＋. SBR obtained using the optimal parameters was about 1.7 times higher than that obtained using the clinical parameters. The differences in the results obtained using the optimal and clinical parameters seemed mainly due to that in the case of the clinical parameters CTAC was not applied.

Key words : Dopamine transporter scintigraphy, Image reconstruction, Single photon emission computed tomography (SPECT), Specific binding ratio (SBR)

(c) Reconstructed by the clinical parameters

(d) Reconstructed by the optimum parameters

(a) L-SBR

(b) R-SBR

Fig. 4　Comparison between the clinical parameters and the optimal parameters by using the clinical data.
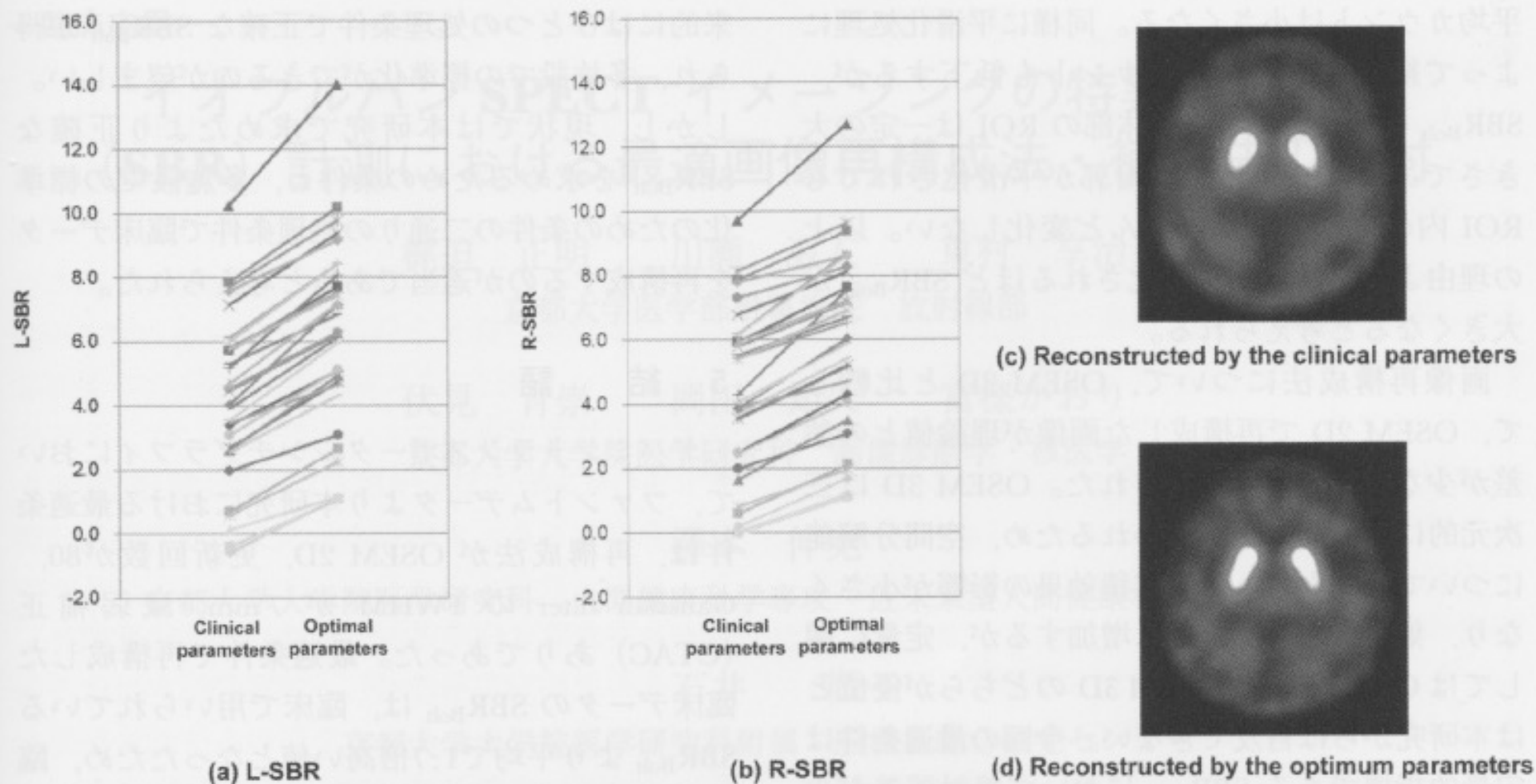
ドパミントランスポータシンチグラフィにおける新規解析手法の有用性の検討

伊藤良典[1)]、原一洋[2)]、藤田尚利[1,3)]、多田智大[1)]、
大野里沙[1)]、村山里奈[1)]、池田陽菜[4)]、越智優佳[4)]、
西尾美穂[4)]、堤貴紀[3)]、小田川哲郎[1)]、田村美香[1)]、
勝野雅央[2)]、阿部真治[3)]、加藤克彦[4)]

1) 名古屋大学大学院医学系研究科医療技術学専攻
2) 名古屋大学大学院医学系研究科神経内科学
3) 名古屋大学医学部附属病院医療技術部放射線部門
4) 名古屋大学大学院医学系研究科総合保健学専攻

Nagoya University Graduate School of Medicine

新規解析手法の概念

➢ 概念
- 各領域にどれだけの集積があれば、撮像した画像に近づくか
  という考えのもと、集積量を探る

近似した

Filtering
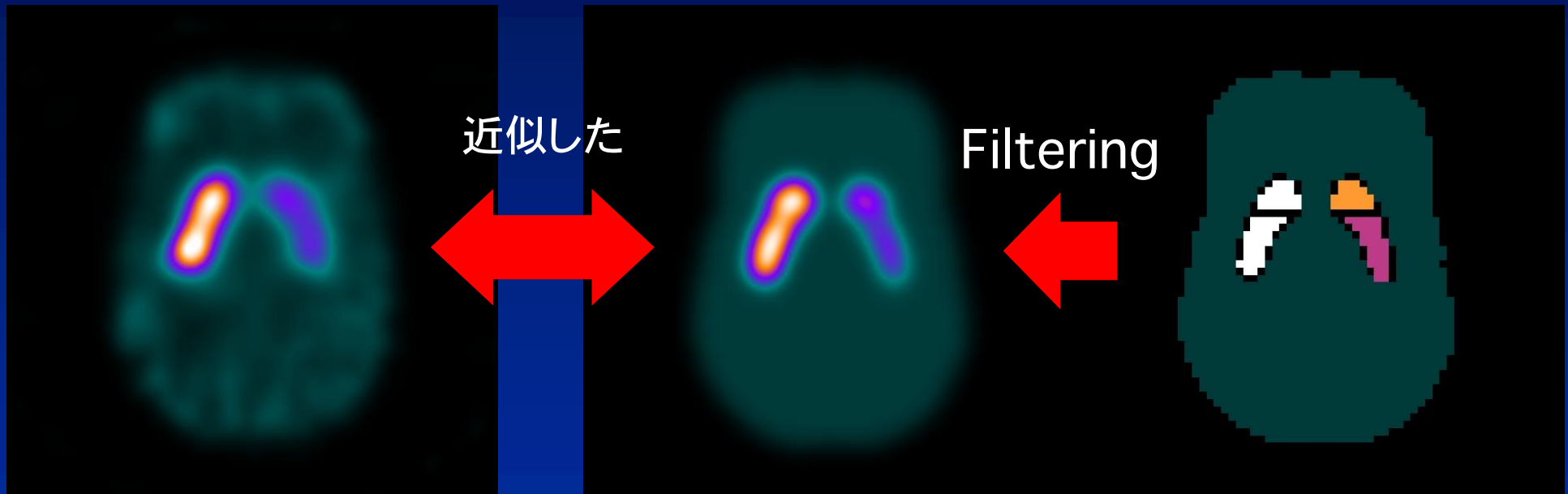
実際に撮像した
SPECT画像

SPECT様画像　　ボケの無い理想画像

集積量を仮定して
作成した画像

Ito Y, et al. J Nucl Med. 2020; 61 (suppl 1): 3130.

Nagoya University Graduate School of Medicine

新規解析手法で得られた成果

➤ ファントムでの成果

ファントムに封入した[123]I溶液のカウント濃度と解析手法で算出されたSPECTカウント濃度に強い相関を認めた。

相関係数: 0.997 ($p < 0.001$)
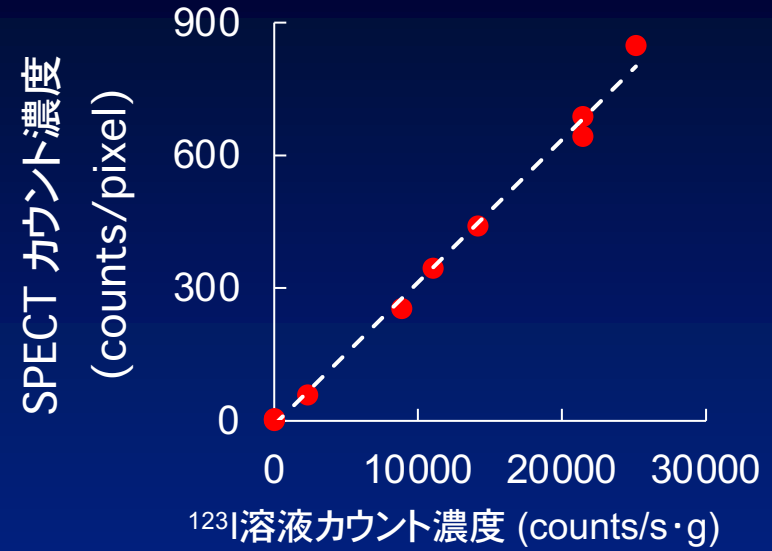
➤ 臨床例での成果

被殻SBRと運動機能スコア (MDS-UPDRS)に相関を認めた。

相関係数: -0.483 ($p = 0.004$)
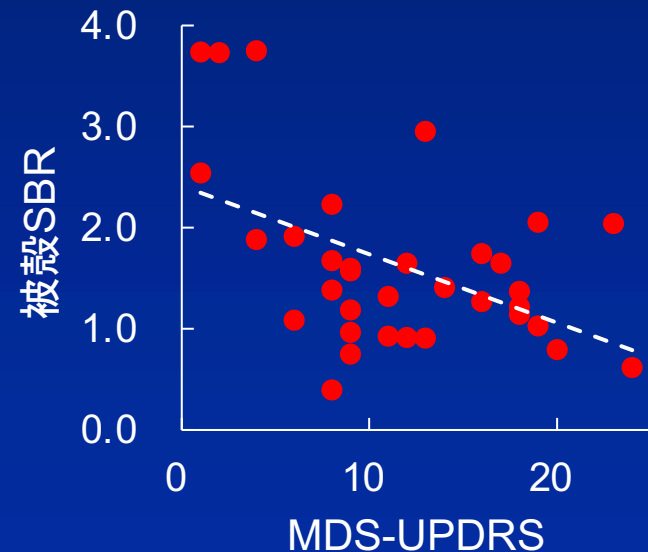
Ito Y, et al. J Nucl Med. 2020; 61 (suppl 1): 3130.

Nagoya University Graduate School of Medicine

RADIATION ONCOLOGY PHYSICS

Novel approach to semi-quantification of tracer accumulation in dopamine transporter scan

Yoshinori Ito[1] | Naotoshi Fujita[2] | Kazuhiro Hara[3] | Tomohiro Tada[1] | Shinji Abe[2] | Masahisa Katsuno[3] | Shinji Naganawa[4] | Katsuhiko Kato[5]

[1]Department of Radiological and Medical Laboratory Sciences, Nagoya University Graduate School of Medicine, Higashi-ku, Nagoya, Japan

[2]Department of Radiological Technology, Nagoya University Hospital, Showa-ku, Nagoya, Japan

[3]Department of Neurology, Nagoya University Graduate School of Medicine, Showa-ku, Nagoya, Japan

[4]Department of Radiology, Nagoya University Graduate School of Medicine, Showa-ku, Nagoya, Japan

[5]Functional Medical Imaging, Biomedical Imaging Sciences, Division of Advanced Information Health Sciences, Department of Integrated Health Sciences, Nagoya University Graduate School of Medicine, Higashi-ku, Nagoya, Japan

Correspondence
Katsuhiko Kato, Functional Medical Imaging, Biomedical Imaging Sciences, Division of Advanced Information Health Sciences, Department of Integrated Health Sciences, Nagoya University Graduate School of Medicine, 1-1-20 Daiko-Minami, Higashi-ku, Nagoya 461-8673, Japan.
Email: katokt@med.nagoya-u.ac.jp

Abstract

Purpose: Accurate tracer accumulation evaluation is difficult owing to the partial volume effect (PVE). We proposed a novel semi-quantitative approach for measuring the accumulation amount by examining the approximate image. Using a striatal phantom, we verified the validity of a newly proposed method to accurately evaluate the tracer accumulations in the caudate and putamen separately. Moreover, we compared the proposed method with the conventional methods.

Methods: The left and right caudate/putamen regions and the whole brain region as background were identified in computed tomography (CT) images obtained by single-photon emission computed tomography (SPECT)/CT and acquired the positional information of each region. SPECT-like images were generated by assigning assumed accumulation amounts to each region. The SPECT-like image, approximated to the actual measured SPECT image, was examined by changing the assumed accumulation amounts assigned to each region. When the generated SPECT-like image most approximated the actual measured SPECT image, the accumulation amounts assumed were determined as the accumulation amounts in each region. We evaluated the correlation between the count density calculated by the proposed method and the actual count density of the ^{123}I solution filled in the phantom. Conventional methods (CT-guide method, geometric transfer matrix [GTM] method, region-based voxel-wise [RBV] method, and Southampton method) were also evaluated. The significance of differences between the correlation coefficients of various methods (except the Southampton method) was evaluated.

Results: The correlation coefficients between the actual count density and the SPECT count densities were 0.997, 0.973, 0.951, 0.950, and 0.996 for the proposed method, CT-guide method, GTM method, RBV method, and Southampton method, respectively. The correlation of the proposed method was significantly higher than those of the other methods.

Conclusions: The proposed method could calculate accurate accumulation amounts in the caudate and putamen separately, considering the PVE.

タウイメージング

^{18}F-THK5351 PET/CT

　第1例 2015年11月11日

Nagoya University Graduate School of Medicine

Studies on Scattered Radiation out of Field of View and Effect of Scatter Correction in 3D brain PET

Masayuki Honda[1], Yasuhiro Sakuragi[2],

Shinji Abe[2], Naotoshi Fujita[2], Tetsuro Odagawa[1],

Keita Kunimoto[1], Katsuhiko Kato[1]

[1] Department of Radiological and Medical Laboratory Sciences, Nagoya University Graduate School of Medicine, Nagoya, Japan
[2] Department of Radiological Technology, Nagoya University Hospital, Nagoya, Japan

Materials

PET-CT systems

Biograph16 (SIEMENS)

The brain phantom IB-10 (Kyoto Kagaku Co., Ltd.)

The cylindrical phantom (YAMATO Jushi Inc.)

Image J

The solution of ^{18}F

The lead-made neck shield
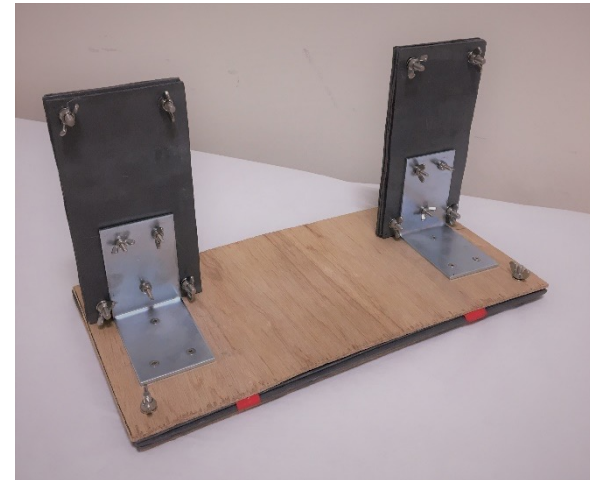
Fig.2 The lead-made neck shield

Honda M, et al. EANM'17, Vienna, Austria.

Conclusion

When the cylindrical phantom was located out of FOV, there was the influence of scattered radiation out of FOV on coincidence events.

When the distance between the cylindrical phantom and the detector was within 10 cm, there was the influence of scattered radiation out of FOV on SUV.

Effect of scattered radiation out of FOV was reduced by using the lead-made neck shield and scatter correction.

Nagoya University Graduate School of Medicine

^{11}C-PiB
[N-methyl-^{11}C]2-(4'-methylaminophenyl)-6-hydroxybenzothiazole
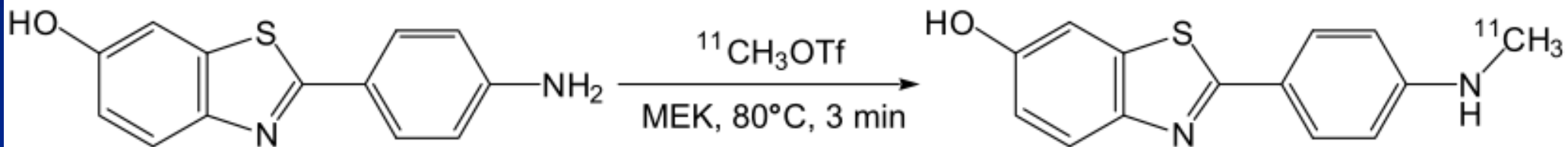
Comparative study of various reference regions for standardized uptake value ratio using ^{11}C-Pittsburgh Compound-B PET and MR images

Tomohiro Tada[1], Naotoshi Fujita[1][2], Yoshinori Ito[1], Risa Ono[1],
Rina Murayama[1], Yoshinori Tsutsumi[2], Haruna Ikeda[3], Yuka Ochi[3],
Miho Nishio[1], Tetsuro Odagawa[1], Mika Tamura[1], Hiroshi Yamaguchi[3],
Shinji Abe[2], Katsuhiko Kato[3]

1) Department of Radiological and Medical Laboratory Sciences, Nagoya University Graduate School of Medicine, Nagoya, Japan
2) Department of Radiological Technology, Nagoya University Hospital, Nagoya, Japan
3) Department of Integrated Health Sciences, Nagoya University Graduate School of Medicine, Nagoya, Japan

Purpose

- Standardized uptake value ratio (SUVR) is used as a quantitative evaluation method.

$$SUVR = \frac{SUV\ (region\ of\ interest)}{SUV\ (reference\ region)}$$

- we aimed to compare the validity of the cerebellar cortex, pons, and corpus callosum as the reference regions.
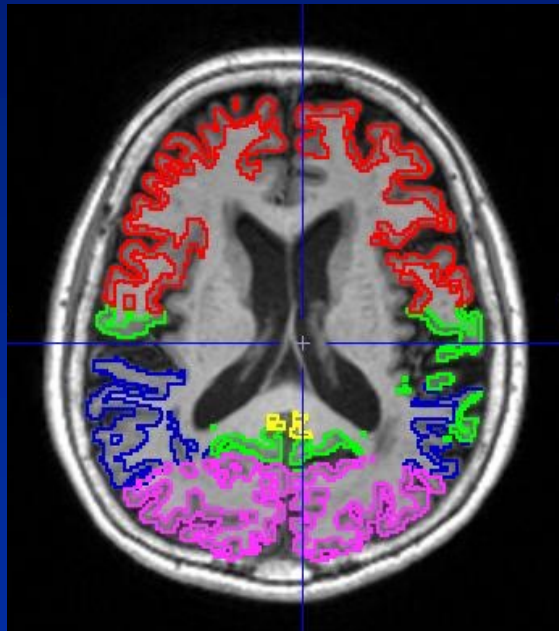
Fig. 1 VOIs of the cortical regions.

● corpus callosum

● pons
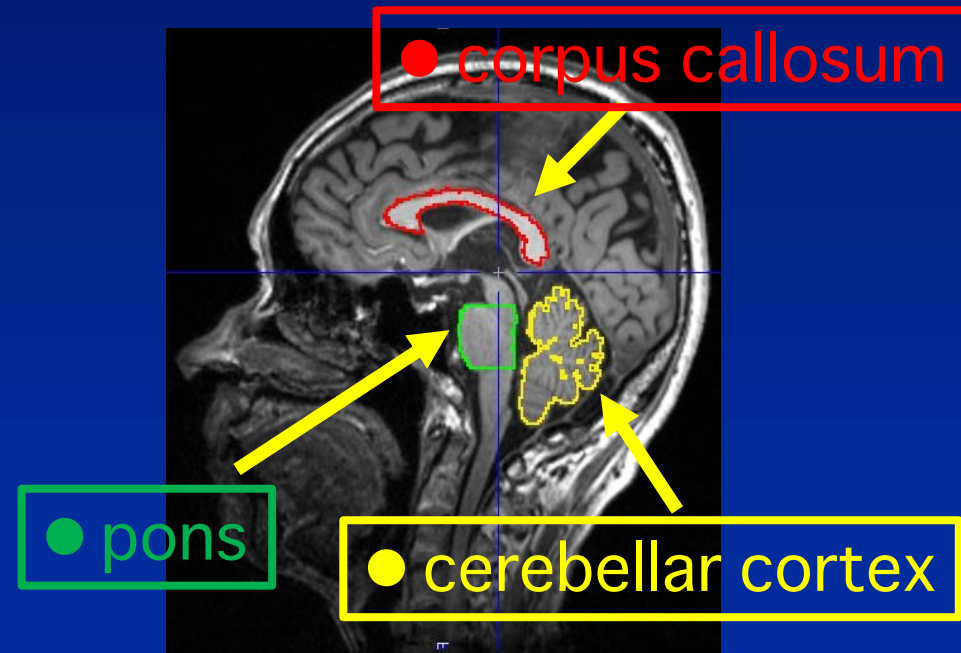
● cerebellar cortex

Fig. 2 VOIs of the reference regions.

多田智大, ら. 日本核医学技術学会総会学術大会, 2020, 神戸.

Nagoya University Graduate School of Medicine

Results

We examined whether the cerebellar cortex, pons, or corpus callosum was a valid reference region.

・MMSE ・ACE-R total
・ACE-R attention ・ACE-R memory

SUVR was best correlated with cognitive functional testing with the cerebellar cortex as the reference region.
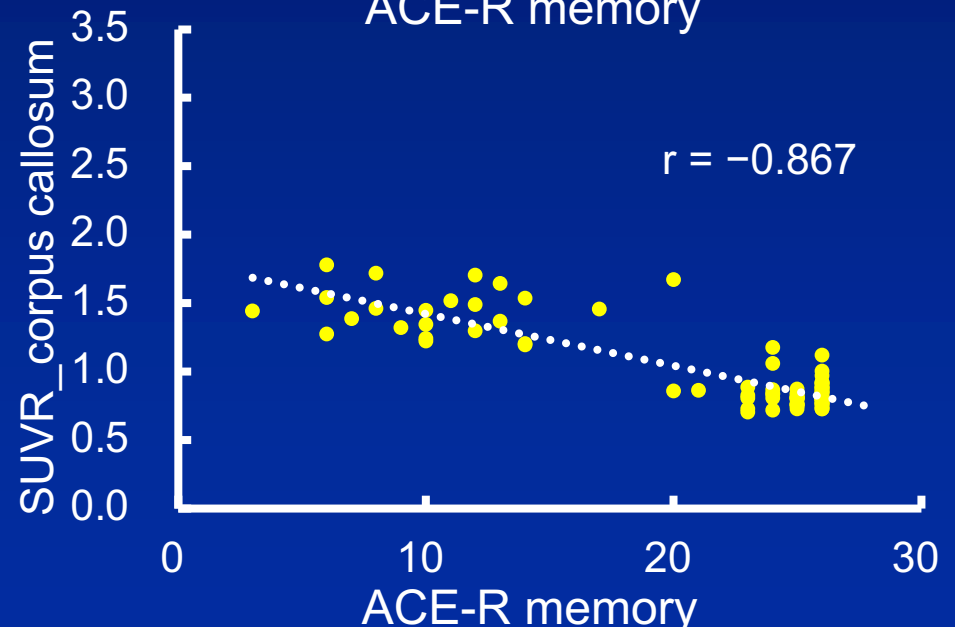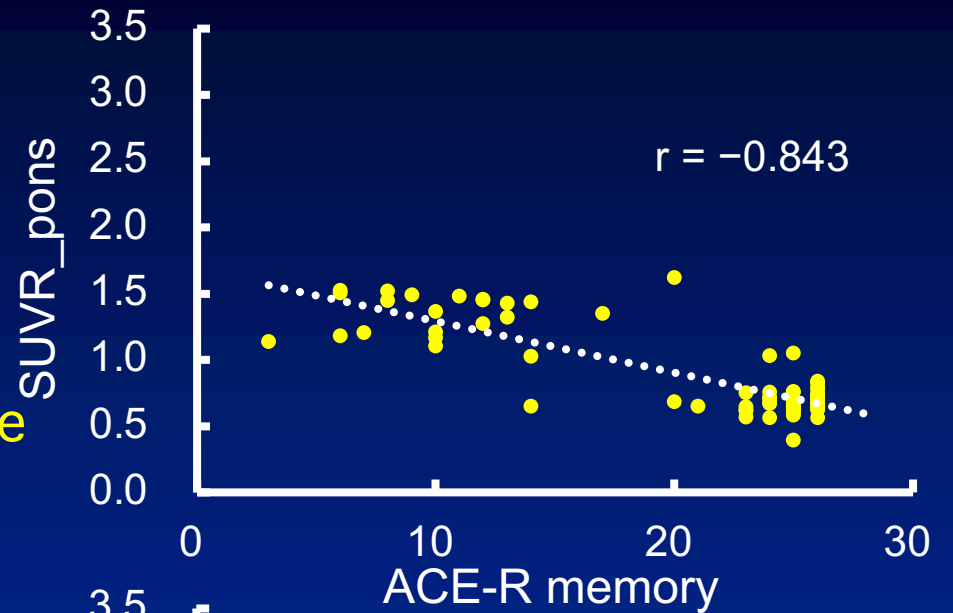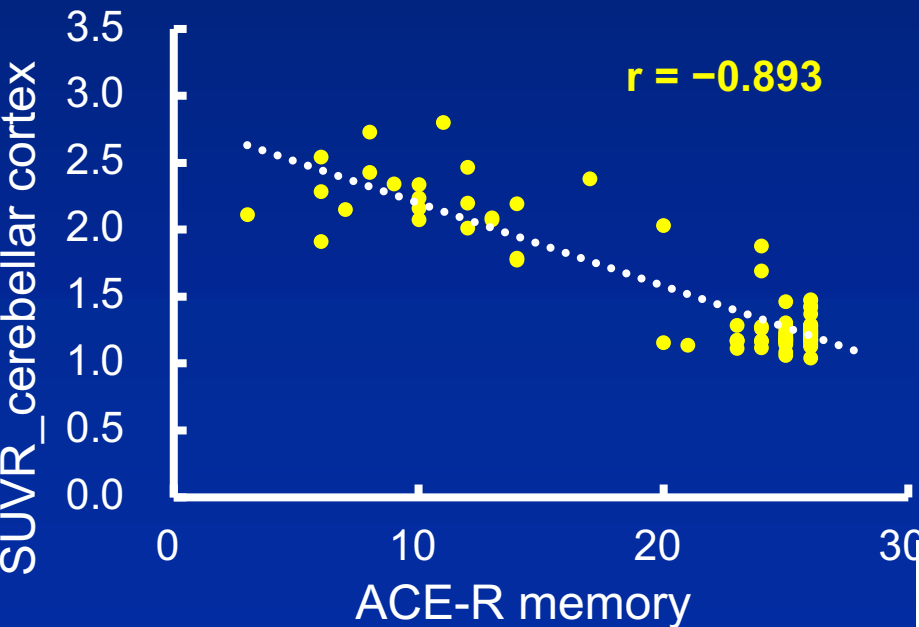
多田智大, ら. 日本核医学技術学会総会学術大会, 2020, 神戸.
Nagoya University Graduate School of Medicine

ORIGINAL ARTICLE

Comparative examination of the pons and corpus callosum as reference regions for quantitative evaluation in positron emission tomography imaging for Alzheimer's disease using ^{11}C-Pittsburgh Compound-B

Tomohiro Tada[1] · Kazuhiro Hara[2] · Naotoshi Fujita[1] · Yoshinori Ito[3] · Hiroshi Yamaguchi[4] · Reiko Ohdake[5] · Kazuya Kawabata[2,6] · Aya Ogura[2] · Toshiyasu Kato[2,7] · Takamasa Yokoi[8] · Michihito Masuda[2,9] · Shinji Abe[1] · Shinichi Miyao[10] · Shinji Naganawa[11] · Masahisa Katsuno[2,12] · Hirohisa Watanabe[5] · Gen Sobue[13] · Katsuhiko Kato[14]

Abstract

Objectives Standardised uptake value ratio (SUVR) is usually obtained by dividing the SUV of the region of interest (ROI) by that of the cerebellar cortex. Cerebellar cortex is not a valid reference in cases where amyloid β deposition or lesions are present. Only few studies have evaluated the use of other regions as references. We compared the validity of the pons and corpus callosum as reference regions for the quantitative evaluation of brain positron emission tomography (PET) using ^{11}C-PiB compared to the cerebellar cortex.

Methods We retrospectively evaluated data from 86 subjects with or without Alzheimer's disease (AD). All subjects underwent magnetic resonance imaging, PET imaging, and cognitive function testing. For the quantitative analysis, three-dimensional ROIs were automatically placed, and SUV and SUVR were obtained. We compared these values between AD and healthy control (HC) groups.

Results SUVR data obtained using the pons and corpus callosum as reference regions strongly correlated with that using the cerebellar cortex. The sensitivity and specificity were high when either the pons or corpus callosum was used as the reference region. However, the SUV values of the corpus callosum were different between AD and HC ($p < 0.01$).

Conclusions Our data suggest that the pons and corpus callosum might be valid reference regions.

Keywords Standardised uptake value ratio · Brain · Positron emission tomography imaging · ^{11}C-Pittsburgh Compound-B · Alzheimer's disease

Introduction

Alzheimer's disease (AD) is pathologically characterised by neurofibrillary tangles and amyloid β (Aβ) deposition. Aβ deposition is a pathological feature that arises from the earliest stages of AD onset and begins decades before the onset of cognitive decline [1]. ^{11}C-Pittsburgh compound-B (PiB) is an amyloid imaging agent developed by Mathis et al., derived from the structure of thioflavin T, which is used to detect Aβ deposition in vitro [2]. Amyloid imaging

with ^{11}C-PiB enables the visualisation of Aβ deposition in the brain. Amyloid imaging has made it possible to evaluate Aβ deposition in the brain before death; however, it still has to be confirmed at autopsy [3]. Therefore, amyloid imaging using positron emission tomography (PET) is important for the early diagnosis of AD. The development of therapeutic agents for AD has been a focal area of research [4, 5]. Besides helping in AD diagnosis, amyloid imaging with ^{11}C-PiB PET also aids in evaluating the therapeutic effect of clinical treatments. Several studies have used the standardised uptake value ratio (SUVR) as a quantitative evaluation of brain PET using ^{11}C-PiB [3, 6, 7]. SUVR is obtained by dividing the SUV of the region of interest (ROI) by that of the reference region. Generally, SUVR is evaluated using the

✉ Katsuhiko Kato
  katokt@med.nagoya-u.ac.jp

Extended author information available on the last page of the article

^{11}C-PiB PET検査における SUVRの年齢による変動

稲垣朝也[1], 藤田尚利[2], 多田智大[2], 岩永陽菜[2][3], 稲垣拓実[3],
磯辺亮太[3], 長原朋香[3], 清瀬裕也[1], 恒川諒太朗[1],
阿部真治[2], 中西恒平[3], 西井龍一[3], 加藤克彦[3]

1) 名古屋大学医学部保健学科 放射線技術科学専攻
2) 名古屋大学医学部附属病院 医療技術部 放射線部門
3) 名古屋大学大学院 医学系研究科 総合保健学専攻

結語

- AD群において、年齢増加に伴うmcSUVRの有意な減少が確認された。

- 部位別では前頭葉、後頭葉での年齢増加に伴うSUVRの有意な減少が確認された。

^{11}C-PiB PET検査における皮質平均SUVR算出手法の比較

稲垣朝也[1]、藤田尚利[2]、多田智大[2]、岩永陽菜[1][2]、磯辺亮太[1]、
長原朋香[1]、恒川諒太朗[1]、阿部真治[2]、南本亮吾[3] 、
原一洋[4]、中西恒平[1]、西井龍一[1]、加藤克彦[1]

1) 名古屋大学大学院 医学系研究科 総合保健学専攻
2) 名古屋大学医学部附属病院 医療技術部 放射線部門
3) 名古屋大学大学院 医学系研究科 総合画像情報解析寄附講座
4) 名古屋大学大学院 医学系研究科 神経内科学

Nagoya University Graduate School of Medicine

Comparison of quantitative assessment for cardiac sarcoidosis inflammation site using ^{18}F-FDG PET/CT images

Rina Murayama[1], Ryota Morimoto[2], Naotoshi Fujita[1],[3],
Yoshinori Ito[1], Risa Ono[1], Tomohiro Tada[1], Haruna Ikeda[1],
Yuka Ochi[1], Miho Nishio[1], Yoshinori Tsutsumi[3], Mika Tamura[1],
Tetsuro Odagawa[1], Shinji Abe[3], Katsuhiko Kato[1]

[1] Department of Radiological and Medical Laboratory Sciences, Nagoya
University Graduate School of Medicine, Nagoya, Japan
[2] Department of Cardiology, Nagoya University Graduate School of
Medicine, Nagoya, Japan
[3] Department of Radiological Technology, Nagoya University Hospital,
Nagoya, Japan

- ^{18}F-FDG PET画像を用いた心臓サルコイドーシス (CS)炎症部位の定量評価は standardized uptake value (SUV),cardiac metabolic volume (CMV),cardiac metabolic activity (CMA)等の指標を用いて行う.

> ・CMV: CS炎症部位の体積　・CMA: CMV×SUVmean

- これらの指標は閾値を用いてCS炎症部位にvolume of interest (VOI)を設定し算出する.しかし,これらの指標を算出する際の閾値は明らかにされていない.

①肝臓のSULmeanとその標準偏差を用いたthreshold

$${}_{0.8}SUL_{LIVER}\ threshold = 肝臓のSULmean × 0.8 + SD × 3.0$$

②左室心プール (LVBP)のSULmeanとその標準偏差を用いたthreshold

$${}_{1.0}SUL_{LVBP}\ threshold = LVBP\ SULmean × 1.0 + SD × 3.0$$

threshold	Method 1 Visual positive (N=53)		Method 2 All examinations (N=81)			
	Examination set VOI exactly	Examination set VOI not exactly	Cutoff Value (CMA)	Sensitivity [%]	Specificity [%]	AUC
${}_{0.8}SUL_{LIVER}$	38 (71.7%)	15 (28.3%)	0.249	96.2	92.9	0.978
${}_{1.0}SUL_{LVBP}$	50 (94.3%)	3 (5.7%)	7.749	94.3	100	0.993

※ 名古屋大学大学院医学系研究科及び医学部附属病院生命倫理委員会承認済 (承認番号 2019-0035)

Case1

◆ CS治療中の症例

$_{0.8}SUL_{LIVER}$ threshold

一部しかVOIが
設定されていない
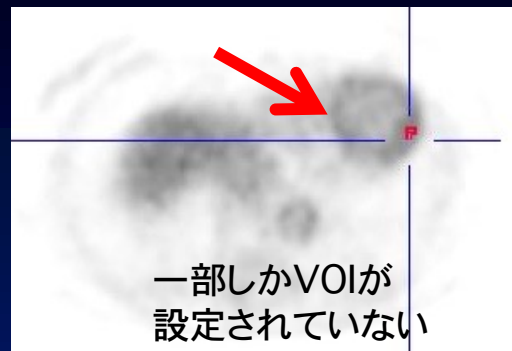
- 肝臓のSULmean: 2.45
- $_{0.8}SUL_{LIVER}$ threshold: 2.60
- CMA: 1.02

$_{1.0}SUL_{LVBP}$ threshold
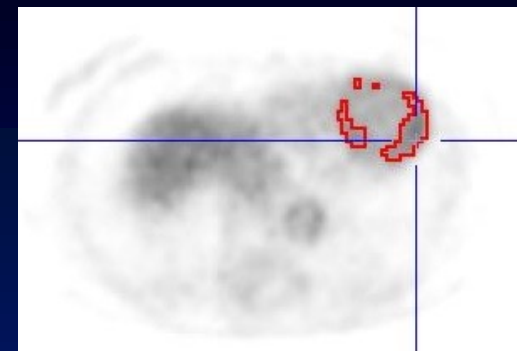
- LVBPのSULmean: 1.61
- $_{1.0}SUL_{LVBP}$ threshold: 1.98
- CMA: 45.6

Case2

◆ 肝臓のSUVが
高い症例

$_{0.8}SUL_{LIVER}$ threshold

一部しかVOIが
設定されていない
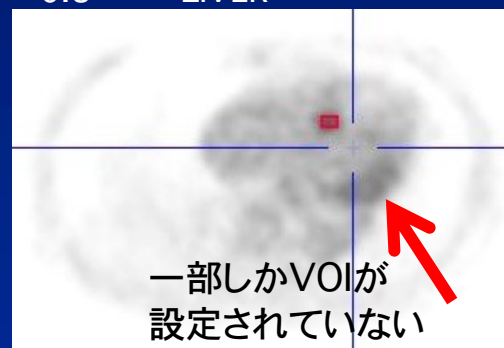
- 肝臓のSULmean: 2.95
- $_{0.8}SUL_{LIVER}$ threshold: 2.97
- CMA: 12.6

$_{1.0}SUL_{LVBP}$ threshold
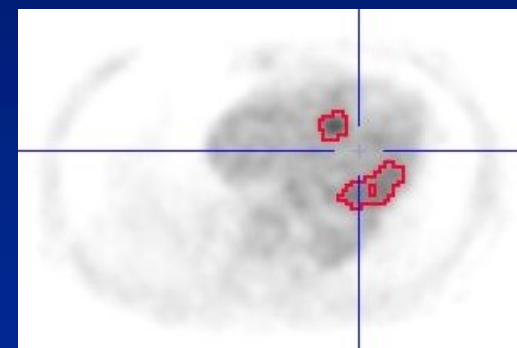
- LVBPのSULmean: 1.73
- $_{1.0}SUL_{LVBP}$ threshold: 2.15
- CMA: 105

- $_{1.0}SUL_{LVBP}$ thresholdを用いて設定したCS炎症部位は$_{0.8}SUL_{LIVER}$ threshold を用いて設定したCS炎症部位よりも臨床診断で指摘されているCS炎症部位に より一致した.

Murayama R, et al. Eur J Nucl Med Mol Imaging. 2020;47: S223.

2019 SNMMI Anaheim 5演題
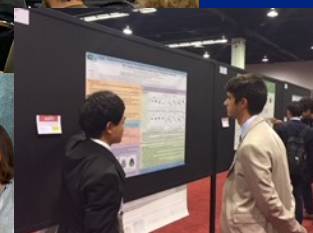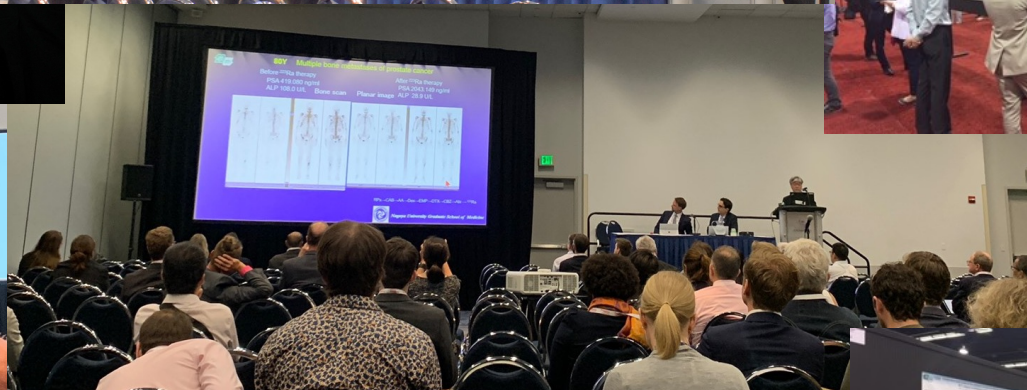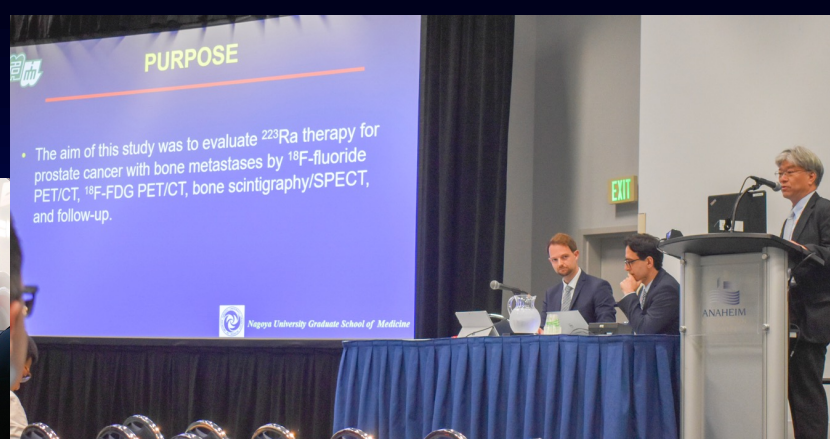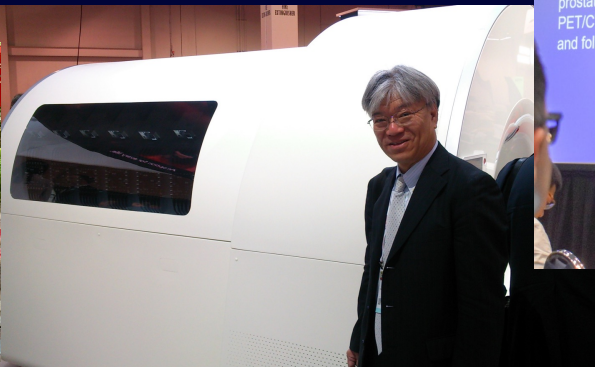
TPO28   Evaluation of the basic characteristics of the cardiac focusing-collimators

Arisa Niwa [1], Hidetaka Kono[2], Shinji Abe[2], Naotoshi Fujita[2], Tomotaka Kumazawa[2], Yusuke Fujita[1], Tetsuro Odagawa[1], Katsuhiko Kato[1]

[1] Department of Radiological and Medical Laboratory Sciences, Nagoya University Graduate School of Medicine, Nagoya, Japan

[2] Department of Radiological Technology, Nagoya University Hospital, Nagoya, Japan

Aim

Recently IQ-SPECT, which consists of cardiac focusing-collimator (SMARTZOOM), cardio-centric acquisition, and resolution recovery iterative reconstruction algorithms (3D-OSEM), has been developed in the field of nuclear cardiology. IQ-SPECT delivers cardiac imaging 4 times faster than conventional SPECT acquisition with scan times as low as 4 minutes per acquisition. This study was performed to evaluate the basic characteristics of the cardiac focusing-collimator such as its influences on the uniformity, resolution, and dose linearity of SPECT images.

Materials and Methods

Gamma camera and SPECT-CT (Fig.1)
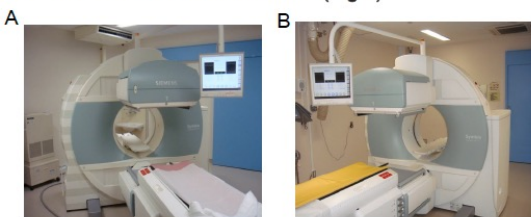
Fig1. Siemens Symbia-T (A) and Siemens Symbia-T6 (B)

Collimator
- Cardiac focusing-collimator (CF)
- Low energy high resolution collimator (LEHR)
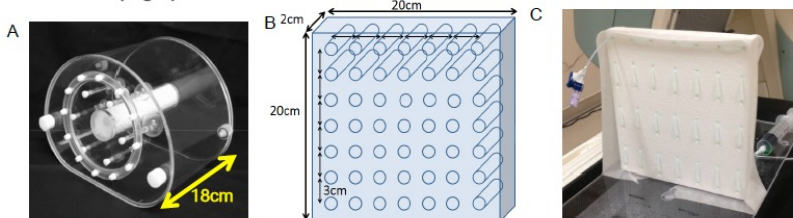
Phantom (Fig.2)

Fig2. NEMA body phantom (A) and line source phantom(B and C)

Line source phantom was made of expanded polystyrene and fluororesin tube. The Tc-99m solution was enclosed into NEMA body phantom and line source phantom. Concentration of the solution enclosed into NEMA body phantom was 38.4 kBq/ml and that enclosed into line source phantom was 4.6×10^3 kBq/ml .
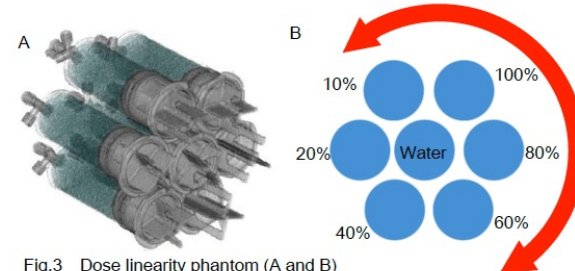
Fig.3   Dose linearity phantom (A and B)

Dose linearity phantom was made of seven syringes (diameter, 45mm). The Tc-99m solution was enclosed into dose linearity phantom. Concentration of the solution varied between 0%(water) and 100%(114kBq/mL).   Each concentration was measured in the well counter and cpm was calculated.
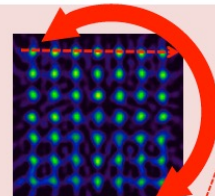
Uniformity of SPECT images

The data was acquired with Siemens Symbia T-series using LEHR and CF, and NEMA body phantom on bed. The data acquisitions were made by regarding the center of the phantoms as the center of the heart in IQ-SPECT. Acquired data were reconstructed, and SPECT images were compared. We drew a circle region of interest (ROI) on the reconstructed SPECT images. The center of the circle was regarded as the rotation center , and the diameters varied between 100mm and 200mm (Fig.4) . We calculated each coefficient of variation (CV) from mean counts and standard deviations (SD) determined on the circle ROIs.
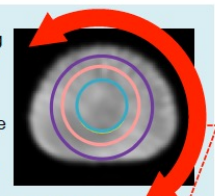
Fig.4 Drawing of circle ROIs

Resolution of SPECT images

We determined line profiles in each line source on the reconstructed images(Fig. 5) and calculated full width half maximum (FWHM) .
For evaluation of the resolution of SPECT images, CT based attenuation correction and scatter correction were not performed.


Fig.5 Determination of line profiles

Dose linearity of SPECT images

Acquired data were reconstructed, and circle ROIs were drawn on the reconstructed SPECT images manually by adjusting the ROI boundaries to the syringe boundaries of the reconstructed SPECT images (Fig.6).
Table 1 shows recording parameters of each collimator.
Table 2 shows reconstruction parameters of each collimator.

Fig.6 Drawing of ROI

Niwa A, et al. EANM'13, Lyon, France.
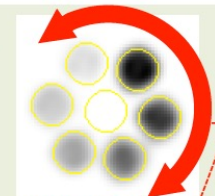
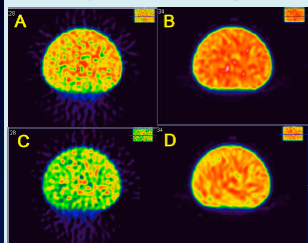# Results

Uniformity of SPECT images

Fig.7 Comparison of SPECT images acquired with NEMA body phantom under various conditions

SPECT images acquired with NEMA body phantom using LEHR in a 360°acquisition range and reconstructed with FBP (A) or with 3D-OSEM(B) , in a 180°acquisition range and reconstructed with FBP (C) or 3D-OSEM (D).
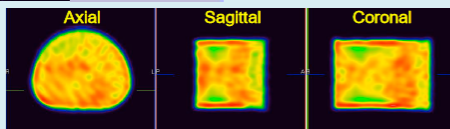

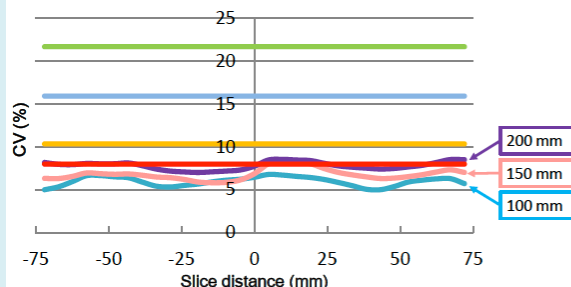Fig.8 SPECT images acquired with NEMA body phantom using CF

Fig.9 Distribution of CV

The vertical axis was for CV and the horizontal axis for the slice distance. The negative side of the horizontal axis is for the foot, and the positive side is for the head.

When SPECT images were acquired with LEHR in a 360°acquisition range, the images were uniform , but the images acquired in a 180°acquisition image showed a lower uniformity (Fig.7). When the images were acquired with CF, the images were uniform at the areas near the rotation center and the center of body axis of the phantom compared with those acquired with LEHR collimator (Figs.7-9).

Resolution of SPECT images

Fig.10 Comparison of SPECT images with line source phantom under various conditions

SPECT images acquired with line source phantom using CF and reconstructed with 3D-OSEM (A), using LEHR in a 360°acquisition range and reconstructed with 3D-OSEM (B) or FBP (C) .
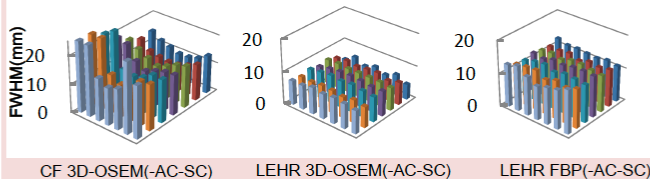

Fig.11 Comparison of distributions of FWHM

FWHM calculated when CF was used and reconstructed with 3D-OSEM (A), FWHM when LEHR was used and reconstructed with 3D-OSEM (B) or FBP (C)

SPECT resolution when CF was used was inferior to that when LEHR collimator was used (Figs.10 and 11).

At the marginal zone
FWHM acquired with CF and reconstructed with 3D-OSEM was higher than that acquired with LEHR and reconstructed with FBP and 3D-OSEM.

At the central zone
FWHM acquired with CF and reconstructed with 3D-OSEM was 2mm lower than that acquired with LEHR and reconstructed with FBP, and 2mm higher than that acquired with LEHR and reconstructed with 3D-OSEM.
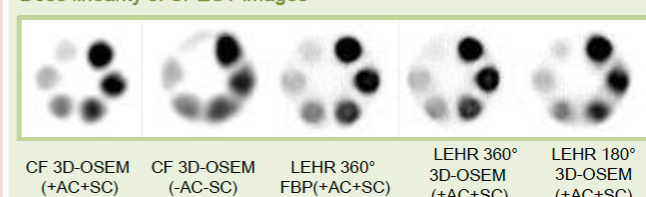
Dose linearity of SPECT images

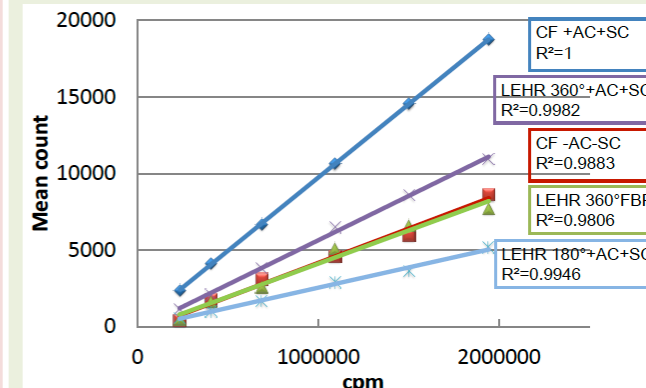Fig.12 Comparison of SPECT images acquired under various conditions

Fig.13 Comparison of the dose linearity of SPECT images acquired under various conditions

Comparison of R-squared value (Fig.13)
LEHR 360°FBP(+AC+SC) < CF 3D-OSEM(-AC-SC)
 < LEHR 180°3D-OSEM(+AC+SC)   < LEHR 360°3D-OSEM(+AC+SC)
 < CF 3D-OSEM(+AC+SC)

SPECT images acquired with CF and reconstructed with 3D-OSEM, CT based attenuation correction, and scatter correction showed almost the same dose linearity as those acquired with LEHR collimation and reconstructed with 3D-OSEM.

Discussion

Uniformity of SPECT images
The uniformity of SPECT images acquired with CF was maintained within a certain range around the rotation center or the body axis of the phantom. The finding is due to the characteristics of CF collimation, namely, the focus of the collimator varies continuously from cone-like in the central region to parallel at the edge (Fig.14).

Fig.14   CF collimator

Resolution of SPECT images
FWHM acquired with CF and reconstructed with 3D-OSEM was better within a certain range around the rotation center (sweet spot) and worse outside the range. The finding is due to the fact that the sweet spot of CF was set in order to correspond to the center of the phantoms.

Dose linearity of SPECT images
SPECT images acquired with CF and reconstructed with 3D-OSEM, CT based attenuation correction, and scatter correction showed R-squared value close to 1. The finding is due to the fact that when CF is used image reconstruction with 3D-OSEM, CT based attenuation correction, and scatter correction improves the SPECT dose linearity.

Conclusion

When CF was used, the uniformity and dose linearity of SPECT images were better , but their resolution was worse than those when LEHR collimator was used.

CERTIFICATE OF ACHIEVEMENT
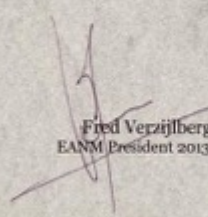
THIS IS TO CERTIFY THAT
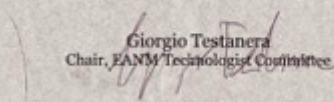
Arisa Niwa

is the 2nd nominee

of the

Best Poster Presentation
Poster Award 2013

EANM Congress 2013, Lyon

Fred Verzijlbergen
EANM President 2013 - 2014

Giorgio Testanera
Chair, EANM Technologist Committee

23rd of October 2013

EANM'13
European Association of Nuclear Medicine

2nd Nominee for Best Poster
Presentation

Evaluation of the basic characteristics of the cardiac
focusing collimators

A. Niwa, S. Abe, T. Ohtagawa, N. Fujita, H. Kuno, T.
Kumazawa, T. Fujita, K. Kato

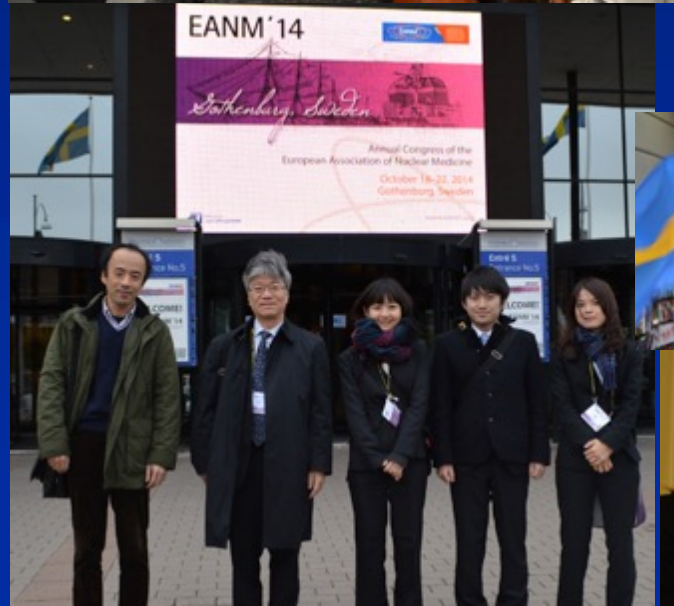Nagoya University Graduate School of Medicine, Nagoya,
JAPAN

2013/10/23 12:06:01

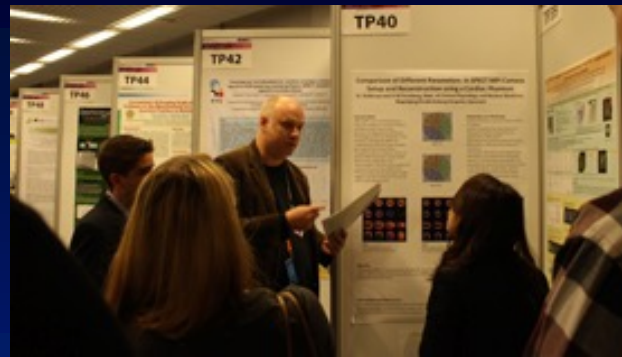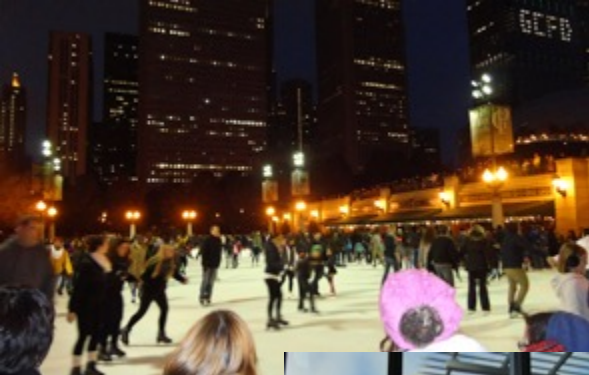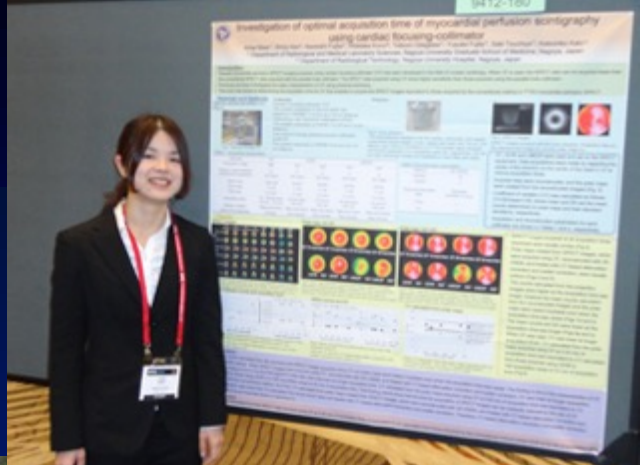# 2013 EANM Lyon
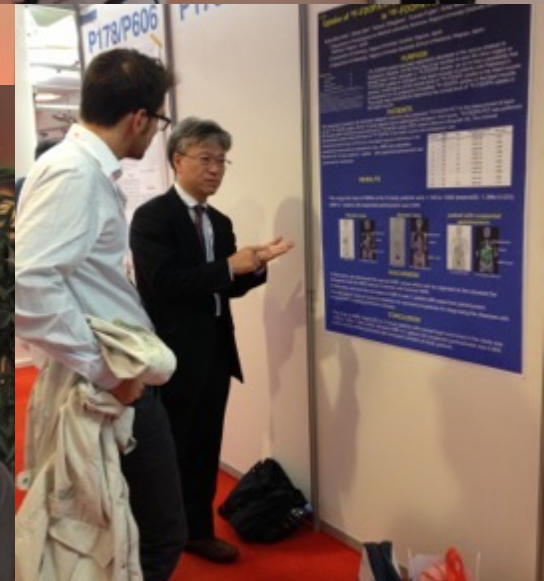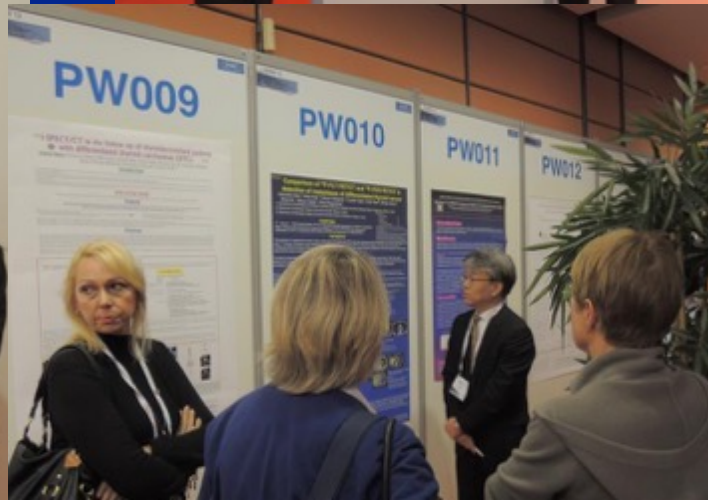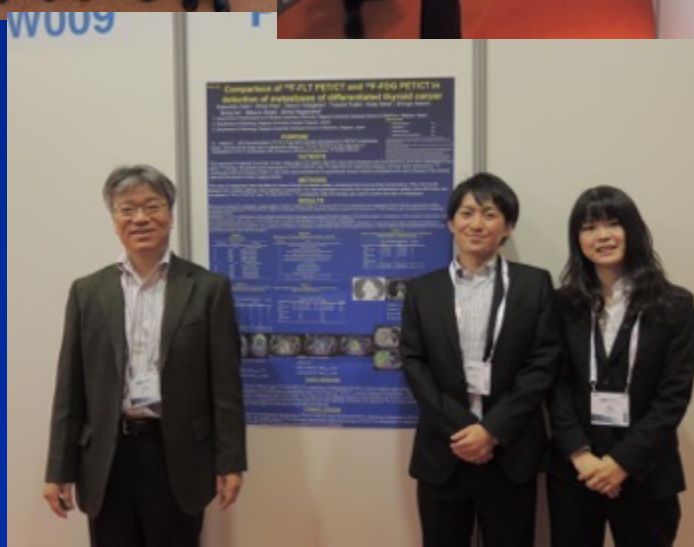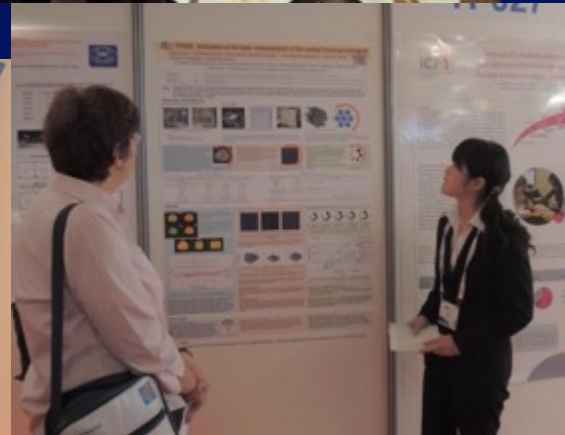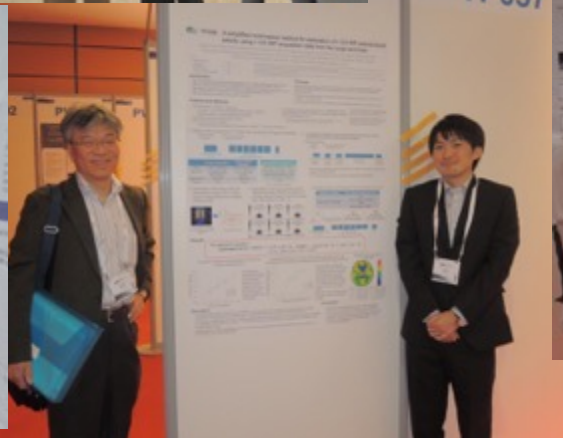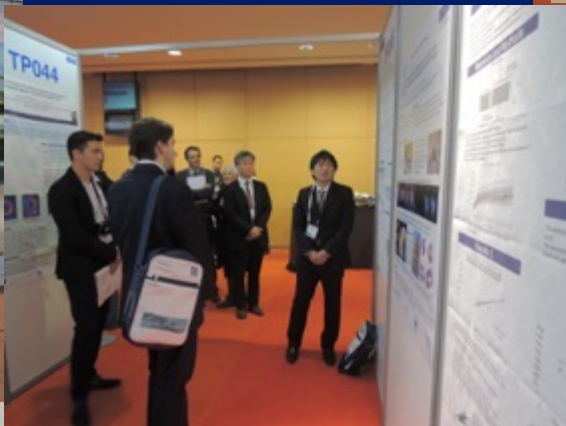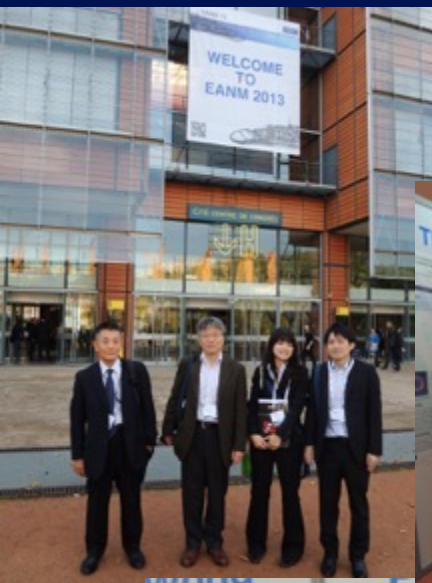
2014 SNM St. Louis

2014 EANM Göteborg

2014 RSNA
Chicago

2015 SPIE
Orlando

OPEN

Assessment of Severity in Chronic Thromboembolic Pulmonary Hypertension by Quantitative Parameters of Dual-Energy Computed Tomography

Yoshinori Tsutsumi, RT,*† Shingo Iwano, MD, PhD,‡ Naoki Okumura, MD, PhD,§ Shiro Adachi, MD, PhD,§ Shinji Abe, RT, PhD,* Takahisa Kondo, MD, PhD,§ Katsuhiko Kato, MD, PhD,† and Shinji Naganawa, MD, PhD‡

Objective: The objective of this study was to assess the correlation between dual-energy computed tomography quantitative parameters and hemodynamics in patients with chronic thromboembolic pulmonary hypertension.

Methods: Dual-energy computed tomography of 52 chronic thromboembolic pulmonary hypertension patients were evaluated retrospectively. The mean lung perfused blood volume (lung PBV) and the mean pulmonary artery (PA) enhancement measured at pulmonary parenchymal phase were compared with the hemodynamics by Spearman rank correlation coefficient (r_s) and receiver operating characteristic analysis.

Results: Lung PBV was correlated with mean pulmonary arterial pressure ($r_s = 0.47$, $P < 0.001$). Pulmonary artery enhancement was correlated with cardiac index ($r_s = -0.49$, $P < 0.001$) and pulmonary vascular resistance ($r_s = 0.48$, $P < 0.001$). The areas under the curves were 0.86 for lung PBV to predict mean pulmonary arterial pressure of >50 mm Hg and 0.86 for PA enhancement to predict pulmonary vascular resistance of >1000 dyne·s/cm[5].

Conclusions: Lung PBV and PA enhancement could be indicators of hemodynamics.

Key Words: Dual-energy computed tomography, chronic thromboembolic pulmonary hypertension, hemodynamics

Chronic thromboembolic pulmonary hypertension (CTEPH) is a specific type of pulmonary hypertension (PH) caused by obstructive vascular remodeling, which lead to increase pulmonary artery (PA) pressure and right heart failure.[1,2] The development of CTEPH has been suggested to be associated with acute pulmonary embolism.[1–3] The incidence of CTEPH within 2 years after acute symptomatic pulmonary embolism has been reported to range from 0.1% to 9.1%.[3]

Chronic thromboembolic pulmonary hypertension is defined as the presence of multiple chronic organized occlusive thromboembolisms in the pulmonary arteries, which accompany PH with a mean pulmonary arterial pressure (mPAP) of 25 mm Hg or more and a pulmonary arterial wedge pressure of 15 mm Hg or less.[1,2] Diagnosis of CTEPH is confirmed by pulmonary arteriography or

contrast-enhanced computed tomography (CT) based on the findings of mismatched lung perfusion using pulmonary ventilation/perfusion scintigraphy.[1,2]

The contrast-enhanced CT findings of CTEPH in the PA are a complete obstruction or partial filling defects such as vessel narrowing, intimal irregularities, and bands and webs caused by chronic organized blood clots.[2,4,5] In addition, the dilatation of the main PA diameter is known to be associated with PH.[6–10] The diameter ratio of the main PA to the ascending aorta (rPA) measured on a CT image is widely used as a noninvasive diagnostic method for PH.[8–10] The rPA is also known to correlate with the mPAP.[8,10] Recently, dual-energy computed tomography (DE-CT) has enabled us to analyze lung perfused blood volume (lung PBV) and is able to generate an iodine map image similar to that obtained by pulmonary perfusion scintigraphy. Its diagnostic utility for the evaluation of pulmonary perfusion in CTEPH has been reported to be equivalent to pulmonary perfusion scintigraphy.[11–13]

Right heart catheterization (RHC) is invasive but essential to evaluate the hemodynamics of CTEPH. The mPAP and pulmonary vascular resistance (PVR) obtained by RHC is one of the prognostic factors in CTEPH patients.[14–16] Therefore, it may be useful to identify high-risk patients by noninvasive CT examination. A few studies reported that quantitative or visual assessment of lung PBV significantly correlated with clinical parameters such as mPAP, PVR, or mosaic attenuation pattern in CTEPH patients.[17–19] It should be noted however that a correlation between quantitative evaluation using DE-CT and hemodynamic severity has not been demonstrated. Therefore, the purpose of this study was to consider whether contrast-enhanced DE-CT could be used to assess the severity of CTEPH.

MATERIALS AND METHODS

Patients

This retrospective study was approved by the institutional review board of Nagoya University Hospital (approval number 2017-0291) with waivers of informed consent from all participants. From April 2014 to July 2017, 58 consecutive patients who underwent DE-CT for the detailed examination or follow-up of CTEPH were treated at our institution. The diagnosis of CTEPH was confirmed by ventilation/perfusion scintigraphy, RHC, and pulmonary arteriography. Patients who underwent pulmonary endarterectomy or balloon pulmonary angioplasty were not included in this study, because of the various time intervals between CT and RHC that were performed before or after treatments. If multiple examinations were performed on a patient during the study period, only the first DE-CT examination was analyzed. This is because multiple examinations become a confounding factor to evaluate CT and RHC parameters. Three patients were excluded because of the presence of pulmonary disease (interstitial pneumonia, atypical mycobacterial disease, or emphysema). One patient was excluded because

Assessment of severity in chronic thromboembolic pulmonary hypertension by quantitative parameters of dual energy computed tomography

（Dual Energy CT から得られる定量値を用いた慢性血栓塞栓性肺高血圧症の重症度評価）

Yoshinori Tsutsumi, Shingo Iwano, Naoki Okumura, Shiro Adachi, Shinji Abe, Takahisa Kondo, Katsuhiko Kato, Shinji Naganawa

CTEPHの定義

CTEPH：慢性血栓性肺高血圧症

（chronic thromoboembolic pulmonary hypertension）

慢性肺血栓塞栓症

血栓溶解療法または抗凝固療法施行

後も6か月以上不変

肺高血圧症

1. 肺動脈圧の上昇
   平均肺動脈(mPAP):25mmHg以上

2. 肺動脈楔入圧(PAWP)が正常
   15 mmHg以下

Tsutsumi Y, et al. J Comput Assist Tomogr. 2020;44(4):578-585.

Conclusion

- Lung PBV値はmPAPと正の相関にあることから、高濃度の造影剤が肺血管内に停滞している可能性があり、肺循環の灌流不良を示している。

- Lung PBV は、血行動態の指標として利用が可能であり、非侵襲的な検査であるDE-CTは、重症のCTEPH患者を識別する上でも有用である。

Tsutsumi Y, et al. J Comput Assist Tomogr. 2020;44(4):578-585.

Magna Cum Laude Radiographer Poster Award

Congratulations go to

Mr. Yoshinori Tsutsumi, Nagoya/JN

in merit of the scientific poster C-0883 entitled:

Assessment of the severity in chronic thromboembolic pulmonary hypertension by quantitative parameters of energy CT

Comparison of low pulmonary perfusion index using ^{99m}Tc-MAA SPECT and hemodynamic parameters in chronic thromboembolic pulmonary hypertension

Yuka Ochi[1], Yoshinori Tsutsumi[3], Naotoshi Fujita[2][3], Yoshinori Ito[2], Risa Oono[2], Tomohiro Tada[2], Rina Murayama[2], Haruna Ikeda[1], Miho Nishio[1], Mika Tamura[2], Tetsuro Odagawa[2], Shinji Yamaguchi[1], Shinji Abe[3], Katsuhiko Kato[1]

[1] Department of Integrated Health Sciences, Nagoya University Graduate School of Medicine, Nagoya, Japan
[2] Department of Radiological and Medical Laboratory Sciences, Nagoya University Graduate School of Medicine, Nagoya, Japan
[3] Department of Radiological Technology, Nagoya University Hospital, Nagoya, Japan
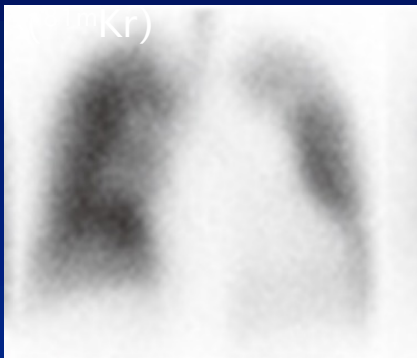
Nagoya University Graduate School of Medicine

Summary

- Right-sided heart catheterization, pulmonary ventilation scintigraphy using ^{81m}Kr, and pulmonary perfusion scintigraphy using ^{99m}Tc-MAA are performed to diagnose chronic thromboembolic pulmonary hypertension (CTEPH).

pulmonary ventilation
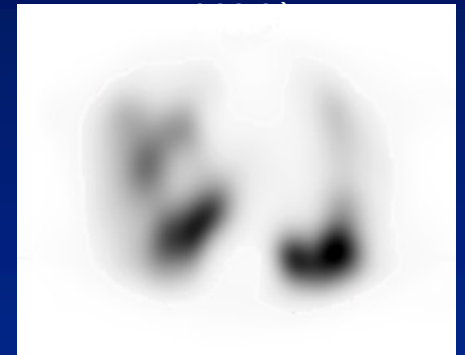planer imaging
(^{81m}Kr)

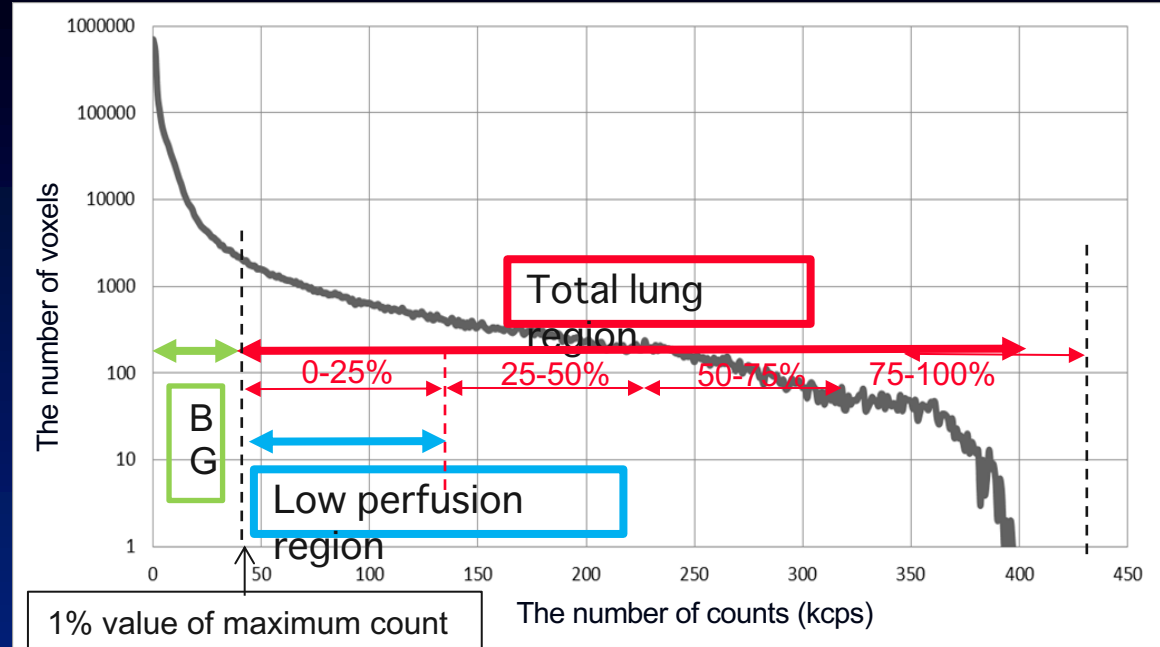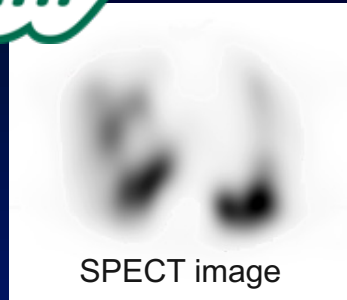pulmonary perfusion
planer imaging (^{99m}Tc-MAA)
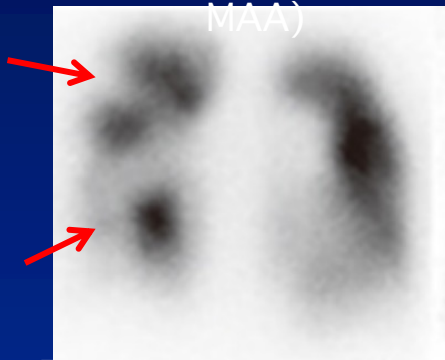
pulmonary perfusion
SPECT imaging (^{99m}Tc-MAA)

- Hemodynamic indicators [mean pulmonary arterial pressure (mPAP) and pulmonary vascular resistance (PVR)] obtained from right heart catheterization are used to assess the severity of CTEPH, but it is highly invasive.

- The aim of this study is investigating whether it is possible to evaluate the severity of CTEPH using the index obtained from SPECT images of pulmonary blood flow scintigraphy using ^{99m}Tc-MAA, which is less invasive.

Ochi Y, et al. J Nucl Med. 2020; 61 (suppl 1): 3087.

SPECT image

Total lung region

0-25%   25-50%   50-75%   75-100%

BG

Low perfusion region

The number of voxels

The number of counts (kcps)

1% value of maximum count

$$\text{Low perfusion index} = \frac{\text{Low perfusion region volume (cm}^3)}{\text{Total lung region volume (cm}^3)}$$

➢ As a result of investigating the correlations between the low perfusion index and the hemodynamic index, there are weak correlations was found between the low perfusion index and mPAP or PVR. (mPAP :r=0.313, p<0.005, PVR :r=0.364, p<0.005)

In the future, further studies will be required, such as changing the BG threshold and determining the threshold for each patient .
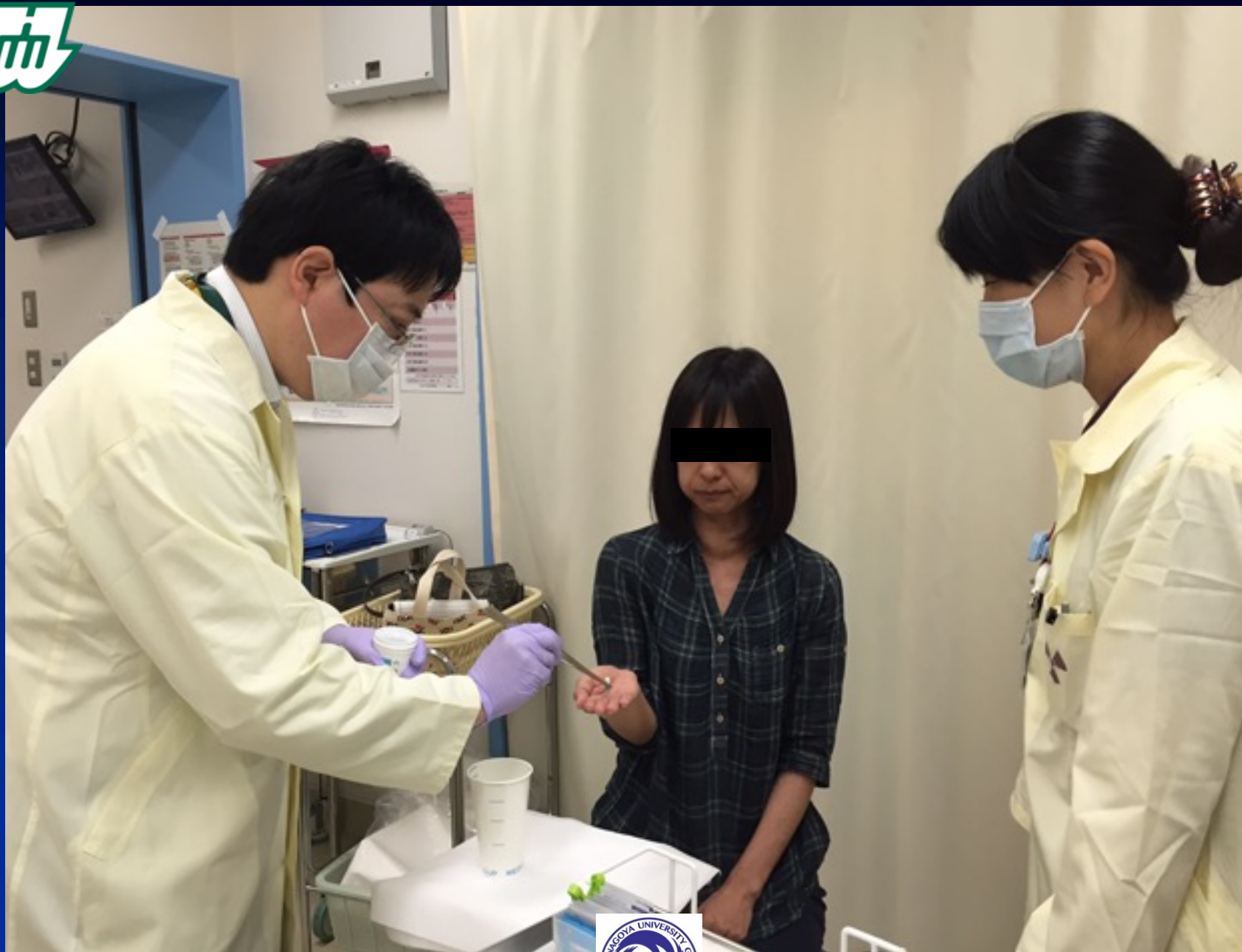
Ochi Y, et al. J Nucl Med. 2020; 61 (suppl 1): 3087.

甲状腺機能亢進症、甲状腺癌の
^{131}I 内用療法

- 70年以上の歴史を有する安全な治療法
- 有用性は国際的に定着
- ^{131}Iカプセルを内服

臨床臨床核医学を改変

Radioiodine treatment of thyroid disease

Muenster University Hospital
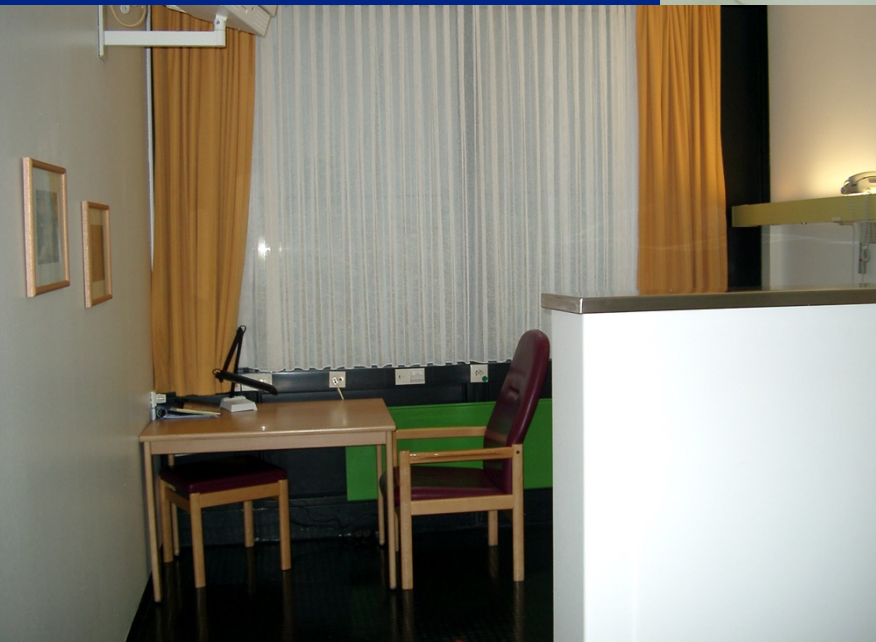
Nagoya University Graduate School of Medicine

ヨウ素制限中の食事

絶対に食べてはならない食品

大量のヨウ素が含まれていて、少しの摂取でも大きな影響を受けます。

海藻類 ・・・ 昆布、わかめ、のり、ひじき、もずくなど

昆布加工品 ・・・ とろろ昆布、おぼろ昆布、昆布佃煮、昆布茶など

昆布だし、風味調味料・・・ 昆布だし、昆布だしを含む風味調味料など

昆布エキス含有食品 ・・・ インスタント味噌汁、だしの素、だし入り醤油など

＊市販の調味料（醤油・みそ・酢を含めて）の中には、
昆布だし、昆布エキスなどを使用しているものがあります。

ヨード強化卵 ・・・ ヨード強化卵は多量のヨウ素が含まれています。

Nagoya University Graduate School of Medicine

ヨウ素制限中の食事

できるだけ食べないように注意する食品

比較的ヨードが多く含まれている食品です。
思いがけない食品や食材にヨードが含まれることがあるので注意が必要です.

テングサ加工品・・・ 　寒天、ところてん、羊羹、こんにゃく

魚介類・・・ 　　　　鱈（たら）および鱈を使用した練り製品

　　　　　　　　　　青身魚・・・さば、いわし、かつお、ぶり、にしん

　　　　　　　　　　赤身魚・・・まぐろ、さけ、ます、ツナ缶など

　　　　　　　　　　貝類、えび、かに

肉類・・・ 　　　　レバー、モツ、ホルモン　等

カラギナン含有食品・・・ 　豆乳、ドレッシング、ゼリー、プリン、アイスクリー

その他の注意・・・ 　補助栄養食品（サプリメント）や自然食品類にも含まれることがあ

　　　　　　　　　　欧米ではヨード添加食塩が使用されていることが多い

☆注意：1回程度の摂取なら繰り返さないように注意すれば心配ありません。

患者様向け ヨウ素制限食のポイント Point 第3版

カレスサッポロ 北光記念病院

監修

栄養科 田村 美香　鷲原 領子
放射線科 中驫 邦博　　院長 櫻井 正之

ヨウ素制限食の食品一覧表

	食べてもよい食品	1回量を1人前程度で制限する食品	禁止食品
穀類	ごはん、パン、めん、スパゲティ、もち、小麦粉など		めん類の時の汁、おにぎりの海苔、食紅を使った赤飯
いも・でん粉類	全ての芋・でん粉 はるさめ・くずきりなど		ひじきの入ったこんにゃく
砂糖・甘味料	さとう・はちみつなど全ての甘味料	黒砂糖	
豆類	ほぼ全ての豆類	木綿豆腐	納豆のたれ（昆布エキス）、だし入り味噌・しょうゆなど
種実類	ごま・くり・落花生など全ての種実類		アーモンド・ピーナツバターなど外国産の食品（ヨウ素添加量）
野菜類	ほぼ全ての野菜類		紅しょうが、梅干、福神漬（人工赤色着色料）
果実類	全ての果実類		チェリー缶（人工赤色着色料）
きのこ類	全てのきのこ類		
藻類			昆布、わかめ、のりなど海藻類全般 NO!
魚介類	エビ・ホタテ貝柱	イカ・タコ・ヒラメ・メバチ・ホッケ・ハマチ・カンパチ・カジキ・アユ・マグロ・アナゴ・サケ	タラ・タラコ・タイ・イワシ・ハタハタ・ワカサギ・シシャモ・アジ・カツオ・ブリ・サバ・サンマ・カレイ・アワビ・サザエ・アンコウきも・ナマコ・カキ・アサリ・練り製品など魚介類全般注意
肉類	全ての肉類		ホルモンなどの内臓類 ウインナー、ハムなどの人工赤色着色料・昆布エキス
卵類		鶏卵	ヨウ素卵（ヨウ素強化）卵豆腐、出し巻き卵、茶わん蒸し（昆布だし）

ヨウ素制限食栄養指導用の小冊子

ヨウ素制限(low iodine diet: LID) 1週間と2週間の比較

名古屋大学大学院医学系研究科医療技術学専攻医用量子科学分野

田村 美香

- バセドウ病の放射性ヨウ素治療の成功率

- 放射性ヨウ素治療の効果判定は、

放射性ヨウ素治療後1年以内に抗甲状腺薬を休薬できた、または、

放射性ヨウ素治療前に抗甲状腺薬を投与されていない患者は治療後

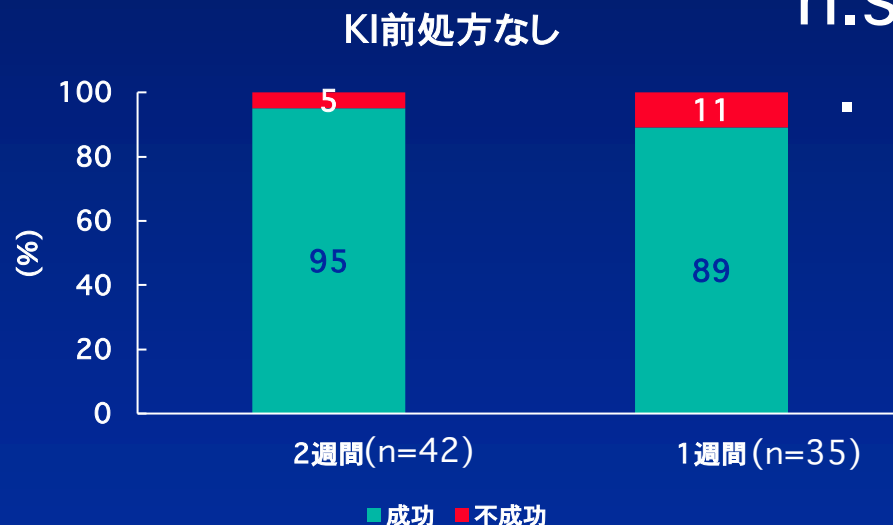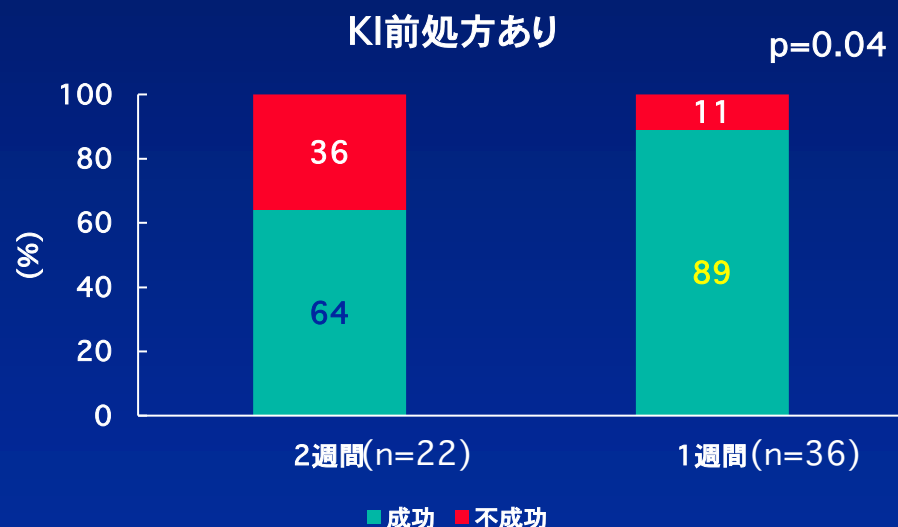1年以内に甲状腺機能が正常化、及び潜在性甲状腺機能低下症な

いし甲状腺機能低下症へ移行した場合を「治療成功」と定義した。

ヨウ素制限 1週間と2週間の比較

・バセドウ病の放射性ヨウ素治療の成功率 Fisher's Exact Test

	p-value	odds ratio
ヨウ化カリウム(KI)前処方 あり　LID 1週間vs.2週間	0.04	0.20
ヨウ化カリウム(KI)前処方 なし　LID 1週間vs.2週間	0.40	2.5

n.s

KI前処方あり p=0.04

KI前処方なし

「KI前処方あり」では、有意に1週間のヨウ素制限の方が成功率が高かった。

「KI前処方なし」では、有意差はなかった

Tamura M, et al. SNMMI 2019.

Nagoya University Graduate School of Medicine

ヨウ素制限(LID) 1週間と2週間の比較

・バセドウ病のLID後の尿中ヨウ素濃度(UICμg/gCRE)の変化

(wilcoxon符号付順位和検定)
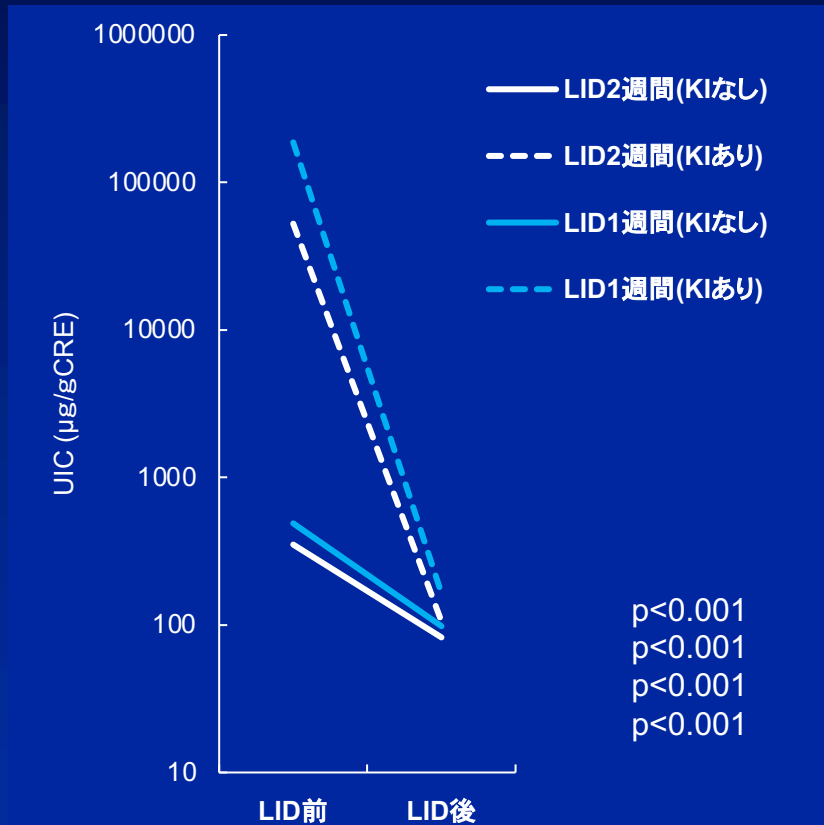
	UIC1	UIC2
LID2週間(KIなし)	350.8±412.7	82.4±144.2
LID2週間(KIあり)	52555.4±77915.1	105.8±95.3
LID1週間(KIなし)	488.5±818.4	98.2±110.1
LID1週間(KIあり)	187085±240187.2	164.3±253.7

LID後のUICは、

いずれの群も有意な低下を認めた。

Tamura M, et al. SNMMI 2019.

ヨウ素制限 1週間と2週間の比較

・ バセドウ病のLID後の尿中ヨウ素濃度(UICμg/gCRE) Fisher's Exact Test

	p-value	odds ratio
ヨウ化カリウム(KI)前処方 あり LID 1週間vs.2週間	0.41	1.68
ヨウ化カリウム(KI)前処方 なし LID 1週間vs.2週間	0.29	1.93

KI前処方あり   n.s

KI前処方なし   n.s

LID2週間 (n=22) LID1週間 (n=36)
■UIC100μg/gCRE未満 ■UIC100μg/gCRE以上

LID2週間 (n=42) LID1週間 (n=35)
■UIC100μg/gCRE未満 ■UIC100μg/gCRE以上
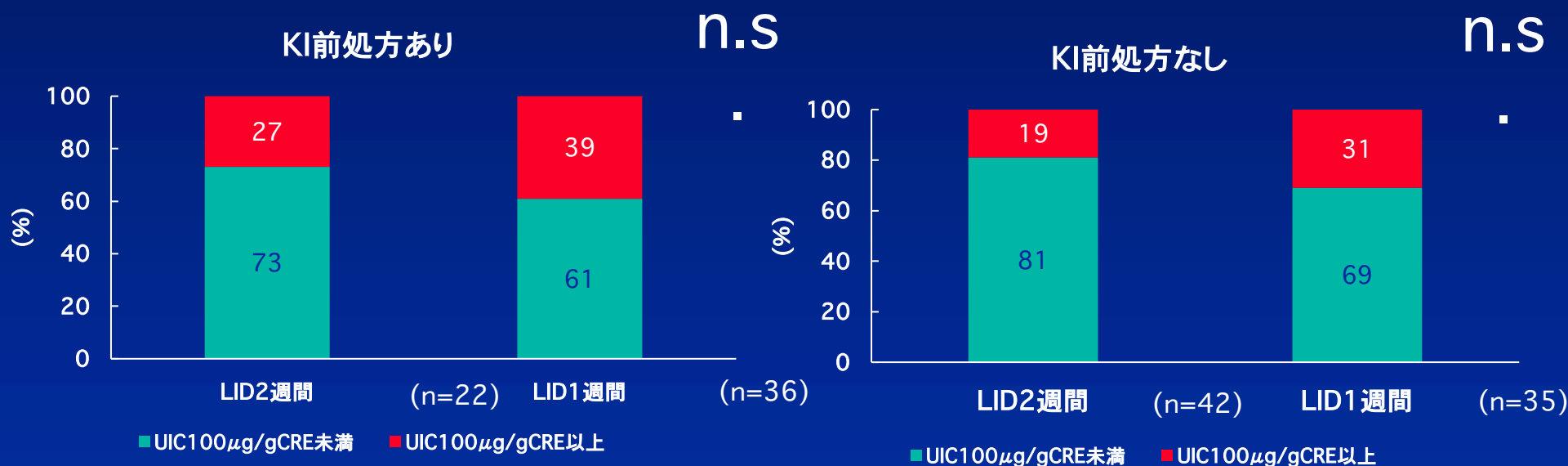
UIC 100μg/gCRE 未満か否かで区分した場合、LID1週間も2週間も有意差を認めなかった。
（WHO区分: 尿中ヨウ素排泄量 <100μg/l …ヨウ素欠乏）

Tamura M, et al. SNMMI 2019.

Nagoya University Graduate School of Medicine

ORIGINAL ARTICLE

Effect of previous administration of potassium iodine and different durations of low iodine diets for radioiodine therapy on the treatment of Graves' disease in iodine-rich areas

Mika Tamura[1,2] · Kunihiro Nakada[3] · Haruna Iwanaga[1,4] · Naotoshi Fujita[4] · Katsuhiko Kato[5]

Abstract

Purpose To examine whether adherence to a low-iodine diet (LID) enhances the therapeutic efficacy of radioiodine therapy (RAI) in Graves' hyperthyroidism (GH) in iodine-rich areas.

Methods We retrospectively evaluated 185 patients with GH from Aichi (n = 114) and Hokkaido (n = 71) Prefectures. Patients aged ≥ 18 years with GH who underwent RAI between December 2012 and March 2022 were divided into subgroups based on pretreatment with anti-thyroid drug (ATD) or potassium iodide (KI). Patients were followed up with LID from 18 days (group A) or 7 days (group H) before RAI to 3 days after RAI. The dose of radioactive iodine 131 (^{131}I) was adjusted to deliver > 100 Gy to the thyroid. The associations between urinary iodine concentration on UIC2 vs. 24hRU and UIC2 vs. the 1-year RAI success rate (SR) were investigated.

Results Compared with UIC1, UIC2 was significantly decreased in all subgroups (P < 0.01). An inverse correlation between UIC2 and 24hRU was observed in the four groups; however, the difference was insignificant. The SR in groups A and H was 85% and 89%, respectively. Univariate analysis revealed no association between UIC2 and SR in each group. Additionally, stratification of the 185 patients into quartiles using UIC2 yielded no significant differences in SR (p = 0.79).

Conclusions LID sufficiently reduced UIC in patients undergoing RAI. Although a lower UIC2 may increase 24hRU, it did not increase the success of RAI. The benefit of LID in enhancing the efficacy of RAI in GH treatment remains uncertain.

Keywords Radioiodine therapy · Low iodine diet · Graves' hyperthyroidism · Urinary iodine concentration · Iodine-rich areas

✉ Katsuhiko Kato
katokt@med.nagoya-u.ac.jp

1 Department of Radiological and Medical Laboratory Sciences, Nagoya University Graduate School of Medicine, Nagoya, Japan

2 Department of Clinical Nutrition, Hokko Memorial Hospital, Sapporo, Japan

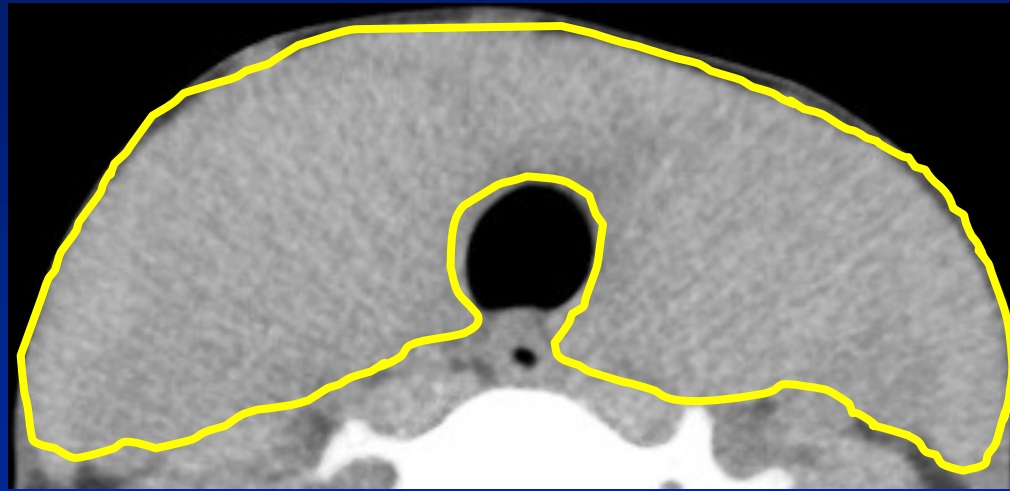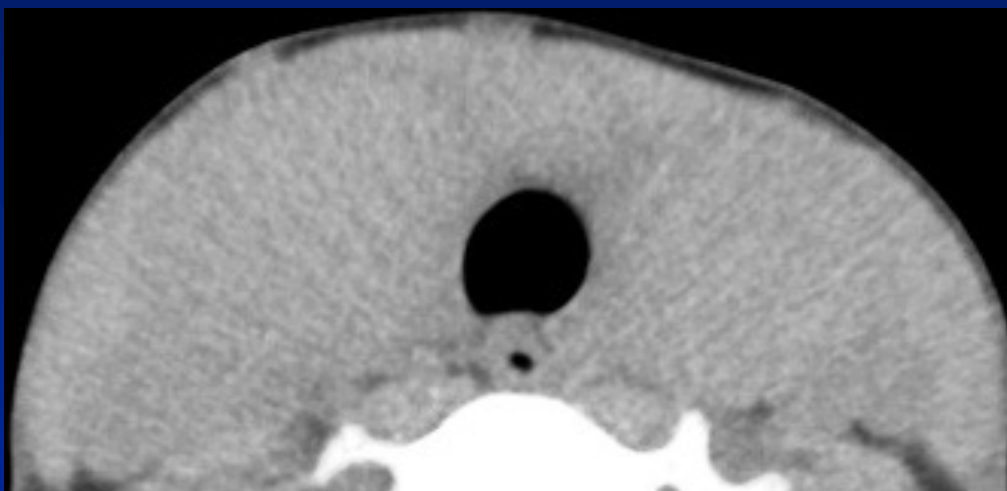3 Department of Radiology, Hokko Memorial Hospital, Sapporo, Japan

4 Department of Radiological Technology, Nagoya University Hospital, Nagoya, Japan

Introduction

Graves' hyperthyroidism (GH) is the most common cause of hyperthyroidism. Anti-thyroid drugs (ATDs), radioactive iodine ^{131}I therapy (RAI), and thyroidectomy are the main treatments for GH [1]. Serious side effects can occur following administration of ATDs and thyroidectomy. RAI is an established and safe treatment option for GH. Identifying the factors that affect RAI efficacy can help improve patient outcomes and reduce healthcare costs associated with GH. These factors include thyroid weight and hormone levels before treatment, duration of ATD use, and other clinical factors [2–4]. Two preparations are recommended before ^{131}I administration to enhance RAI efficacy: withdrawal

甲状腺重量推定法

頸部単純CT（5㎜スライス）　　　スライス毎にROIを設定

推定重量（g）＝ROIの面積（mm²）×5（mm）×比重1（g/mm³）

Nagoya University Graduate School of Medicine

甲状腺短径の測定長または測定断面積の違いによる甲状腺体積の変動
−X線CT画像を用いた甲状腺体積の楕円体近似法の検証−

Quimbyの式

$$投与放射能 = 単位変換係数 \times \frac{甲状腺吸収線量 \times 甲状腺体積}{甲状腺ヨウ素摂取率 \times 有効半減期}$$

甲状腺体積測定法について

・一般的には**超音波画像**にて行う（簡便さとコスト的観点から）
・体積測定は**楕円体近似法**を用いる
左葉,右葉,峡部に対して,長径,短径,横径から
体積 ＝ π／６×長径×短径×横径 [cm^3] を求め合計する

X線CT画像を用いた体積測定

横断像から甲状腺領域を抽出し,各スライスの面積を算出
体積 ＝ ∑（各スライスの面積×スライス厚）[cm^3]

ここが〇 超音波画像を用いた体積算出に比較して**正確さは高い**
ここが× 甲状腺部分をトレースする作業が**煩雑,放射線被ばく**を有する

楕円体近似法における甲状腺の測定長（特に短径,横径に着目）
によって,甲状腺体積がどの程度変動するかを検証した
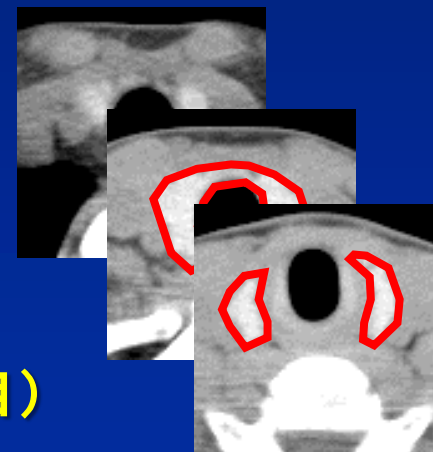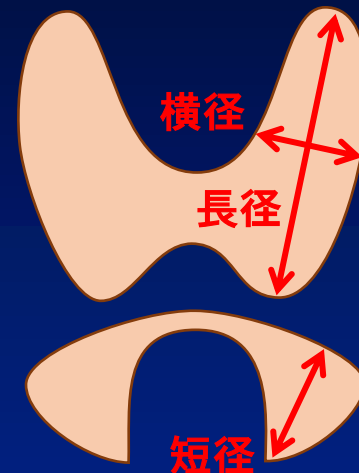
横径
長径
短径

Nagoya University Graduate School of Medicine

三次元的甲状腺体積測定（V_{CT}）

Axial plane	■ Thyroid ■ Artery ■ Vein ■ Trachea
Sagittal plane	Coronal plane
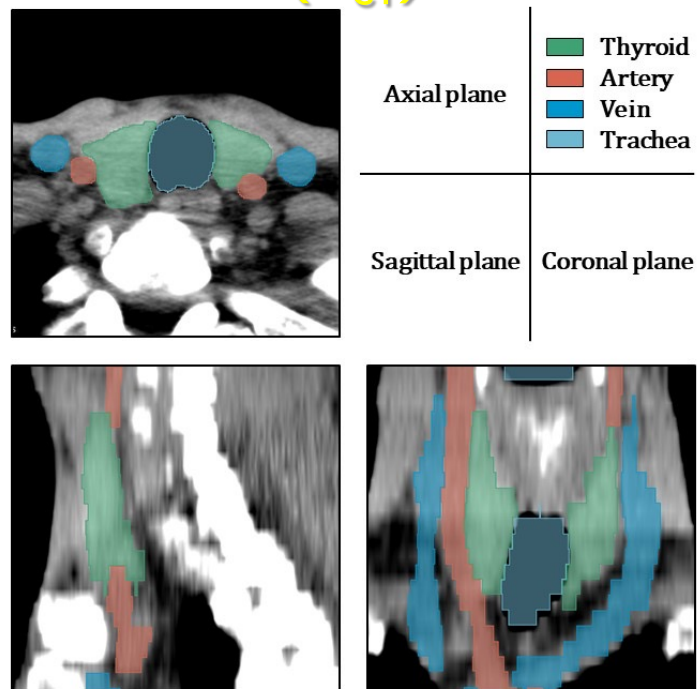
撮影した5mmスライス/5mm間隔のCT画像から用手的に甲状腺領域を抽出し,各スライスにおける甲状腺体積の総和として算出した

楕円体近似を用いた体積測定（$V_{ellipsoid}$）

各葉で楕円体近似体積を計算

Centroid of the thyroid ROI

任意の径を取得

Cross-sectional plane
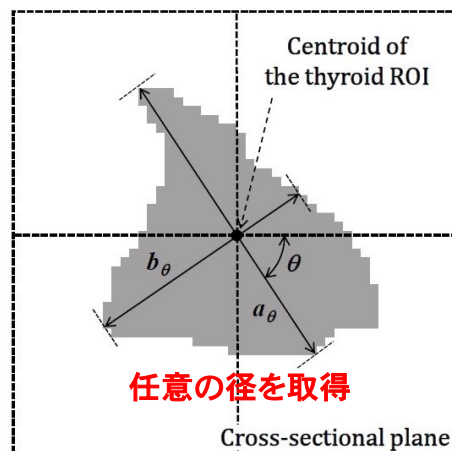
Ellipsoid approximation
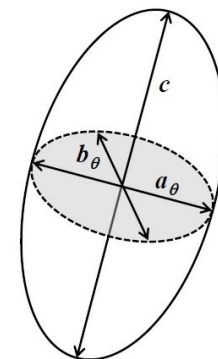
$$V_{ellipsoid}(\theta_L, \theta_R) = \left(\frac{\pi}{6} \times a_{\theta_L} \times b_{\theta_L} \times c_L\right)_{Left\,lobe} + \left(\frac{\pi}{6} \times a_{\theta_R} \times b_{\theta_R} \times c_R\right)_{Right\,lobe}$$

(8100 volumes)　　　　(90 volumes)　　　　(90 volumes)

The Mean volume of the 8100 thyroid volumes	: $V_{ellipsoid,mean}$
The volume using the maximum diameter (either a_θ or b_θ) combined with its orthogonal diameter	: $V_{ellipsoid,maxlength}$
The maximum volume among the 8100 thyroid volumes	: $V_{ellipsoid,maxvolume}$
The minimum volume among the 8100 thyroid volumes	: $V_{ellipsoid,minvolume}$

円相当径 $R[cm] = 2\sqrt{S/\pi}$　　　を用いた方法
（ $V_{ellipsoid,Heywood}$ ）

$$V_{ellipsoid,Heywood}\,[cm^3] = \left(\frac{\pi}{6} \times R_L \times R_L \times c_L\right)_{Left\,lobe} + \left(\frac{\pi}{6} \times R_R \times R_R \times c_R\right)_{Right\,lobe}$$

上記の5手法（$V_{ellipsoid}$）について,CT画像から三次元的に算出した甲状腺体積（V_{CT}）と比較し,楕円体近似の妥当性と最適な手法について検討した

Fujita N, et. al. Variation in thyroid volumes due to differences in the measured length or area of the cross-sectional plane: A validation study of the ellipsoid approximation method using CT images. J Appl Clin Med Phys. 2021;22(4):15-25.

Relationship between V_{CT} and the five approximate volumes.
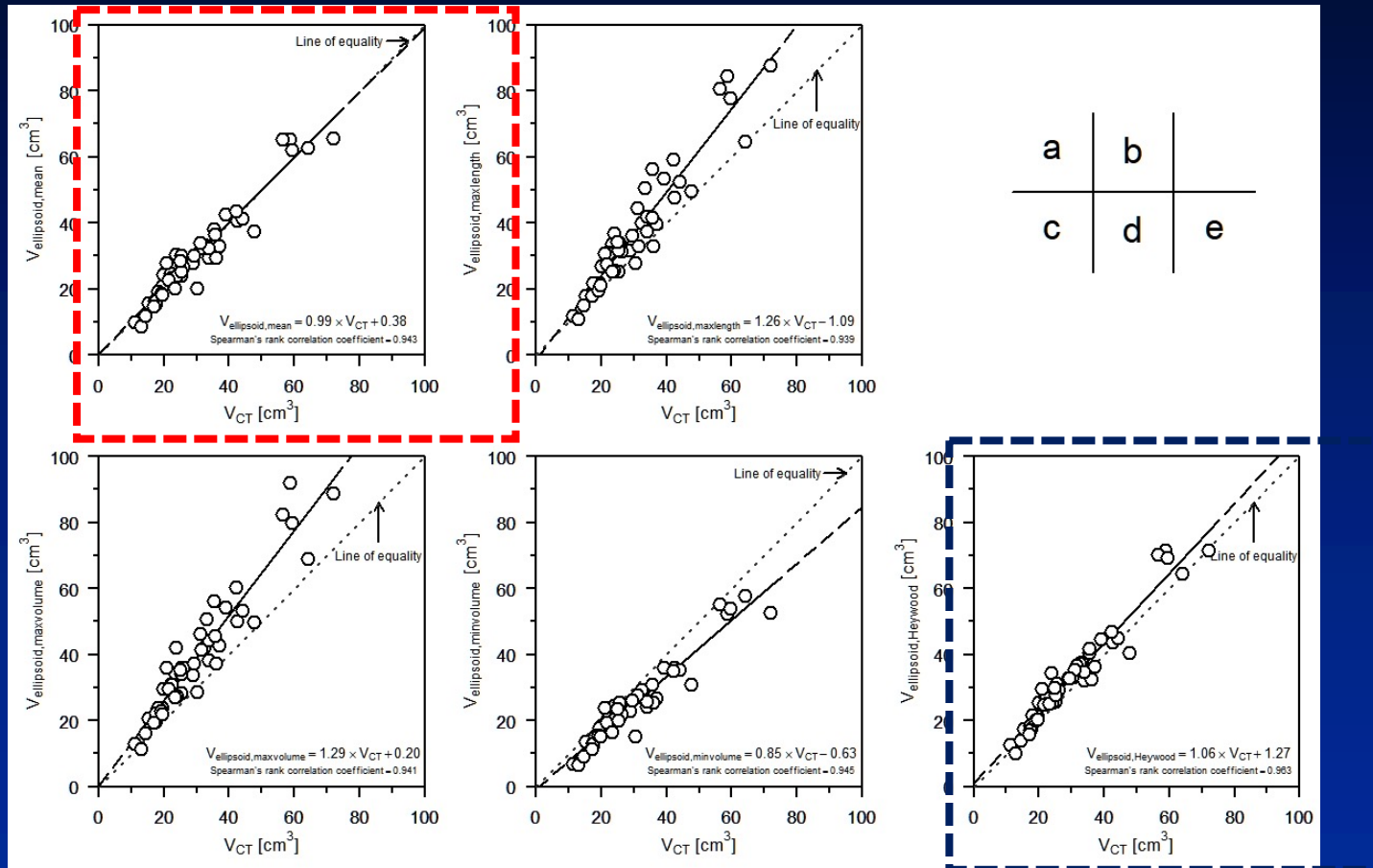
・任意の*a,b*の長さをもとに楕円体近似すると甲状腺体積は変動する
・楕円体近似体積の平均値を用いた場合（ $V_{ellipsoid,mean}$;赤枠），円相当径を用いた場合
の楕円体近似体積（ $V_{ellipsoid,Heywood}$;青枠）はV_{CT}と良好な一致関係を認める

Fujita N, et. al. Variation in thyroid volumes due to differences in the measured length or area of the cross-sectional plan
A validation study of the ellipsoid approximation method using CT images. J Appl Clin Med Phys. 2021;22(4):15-25.

Error rate between V_{CT} and the five approximate volumes.

平均誤差は10〜20%程度,
場合によっては誤差が50%を
超える症例もあった
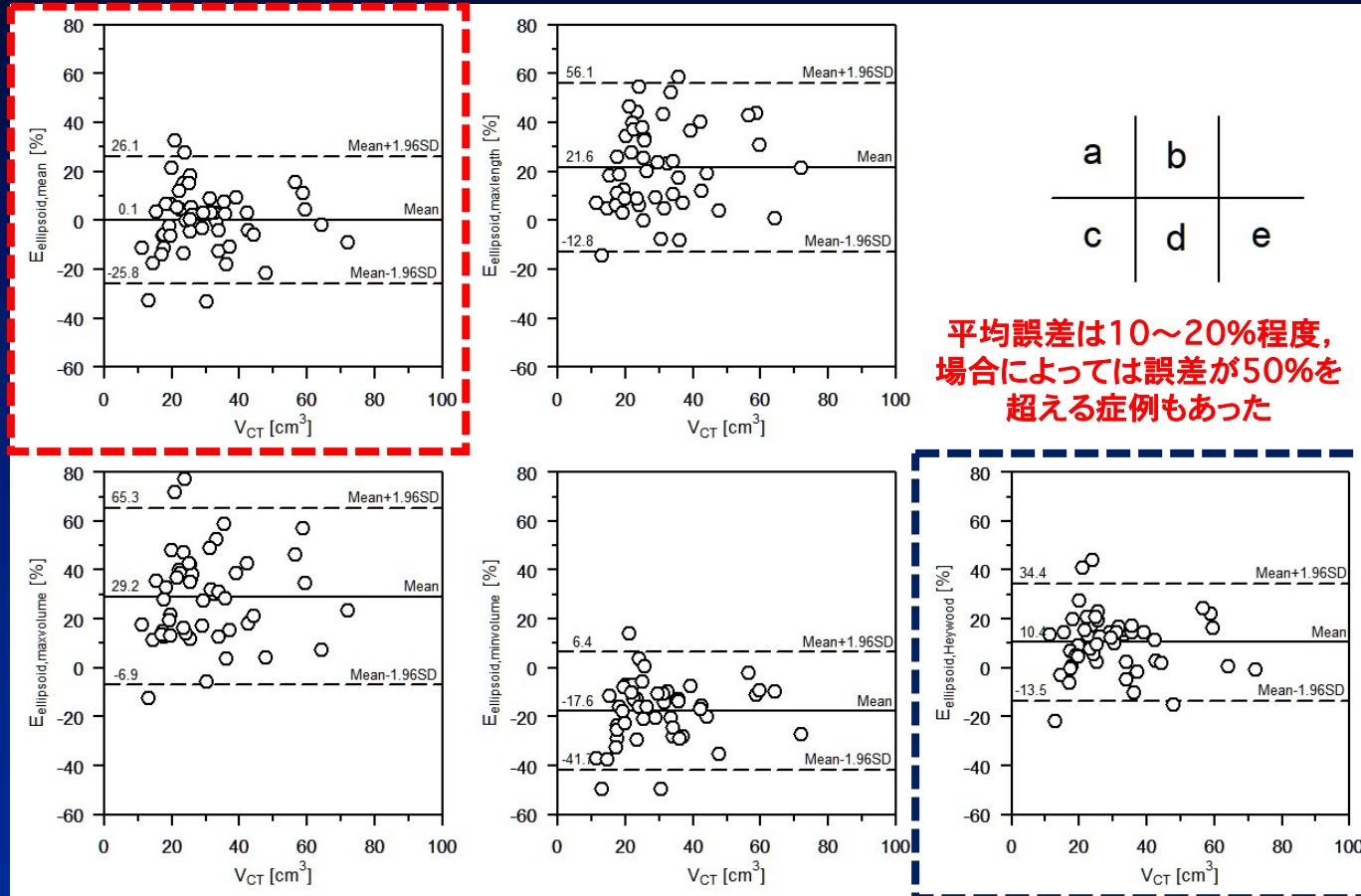
・楕円体近似による甲状腺体積測定は,完全な代替手段にはなりえないかもしれない
・十分な測定精度を必要とする場合には,三次元的な甲状腺体積測定を行う必要がある

Fujita N, et. al. Variation in thyroid volumes due to differences in the measured length or area of the cross-sectional plan
A validation study of the ellipsoid approximation method using CT images. J Appl Clin Med Phys. 2021;22(4):15-25.

WILEY

Variation in thyroid volumes due to differences in the measured length or area of the cross-sectional plane: A validation study of the ellipsoid approximation method using CT images

Naotoshi Fujita[1,2] | Katsuhiko Kato[3] | Shinji Abe[1] | Shinji Naganawa[4]

[1]Department of Radiological Technology, Nagoya University Hospital, Nagoya, Japan

[2]Department of Radiological and Medical Laboratory Sciences, Nagoya University Graduate School of Medicine, Nagoya, Japan

[3]Functional Medical Imaging, Biomedical Imaging Sciences, Division of Advanced Information Health Sciences, Department of Integrated Health Sciences, Nagoya University Graduate School of Medicine, Nagoya, Japan

[4]Department of Radiology, Nagoya University Graduate School of Medicine, Nagoya, Japan

Author to whom correspondence should be addressed. Katsuhiko Kato
E-mail: katokt@med.nagoya-u.ac.jp

Abstract

Purpose: This study examined the variation in the thyroid volume determined by the ellipsoid approximation method due to differences in the measured length or area of the cross-sectional plane of CT images.

Methods: Forty-five patients with Graves' disease were included in this retrospective study. We designated the three-dimensional thyroid volumes extracted manually (V_{CT}) as the reference data and calculated five approximate volumes for comparison: (a) the mean volume of 8100 different thyroid volumes depending on the diameter of the cross-sectional plane at the midpoint of the major axis, ($V_{ellipsoid,mean}$); (b) the volume using the maximum diameter and its orthogonal diameter, ($V_{ellipsoid,maxlength}$); (c) the maximum ($V_{ellipsoid,maxvolume}$); (d) minimum ($V_{ellipsoid,minvolume}$) of the 8100 thyroid volumes; and (e) the volume determined with an equivalent circle diameter, ($V_{ellipsoid,Heywood}$).

Results: Thyroid volumes obtained via the ellipsoid approximation method varied depending on the diameter of the cross-sectional plane and included a mean error of approximately 20%, while the concordance correlation coefficient (CCC) differed for each approximate volume. Among these volumes, $V_{ellipsoid,mean}$ and $V_{ellipsoid,Heywood}$ were in good agreement with V_{CT}, according to single regression analyses and the resultant CCC values, with mean errors of 0.1% and 10.4%, respectively.

Conclusion: While $V_{ellipsoid,Heywood}$ approximated thyroid volumes with vastly reduced errors, we recommend utilizing three-dimensional thyroid volumetry if measurement accuracy is required.

KEY WORDS

CT, ellipsoid approximation, graves' disease, internal radioiodine therapy, thyroid, volumetry

1 | INTRODUCTION

Internal radioiodine therapy (iodine-131) is a treatment for Graves' disease.[1] In radioiodine therapy for Graves' disease, the administered radioactivity is often determined based on the patient's thyroid volume.[2-4] Therefore, accurate thyroid volumetry before radioiodine therapy leads to the accurate determination of the administered radioactivity, thereby ensuring the therapeutic effect. Thyroid

^{131}I 投与量を目標吸収線量を70〜200Gy

Quimbyの式：

$$\frac{\text{投与量}}{\text{（MBq）}} = \frac{\text{吸収線量（cGy）} \times \text{甲状腺重量（g）}}{5.4 \times 24\text{時間ヨード摂取率（％）} \times \text{有効半減期（日）}}$$

吸収線量　　70〜200 Gy (7000〜20000 cGy)

バセドウ（グレーブス）病患者を対象としたSPECT定量画像とヨウ素の体内動態を用いた甲状腺吸収線量算出法

Quimbyの式

$$投与放射能 = 単位変換係数 \times \frac{甲状腺吸収線量 \times 甲状腺体積}{甲状腺ヨウ素摂取率 \times 有効半減期}$$

➡ 式中の甲状腺吸収線量は ^{131}I投与放射能から逆算される「**目標値**」ないし「**推定値**」

= Pre-therapeutic dosimetry

⬍ 実際の甲状腺吸収線量が適切に測定できていないという問題点
＝ 甲状腺吸収線量がわからないため,治療効果を予測できない

内用療法時のSPECT画像から ^{131}I の取り込みや分布を可視化し,そこから甲状腺吸収線量を「**実測値**」として算出できないか？

= Post-therapeutic image-based dosimetry

MIRD*ガイドラインにおけるvoxel dosimetry を拡張し,SPECT定量画像とヨウ素の体内動態を用いた甲状腺吸収線量算出法を提案した

* MIRD: Medical Internal Radiation Dose Committee

Fujita N, et. al. Investigation of post-therapeutic image-based thyroid dosimetry using quantitative SPECT/CT, iodine biokinetics, and the MIRD's voxel S values in Graves' disease. EJNMMI Phys. 2020; 7(1): 6. doi: 10.1186/s40658-020-0274-7.

Nagoya University Graduate School of Medicine

・従来手法 D_{EANM} :EANM-based thyroid dosimetry (Pre-therapeutic dosimetry)

Hänscheid H, et. al. Eur J Nucl Med Mol Imaging. 2013; 40(7): 1126–34

$$D_{EANM}[Gy]=A\cdot\bar{E}\cdot\int_0^\infty RIU(t)dt\,/V=\frac{A_a\cdot\bar{E}\cdot k_t}{V\cdot k_B\cdot k_T}$$

V:甲状腺体積[cm^3], A_a:投与放射能[MBq], $\bar{E}$:^{131}I 単位崩壊あたりの平均沈着エネルギー[MBq d Gy^{-1} cm^{-3}]

$RIU(t)$:時刻 t における甲状腺ヨウ素摂取率

k_t:血中から甲状腺への移行定数[d^{-1}], k_B:血中外への移行定数[d^{-1}], k_T:甲状腺外への移行定数[d^{-1}]

・提案手法 D_{image} :Post-therapeutic image-based dosimetry

➡ 内用療法時のSPECT画像から甲状腺吸収線量を「実測値」として算出する

$$D_{image}(x,y,z)[Gy]=\int_0^\infty \frac{C_{thyroid}(x,y,z)\cdot S_{vol}}{T_{thyroid}\cdot RIU(24h)}\cdot RIU(t)dt\otimes k_S$$

$$\bar{D}_{image,PVC}[Gy]=\frac{\bar{D}_{image}}{W_{PVC}}$$

甲状腺領域内の平均吸収線量を$\bar{D}_{image}$
とし，部分容積効果を補正したもの

$C_{thyroid}$:甲状腺SPECT画像のボクセルカウント, $T_{thyroid}$:甲状腺SPECT画像の撮像時間[sec.],
S_{vol}:system volume sensitivity [MBq/cps], k_s:voxel S value* [mGy・MBq^{-1}・sec^{-1}]

* Bolch WE, et. al. J Nucl Med. 1999; 40(1): 11S–36S.

Fujita N, et. al. Investigation of post-therapeutic image-based thyroid dosimetry using quantitative SPECT/CT, iodine biokinetics, and the MIRD's voxel S values in Graves' disease. EJNMMI Phys. 2020; 7(1): 6. doi: 10.1186/s40658-020-0274-
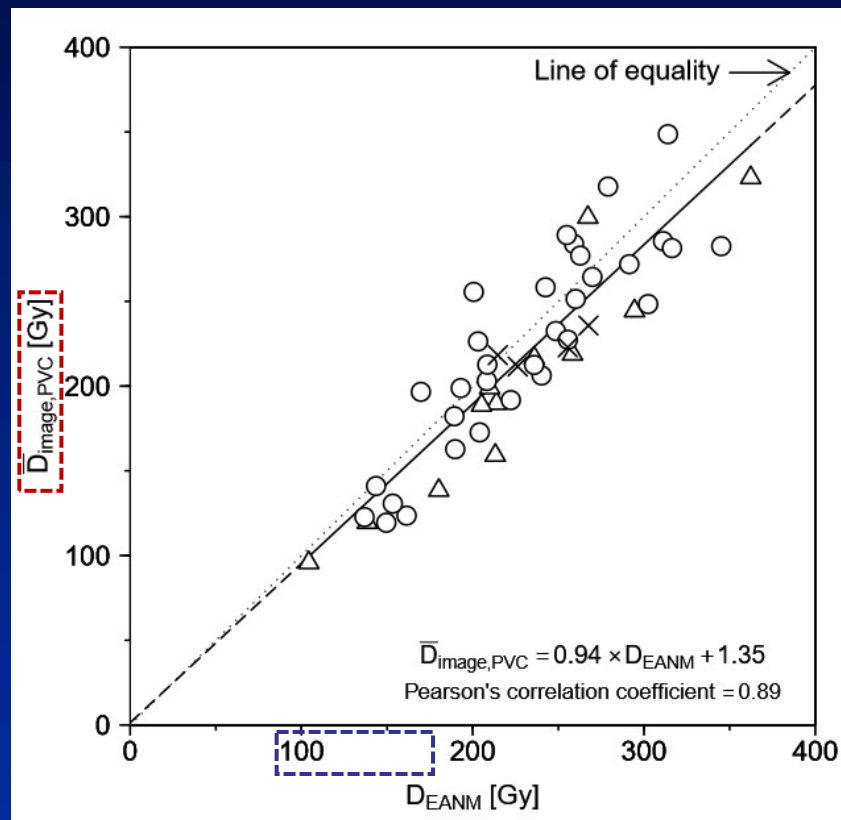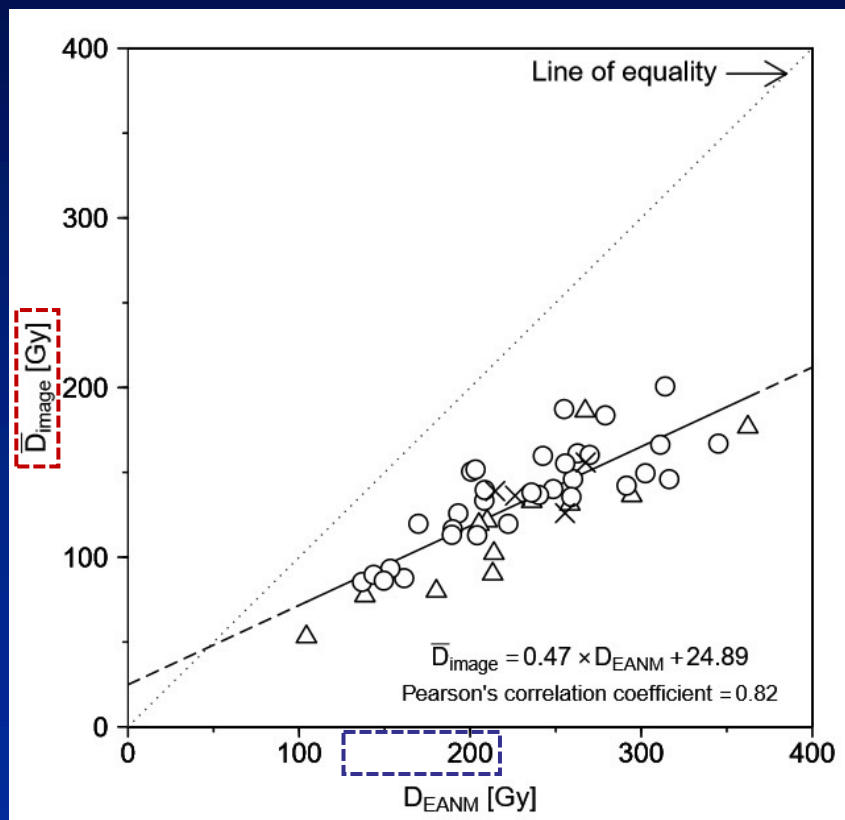
D_{EANM} と $\bar{D}_{image}$,$\bar{D}_{image,PVC}$ の関係（左図：$\bar{D}_{image}$ ，右図：$\bar{D}_{image,PVC}$）

〇：甲状腺機能低下状態, △：甲状腺機能正常状態, ×：甲状腺機能亢進状態

部分容積効果補正なし	部分容積効果補正あり

左図:
$$\bar{D}_{image} = 0.47 \times D_{EANM} + 24.89$$
Pearson's correlation coefficient = 0.82

右図:
$$\bar{D}_{image,PVC} = 0.94 \times D_{EANM} + 1.35$$
Pearson's correlation coefficient = 0.89

D_{EANM}
230.2 ± 56.7 Gy
（104.3-362.3）

$\bar{D}_{image}$
132.6 ± 32.2 Gy
（53.1-200.7）

$\bar{D}_{image,PVC}$
217.9 ± 59.8 Gy
（95.7-348.6）

提案手法は,部分容積効果を補正した 場合,EANM-based thyroid dosimetry（従来手法）と一致する傾向を認めた

Fujita N, et. al. Investigation of post-therapeutic image-based thyroid dosimetry using quantitative SPECT/CT, iodine biokinetics, and the MIRD's voxel S values in Graves' disease. EJNMMI Phys. 2020; 7(1): 6. doi: 10.1186/s40658-020-0274-
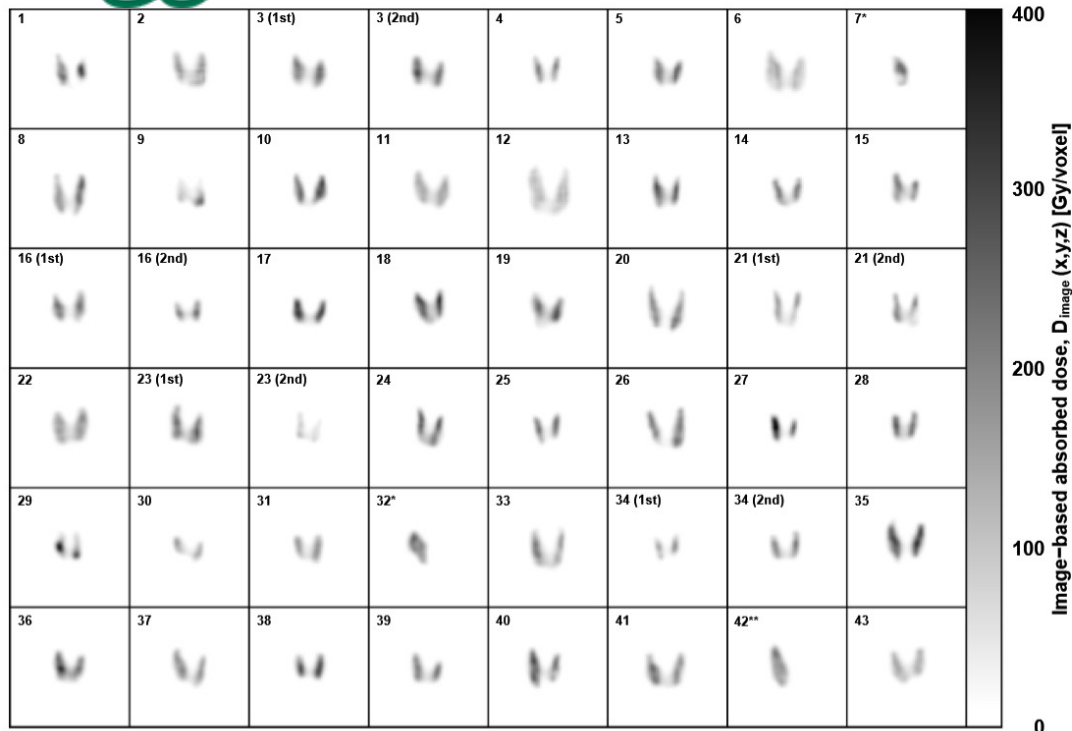
Absorbed dose image of thyroid obtained from each patient.

従来手法は,甲状腺に対するヨウ素の集積を「推定」することで甲状腺吸収線量を計算

⇕

提案手法は,ボクセル単位で吸収線量を計算するため,内用療法時の^{131}Iの直接的な可視化と,局所的な線量分布を把握できる

⬇

将来的に治療効果予測に応用できるかもしれない

提案手法であるpost-therapeutic image-based dosimetryが,線量-効果判定を行うにあたり,現在の標準手法であるpre-therapeutic dosimetryの代替手段になり得る

Fujita N, et. al. Investigation of post-therapeutic image-based thyroid dosimetry using quantitative SPECT/CT, iodine biokinetics, and the MIRD's voxel S values in Graves' disease. EJNMMI Phys. 2020; 7(1): 6. doi: 10.1186/s40658-020-0274-7

Investigation of post-therapeutic image-based thyroid dosimetry using quantitative SPECT/CT, iodine biokinetics, and the MIRD's voxel S values in Graves' disease

Naotoshi Fujita[1,2], Yumiko Koshiba[1], Shinji Abe[1] and Katsuhiko Kato[2*]

* Correspondence: katokt@met. nagoya-u.ac.jp
[2]Department of Radiological and Medical Laboratory Sciences, Nagoya University Graduate School of Medicine, 1-1-20 Daiko-Minami, Higashi-ku, Nagoya 461-8673, Japan
Full list of author information is available at the end of the article

Abstract

Background: Before radioiodine therapy for Graves' disease, the estimated thyroid-absorbed dose is calculated based on various clinical parameters. However, the actual accumulation of iodine in the thyroid during radioiodine therapy is not determined. We validated the feasibility of post-therapeutic image-based thyroid dosimetry through quantitative single-photon emission computed tomography (SPECT) imaging and thyroid biokinetics and expanding the Medical Internal Radiation Dose Committee's (MIRD) voxel dosimetry guidelines.

Methods: Forty-three patients with Graves' disease who underwent radioiodine therapy were chosen as subjects for this retrospective analysis. We acquired patients' SPECT images 24 h after oral administration. SPECT images were quantified using system volume sensitivity to calculate time-integrated activity coefficients on a voxel basis. Absorbed dose was obtained by convolving MIRD guideline voxel S values with time-integrated activity coefficients. To determine accuracy, we compared the results obtained using the post-therapeutic image-based absorbed-dose method ($\overline{D}_{image,PVC}$) with absorbed doses calculated using the method described by the European Association of Nuclear Medicine (pre-therapeutic method; D_{EANM}).

Results: Using image-based dosimetry as post-therapeutic dosimetry, we visualized the local accumulation and absorbed dose distribution of iodine in the thyroid. Furthermore, we determined a strong correlation (Pearson's correlation coefficient = 0.89) between both dosimetries, using the regression equation: $\overline{D}_{image,PVC} = 0.94 \times D_{EANM} + 1.35$.

Conclusion: Post-therapeutic image-based doses absorbed in the thyroid resembled those of pre-therapeutic EANM method-based absorbed doses. Additionally, the post-therapeutic image-based method had the advantage of visualizing thyroid iodine distribution, thus determining local dose distributions at the time of treatment. From these points, we propose that post-therapeutic image-based dosimetry could provide an alternative to standard pre-therapeutic dosimetry to evaluate dose response.

Keywords: Absorbed dose, Graves' disease, Internal radionuclide dosimetry, Radioiodine therapy, SPECT/CT, Thyroid

TP008 Studies on measurement of thyroid uptake rate on ^{131}I scintigraphy images

Yumiko Koshiba[1], Shinji Abe[2], Saki Tsuchiya[1], Naotoshi Fujita[2], Tetsuro Odagawa[1], Katsuhiko Kato[1]

[1] Department of Radiological and Medical Laboratory Sciences, Nagoya University Graduate School of Medicine, Nagoya, Japan

[2] Department of Radiological Technology, Nagoya University Hospital, Nagoya, Japan

Purpose

- Measurement of ^{131}I thyroid uptake rate (TUR) is usually performed before the internal ^{131}I therapy for patients with Graves' disease, and the dose of ^{131}I to be administered is determined from the data of TUR.
- In the previous study using a thyroid phantom, we found that TUR could be measured on the planar and SPECT/CT images with less than 5% of errors.
- In this study, we compared the TUR values before and after ^{131}I therapy using clinical data obtained from the planar and SPECT/CT images.

Patients and Methods

- TUR measurement system (AZ-800, Anzai Medical) (Fig. 1)
- Gamma camera and SPECT-CT (Fig. 2)
- High energy collimator
- Image J (National Institutes of Health)
- ^{131}I capsule (37 ~ 481 MBq)

- Consective 27 patients with Graves' disease treated with ^{131}I therapy in Nagoya University Hospital between December 2014 and August 2015 (male/female: 6/21, age: 17-79 y, mean±s.n.: 50.0±14.2 y).
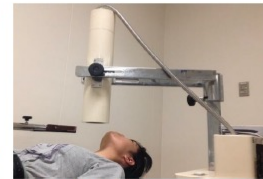

Fig. 1 TUR measurement system

Fig. 2 Siemens Symbia-T6

Table 1 Acquisition parameters (A: Planar, B: SPECT/CT)

(A)
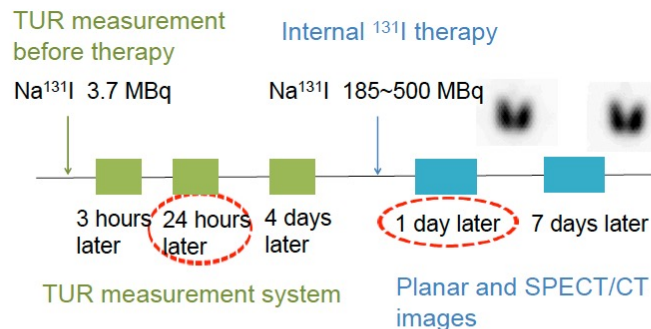
Matrix size	256 × 256
Zoom rate	× 3.2
Acquisition time	1 min

(B)

Acquisition range	360°
Acquisition angle	6° (30 views)
Matrix size	128 × 128
Zoom rate	× 1.45
Pixel size	3.3 mm
Acquisition time	5 min
Acquisition orbit	Non-circular
Detector motion	Continuous

Table 2 Reconstruction parameters

Reconstruction	3D-OSEM
Iteration	15
Subset	6
Post-reconstruction filter	Gaussian (FWHM: 6 mm)
CTAC,SC	+

※The study was performed according to the approval of the Ethics Committee of Medicine at Nagoya University for Human Studies (No.15-303).

1. Outlines of the procedures of TUR measurement

TUR measurement before therapy

Internal ^{131}I therapy

Na^{131}I 3.7 MBq

Na^{131}I 185~500 MBq

3 hours later   24 hours later   4 days later   1 day later   7 days later

TUR measurement system

Planar and SPECT/CT images

The TUR values calculated with the planar and SPECT/CT images which were obtained 1 day after internal ^{131}I therapy were compared with those measured by the TUR measurement system before ^{131}I therapy.

2. Measurement of TUR

First, using the planar and SPECT/CT images acquired with the ^{131}I capsule, the equation for indicating the relationship between the ^{131}I radioactivity and the counts on the planar and SPECT/CT images were established (Fig. 3). Using the equation, the counts on the planar and SPECT/CT images corresponding to the ^{131}I dose administered were determined.

The TUR values were calculated with the planar and SPECT/CT images. Rectangular ROIs were drawn on planar images and SPECT/CT axial images, and total counts were measured using Image J. Background counts were obtained by using average counts of rectangular ROIs at the four corners on the images (Fig. 4 and 5).

TUR was calculated as follows;

$$TUR\ [\%] = (T - B)/A \times 100$$

- T: Total counts of the thyroid images [counts]
- B: Background counts of the thyroid images [counts]
- A: Counts on the images corresponding to the ^{131}I dose administered [counts]
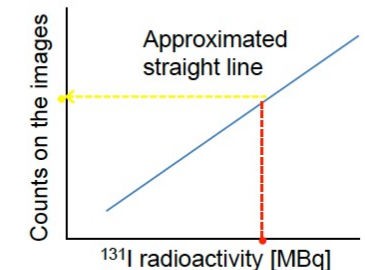

Fig. 3 Determination of the counts on the images corresponding to the ^{131}I dose administered
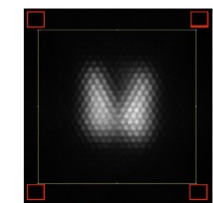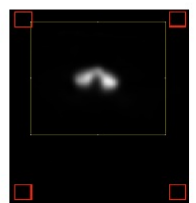

Fig. 4 Planar image   Fig. 5 SPECT/CT image

Results

- The TUR values measured on the planar and SPECT/CT images after ^{131}I therapy closely correlated with those measured by the TUR measurement system before ^{131}I therapy (R>0.7) (Fig. 6).
- In the results of Bland-Altman Plots, systematic error was found between the TUR values before and after ^{131}I therapy, and the TUR values measured after ^{131}I therapy tended to be smaller than those measured before the therapy (Fig. 7).
- The intervals of 95%LOA in the planar and SPECT/CT images were 25.9% and 26.7%, respectively.
- In relation to 95%LOA and the mean differences, there were no clinically significant differences between the TUR values measured on the planar and those measured on the SPECT/CT images.

Discussion

- The TUR values measured after ^{131}I therapy tended to be smaller than those measured before the therapy. There might be the following reasons for this finding.
  - The difference in the TUR values due to influence of the restriction of iodine intake.
  - The difference in the accuracy of the measurements of TUR values.
  - The difference in shapes between ^{131}I capsule and the thyroid gland. In establishment of the equation for indicating the relationship between the ^{131}I radioactivity and the counts on the images, images acquired with the ^{131}I capsule were used.
- The intervals of 95%LOA in both the planar images (25.9%) and the SPECT/CT images (26.7%) were wide. Four of the total 27 cases showed more than 15% difference between the TUR values before and after the therapy. Therefore, clinical cases may occur whose TUR values measured after ^{131}I therapy significantly differ from those measured before the therapy. Relatively small sample size in this study (n=27) might cause the wide intervals of 95%LOA. Further studies with increased numbers of cases will be needed.
- Essentially the same TUR values were obtained with use of both the planar and the SPECT/CT images. Further studies will be conducted by using SPECT/CT to elucidate the relationship between the effect of ^{131}I therapy and the dose of ^{131}I actually absorbed into the thyroid gland.

Conclusion

- The results suggest a possibility that clinical cases may occur whose TUR values measured after ^{131}I therapy significantly differ from those measured before the therapy.
- Essentially the same TUR values were obtained with use of both the planar and SPECT/CT images.
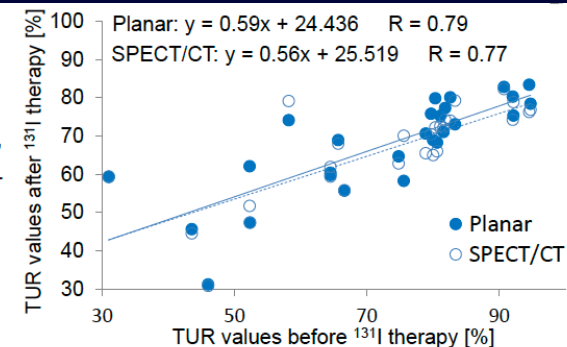

Planar: y = 0.59x + 24.436   R = 0.79
SPECT/CT: y = 0.56x + 25.519   R = 0.77

Fig. 6 The relationships between the TUR values after ^{131}I therapy and those before ^{131}I therapy

(A) Mean difference (5.2%), 95%CI, 95%LOA, r = 0.43 (p<0.05)
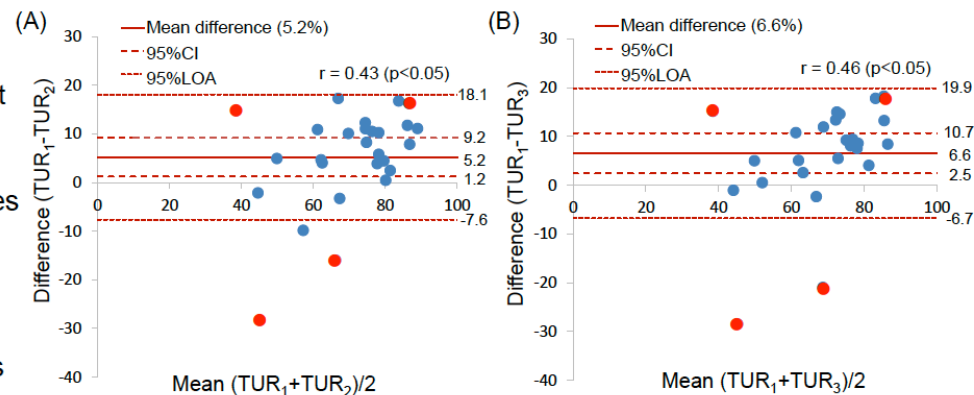(B) Mean difference (6.6%), 95%CI, 95%LOA, r = 0.46 (p<0.05)

Fig. 7 Bland-Altman Plots. (A) Difference between the TUR values measured before ^{131}I therapy (TUR$_1$) and those measured on the planar images after the therapy (TUR$_2$). (B) Difference between the TUR values measured before ^{131}I therapy (TUR$_1$) and those measured on the SPECT/CT images after the therapy (TUR$_3$).
※The cases showing more than 15% difference between the TUR values before and after the therapy are colored red.

TP003 # Dosimetry of absorbed doses of Radioiodine-131 in Therapy for Hyperthyroidism

Yumiko Koshiba[1], Shinji Abe[2], Naotoshi Fujita[2], Takuya Nishimoto[2], Yasuhiro Sakuragi[2],
Keita Kunimoto[1], Masayuki Honda[1], Tetsuro Odagawa[1], Katsuhiko Kato[1]

[1] Department of Radiological and Medical Laboratory Sciences, Nagoya University Graduate School of Medicine, Nagoya, Japan
[2] Department of Radiological Technology, Nagoya University Hospital, Nagoya, Japan

Purpose

- It is important to evaluate accurately absorbed doses of ^{131}I in therapy for patients with Graves' disease. Therapeutic effects may be estimated more accurately by evaluating quantitatively absorbed doses in the thyroid gland.
- The purpose of this study was to evaluate the absorbed doses of ^{131}I in the thyroid gland in therapy for patients with Graves' disease using the SPECT/CT images acquired after the therapy.

Materials

- Gamma camera and SPECT/CT:
  - Symbia T6 (Siemens Healthcare)
  - Collimator: high energy (HE)
- Thyroid uptake ratio (TUR) measurement system:
  - AZ-800 (Anzai Medical)
- Well counter: ACCUFLEX γ 7001 (Aloka)
- Processing and analyzing software:
  - Syngo MI Applications VA60A (Siemens Healthcare)
  - Image J (National Institutes of Health)
- Pool phantom
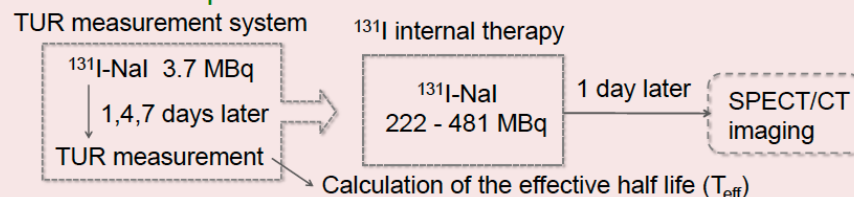- ^{131}I capsule (222 ~ 481 MBq)
- Solution of ^{131}I

Patients

27 patients with hyperthyroidism who received ^{131}I therapy between December 2014 and June 2016 (the total cases of the treatment were 30).

Male/Females: 5/22
Age range: 27 – 79 years
(52.6 ± 12.9 years)

※The study was performed according to the approval of the Ethics Committee of Medicine at Nagoya University for Human Studies (No.15-303).

Outlines of the procedures of the treatment

TUR measurement system ^{131}I internal therapy

^{131}I-NaI 3.7 MBq
↓ 1,4,7 days later
TUR measurement

→ ^{131}I-NaI 222 - 481 MBq → 1 day later → SPECT/CT imaging

Calculation of the effective half life (T_{eff})

Methods

1. Calculation of cross calibration factor (CCF)

- A solution of ^{131}I was enclosed into the pool phantom. Its SPECT-CT data were acquired and the radioactivity of the ^{131}I solution was measured by the well counter. Circular ROIs were drawn on the axial images and average counts per voxel were measured using Image J. CCF was calculated as follows;
  CCF=W/P (P: the average counts per voxel of the images [counts/voxel], W: the radioactivity of the ^{131}I solution measured by the well counter [MBq/ml]).
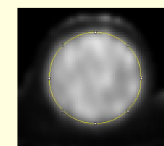

Fig.1 SPECT/CT image of the pool phantom

2. Calculation of absorbed dose at the voxel level

The voxel S value Approach[1]

Voxel$_k$: target voxel   Voxel$_h$: source voxel

$$D(voxel_k) = \sum_{h=0}^{N} \tilde{A}voxel_h \cdot S(voxel_k \leftarrow voxel_h)$$

D($voxel_k$): Dose at the $voxel_k$
$\tilde{A}$($voxel_h$): Accumulated activities at the $voxel_h$
S($voxel_k \leftarrow voxel_h$): The mean absorbed dose to the target $voxel_k$ per radioactive decay in the source $voxel_h$

※ A case in which target $voxel_k$ is surrounded by N source voxels

1) Wesley E. Bolch, et al.: MIRD Pamphlet No.17: The Dosimetry of Nonuniform Activity Distributions-Radionuclide S Values at the Voxel Level. J Nucl Med. 40: 11s-36s, 1999
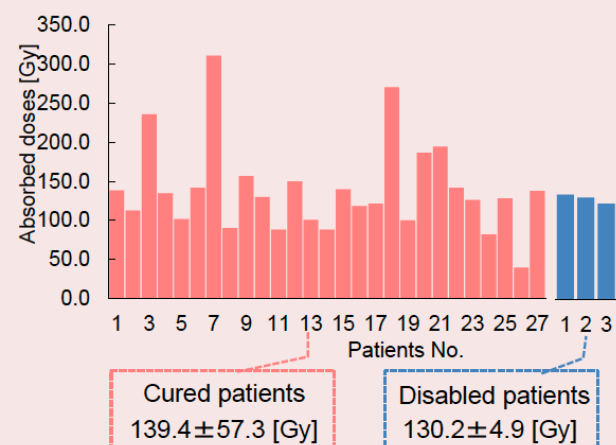
Results

The virtually mean absorbed doses

Cured patients
139.4±57.3 [Gy]

Disabled patients
130.2±4.9 [Gy]

Fig. 2 The virtually mean absorbed doses for each patient

% difference: $(D_{expected} - D_{virtual}) / D_{expected}$

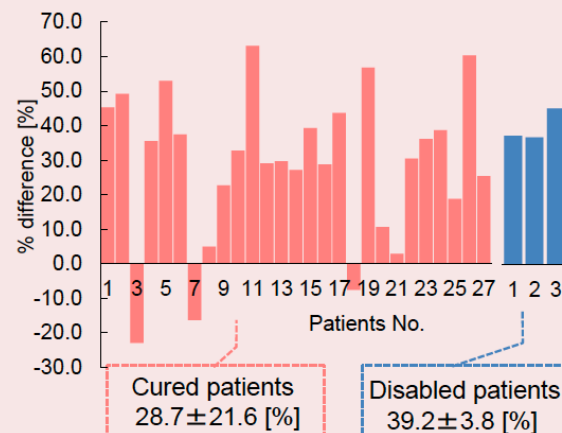Cured patients
28.7±21.6 [%]

Disabled patients
39.2±3.8 [%]

Fig. 3 Percentage difference in the virtually mean absorbed doses for the expected absorbed doses

Conclusion

- The absorbed doses of ^{131}I in therapy for patients with Graves' disease were obtained by using the SPECT/CT images acquired after the therapy.
- The results reflected the therapeutic effect.
- Further studies with an increased number of cases will be needed to evaluate the relationship between the absorbed doses and the therapeutic effects.

Discussion

% difference

- Cured patients: 28.7±21.8%, Disabled patients: 39.2±3.8%

  T_{eff}: 6.4±1.7 [day]
  U: 70.0±17.9 [%]

  T_{eff}: 5.8±0.5 [day]
  U: 77.1±11.1 [%]

➤ The difference between the virtually mean absorbed doses and the expected absorbed doses in the cured patients was smaller than that in the disabled patients.

➤ The effective half life seemed to be more important than the other factors affecting the absorbed doses.

Conformity index: CI

$$V_x / V_{thyroid} = \frac{\text{The volume irradiated with } x \text{ percent of the prescription dose [cm}^3\text{]}}{\text{The volume of the thyroid [cm}^3\text{]}}$$

	Cured patients	Disabled patients
$V_{100} / V_{thyroid}$	0.19±0.16	0.11±0.02
$V_{90} / V_{thyroid}$	0.26±0.18	0.16±0.02
$V_{50} / V_{thyroid}$	0.70±0.26	0.59±0.02

➤ CI: Cured patients＞Disabled patients
 → Ununiform distribution of ^{131}I may influence to the therapeutic effec

Koshiba Y, et al. EANM'16, Barcelona, Spain.

Nagoya University Graduate School of Medicine

甲状腺機能亢進症、甲状腺癌の^{131}I内用療法

- 500MBq(13.5mCi)まで外来で投与可能
- 500MBq(13.5mCi)以上は放射線治療病室へ収容が必要
- 退室の基準(500MBq、1mの距離で1cm線量当量率は30μSv/hr)

（医薬発第70号通達）
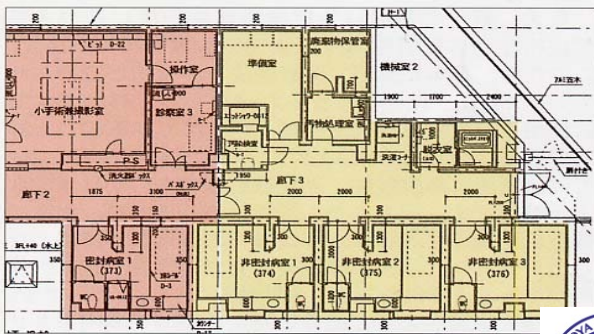
- 甲状腺癌治療(低用量アブレーション) 1110 MBq (30mCi)

（医政発第1108第2号通達）

RI内用療法を受けた患者の安全管理

治療には多量のRIを用いる

　→　家族や公衆の被ばくを低減するため、
　　退出基準に従って、一定期間患者を放射線治療病室
　に入院させる

放射線治療病室

RI治療室
3E病棟

Nagoya University Graduate School of Medicine

当院でのバセドウ病に対する内用療法症例

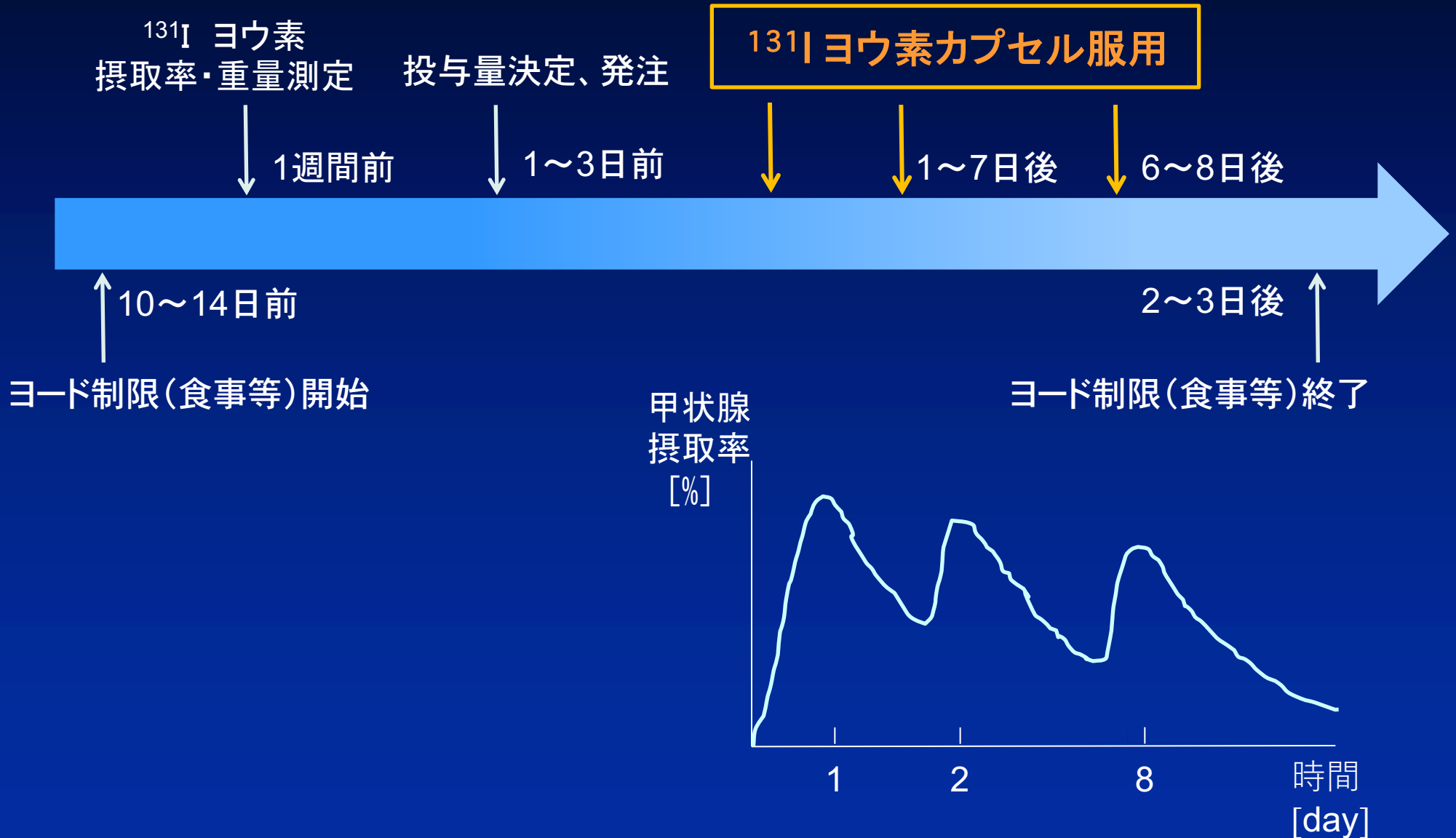2001年5月〜2025年2月に内用療法を行った、693例のうち重量が多かった例は

順位	年齢/性別	甲状腺重量(g)
1	80/F	672
2	66/F	482
3	49/M	465
4	67/F	451
5	45/M	413
6	65/F	410
7	47/F	399
8	33/F	383
9	66/F	369
10	49/M	361
11	48/M	343
12	52/F	336
13	33/M	332
14	43/F	315
15	47/F	306
16	27/F	300

^{131}I内用療法スケジュール(通常)
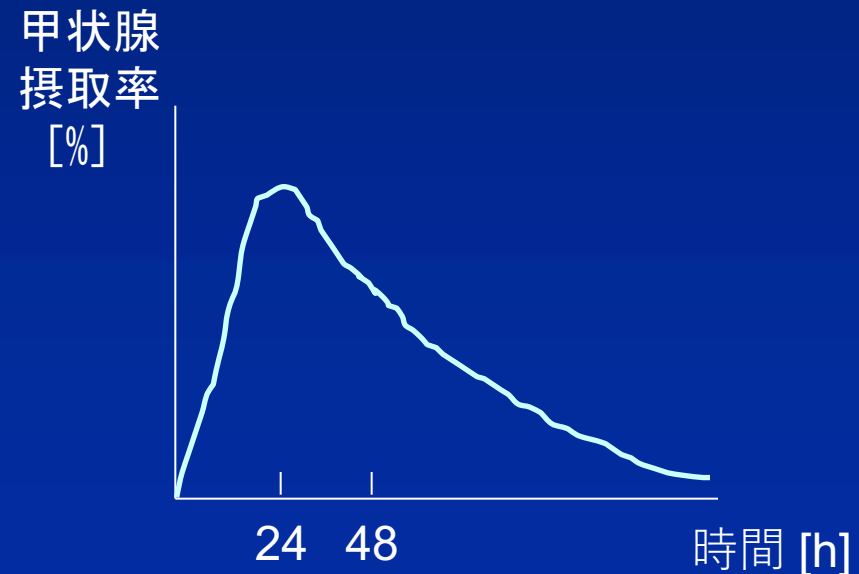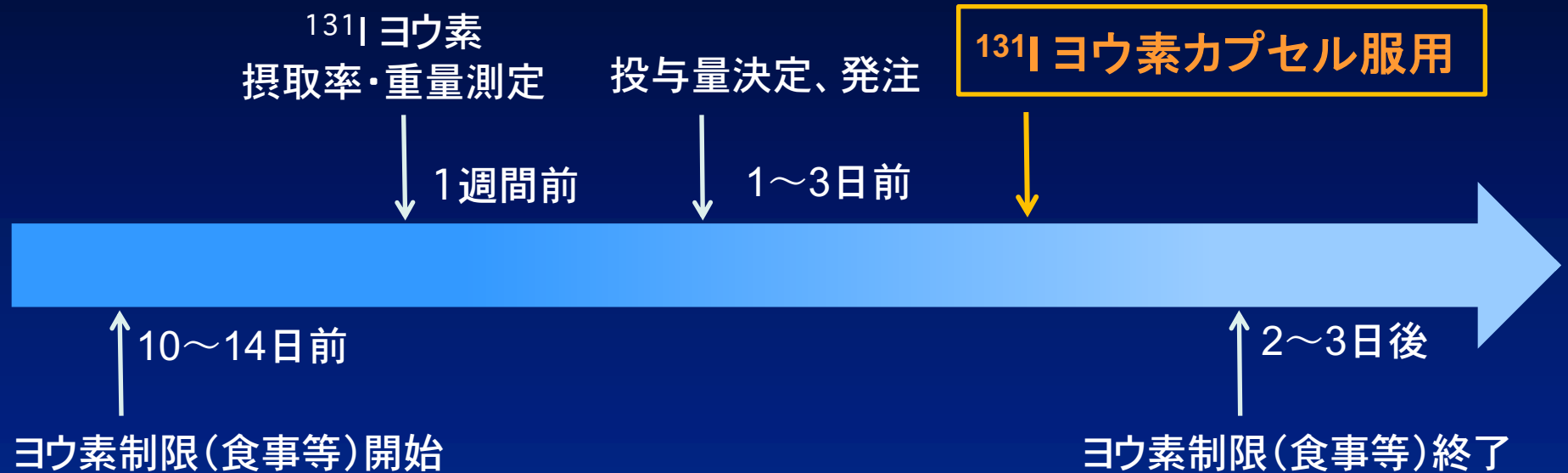
^{131}I ヨウ素
摂取率・重量測定

投与量決定、発注

^{131}I ヨウ素カプセル服用

1週間前

1～3日前

10～14日前

2～3日後

ヨウ素制限（食事等）開始

ヨウ素制限（食事等）終了

甲状腺
摂取率
[％]

24 48

時間 [h]

Yumiko Koshiba, et al. EANMMI 2016.

131I内用療法スケジュール(分割照射)

131I ヨウ素
摂取率・重量測定

投与量決定、発注

131Iヨウ素カプセル服用

1週間前

1〜3日前

1〜7日後

6〜8日後

10〜14日前

2〜3日後

ヨード制限(食事等)開始

ヨード制限(食事等)終了

甲状腺
摂取率
[%]

1　　　2　　　　8

時間
[day]

Yumiko Koshiba, et al. EANMMI 2016.

2663 Studies on Fractionated Administration of Radioiodine-131 in Therapy for Hyperthyroidism

Yumiko Koshiba[1], Shinji Abe[2], Naotoshi Fujita[2], Takuya Nishimoto[2], Yasuhiro Sakuragi[2], Tetsuro Odagawa[1], Katsuhiko Kato[1]

[1]Department of Radiological and Medical Laboratory Sciences, Nagoya University Graduate School of Medicine, Nagoya, Japan

[2]Department of Radiological Technology, Nagoya University Hospital, Nagoya, Japan

Background

- The radioiodine-131 therapy for hyperthyroidism

Criteria for ^{131}I therapy in Japan:

The dose of ^{131}I to be administered or residual radioactivity must not exceed 500 MBq.

✓ Dose of ^{131}I to be administered ≦ 500 MBq
→ Patients receive the ^{131}I therapy in outpatient clinics.

✓ Dose of ^{131}I to be administered > 500 MBq
→ Patients have to be treated in hospitals.

The dose of ^{131}I to be administered [MBq] =

$$\frac{\text{The absorbed dose [cGy]} \times \text{The weight of the thyroid [g]}}{5.4 \times \text{Thyroid uptake rate [\%]} \times \text{The effective half life [day]}}$$

Some patients need > 500 MBq of ^{131}I because of the large weight of the thyroid.

However —
- The number of patients with hyperthyroidism or thyroid cancer who need ^{131}I therapy ↑
- The number of sickrooms for ^{131}I therapy ↓

↳ The number of patients who can be treated in hospitals is limited.

→ It is desirable that ^{131}I therapy can be performed in outpatient clinics regardless of the dose of ^{131}I to be administered.

Although fractionated administration in every 3~6 months is generally performed in Japan, it is time-consuming.

It is desirable that patients can be treated by fractionated administration with shorter intervals.

Purpose

To evaluate the effectiveness of fractionated administration of ^{131}I for patients with hyperthyroidism who needed the ^{131}I therapy with > 500 MBq, we compared the expected absorbed doses and the virtually absorbed doses. The fractionated administration was performed in out patient clinics at intervals of ≦ 8 days.

Materials

- Gamma camera: Symbia T6 (Siemens)
  Collimator: high energy (HE)
- Thyroid uptake ratio (TUR) measurement system: AZ-800 (Anzai Medical) (Fig.1)
- Processing and analyzing software:
  Syngo MI Applications VA60A (Siemens)
  Image J (National Institutes of Health)
- ^{131}I capsule (47~481 MBq)
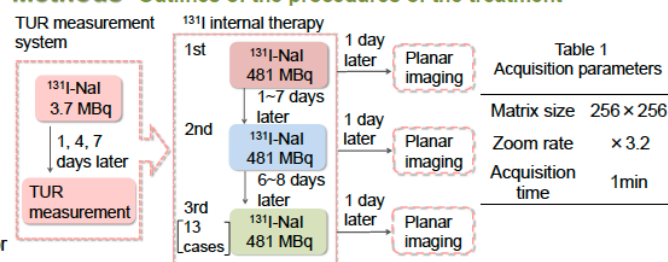
Fig.1 TUR measurement system

Patients

30 patients with hyperthyroidism who received ^{131}I therapy between July 2012 and November 2015 (The total cases of the treatment were 37).

Male/Females: 8/22
Age range: 17 – 78 years
(44.2 ± 14.4 years)

※ The study was performed according to the approval of the Ethics Committee of Medicine at Nagoya University for Human Studies (No.15-303).

Methods Outlines of the procedures of the treatment

TUR measurement system

^{131}I internal therapy

1st ^{131}I-NaI 481 MBq →1 day later→ Planar imaging

^{131}I-NaI 3.7 MBq
1, 4, 7 days later
TUR measurement

1~7 days later
2nd ^{131}I-NaI 481 MBq →1 day later→ Planar imaging

6~8 days later
3rd [13 cases] ^{131}I-NaI 481 MBq →1 day later→ Planar imaging

Table 1 Acquisition parameters

Matrix size	256×256
Zoom rate	×3.2
Acquisition time	1min

Comparison between the virtually absorbed doses and the expected absorbed doses

- The virtually absorbed doses were calculated with the data acquired from the planar images.
- Rectangular ROIs were drawn on the planar images.
  → Total counts were measured using Image J.
- ➢ Correlation between ^{131}I activity and counts on the images
  - The planar images acquired with the ^{131}I capsule
    → The equation for indicating the relationship between the ^{131}I radioactivity and the counts on the planar images was established (Fig.3).
    ↓
    Determination of the ^{131}I radioactivity corresponding to the counts on the images
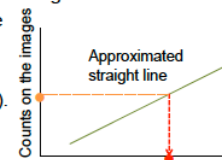
Fig.2 Planar image

Fig.3 Determination of the counts on the images corresponding to the ^{131}I dose administered

- The expected absorbed doses and the virtually absorbed doses were calculated according to the Quimby formula;

  Expected absorbed doses [cGy] = $(5.4 \times T_{eff} \times D_{admin} \times U) / W$

  Virtually absorbed doses [cGy] = $(5.4 \times T_{eff} \times D_{image}) / W$

  T_{eff}: The effective half life [day] D_{admin}: ^{131}I dose administered [MBq]
  U: Thyroid uptake rate [%] W: The weight of the thyroid [g]
  D_{image}: ^{131}I radioactivity corresponding to the counts on the planar images [MBq]

- Virtually absorbed doses-to-expected absorbed doses ratio (VER)
  = Expected absorbed doses / Virtually absorbed doses
  = $D_{admin} \times U / D_{image}$
  → We compared VER obtained after the second and third administrations with that obtained after the first administration.

Classification of therapeutic effects

Cured — Normalization or decline in the function of the thyroid grand → ^{131}I treatment has ended.

Improved — Improvement of the blood test results, clinical findings, and weight of the thyroid gland → However, the ^{131}I treatment has not yet ended.
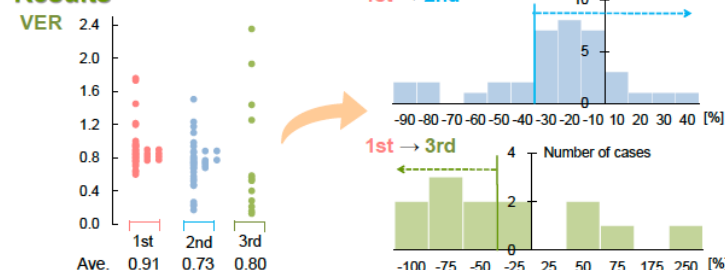
Results

VER

Fig.4 VER in each administration

	1st	2nd	3rd
Ave.	0.91	0.73	0.80

1st → 2nd Number of cases
-90 -80 -70 -60 -50 -40 -30 -20 -10 10 20 30 40 [%]

1st → 3rd Number of cases
-100 -75 -50 -25 25 50 75 175 250 [%]

Fig.5 Distribution of rate of change in VER

Therapeutic effects

30 patients

Cured — 28 patients (93%)
✓ The number of fractions: Two (18 patients), Three (10 patients)
✓ VER: 0.83±0.26
✓ Weight of the thyroid gland: 134.1±68.0 g
✓ Age: 44.4±13.5

Improved — 2 patients (7%)
✓ The number of fractions: Two (1 patient), Three (1 patient)
✓ VER: 0.69±0.16
✓ Weight of the thyroid gland: 333.6±148.8 g
✓ Age: 41.0±21.0

Discussion

VER
- Average: 0.91 (1st), 0.73 (2nd), 0.80 (3rd) (Fig.4)
  - 1st→2nd : The rate of change in VER were more than -30% in 28 cases (76%).
  - 2nd→3rd : The rate of change in VER were less than -50% in 7 cases (54%) (Fig.5).
- ➢ High therapeutic effects are expected by twice divided ^{131}I therapy.
- ➢ Further studies with increased numbers of cases will be needed to evaluate the effectiveness of three times administrations.

Therapeutic effects
- VER of the patients who were improved is not very small compared to the VER of the patients who were cured. → Therapeutic effects are expected.
- Weight of the thyroid grand of the 2 patients who were improved are so large.
  → If sufficient dose of ^{131}I is administered to 2 patients by retreatment, they may be cured.

Conclusions

- Results suggest that high therapeutic effects on hyperthyroidism are expected by twice divided ^{131}I administrations.
- Further studies with increased numbers of cases will be needed to evaluate the effectiveness of three times divided ^{131}I administrations.
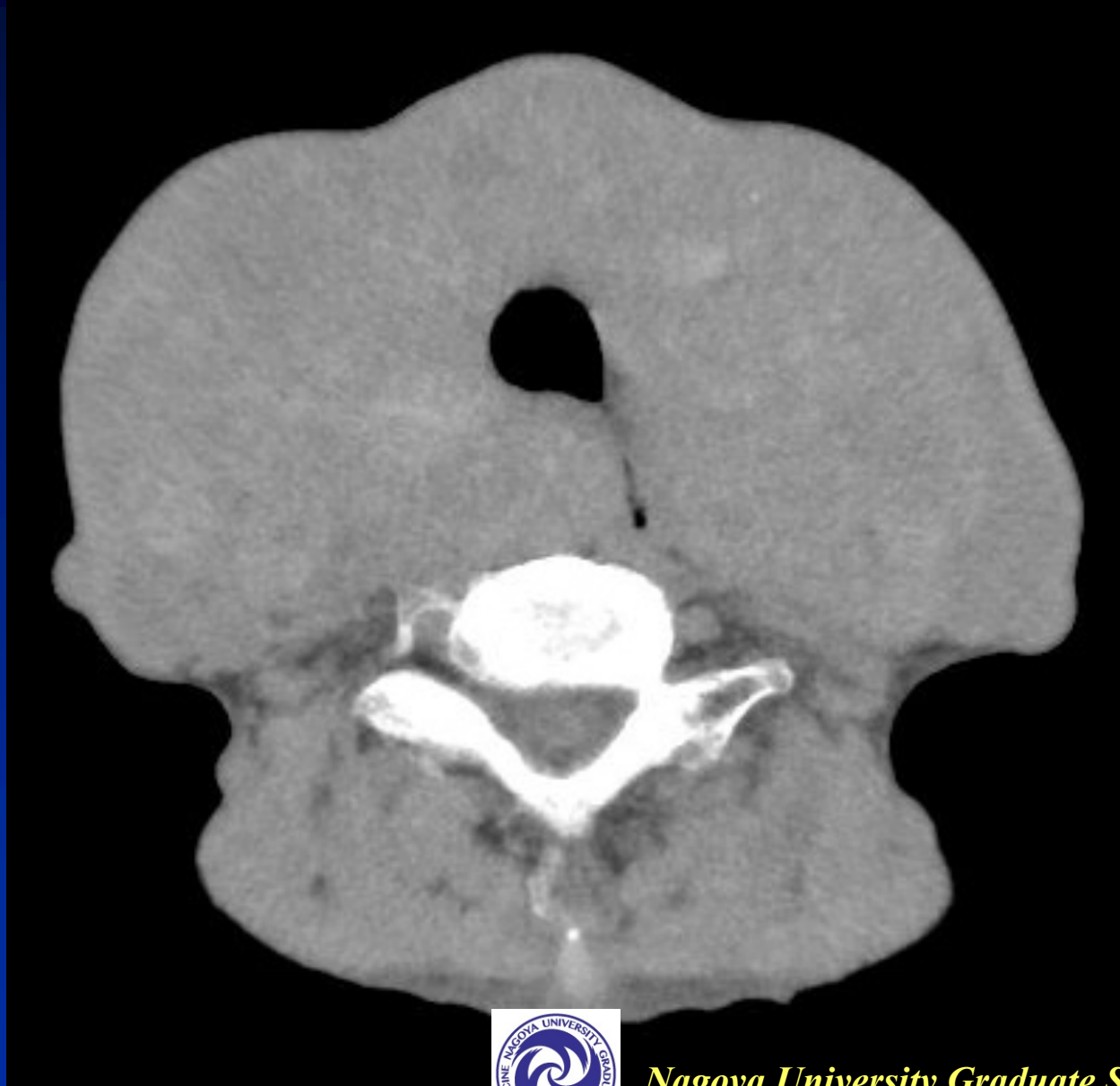
治療前　　　　　　　　　　　　　　治療後

Nagoya University Graduate School of Medicine

80歳代　甲状腺重量 672g
治療前
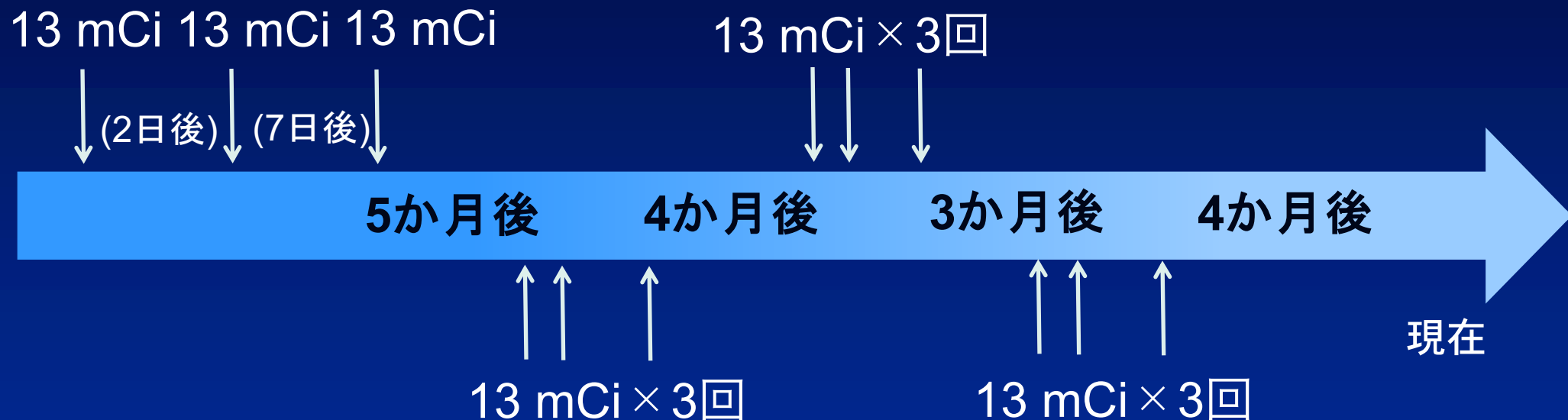
甲状腺機能亢進症における甲状腺CT値と甲状腺機能の関係性

◆甲状腺機能を評価する新しい指標の探索

- X線CT画像において、原子番号の大きいヨウ素を多く含む甲状腺はCT値が高くなり、正常な甲状腺のCT値はおおよそ110 Hounsfield unit (HU)となる。

- 一方でバセドウ病は、甲状腺CT値が正常よりも有意に低いという報告がある[1]。
  ➢ 甲状腺CT値が甲状腺の機能を反映している可能性がある。

Iwanaga H, et al. Correlation between the thyroid computed tomography value and thyroid function in hyperthyroidism: a retrospective study. Ann Nucl Med. 2024;38(8):659-665.

[1] Iida Y, et al. Thyroid CT number and its relationship to iodine concentration. Radiology. 1983;147:793–795.

バセドウ病の患者50例について、甲状腺平均CT値と下記のパラメータとの相関関係を調べた。

甲状腺重量
24時間ヨウ素摂取率
有効半減期

Free triiodothyronine (FT3)
Free thyroxine (FT4)
Thyroid stimulating hormone (TSH)
TSH receptor antibody (TRAb)

1 Min/Max: -6 /125
1 Mean/SD: 90.8 /15.7
1 Area: 5.22 sq.cm
1 Pixel: 3435

2 Min/Max: 6 /126
2 Mean/SD: 92.8 /1
2 Area: 8.30 sq.cm
2 Pixel: 5456
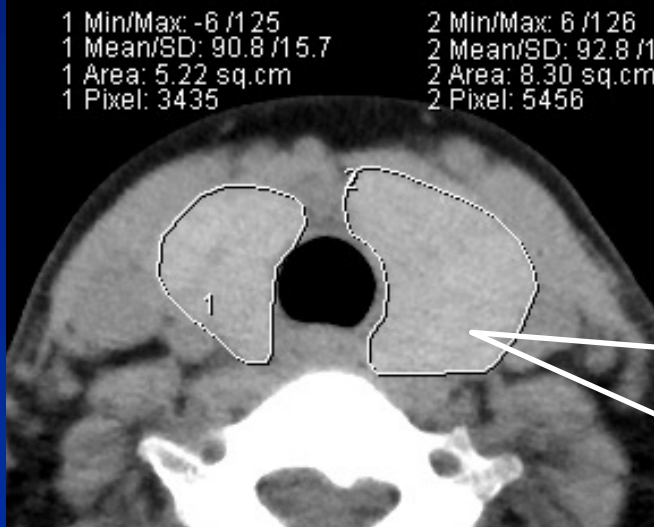
甲状腺CT値はX線CT画像上の甲状腺全体にROIを設置して算出した。

頚部X線CT画像

- 甲状腺CT値と有効半減期との間に有意な正の相関、TRAb値との間に弱い負の相関がみられた。

- 有効半減期は甲状腺のヨウ素排出の速度を表す。

➤ 甲状腺CT値は甲状腺のヨウ素排出に関わる因子と関係があると考えられる。

Effective half live (day) / Thyroid CT value (HU)

$y = 0.09x + 1.45$
$r = 0.69$, $p < 0.01$
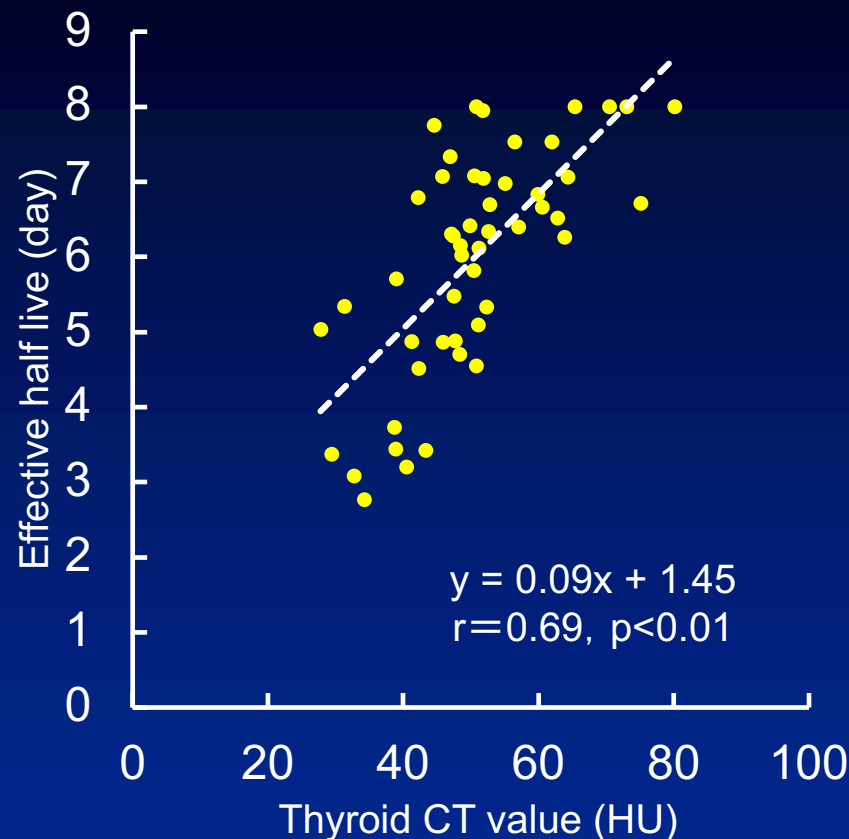
甲状腺CT値と有効半減期の関係

甲状腺CT値は主にヨウ素排出に関する因子と関係があり、甲状腺機能を反映していることが示唆された。

Ikeda H, et al. Correlation between thyroid computed tomography density and thyroid function in hyperthyroidism. J Nucl Med. 2020;61:3081.

ORIGINAL ARTICLE

Correlation between the thyroid computed tomography value and thyroid function in hyperthyroidism: a retrospective study

Haruna Iwanaga[1,2] · Naotoshi Fujita[1] · Shinji Abe[1] · Shinji Naganawa[3] · Katsuhiko Kato[4]

Abstract

Objective Radioiodine (I-131) therapy for hyperthyroidism is a well-established and safe treatment option. This study aimed to investigate the relationship between the computed tomography (CT) value and the function and volume of the thyroid gland by identifying the factors that induce changes in the CT value of patients with hyperthyroidism.

Methods This retrospective study evaluated 38 patients with Graves' disease and 10 patients with Plummer disease. To obtain the mean CT value and volume of the thyroid gland, the entire thyroid gland was set as the region of interest. A test dose of 3.7 MBq I-131 was administered before initiating I-131 therapy, and the radioiodine uptake (RIU) rate was assessed after 3, 24, 96, and 168 h. An approximate curve was plotted based on the RIU values obtained, and the effective half-life (EHL) was calculated. The correlation between the mean CT value and the volume of the thyroid gland, 24-h RIU, EHL, and the free triiodothyronine (FT3), free thyroxine (FT4), thyroid-stimulating hormone (TSH), and TSH receptor antibody (TRAb) levels was evaluated.

Results The CT value exhibited a significant positive correlation with EHL in patients with Graves' disease ($r = 0.62$, $p < 0.0001$) as well as patients with Plummer disease ($r = 0.74$, $p < 0.05$). However, it did not display any correlation with the remaining parameters.

Conclusion The CT value is significantly correlated with EHL, suggesting that it reflects thyroid function and is mainly related to the factors associated with iodine discharge.

Keywords Graves · Disease · Plummer disease · CT value · Radioiodine therapy · Effective half-life · Thyroid

List of abbreviations

CT	Computed tomography
EANM	European association of nuclear medicine
EHL	Effective half-life
FT3	Free triiodothyronine
FT4	Free thyroxine
HU	Hounsfield units
I-131	Radioiodine
RIU	Radioiodine uptake
TRAb	TSH receptor antibody
TSH	Thyroid-stimulating hormone

✉ Katsuhiko Kato
katokt@med.nagoya-u.ac.jp

1. Department of Radiological Technology, Nagoya University Hospital, Nagoya, Japan

2. Department of Radiological and Medical Laboratory Sciences, Department of Integrated Health Science, Nagoya University Graduate School of Medicine, Nagoya, Japan

3. Functional Medical Imaging, Biomedical Imaging Sciences, Division of Advanced Information Health Sciences, Department of Integrated Health Sciences, Nagoya University Graduate School of Medicine, Nagoya, Japan

4. 1-20, Daikominami 1-Chome, Higashi-Ku, Nagoya 461-8673, Japan

Introduction

Iodine is stored in the thyroid gland for the synthesis of thyroid hormones. Therefore, thyroid glands, which contain a large amount of iodine with a high atomic number, tend to exhibit a relatively high computed tomography (CT) value. The normal thyroid CT value is approximately 110 Hounsfield units (HU) [1, 2]. In contrast, the CT value of patients with Graves' disease, a form of hyperthyroidism, is lower than the normal CT value [2]. Although the CT value may reflect thyroid function [1, 3–6] the relationship between the CT value and thyroid function has not yet been
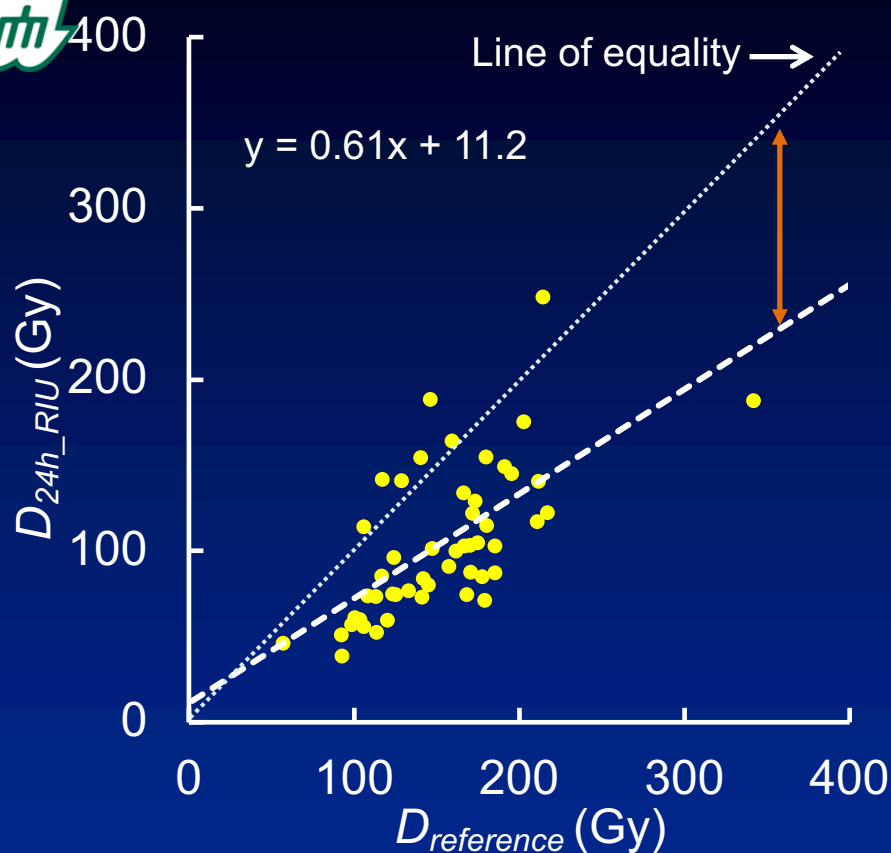
甲状腺CT値を用いたI-131内用療法の投与放射能決定法の検討

◆投与放射能決定法 (吸収線量推定法)の簡略化

- 吸収線量算出のために必要な、ヨウ素の体内動態を評価する検査は複数回の計測が必要となる。
  - ➢ 時間がかかり、煩雑である。

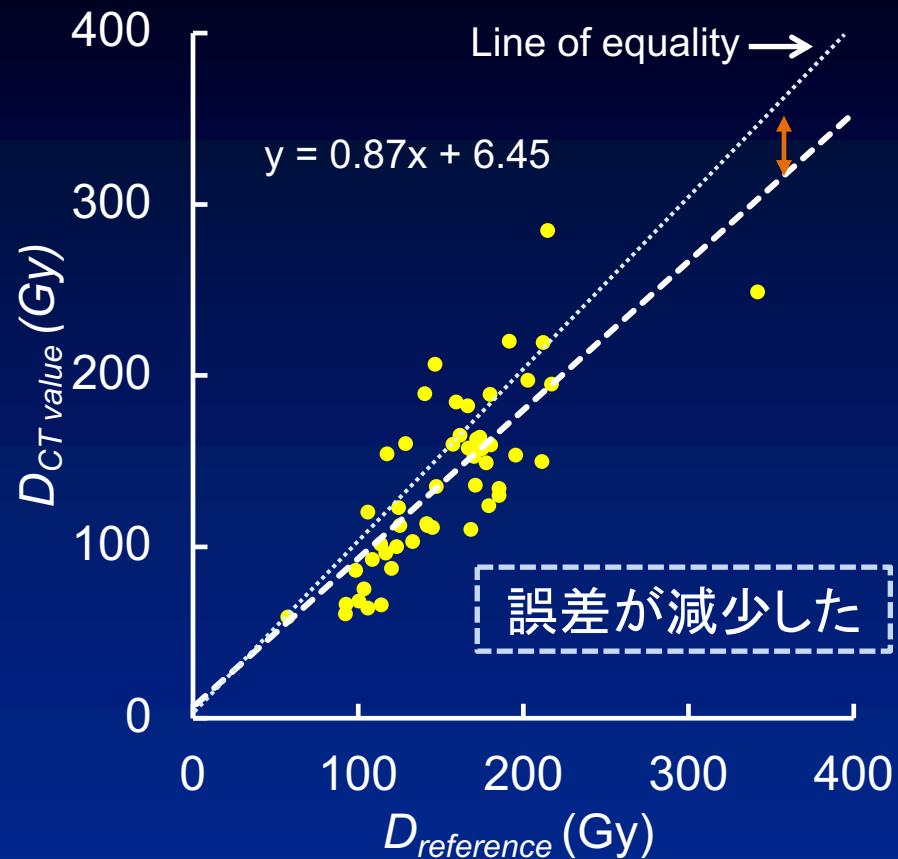- 多くの施設では複数回の測定を行わず、24時間ヨウ素摂取率のみから推定吸収線量を算出している。
  - ➢ 測定点が少ないと誤差が大きくなる。

> 24時間ヨウ素摂取率のみを用いて吸収線量を算出する場合、甲状腺CT値を用いて吸収線量の推定精度を向上させることが可能であるかを検討した。

y = 0.61x + 11.2

Line of equality →

D_{24h_RIU} (Gy)

$D_{reference}$ (Gy)

y = 0.87x + 6.45

Line of equality →

$D_{CT\,value}$ (Gy)

$D_{reference}$ (Gy)

誤差が減少した

24時間ヨウ素摂取率のみ
D_{24h_RIU}

甲状腺CT値で補正
$D_{CTvalue}$

ヨウ素摂取率を複数回測定できない場合、甲状腺CT値を用いて吸収線量の推定精度が向上できることが示唆された。

Ikeda H, et al. Dosimetry prior to I-131 therapy in hyperthyroidism using thyroid computed tomography value. Eur J Nucl Med Mol Imaging. 2021;48:s603.

■ 第77回日本放射線技術学会総会学術大会, 2021.4.15–18, 横浜.

- CyPos賞 Bronze Award

甲状腺機能亢進症のI-131内用療法における治療効果予測因子の検討

池田陽菜、藤田尚利、山口博司、西尾美穂、阿部真治、加藤克彦

CyPos賞 Bronze Award

■ 2021 SNMMI Washington D.C.

68th Annual Meeting - Virtual Edition of the Society of Nuclear Medicine and Molecular Imaging - SNMMI'21, 2021.6.11–15, Virtual Edition.

- 2021 ERF SNMMI-TS Professional Development Grant Award for the SNMMI Annual Meeting for technologists and technologist students

- International Best Abstract Award

Predictive Factors of the Therapeutic Effect of I-131 Therapy for Hyperthyroidism

Haruna Ikeda, Miho Nishio, Yuka Ochi, Mika Tamura, Katsuhiko Kato

TP32   Basic studies on measurement of ^{131}I activity using SPECT-CT

Saki Tsuchiya[1], Shinji Abe[2], Naotoshi Fujita[2] Hidetaka Kono[2], Arisa Niwa[1], Yusuke Fujita[1], Tetsuro Odagawa[1], Katsuhiko Kato[1]

[1] Department of Radiological and Medical Laboratory Sciences, Nagoya University Graduate School of Medicine, Nagoya, Japan

[2] Department of Radiological Technology, Nagoya University Hospital, Nagoya, Japan

Purpose

- We evaluate visually hot spots of scintigrams (SPECT-CT + planar) for the diagnosis of metastases and relapses of thyroid cancer after ^{131}I therapy. However, they don't always provide accurate information because image quality is not necessarily good.
- The purpose of this study is to enhance their diagnostic accuracy by analyzing the scintigrams quantitatively.

Materials and Methods

Image acquisitions

- Gamma camera and SPECT-CT (Fig.1)
- High energy collimator
- Well counter   ACCUFLEX γ 7001 (Aloka)
- Image j
- Pool phantom (Fig.2-A)
- Cylindrical and spherical phantom (Fig.2-B)
- Solution of ^{131}I

Table 1 Acquisition parameters

Acquisition range	360°
Acquisition angle	6°(60views)
Matrix size	128×128
Zoom rate	×1.0
Pixel size	3.3mm
Acquisition time	240min
Acquisition orbit	non-circular
Detector motion	continuous

Table 2 Reconstruction parameters

Reconstruction	3D-OSEM	FBP
Iteration	15	
Subset	6	
Post-reconstruction filter	Gaussian (FWHM:8mm)	
CTAC, SC	+	+
Pre-reconstruction filter		Butterworth
Cutoff frequency		0.6cycles/cm
Order		8

Fig.1 Siemens Symbia-T6

Calculation of cross calibration factor (CCF)

- A solution of ^{131}I was enclosed into the pool phantom. Its SPECT-CT data were acquired and the radioactivity of the ^{131}I solution was measured by the well counter. The data acquired by SPECT-CT were reconstructed by 3D-OSEM and FBP, and attenuation and scattering corrections were made. Circular ROIs were drawn on the axial images and average counts per pixel were measured using Image J. CCF was calculated as follows ; CCF=W/P (P : the average counts per pixel of the images [counts/pixel], W : the radioactivity of the ^{131}I solution measured by the well counter [cps/g]). The experiment was repeated once a week for 3 weeks.

Estimation of ^{131}I activity

- A solution of ^{131}I was enclosed into the cylindrical and spherical phantom. The methods of data acquisition, measurement of radioactivity using well counter, reconstruction, attenuation and scattering corrections, and measurement of the average counts per pixel of the images were same as in calculating CCF. Using CCF and the average counts per pixel of the images, we calculated the radioactivity of the ^{131}I solution enclosed into the cylindrical and spherical phantom, and compared them with the actually measured ^{131}I activity using the well counter. In addition, recovery coefficients (RC) for the error in the calculated values were obtained as follows ; RC=C/M (C : the calculated activity [cps/g], M : the actually measured activity [cps/g]).

Cylinder 45mm 35mm 65mm 12mm 20mm

Sphere 28mm 75mm 45mm 14mm 60mm

※ ■ : ^{131}I
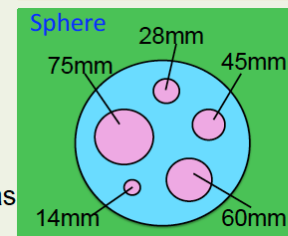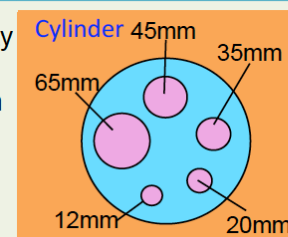 ■ : Agar

(A) 25cm 13cm

(B) 20cm 20cm
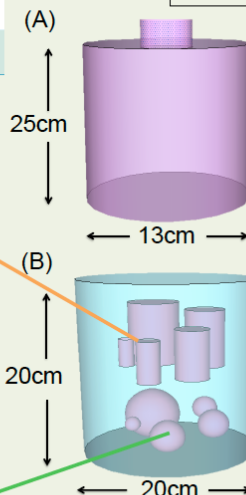
Fig.2 Pool phantom(A) and cylindrical and spherical phantom(B)

Results

Calculation of CCF

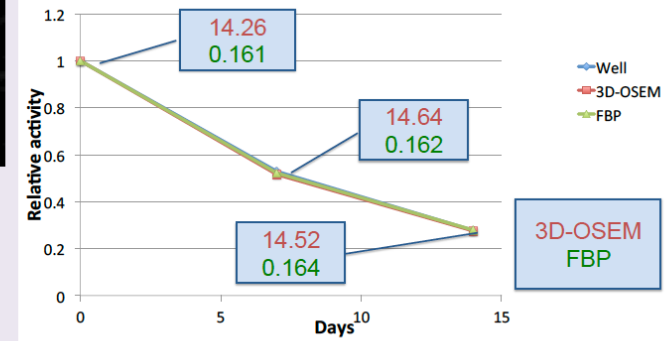- Fig.3 shows SPECT-CT images of the pool phantom.
- The average counts per pixel of the images and the radioactivity of the ^{131}I solution measured by the well counter declined at the same rate. We acquired almost the same CCF values in 3 experiments (Fig.4).

Estimation of ^{131}I activity

- Fig.5 shows SPECT-CT images of the cylindrical and spherical phantom.
- We found that the calculated ^{131}I activities from the images tended to be less compared with the actually measured values when the size of hot spots became smaller, although the same solution of ^{131}I was enclosed into the phantoms (Fig.6). The error in the calculated activities due to the smaller size of hot spots happened almost three times more markedly than FWHM acquired at the same condition (Fig.7). We obtained the recovery coefficients and regression equations for the error in the calculated values of ^{131}I activity from the images depending on the smaller diameter of hot spots (Fig.8).

(A) (B)

Fig.3 SPECT-CT images of the pool phantom (A:3D-OSEM, B:FBP)

Fig.4 Decline of the average counts per pixel of the images and the radioactivity of the ^{131}I solution measured by the well counter (the values were expressed as relative ones to those of the first experiment).

(A) (B) (C) (D)

Fig.5 SPECT-CT images of the cylindrical and spherical phantom
(A : cylinder/3D-OSEM, B : sphere/3D-OSEM, C : cylinder/FBP, D : sphere/FBP)
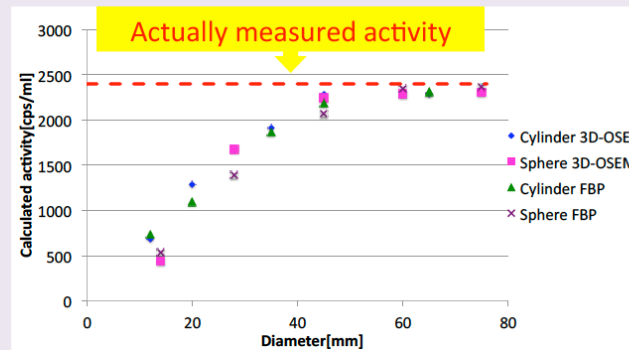
Fig.6 Relationship between the calculated values of ^{131}I activity from the images and the diameter of hot spots
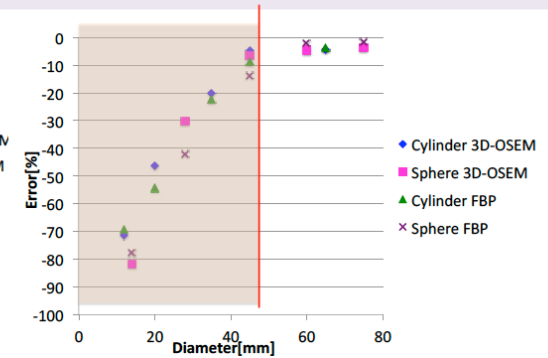
Fig.7 Relationship between the error in the calculated values of ^{131}I activity from the images and the diameter of hot spots

Discussion

- We acquired CCF values which are utilizable to estimate ^{131}I activity from the average counts per pixel of the images.
- The main cause for the error in the calculated values of ^{131}I activity due to the smaller size of hot spots seems partial volume effects based on use of the high-energy collimator. Then we obtained the recovery curves and regression equations, which may be useful to correct the error in the calculated values of ^{131}I activities due to the smaller size of hot spots.

Conclusion

- The results of this study indicate that the smaller size of hot spots lessens the calculated ^{131}I activity, and that an adequate correction for the error in calculated ^{131}I activity is needed for the quantitative analysis of clinical images. We will examine whether the accurate activity can be determined from the scintigrams if the corrections are made using the recovery curves and regression equations obtained in this study.

(A) $y = -1E-05x^3 + 0.0008x^2 + 0.0127x - 0.0056$
$R^2 = 0.97574$

(B) $y = -6E-06x^3 + 0.0004x^2 + 0.0169x + 0.0041$
$R^2 = 0.98389$

Fig.8 Relationship between the recovery coefficient for the error in the calculated values of ^{131}I activity from the images and the diameter of hot spots (A : 3D-OSEM, B : FBP)

Tsuchiya S, et al. EANM'14, Gothenburg, Sweden.

TP020 Comparative study on recovery coefficients of SPECT-CT

Saki Tsuchiya[1], Shinji Abe[2], Naotoshi Fujita[2], Yumiko Koshiba[1], Tetsuro Odagawa[1], Katsuhiko Kato[1]

[1]Department of Radiological and Medical Laboratory Sciences, Nagoya University Graduate School of Medicine, Nagoya, Japan

[2]Department of Radiological Technology, Nagoya University Hospital, Nagoya, Japan

Aim

- Nuclear medicine imaging is ready to be affected by the partial volume effect (PVE) because of its lower spatial resolution than other modalities. Calculation of recovery coefficients (RCs) are usually conducted for assessment of the quantitativity.
- RCs of hot spots may change due to the difference in shapes and reconstruction methods even if their volumes are the same.
- In this study, we compared RCs of hot spots having the same volume but different shapes.

Materials and Methods

- Gamma camera and SPECT-CT
  Symbia T6 (Siemens Healthcare)
  Collimator: LEHR
- Well counter: ACCUFLEXγ 7001 (Aloka)
- Processing and analyzing software:
  Syngo MI Applications VA60A (Siemens Healthcare)
  Image J (National Institutes of Health)
- Pool phantom (Fig. 1-a)
- Spherical phantom (Fig. 1-b)
- Irregularly shaped phantom (fig. 1-c, 1-d)
- Solution of Tc-99m

Table 1 Acquisition parameters	
Acquisition range	360°
Angular step	6° (60 views)
Energy window	142.7 keV±10.5%
Matrix size	128 × 128
Zoom rate	× 1.0
Voxel size	4.8 mm
Acquisition time	40 sec/view
Acquisition orbit	Non-circular
Detector motion	Continuous

Table 2 Reconstruction parameters	
Reconstruction method	3D-OSEM
Subset	6
Iteration	3, 5, 7, 10, 20, 30, 40
Post-reconstruction filter	None, Gaussian (FWHM:2〜10 mm)
Attenuation correction	CTAC
Scatter correction	DEW

Fig. 1
(a) Pool phantom
(b) Spherical phantom
(c) Irregularly shaped phantom
(d) Internal containers of the irregularly shaped phantom

■ : Water/Agar
■ : Tc-99m

Image acquisition and reconstruction

A solution of Tc-99m was enclosed into the spherical and the irregularly shaped phantoms. SPECT-CT data of the phantoms were acquired and reconstructed using 3D-OSEM. Varied conditions on the subsets × iterations (SI) and FWHM of the Gaussian filter were used for the reconstruction of images. The radioactivity of the solution was measured by the well counter.

Image analysis

ROIs were drawn on the reconstructed images, and the average counts per pixel were measured. Methods for placing ROIs were (1) two-dimensional method (Fig. 2-a), and (2) three-dimensional method (Fig 2-b). RCs were acquired in the way showing in Fig. 3. RCs of the spherical and the irregularly shaped phantoms having the same volume were compared. And differences in the RCs (D values) were obtained using following equation; D value [%] = (RCi − RCs) / RCs × 100 (RCi : RC of the irregularly shaped phantom, RCs: RC of the spherical phantom).
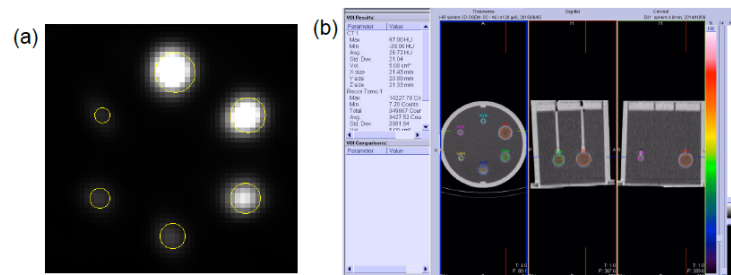
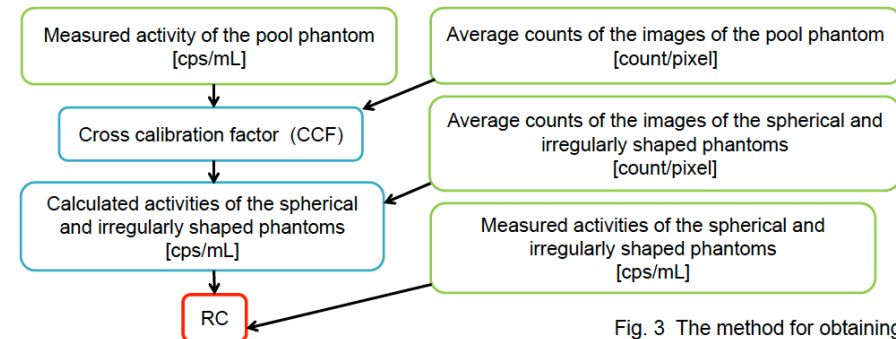Fig. 2 (a) Two-dimensional (2D) method
(b) Three-dimensional (3D) method

Fig. 3 The method for obtaining RCs

Results

- Figs. 4 and 5 show the relationships between the RC and the diameter of hot spots (recovery curves) obtained using the spherical phantom. Slopes of the recovery curves became gentler with an increase of the SI in both methods. On the other hand, slopes of the recovery curves became steeper with an increase of the FWHM of Gaussian filter in both methods.
- Fig. 6 shows the relationship between the D value and the SI. In both methods, absolute D values became smaller when the SI ≧ 120.
- Fig. 7 shows the relationship between the D value and the FWHM of Gaussian filter. On the whole, absolute D values seem to be the smallest when the FWHM 6~8 mm in both methods.
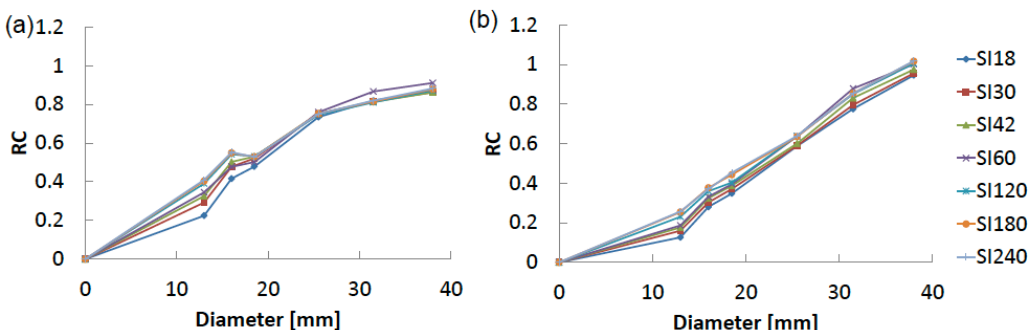
Fig. 4 Relationship between the RC and the diameter of hot spots of the spherical phantom when the FWHM of Gaussian filter was 6 mm and the SI varied (a：2D method, b：3D method)
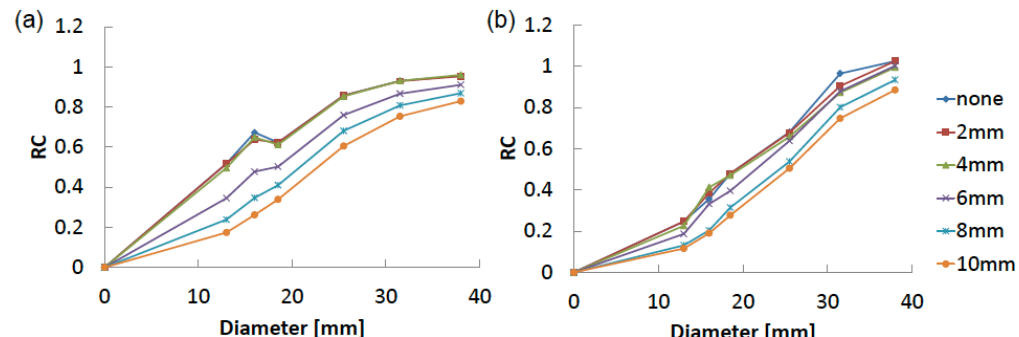
Fig. 5 Relationship between the RC and the diameter of hot spots of the spherical phantom when the SI was 60 and the FWHM of Gaussian filter varied (a：2D method, b：3D method)
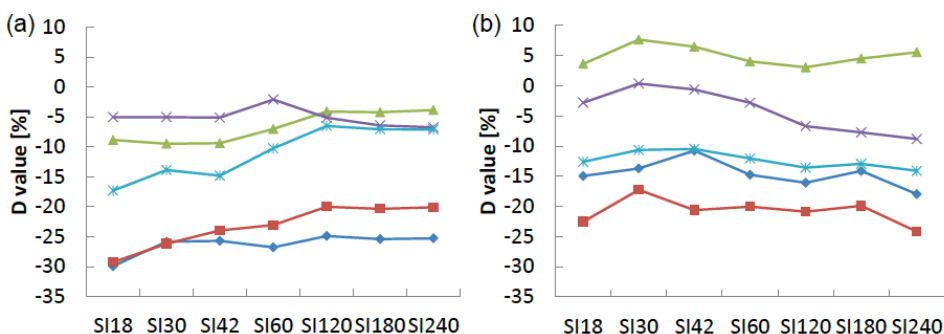
Fig. 6 Relationship between the D value and the SI when the FWHM of Gaussian filter was 6 mm (a：2D method, b：3D method)
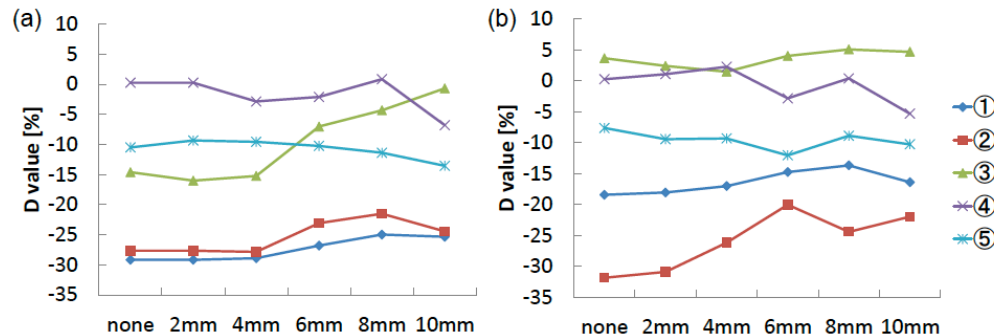
Fig. 7 Relationship between the D value and the FWHM of Gaussian filter when the SI was 60 (a：2D method, b：3D method)

Discussion

- The quantitativity was improved with an increase of the SI and a decrease of the FWHM of Gaussian filter (Figs. 4 and 5). The RCs tended to decrease with a decrease of cross section and side because of stronger effect of the PVE (Figs. 6 and 7).
- When we used 2D method, the D value tended to be smaller by using ≧ 120 of the SI and Gaussian filter whose FWHM was 6~8 mm. As for 3D method, the D value tended to be smaller by using 30~60 of the SI Gaussian filter whose FWHM was 6~8 mm. Considering both stability of the RCs and quantitativity, the most adequate parameters seem to be as follows; 120 or 180 of the SI and Gaussian filter whose FWHM is 6 mm in 2D method, and 60 of the SI and Gaussian filter whose FWHM is 6 mm in 3D method.
- The stability of the RCs and quantitativity were improved by using adequate parameters, although degree of the improvement was limited. The development of new analytical methods will be needed. Besides the stability and quantitativity, visual and physical image qualities are important and should also be improved.

Conclusion

We compared RCs of hot spots having the same volume but different shapes. RCs varied due to shapes of hot spots and reconstruction parameters.
The stability of the RCs and quantitativity were improved by using the adequate parameters.
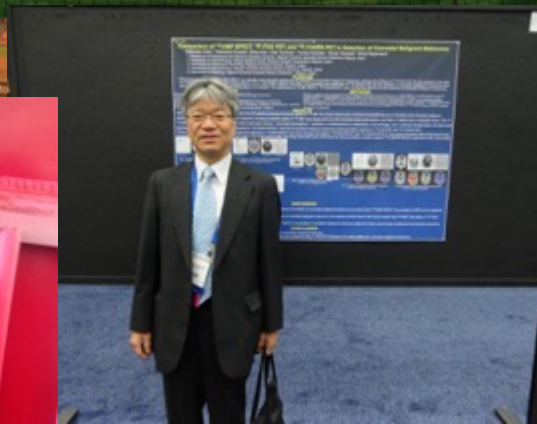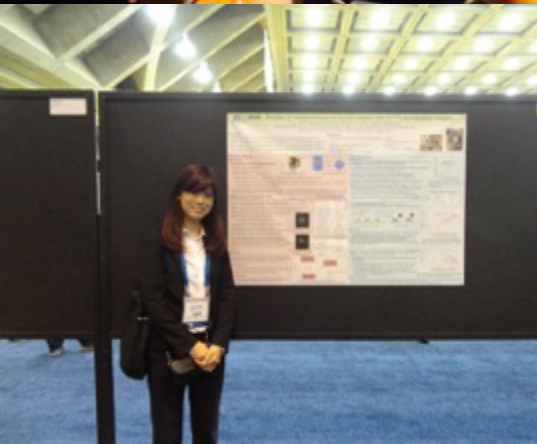
Oral Presentations by Selected Students
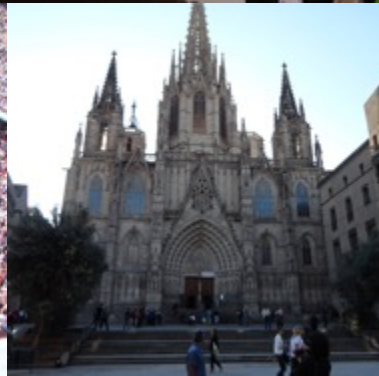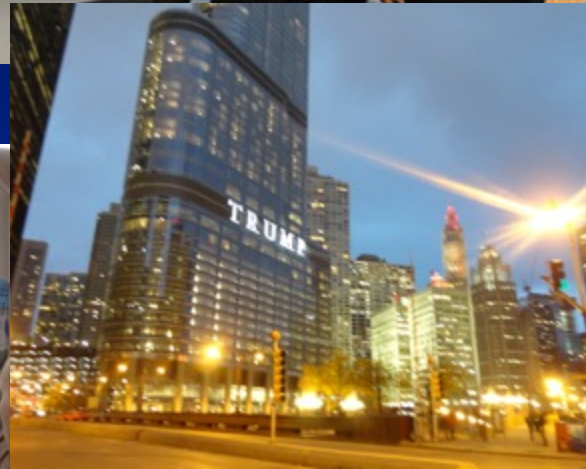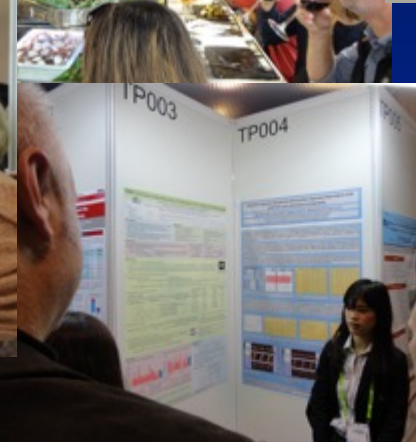学生選抜セッション（学生選抜研究発表）

4月16日(木)14：00～16：30(F201)
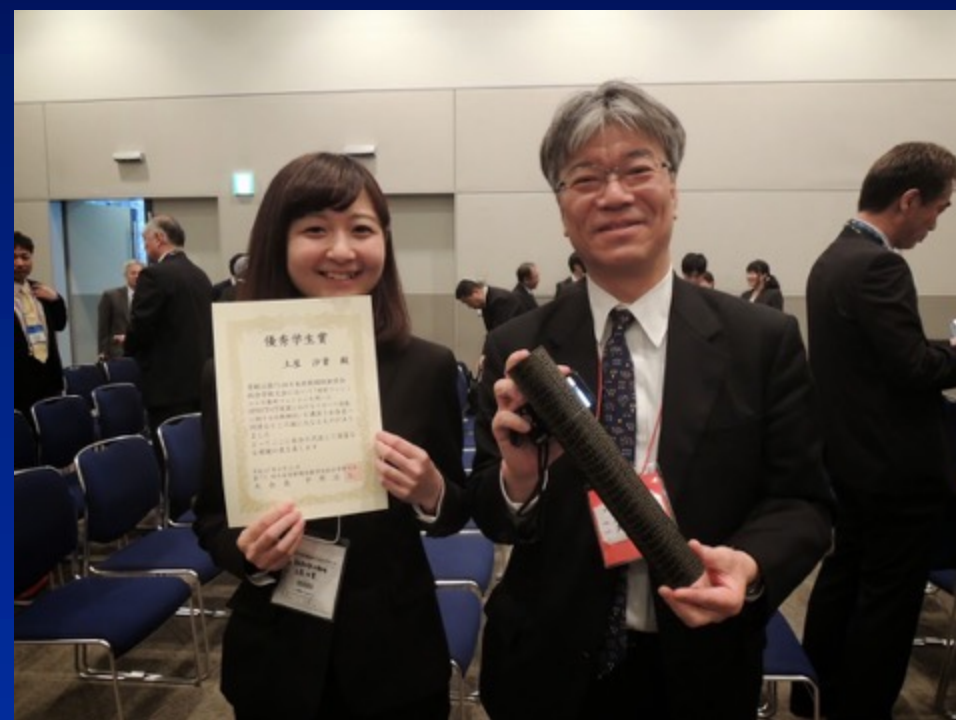
2015 SNM Baltimore

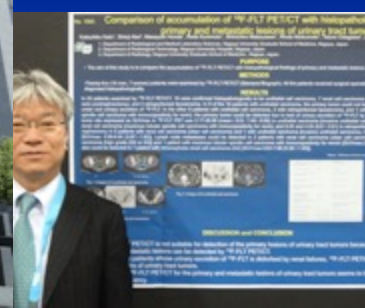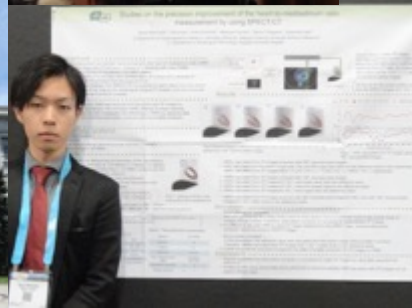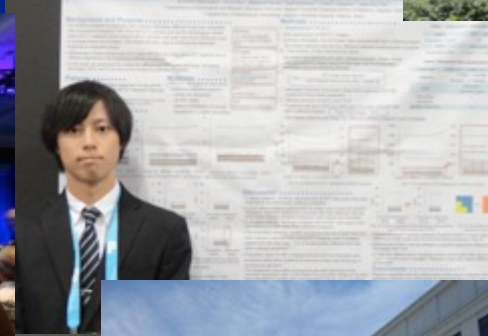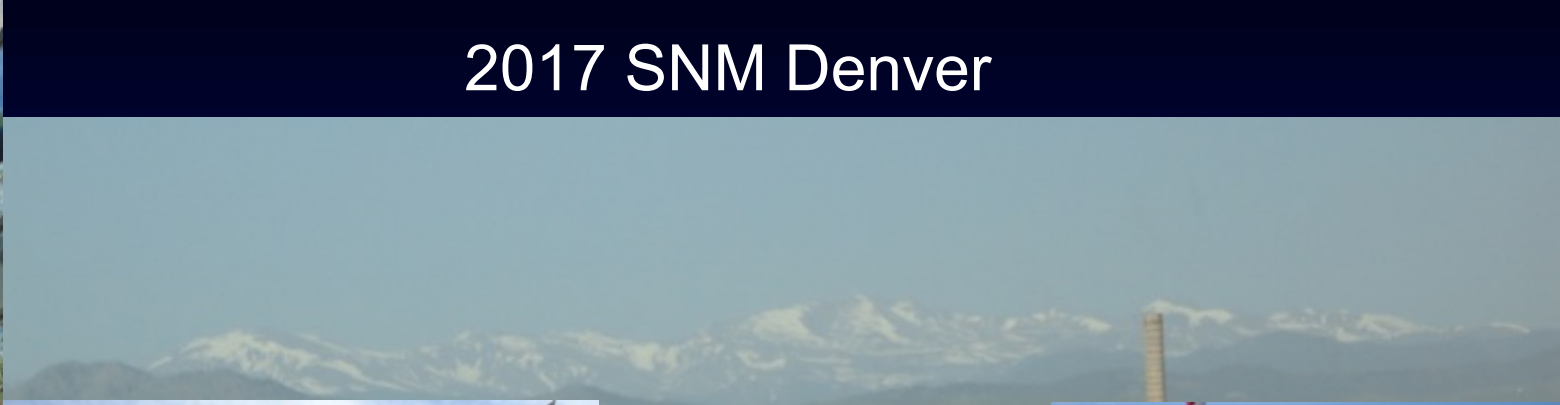2015 EANM Hamburg　5演題　　　　　　2015 RSNA Chicago

2016 EANM Barcelona　5演題
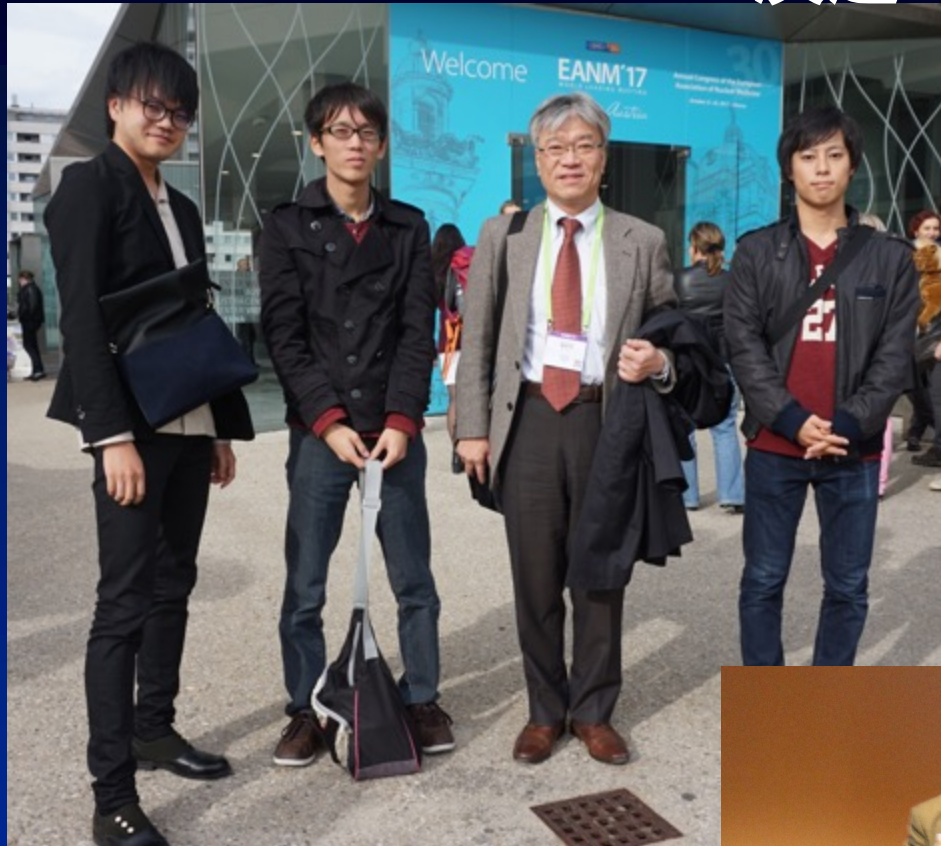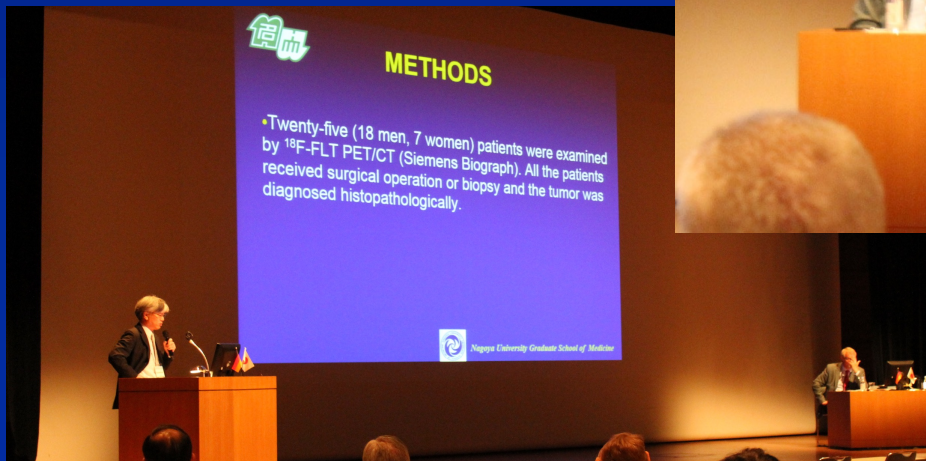
2016 RSNA Chicago

2017 EANM Wien　4演題

2017 RSNA Chicago

2018 日独放射線交流計画

2018 WFNMB世界核医学会 Melbourne

2018 SNM Philadelphia 4演題

2018 EANM Düsseldorf　3演題

2018 RSNA Chicago

—原 著—

分化型甲状腺癌のアブレーション効果判定に関する多施設共同研究に向けた技術的検討：アンケート調査とファントム評価

土屋 沙貴[1]　　阿部 真治[1]　　藤田 尚利[1]
西本 卓矢[1]　　櫻木 庸博[1]　　小芝有美子[2]
米田 和夫[1]　　加藤 克彦[2]

1）名古屋大学医学部附属病院医療技術部放射線部門
2）名古屋大学大学院医学系研究科医療技術学専攻

Technical Validation of Imaging Parameters for Multicenter Study about Effect Measurement of Remnant Ablation in Patients with Differentiated Thyroid Cancer : Questionnaire Survey and Phantom Experiment

Saki Tsuchiya[1], Shinji Abe[1], Naotoshi Fujita[1],
Takuya Nishimoto[1], Yasuhiro Sakuragi[1], Yumiko Koshiba[2],
Kazuo Yoneda[1] and Katsuhiko Kato[2]

1) Department of Radiological Technology, Nagoya University Hospital
2) Department of Radiological and Medical Laboratory Sciences,
Nagoya University Graduate School of Medicine

Summary

Toward multicenter study about effect measurement of ablation in cases thyroid remnant tissue using I-131 after total thyroidectomy (remnant ablation) in Japan, obtaining clinical data has been performed. In this study, we made a survey by questionnaire on equipment and acquisition parameters used for diagnostic scintigraphy from eight hospitals that have been performed remnant ablation. And we performed a phantom study based on acquisition parameters in our hospital in order to evaluate the visually detectable activity of residual tissue. In this study, we acquired data of whole body (WB), planar, and single photon emission computed tomography (SPECT) images using neck phantom with I-131 NaI capsule. According to the survey by questionnaire, the dose of I-131, intervals between ingestion and imaging, and bed speed of WB differed among eight hospitals. In the phantom study, we could detect low radioactivity of 1.66 kBq (WB, bed speed : 10 cm/min), 1.39 kBq (planar, 5 min acquisition), and 4.69 kBq (SPECT). The detectability was improved by extending the acquisition time in WB and planar imaging. Hence it is necessary to perform phantom experiment at other hospitals and standardize some imaging parameters such as bed speed of WB and acquisition time of planar imaging. And we need to examine criteria to determine whether remnant ablation succeeded from not only technical but also clinical aspect.

Table 1　Answers of questionnaires : protocols and gamma cameras
アブレーション実施施設に対するアンケートの回答：収集プロトコルと使用機器

Institute	Isotope	Dose [MBq (mCi)]	Intervals between isotope therapy and tracer study [months]	Intervals between uptake and imaging [days]	Model name (Manufacturer)	Collimator	Thickness of scintillator [inch]
A	I-131	185 (5)	7	4	Symbia T6 (Siemens)	HE	3/8
B	I-131	370 (10)	9	3	Symbia E (TOSHIBA)	HE	3/8
C	I-131	370 (10)	3–6	1 and 3	E.CAM (TOSHIBA)／Symbia T16 (Siemens)	HE	5/8
D	I-131	185 (5)	12	3	Infinia (GE)	HE	3/8
E	I-131	185(5)	6	5	Infinia (GE)	HE	3/8
F	I-123	18.5 (0.5)	6	1	SKYLlight (Philips)	LEGP	3/8
G	None	—	—	—			
H	None	—	—	—			

Table 2　Answers of questionnaires : acquisition parameters
アブレーション実施施設に対するアンケートの回答：収集条件

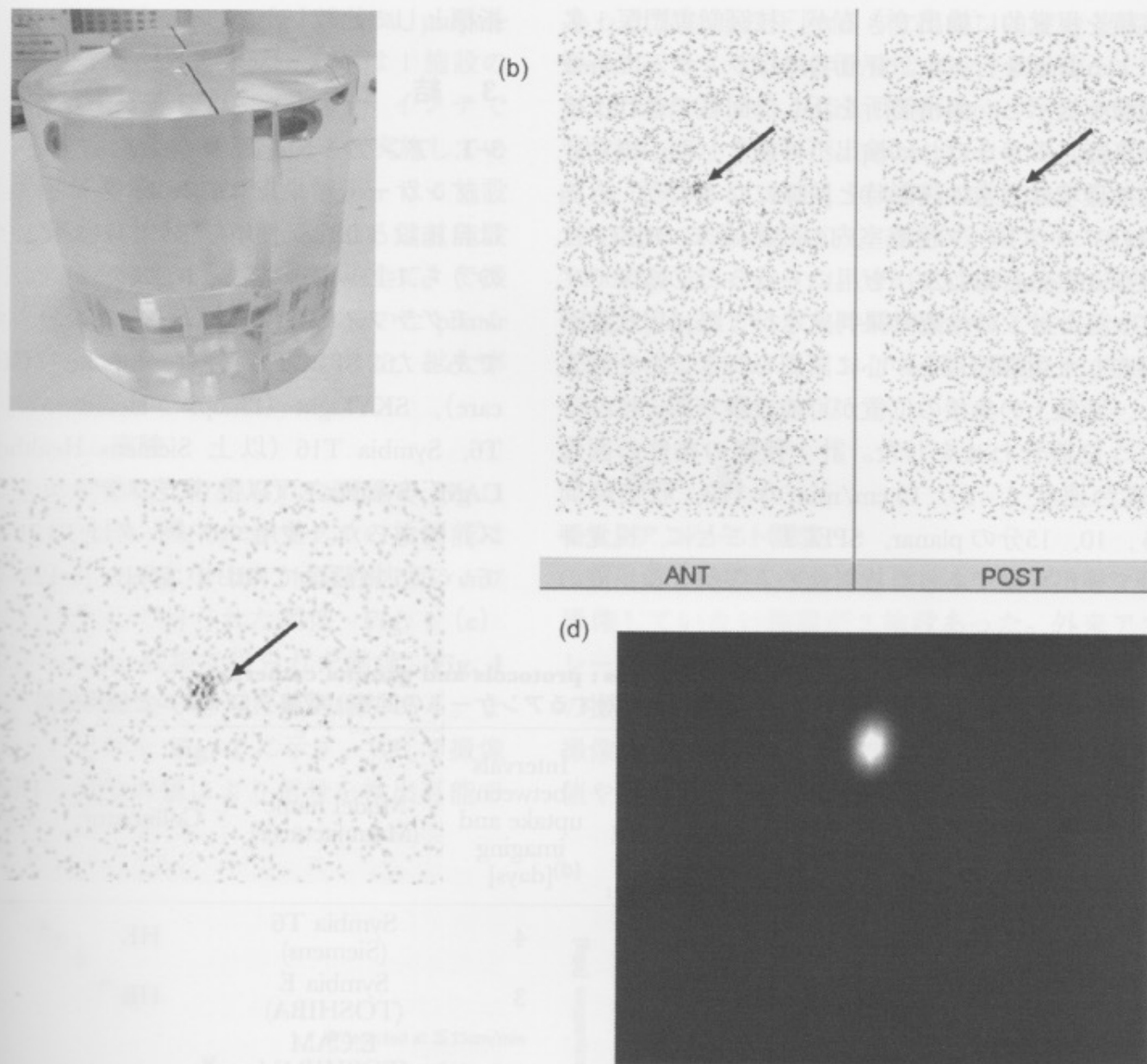| Institute	WB			Planar			SPECT
	Matrix	Magnification	Bed speed [cm/min]	Matrix	Magnification	Acquisition time [sec]	
A	256×1,024	1.00	15	—	—	—	○
B	256×1,024	1.00	15	128×128	1.00	600	○
C	256×1,024	1.00	8	—	—	—	○
D	256×1,024	1.00	8	—	—	—	○
E	256×768	1.00	5	—	—	—	○
F	512×1,024	1.00	7	—	—	—	×
G	—	—	—	—	—	—	—
H	—	—	—	—	—	—	—

Fig. 1　Neck phantom　(a: structure of the phantom,　b: WB,　c: planar,　d: SPECT)
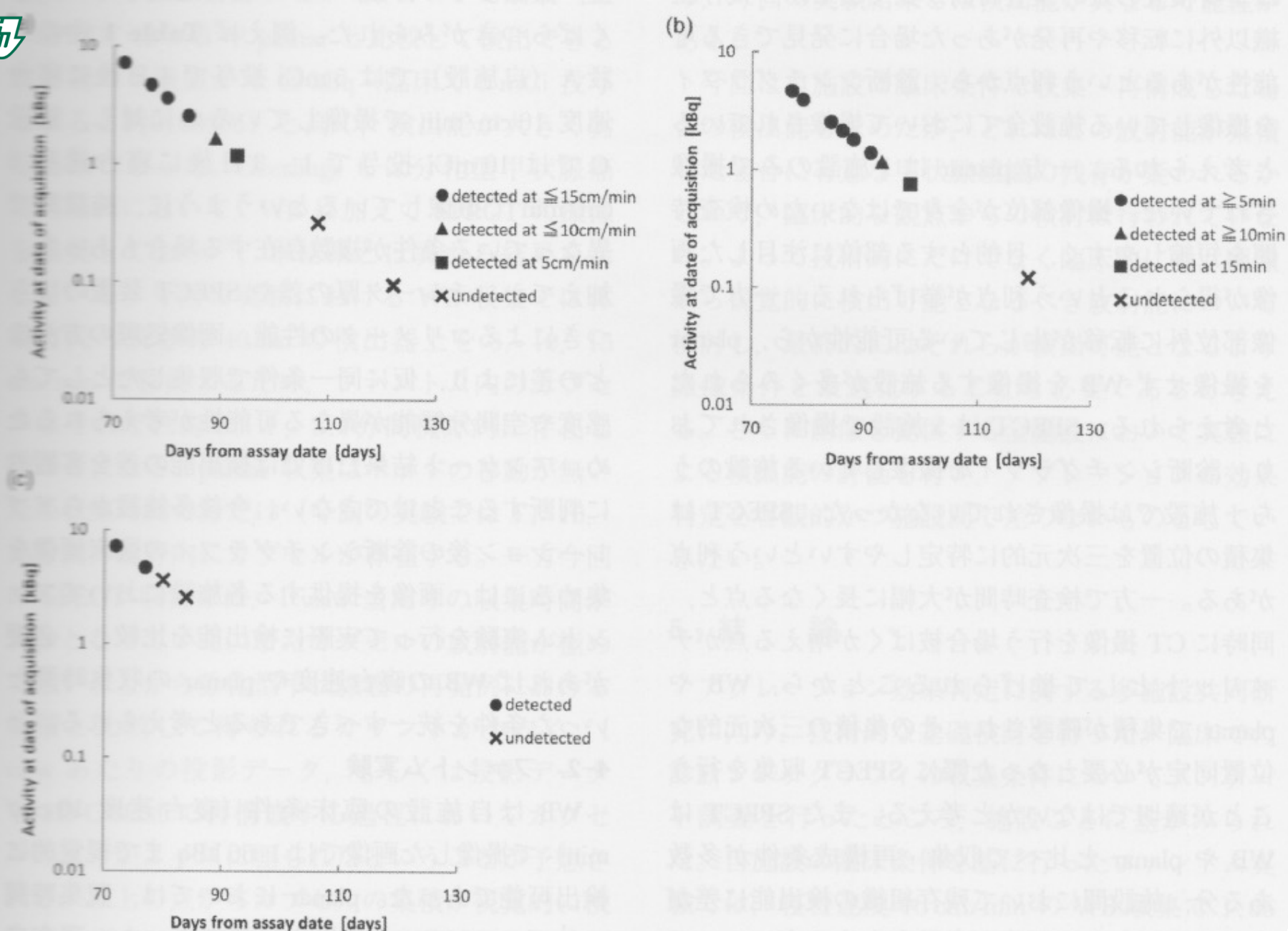頸部ファントム　(a: ファントム写真,　b: WB 像,　c: プラナー像,　d: SPECT 像)

Fig. 2 **Results of visual evaluation** （a：WB, b：planar, c：SPECT）
視覚評価の結果 （a：WB, b：プラナー像, c：SPECT）

ソマトスタチン受容体シンチグラフィにおけるファントムを用いた撮像条件の基礎的検討

西尾美穂[1)]、藤田尚利[2,3)]、伊藤良典[2)]、
大野里沙[2)]、多田智大[2)]、村山里奈[2)]、
池田陽菜[1)]、越智優佳[1)]、田村美香[2)]、
小田川哲郎[2)]、阿部真治[3)]、片渕哲朗[4)]、加藤克彦[1)]

[1)]名古屋大学大学院医学系研究科総合保健学専攻
[2)]名古屋大学大学院医学系研究科医療技術学専攻
[3)]名古屋大学医学部附属病院医療技術部 放射線部門
[4)]岐阜医療科学大学保健科学部放射線技術学科

方法

撮像条件

	エネルギーウィンドウ幅 (%)	サブウィンドウ幅 (%)	ピクセルサイズ (mm)	散乱減弱補正
A1	±7.5	5	3.3	○
A2	±7.5	5	3.3	×
B	±7.5	5	**4.8**	○
C	±7.5	**3**	3.3	○
D	**±10**	5	3.3	○
E	**±10**	5	**4.8**	○

10mm (11kBq/mL)
22mm (11kBq/mL)
5mm (11kBq/mL)
37mm (0kBq/mL)
28mm (11kBq/mL)
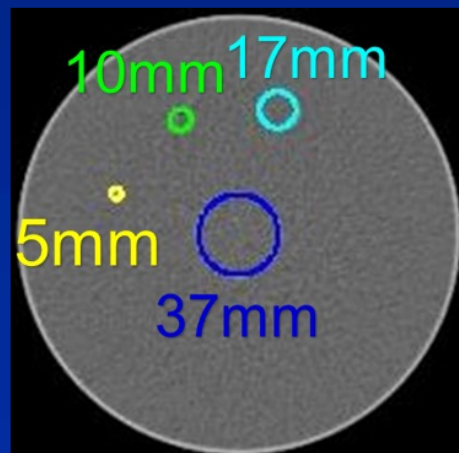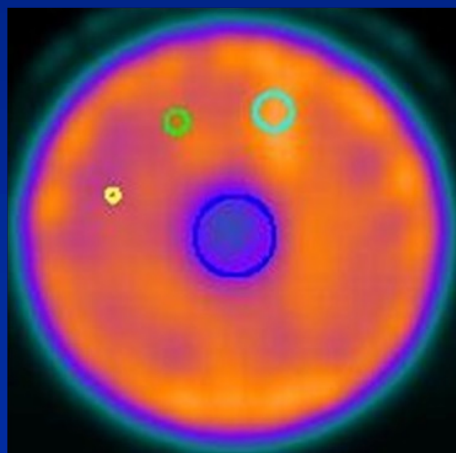
CT画像

SPECT画像

5つの指標

① Scatter Ration (SR): 散乱成分の割合

$$SR = \frac{水部分ROIの平均値}{B.G.ROIの平均値} \times 100 \ [\%]$$

② Coefficient of Variation (CV): 変動係数

$$CV = \frac{B.G.ROIの標準偏差}{B.G.ROIの平均値} \times 100 \ [\%]$$

③ Recovery Coefficient (RC): リカバリー係数

$$RC = \frac{C_j}{C_{28mm}}$$
$$RC = \sum (1 - RCj)$$

jは各球の大きさ、C_jは各球のROI内の最大値
C_{28mm}は28mm径でのROI内の最大値

④コントラスト

$$コントラスト = \frac{各球の平均カウント - B.G.の平均カウント}{各球の平均カウント}$$

⑤ Contrast Noise Ratio (CNR): コントラストノイズ比

$$CNR = \frac{各球の平均カウント - B.G.の平均カウント}{B.G.の標準偏差}$$

22mm
(11kBq/
37m
(0kBq

結果

5つの指標を順位に応じて
スコアリングし、
合計点で総合的に
評価した。

$$\begin{pmatrix} 1位→5点 & 4位→2点 \\ 2位→4点 & 5位→1点 \\ 3位→3点 & 6位→0点 \end{pmatrix}$$

合計点
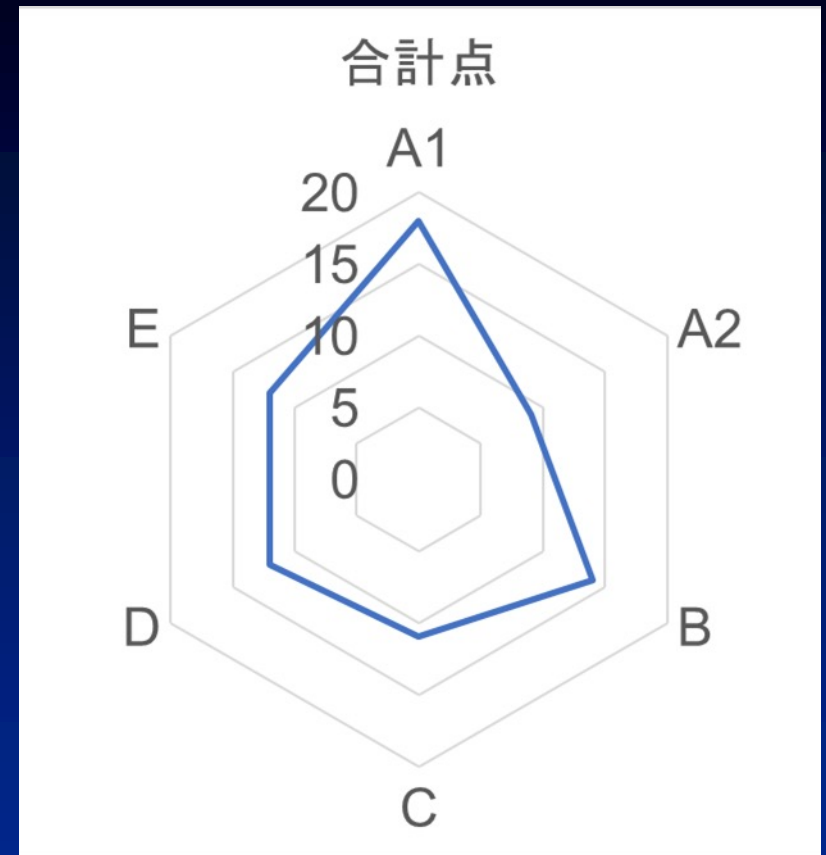
ソマトスタチン受容体シンチグラフィの撮像条件は、
メインウィンドウ幅±7.5%、サブウィンドウ幅5%、
ピクセルサイズ3.3mmが適切であると考えられる。

1830 Studies on variation of the standardized uptake value and metabolic tumor volume in analysis software for PET/CT using digital phantoms

Shinichiro Matsuzawa[1], Shinji Abe[2], Ryuto Mukumoto[1], Chinatsu Hasegawa[1], Tetsuro Odagawa[1], Katsuhiko Kato[1]

1) Department of Radiological and Medical Laboratory Sciences, Nagoya University Graduate School of Medicine, Nagoya, Japan.
2) Department of Radiological Technology, Nagoya University Hospital, Nagoya, Japan.

Purpose

For PET/CT, in indices such as standardized uptake value (SUV) and metabolic tumor volume (MTV) may occur even with the use of the same PET scanner because different algorithms are used in different analysis software programs.

In this study, we examined the causes for differences among 6 analysis software programs using digital phantoms.

Materials

Analysis software programs
• Metavol (v.1, Hokkaido University + University of California, Los Angeles)
• GI-PET (AZE Virtual Place Hayabusa ver 6.0, AZE, Japan)
• FUSION Plus (ver 4.11.1.0j, J-MAC SYSTEM, Japan)
• syngo.via (VB20a, Siemens)
• PMOD (version 3.9, PMOD)
• Advantage Workstation (Volume Share 5, GE)

Methods

The first type of phantom was used to examine the influence of the slice thickness change on SUV and MTV.

Each slice consisted of twenty-five 4mm × 4mm pixels, each with the same values given in SUV. (Fig. 1) Eight rectangular phantoms were then made by increasing the slice thickness from 1 mm to 8 mm. (Fig. 2)
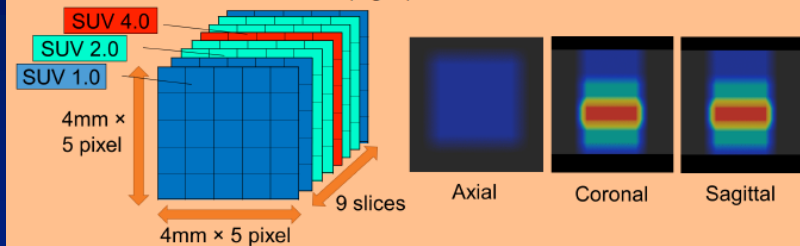

SUV 4.0
SUV 2.0
SUV 1.0
4mm × 5 pixel
9 slices
4mm × 5 pixel
Axial   Coronal   Sagittal

Fig.1 First type of phantom

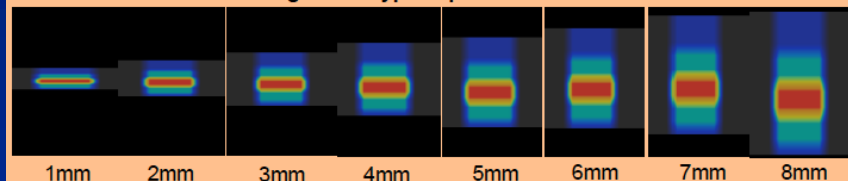1mm   2mm   3mm   4mm   5mm   6mm   7mm   8mm

Fig.2 Eight kinds of phantoms

The second type of phantom was used to examine the measurement accuracy of the SUV peak. Voxels had dimensions 4mm × 4mm × 4mm. A red voxel indicated an SUV scale value of 5.0. A yellow cube indicated an SUV scale value of 4.0. Blue rectangular areas indicated SUV scale values of 1.0.
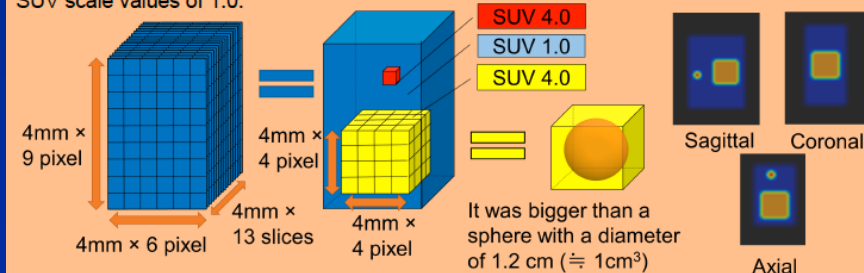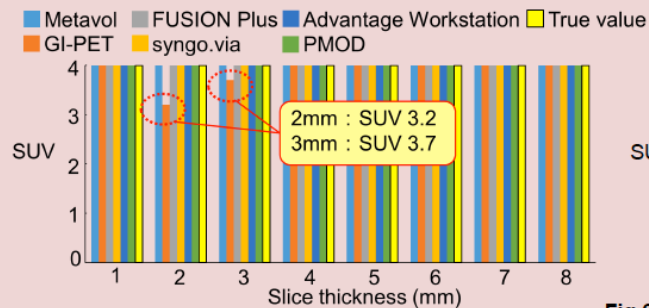

4mm × 9 pixel
4mm × 4 pixel
SUV 4.0
SUV 1.0
SUV 4.0
4mm × 6 pixel   4mm × 13 slices   4mm × 4 pixel
It was bigger than a sphere with a diameter of 1.2 cm ($\fallingdotseq$ 1cm^3)
Sagittal   Coronal   Axial

Fig.3 Second type of phantom

Results

Legend: Metavol, FUSION Plus, Advantage Workstation, True value, GI-PET, syngo.via, PMOD

2mm : SUV 3.2
3mm : SUV 3.7

SUV / Slice thickness (mm)

Fig.4 Comparison of SUVmax between 6 software programs

SUV 1.6
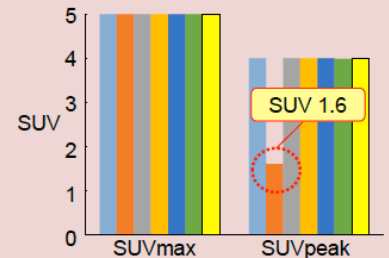
SUVmax   SUVpeak

Fig.6 Comparison of SUVmax and SUVpeak between 6 software programs
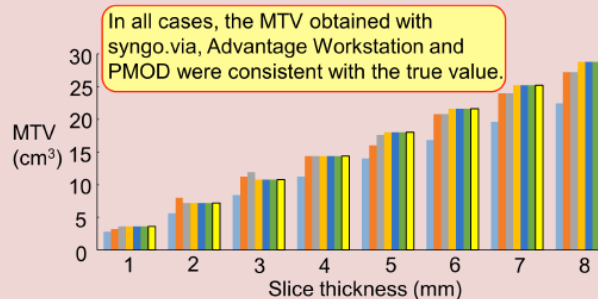
When slice thickness was 2 or 3 mm, SUVmax obtained with GI-PET was lower than the true value.

In all cases, the MTV obtained with syngo.via, Advantage Workstation and PMOD were consistent with the true value. Using other software programs, however, some of the MTV obtained were not consistent with the true value.

SUVpeak obtained with GI-PET was lower than the true value.

In all cases, the MTV obtained with syngo.via, Advantage Workstation and PMOD were consistent with the true value.

MTV (cm^3) / Slice thickness (mm)

Fig.5 Comparison of MTV between 5 software programs

Discussion

As a new slice was made by piling slices to make cubic voxels for GI-PET, voxel values were averaged. Therefore, the SUVmax value was lower than the true value.

Differences in MTV among GI-PET, FUSION Plus and the true value seem to occur due to using different voxels.

Differences in MTV between Metavol and the true value seem to occur due to the fact that Metavol could not measure the outermost data.

In GI-PET, SUVpeak was defined as "the average value in 1-cm^3 sphere centered on the pixel showing the maximum value." Difference in SUVpeak seemed due to difference in the definition of SUVpeak.

Conclusions

In conclusion, the differences in the indices obtained with the 6 software programs are attributable to varied handling of PET slice thicknesses and the definition of SUVpeak.

1841   Influence of scatter correction on measurement of the heart-to-mediastinum ratio by SPECT-CT

Ryuto Mukumoto[1], Tetsuro Odagawa[1], Naotoshi Fujita[2], Shinichiro Matsuzawa[1],
Chinatsu Hasegawa[1], Shinji Abe[2], Katsuhiko Kato[1]

[1] Department of Radiological and Medical Laboratory Sciences, Nagoya University Graduate School of Medicine
[2] Department of Radiological Technology, Nagoya University Hospital

Background

- In the myocardium sympathetic nerve scintigraphy, the heart-to-mediastinum ratio (HMR) is used for diagnosis of Parkinson's disease and dementia with Lewy bodies.
- HMR is an indicator of myocardial I-123 MIBG uptake.
- It is difficult to accurately quantify HMR because of the presence of 529 keV scatter component from I-123 MIBG.
- Using the SPECT-CT data, it is possible to quantify the HMR measurement by making synthetic planar images (SP images).
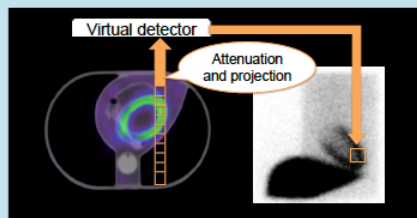
(Fig. 1) How to make SP images.
We used the attenuation map for SPECT images and acquired SP images by attenuating and forward projecting the count per pixel.

The method of scatter correction for removing scatter component by setting multiple energy window.

- I-123 Dual Window (IDW) method
  - Remove 524 keV scatter component of I-123 MIBG, and improve the fluctuation of quantitative value.
- Triple Energy Window (TEW) method
  - It is available for nuclide with multiple energy windows, and possible to set the energy window easily. An image with good contrast can be obtained.

- Using planar images, we calculated HMR from the mean count of the myocardium and mediastinum by setting ROI.
- SPECT images were reconstructed using 360° data and 180° data from each projection angles with or without SC.

Table1. Parameters for data acquisition

Planar		SPECT-CT	
Matrix size	256×256	Acquisition range	360°
Pixel size	1.35 mm	Angular step	3°(60 view)
zoom	1.78	Matrix size	128×128
Acquisition time	5 min	zoom	1.23
		Acquisition time	30 min
SC	IDW TEW	Detector motion	Continuous
		Acquisition orbit	Non-circular

Table2. Parameters for reconstruction

Method	3D-OSEM
Iteration	12
Subset	6
Pixel size	4.8 mm
Post - reconstruction filter	Gaussian (9.6 mm)
Attenuation correction (CTAC)	+ +
Scatter correction (SC)	+ −
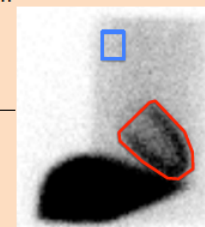
(Fig.2) Setting ROI

Results

- HMR calculated from planar images were 2.51(IDW), 2.58(TEW).
- HMR calculated from SP images were 2.36(SC-) and 2.58(SC+)
- HMR measured from SP images (SC+) were close to the HMR measured from planar image (TEW), and SP images (SC+) made myocardium clear visually.
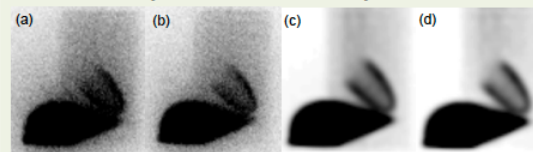
(Fig.3) Planar images with SC (IDW (a), TEW (b)) and SP images with SC (c), without SC (d).

HMR (TEW)=2.58
HMR (SC+)=2.55±0.04
HMR (IDW)=2.51
HMR (SC-)=2.35±0.03
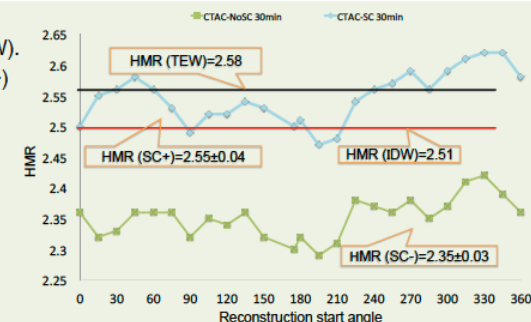
(Fig. 4) The result of HMRs calculated from SP images gained from 180° reconstruction images.

Purpose

- We compared the HMRs calculated from SP images and planar images with or without scatter correction. We investigated the influence of scatter correction on HMR calculated from SP images.

Materials

- Gamma camera and SPECT-CT : Symbia T (SIEMENS)
- Collimator : Low medium energy general purpose collimator (LMEGP)
- Phantom : HL phantom (KYOTO KAGAKU Co., Ltd.)
- Radioisotope : I-123 MIBG

Methods

- We defined the radioactivity concentrations as shown below, and enclosed I-123 MIBG solutions into the respective areas of the torso phantom.
  - myocardium : 38.7 kBq/ml, mediastinum : 2.54 kBq/ml, right lung : 24.8 kBq/ml, left lung : 19.2 kBq/ml, liver : 18.3 kBq/ml
- Planar images were acquired with scatter correction using two kinds of methods (IDW, TEW).

Discussion

- HMR measured from SP images (SC+) were close to the HMR measured from planar image (TEW)
  - In SPECT-CT, scatter correction is performed by setting multiple energy windows, estimating and removing scatter components.

  The effect of scatter correction was high, and the boundary of myocardium was clear.

- The change of HMR measured from SP images when the reconstruction start angle is changed.
  - SC-   360° reconstruction : HMR = 2.36
          180° reconstruction : HMR = 2.35±0.03
  - SC+   360° reconstruction : HMR = 2.58
          180° reconstruction : HMR = 2.55±0.04
  - The value of HMR depends on the reconstruction start angle.

  It suggested that reconstruction angles are appropriate starting from close to the heart.

Conclusion

- In this study, we investigated the influence of scatter correction on HMR calculated from SP images.
- By using SP images (SC+), the quantitative of HMR measurement is improved.
- Further analyses with clinical data will be needed.

Mukumoto R, et al. SNM'18, Philadelphia, United state.

タングステン機能紙を用いた核医学画像フィルタの基礎実験 ～123I におけるファントムの評価～

淺野有紀[1]、今津咲来[2]、曽根千尋[2]、
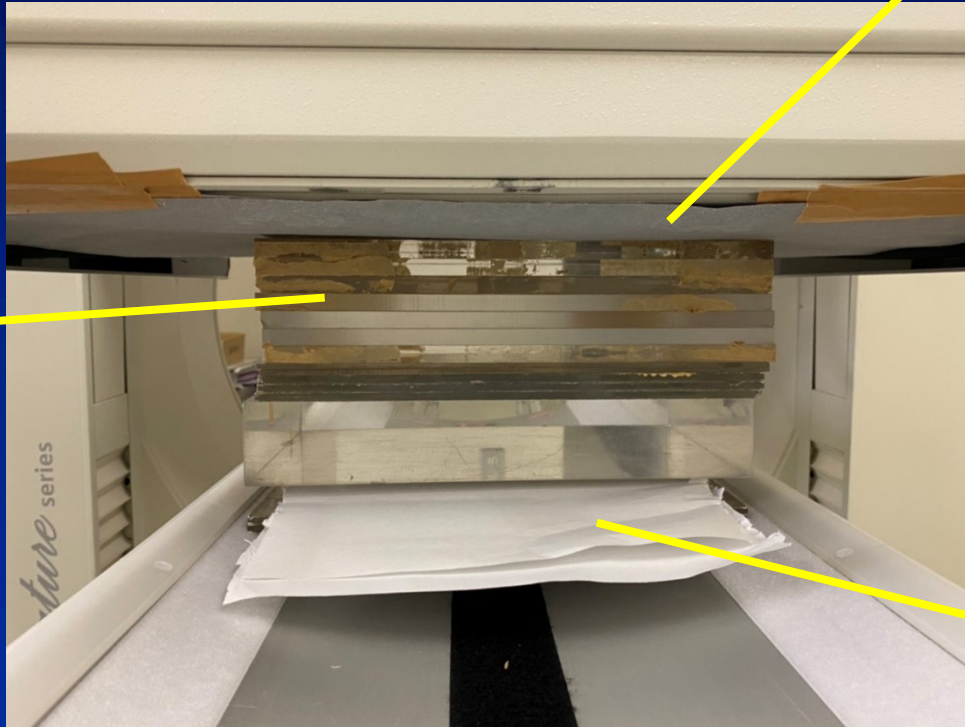
藤田尚利[3]、池田陽菜[1]、越智優佳[1]、

西尾美穂[1]、片渕哲朗[2]、加藤克彦[1]

1) 名古屋大学大学院 医学系研究科 総合保健学専攻
2) 岐阜医療科学大学 保健科学部 放射線技術学科
3) 名古屋大学医学部附属病院医療技術部放射線部門

方法：配置方法

タングステン機能紙

アクリル板

ファントム

^{123}I-MIBGシンチグラフィにおける H/M比を得る新規解析手法 ～3次元数値ファントムによる検証～

磯辺亮太[1], 伊藤良典[2], 藤田尚利[3], 西井龍一[1]
南本亮吾[1], 中西恒平[1], 岩永陽菜[3], 長原朋香[1]
稲垣朝也[1], 恒川諒太郎[1], 加藤克彦[1]

1) 名古屋大学大学院 医学系研究科 総合保健学専攻
2) 名古屋市立大学医学部附属西部医療センター 中央放射線部
3) 名古屋大学医学部附属病院 医療技術部 放射線部門
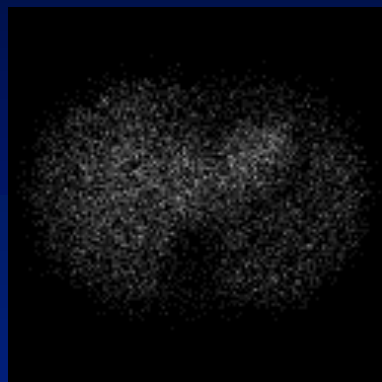
Nagoya University Graduate School of Medicine

インクジェットプリンタを用いた
3次元用ペーパーファントムの
作成と応用に関する研究

名古屋大学大学院 医学系研究科 総合保健学専攻　長原 朋香

作成方法

(1) デザインを作成する
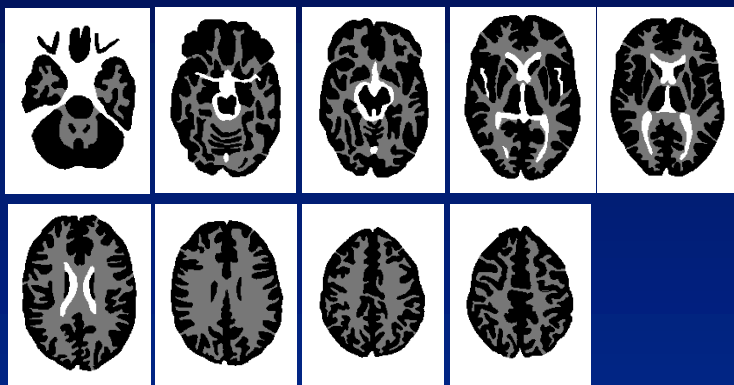
(2) ペーパーファントムを印刷する

インクジェットプリンタ
（RI＋黒インク）で印刷する

(3) PET用ペーパーファントムを作成する

ペーパー
ファントム
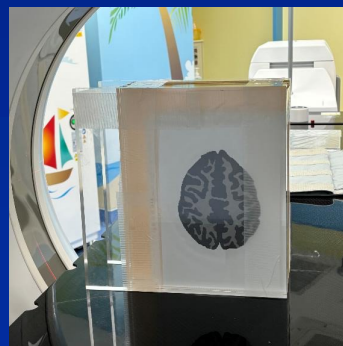
(4) PET収集を行う
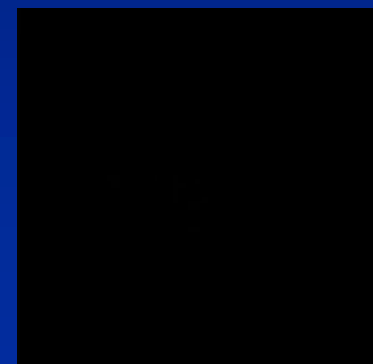
卒業研究 57名

- 平成21年度
- 桑原早那香・眞田那奈子 ^{131}Iの測定機器による甲状腺摂取率の違い
- 田島洋子 ^{131}I-MIBG心筋シンチグラフィにおけるコリメータの比較に関する研究
- 都築恭太郎 名古屋大学医学部附属病院PET検査室における従事放射線技師の被曝量に関する検討
- 平成22年度
- 磯貝静紀 名古屋大学附属病院RI検査室における^{123}I-MIBGを用いた心筋交感神経機能シンチグラフィの心縦隔比の正常値の検討
- 鈴木悠介 ^{123}I溶液を用いた球体ファントムにおける径の違いによる描出能の検討
- 宮地優也 円柱状ファントムによる^{123}Iを用いた低濃度領域における収集時間の短さと放射能濃度の低さの限界の検討
- 安原大雅 ^{18}F-FDG PET/CTにおける肝の生理的集積の検討
- 郡倫一 ^{123}Iによるコイン状線源を用いた描出能の検討
- 平成23年度
- 近藤彩香 ^{123}I-IMPを使用した脳血流SPECT定量解析における新しい非採血法と一点動脈採血法との比較
- 田部敬子 ^{18}F-FDG PET/CTの撮像体位によって生ずるアーチファクトが肝臓の集積に与える影響：両腕を挙げて撮像した場合と下げて撮像した場合の比較
- 森島彩乃 骨シンチグラフィ診断支援ソフトウエアの基本的特性および診断精度の評価
- 米山友明 名古屋大学医学部附属病院におけるPETおよびPET/CT装置の描出能の検討
- 平成24年度
- 小出若葉 骨シンチグラフィ用コンピュータ支援診断ソフトウエアにおけるprefiltering処理の有用性に関する検討
- 小南かすみ Planer Imagingの画質改善ソフトウエアを使った核医学画像の評価
- 丹羽亜利紗 心臓用多焦点型ファンビームコリメータを用いた心筋SPECTによる至適収集時間の検討
- 藤田佑介 ^{123}I-IMP ARG法による脳血流測定法における定量性に影響を与える因子に関する検討
- 平成25年度
- 磯村泰己 ^{123}I-IMPを用いたグラフプロット法による脳血流測定法
- 大峽悠紀 PERCISTを用いた^{18}F-FDG PET/CTによる悪性リンパ腫の治療効果判定の研究
- 土屋沙貴 SPECT-CT装置を用いた^{131}Iの比放射能の推定に関する基礎的検討
- 平成26年度
- 石原加純 ドパミントランスポータシンチグラフィにおける最適収集処理条件の検討
- 小芝有美子 ^{131}Iシンチグラフィによる甲状腺摂取率に関する研究
- 小西翔子 アルゴリズムの異なる解析ソフトにおける心内腔容積の比較
- 鈴村瞳 空間分解能の異なるPET装置におけるSUVの比較に関する研究
- 平成27年度
- 大村優奈 異なる解析ソフトによるSUV比較に関する研究
- 国本啓太 多焦点型ファンビームコリメータを用いた心筋2核種同時収集法に関する検討
- 服部汐里 ドパミントランスポータシンチグラフィの視覚評価の正当性に関する研究
- 本田将之 脳タウイメージング撮像における視野外からの散乱線の影響

Nagoya University Graduate School of Medicine

- 平成28年度
- 遠藤嵩士 ドパミントランスポータシンチグラフィにおける解析ソフトの有用性に関する研究
- 松澤伸一郎 PET解析ソフトウエアにおける計測精度に関する検討
- 椋本竜斗 SPECT-CT装置を用いた心縦隔比の計測精度向上に関する研究
- 柳秀輝 甲状腺機能亢進症の131I内用療法における吸収線量に関する検討
- 平成29年度
- 加藤未来 ^{123}I-MIBG-^{201}TlCl2核種同時収集を用いた心筋交感神経シンチグラフィにおいて^{201}TlClが心縦隔比へ与える影響
- 長谷川千夏 骨シンチグラフィの定量解析に用いるBCFの測定精度に関する検討
- 原陽子 SPECT撮像における^{123}I-MIBG定量化に向けた基礎的検討
- 藤嶋孝太 ^{99m}Tc-MAG3腎動態シンチグラフィおよびイヌリンクリアランス試験で得られる腎機能評価指標の相関分析
- 平成30年度
- 伊藤良典 ドパミントランスポータシンチグラフィにおける部分容積効果を考慮した半定量指標算出の検討
- 大野里沙 ^{18}F-fluoride PET/CT画像および^{18}F-FDG PET/CT画像における正常骨と骨転移のカットオフ値決定に向けた検討
- 多田智大 ^{11}C-PiBを用いたPET画像におけるアルツハイマー型認知症の評価方法
- 村山里奈 心サルコイドーシス^{18}F-FDG PET検査における病変部位検出のための至適閾値に関する基礎的検討
- 令和元年
- 池田陽菜 甲状腺機能亢進症における甲状腺CT値と甲状腺機能の関係性
- 越智優佳 慢性血栓塞栓性肺高血圧症における99mTc-MAA SPECT-CTを用いた肺灌流指数と右心カテーテル検査から得られる各種評価指標との関係の検討
- 奥田迅一郎 Support vector machineを用いた223Ra内用療法の治療効果予測
- 令和2年度
- 大原千乃 頸部X線CT画像から得られた甲状腺重量の計測者間比較
- 酒井惟司 アルツハイマー型認知症における自動領域抽出機能を用いた^{11}C-PiB特異的集積部位の領域別集積量の検討
- 樋口真帆 骨密度及び年齢が^{18}F-fluoride PET/CT及び18F-FDG PET/CTにおける正常骨のstandardized uptake valueに与える影響
- 令和3年度
- 稲垣拓実 ^{111}In溶液のファントム吸着に関する検討 〜濃度及びpHが及ぼす影響について〜
- 大工凌矢 肺血流シンチグラフィにおける肺血流領域決定のための至適閾値の検討
- 林岳弥 PET/CT装置における画像再構成法の違いによるPET画像の物理的評価
- 令和4年度
- 磯邊亮太 ^{123}I-MIBGシンチグラフィにおけるH/M比を得るための逐次近似を用いた新規解析手法の検討
- 高井春風 ^{18}F-fluoride PET/CT及び18F-FDG PET/CT画像で肋骨の転移性骨腫瘍を鑑別できるか？
- 増井里紗 ^{18}F-FDG PET/CT画像による肺癌の縦隔リンパ節転移評価に有効な客観的指標の検討
- 令和5年度
- 稲垣朝也 ^{11}C-PiB PET検査における年齢とSUVRの関係の検討
- 清瀬裕也 肺高血圧症における^{99m}Tc-MAA planar画像と99mTc-MAA SPECT画像の集積分布の比較
- 恒川諒太郎 肺高血圧症における99mTc-MAA Planar画像の集積分布と右心カテーテル検査で得られる諸指標との関係
- 令和6年度
- 李 丞鎬 虚血性心疾患における負荷心筋血流シンチのSDS値と負荷心エコーのWMA値の比較
- 葛禹彤 ^{11}C-methionine PET画像を用いたRadiomics解析によるgliomaのグレード2と3の鑑別

大学院前期課程 23名

- 末澤正太郎 ^{111}Inのデュアルフォトピークを用いたプラナー収集による放射能量推定
- 丹羽亜利紗 心臓用多焦点型ファンビームコリメータを用いた心筋血流シンチグラフィの至適収集条件に関する研究
- 藤田佑介 肺及び脳からの^{123}I-IMP収集データを用いた非侵襲的脳血流量測定法の簡素化と有用性の実証
- 土屋沙貴 ^{131}Iシンチグラフィを用いた甲状腺癌全摘術後の転移巣の評価に関する研究
- 小芝有美子 甲状腺機能亢進症に対する^{131}I内用療法後の甲状腺への^{131}I集積定量と治療効果予測に関する検討
- 国本啓太 心臓用多焦点型ファンビームコリメータを用いたTl-201とI-123による心筋2核種同時収集法に関する研究
- 本田将之 [^{18}F]THK-5351を用いる脳PETタウイメージング検査において脳以外の高集積部位からの放射線がstandardized uptake valueに与える影響に関する研究
- 松澤伸一郎 PET解析ソフトウェアの違いがstandardized uptake value、metabolic tumor volume、total lesion glycolysisへ与える影響に関する研究
- 椋本竜斗 ^{123}I-MIBGを用いた心筋交感神経シンチグラフィ検査におけるSPECT-CTデータを利用した心縦隔比計測精度の向上に関する研究
- 長谷川千夏 骨転移に対するRI内用療法の治療効果判定：骨SPECT, 18F-fluoride PET/CT, 18F-FDG PET/CT画像から測定した半定量的指標の比較
- 伊藤良典 ドーパミントランスポータSPECTにおける新規解析手法の有用性の検討－類似画像探索による集積量の決定－
- 大野里沙 ^{18}F-fluoride PET/CT及び^{18}F-FDG PET/CTにおける正常骨と骨転移の至適カットオフ値の検討
- 多田智大 ^{11}C-Pittsburgh Compound-B (^{11}C-PiB)を用いたPET画像における^{11}C-PiB集積の定量評価と認知機能との関係に関する研究
- 村山里奈 ^{18}F-FDG PET/CT画像を用いた心臓サルコイドーシス病変の定量評価に関する検討
- 池田陽菜 甲状腺機能亢進症に対する放射性ヨウ素内用療法の治療反応性予測と投与放射能・吸収線量決定法に関する研究
- 越智優佳 慢性血栓塞栓性肺高血圧症における^{99m}Tc-MAA SPECTを用いた定量的指標と右心カテーテル検査より得られる血行動態指標との関係の検討
- 西尾美穂 ソマトスタチン受容体シンチグラフィにおける撮像・処理条件の基礎的検討
- 稲垣拓実 放射性医薬品の合成樹脂への吸着に関する基礎的検討
- 淺野有紀 核医学画像の画質改善及び核医学検査における被曝低減のためのタングステン機能紙の活用
- 磯邊亮太 ^{123}I-MIBGシンチグラフィにおけるH/M比を得る新規解析手法の検討
- 長原朋香 インクジェットプリンタを用いた3次元用ペーパーファントムの作成と応用に関する研究
- 稲垣朝也 アミロイドPET検査における皮質平均SUVR算出手法の比較
- 恒川諒太郎 肺高血圧症における99mTc-MAA Planar画像・SPECT画像の集積分布と右心カテーテル検査で得られる諸指標との関係

大学院後期課程　10名

- 伊藤信嗣 Comparison of ^{18}F-FDG PET and bone scintigraphy in detection of bone metastases of thyroid cancer
- 阿部真治 ^{123}I-IMPの肺野と脳の時系列収集データを用いた非採血脳血流定量推定法の検討
- 太田尚寿 Comparison of ^{18}F-fluoride PET/CT, ^{18}F-FDG PET/CT and bone scintigraphy (planar and SPECT) in detection of bone metastases of differentiated thyroid cancer: a pilot study
- 佐々直人 Evaluation of 11C-choline PET/CT for Primary Diagnosis and Staging of Urothelial Carcinoma of the Upper Urinary Tract
- 石口裕章 Diagnostic performance of ^{18}F-FDG PET/CT and whole-body diffusion-weighted imaging with background body suppression (DWIBS) in detection of lymph node and bone metastases from pediatric neuroblastoma
- 藤田尚利 甲状腺機能亢進症に対する放射性ヨウ素内用療法における投与放射能決定法の再構築と甲状腺吸収線量を用いる治療効果予測法の確立
- 堤貴紀　Dual-Energy CTから得られる定量値を用いた慢性血栓塞栓性肺高血圧症の重症度評価
- 大橋俊夫 MRI による内リンパ水腫の評価 ― 非造影法と造影法の比較 ―
- 田村美香 Effect of previous administration of potassium iodine and different durations of low iodine diets for radioiodine therapy on the treatment of Graves' disease in iodine-rich areas(ヨウ素摂取量が多い地域におけるバセドウ病放射性ヨウ素内用療法に対するヨウ化カリウムとヨウ素制限期間の影響)
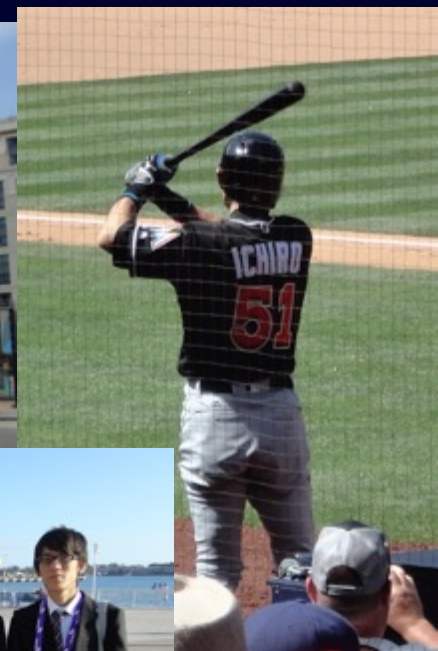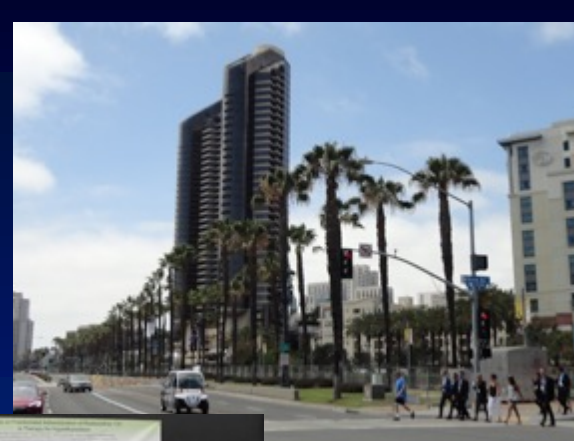- 岩永(池田)陽菜 甲状腺機能亢進症における甲状腺CT値と甲状腺機能の関係性および放射性ヨウ素内用療法の治療効果予測
- 小田川哲郎 ･･･････

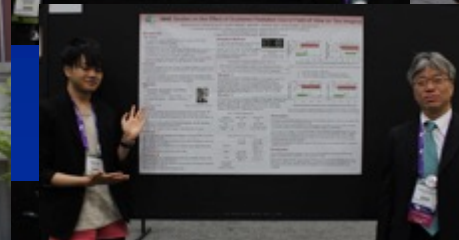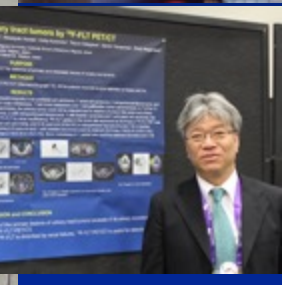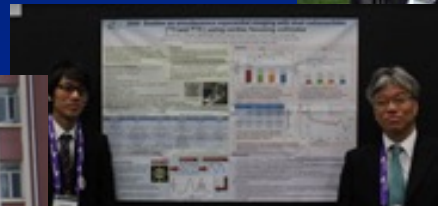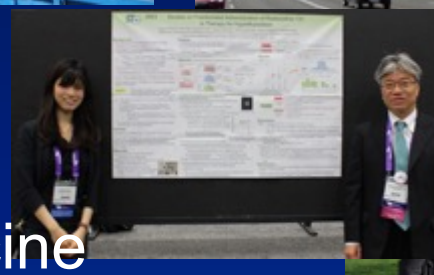*Nagoya University Graduate School of Medicine*
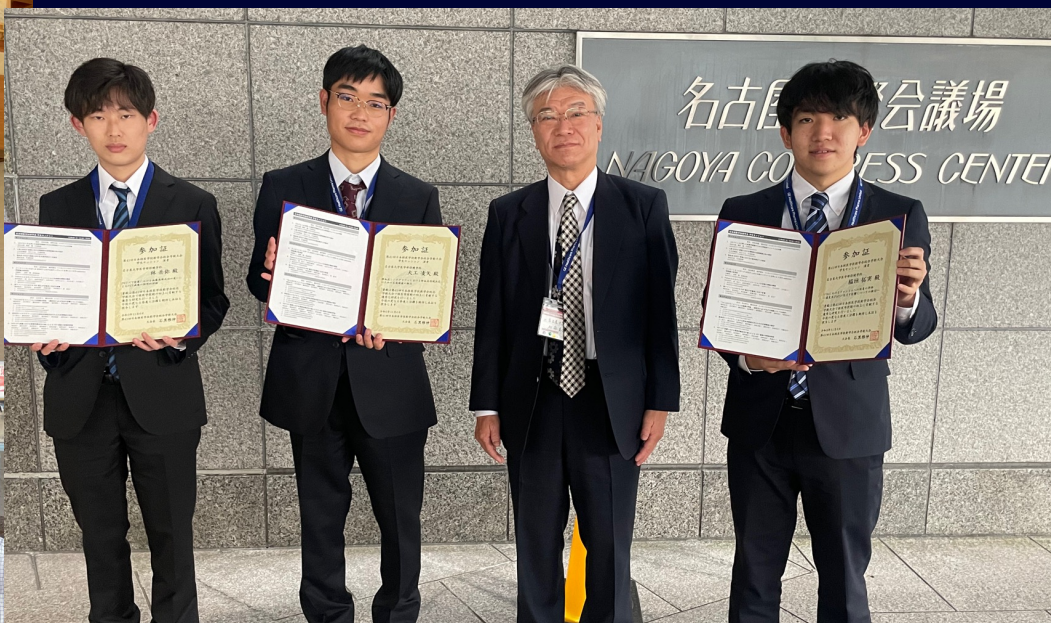
2016 日独放射線交流計画
München

2016 SNM San Diego

2016 2nd Asian Nuclear Medicine
Academic Forum 上海

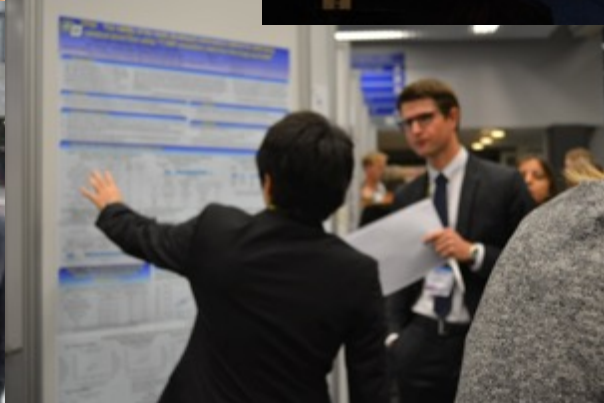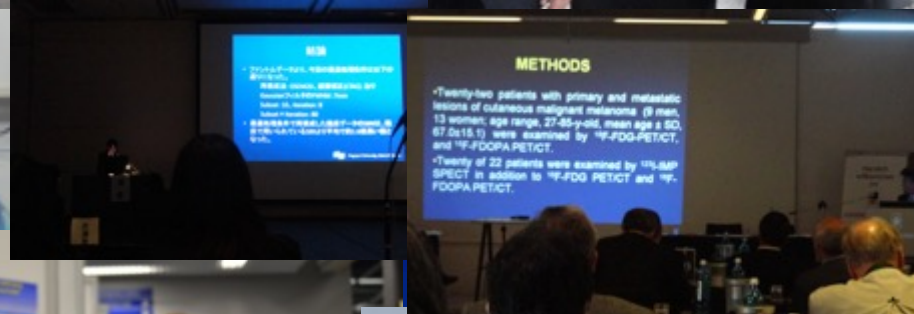*Nagoya University Graduate School of Medicine*

研究室

Nagoya University Graduate School of Medicine

Nagoya University Graduate School of Medicine

Nagoya University Graduate School of Medicine

長い間本当にありがとうございました。